

**MOLECULAR DYNAMICS SIMULATIONS ON THE STRUCTURE AND  
INTERFACIAL INTERACTIONS OF POLYETHYLENE-ORGANOCLAY  
NANOCOMPOSITES**

**Ph.D. Thesis by  
Erol YILDIRIM**

**Department : Chemistry**

**Programme : Chemistry**

**DECEMBER 2011**



**MOLECULAR DYNAMICS SIMULATIONS ON THE STRUCTURE AND  
INTERFACIAL INTERACTIONS OF POLYETHYLENE-ORGANOCLAY  
NANOCOMPOSITES**

**Ph.D. Thesis by  
Erol YILDIRIM  
(509052202)**

**Date of submission : 07 October 2011  
Date of defence examination: 06 December 2011**

**Supervisor (Chairman) : Prof. Dr. Mine YURTSEVER (ITU)  
Members of the Examining Committee : Prof. Dr. Nurseli UYANIK (ITU)  
Prof. Dr. Viktorya AVIYENTE (BU)  
Prof. Dr. Levent DEMIREL (KU)  
Assoc. Prof. Dr. Gökтуğ AHUNBAY (ITU)**

**DECEMBER 2011**





**İSTANBUL TEKNİK ÜNİVERSİTESİ ★ FEN BİLİMLERİ ENSTİTÜSÜ**

**POLİETİLEN-ORGANOKİL NANOKOMPOZİTLERİNİN YAPISAL  
ÖZELLİKLERİNİN VE ARAYÜZEY ETKİLEŞİMLERİNİN MOLEKÜLER  
DİNAMİK SİMÜLASYON YÖNTEMLERİYLE İNCELENMESİ**

**DOKTORA TEZİ  
Erol YILDIRIM  
(509052202)**

**Tezin Enstitüye Verildiği Tarih : 07 Ekim 2011**

**Tezin Savunulduğu Tarih : 06 Aralık 2011**

**Tez Danışmanı : Prof. Dr. Mine YURTSEVER (İTÜ)  
Diğer Jüri Üyeleri : Prof. Dr. Nurseli UYANIK (İTÜ)  
Prof. Dr. Viktorya AVİYENTE (BÜ)  
Prof. Dr. Levent DEMİREL (KÜ)  
Doç. Dr. Göktuğ AHUNBAY (İTÜ)**

**ARALIK 2011**



## FOREWORD

I would like to thank my supervisor Prof. Dr. Mine Yurtsever for her helps, guidance and patience as well as for her psychological support and confidence in me through my studies for this thesis. I am grateful for her directness, her ideas, for giving me opportunities and for providing me well-organized inspiring research environment.

I would like to thank my thesis tracking committee members, Prof. Dr. Nurseli Uyanık and Prof. Dr. Levent Demirel for sharing their scientific knowledge with me and for their useful discussions and suggestions.

I would like to thank Assoc. Prof. Nurcan Tüzün and my friends, Cihan Özen and Gonca Güzel for their continuous support.

I wish to acknowledge computer time provided by High Performance Computing Center and TUBITAK. Finally, I would like to thank my family. I owe them a great deal.

December 2011

Erol YILDIRIM

Chemistry



## TABLE OF CONTENTS

	<u>Page</u>
<b>FOREWORD .....</b>	<b>v</b>
<b>TABLE OF CONTENTS.....</b>	<b>vii</b>
<b>ABBREVIATIONS .....</b>	<b>ix</b>
<b>LIST OF TABLES .....</b>	<b>xi</b>
<b>LIST OF THE FIGURES .....</b>	<b>xiii</b>
<b>SUMMARY .....</b>	<b>xvii</b>
<b>ÖZET.....</b>	<b>xix</b>
<b>1. INTRODUCTION.....</b>	<b>1</b>
1.1 Nanocomposites .....	1
1.2 Nanofillers.....	2
1.3 Clays.. .....	3
1.3.1 2:1Phyllosilicates.....	4
1.3.2 Montmorillonite.....	6
1.4 Theoretical Studies on Clay Structures .....	10
1.5 Organoclays .....	11
1.5.1 Synthesis of organoclays .....	12
1.5.2 Properties of organoclays.....	14
1.5.3 Characterisation of organoclays .....	16
1.5.4 Organic compounds used to prepare organoclays .....	18
1.5.5 Theoretical studies on organoclays .....	21
1.6 Polymer Layered Silicate Nanocomposites .....	23
1.6.1 Polymers used in PLSN .....	24
1.6.2 Definitions.....	25
1.6.3 Preparation of polymer nanocomposites.....	28
1.6.4 Properties and applications of PLSN.....	34
1.7 Characterization of PLSN .....	38
1.8 Polyolefin Nanocomposites .....	43
1.8.1 Polyethylenes .....	45
1.8.2 Polyethylene compatibilizers .....	46
1.8.3 Synthesis and properties of polyethylene nanocomposites.....	50
1.9 Theoretical Studies on PLSN.....	54
1.9.1 Molecular Dynamics and Monte Carlo studies.....	57
1.9.2 Thermodynamics of PLSN .....	58
1.10 Purpose of the Thesis .....	61
<b>2. A COMPARATIVE STUDY ON THE EFFICIENCIES OF POLYETHYLENE COMPATIBILIZERS BY USING THEORETICAL METHODS.....</b>	<b>65</b>
2.1 Theoretical Calculations .....	67
2.1.1 Simulations of polymer chains in amorphous cell .....	67
2.1.2 Determination interaction parameters and reactivities .....	67
2.1.3 Structural Properties of polyethylene compatibilizers.....	69

2.2 Results and Discussion.....	69
2.2.1 Simulations of polymers in amorphous cell .....	69
2.2.2 Determination interaction parameters and reactivities .....	72
2.2.3 Structural properties of PECs .....	81
<b>3. DETERMINATION OF STRUCTURES AND ELECTRONIC PROPERTIES OF MONTMORILLONITE CLAY .....</b>	<b>87</b>
3.1 Theoretical Methods in the Clay Research.....	89
3.2 Theoretical Methods Used in the Study .....	90
3.2.1 Determination of structures and electronic properties by DFT methods.....	90
3.2.2 Hard-soft acid base principle .....	92
3.3 Results and Discussions .....	95
3.3.1 Determination of structures and electronic properties by DFT methods.....	95
3.3.2 Hard-soft acid base principle .....	100
<b>4. MOLECULAR DYNAMICS SIMULATION STUDY ON THE BASAL SPACING AND LAYERING BEHAVIOUR OF CATIONIC SURFACTANTS IN ORGANOCLOYS .....</b>	<b>103</b>
4.1 Theoretical Methods.....	107
4.1.1 Modeling methods of organoclays.....	107
4.1.2 Surfactants used in the calculations .....	111
4.2 Results and Discussions .....	114
4.2.1 General structure and basal spacings in organoclays at equilibrium .	114
4.2.2 Interaction behaviour of head groups on the clay surface.....	117
4.2.3 Effect of cation exchange capacity on the organoclay structure .....	122
4.2.4 Effect of number of chains in surfactants on the organoclay structure.....	125
4.2.5 Effects of alkyl tail length of surfactants on the organoclay structure.....	127
4.2.6 Effect of head group volume of surfactants on the organoclay structure....	129
<b>5. BINARY INTERACTIONS IN POLETHYLENE-ORGANOCCLAY NANOCOMPOSITES .....</b>	<b>133</b>
5.1 Theoretical Methods Used to Calculate Binary Mixing Energies .....	134
5.2 Structures Used in Calculations of Binary Mixing Energies.....	137
5.3 Results and Discussions .....	140
5.3.1 Validation of the method .....	140
5.3.2 Binary mixing energies and minimum energy structures.....	141
<b>6. MOLECULAR DYNAMIS SIMULATIONS OF POLYETHYLENE ORGANOCCLAY NANOCOMPOSITES .....</b>	<b>151</b>
6.1 Structures Used in MD Calculations.....	152
6.2 Modeling Methods and Molecular Dynamics Strategy .....	155
6.3 Results and Discussions .....	157
6.3.1 Structure and molecular organisation in PE-organoclay nanocomposites.....	157
6.3.2 Interaction energies between the constituents .....	172
<b>7. CONCLUSIONS AND RECOMMENDATIONS.....</b>	<b>181</b>
<b>REFERENCES .....</b>	<b>185</b>
<b>CURRICULUM VITAE.....</b>	<b>205</b>

## ABBREVIATIONS

<b>AA</b>	: Acrylic acid
<b>CEC</b>	: Cation Exchange Capacities
<b>CP</b>	: Compatibilizer precursor
<b>DD</b>	: Dodecyl
<b>DFT</b>	: Density Functional Theory
<b>DSC</b>	: Differential scanning calorimetry
<b>EA</b>	: Electron affinity
<b>ESP</b>	: Electrostatic potentials
<b>EVA</b>	: Ethylene vinyl acetate
<b>F</b>	: Fukui reactivity indice
<b>FH</b>	: Flory Huggins
<b>FTIR</b>	: Fourier transform infrared spectroscopy
<b>GMA</b>	: Glycidyl methacrylate
<b>HD</b>	: Hexadecyl
<b>HDPE</b>	: High density polyethylene
<b>HRR</b>	: Heat release rates
<b>HSAB</b>	: Hard-Soft acid base principle
<b>IA</b>	: Itaconic acid
<b>IP</b>	: Ionization potential
<b>LDPE</b>	: Low density polyethylene
<b>LLDPE</b>	: Linear low density polyethylene
<b>MA</b>	: Maleic anhydride
<b>MC</b>	: Monte Carlo
<b>MD</b>	: Molecular Dynamics
<b>MMT</b>	: Montmorillonite
<b>NMR</b>	: Nuclear magnetic resonance
<b>OD</b>	: Octadecyl
<b>OMMT</b>	: Organically modified montmorillonite
<b>PA</b>	: Polyamide
<b>PCN</b>	: Polymer-clay nanocomposites
<b>PE</b>	: Polyethylene
<b>PEC</b>	: Polyethylene Compatibilizers
<b>PET</b>	: Polyethylene terephthalate
<b>PLA</b>	: Poly(lactic acid)
<b>PLNS</b>	: Polymer-layered silicate nanocomposites
<b>PNC</b>	: Polymer nanocomposite
<b>PO</b>	: Polyolefin
<b>POSS</b>	: Polyhedral oligomeric silsesquioxanes
<b>PVA</b>	: Polyvinyl acetate
<b>PW91</b>	: Perdew-Wang 91 functional
<b>PW-DFT</b>	: Plane wave Density Functional Theory
<b>S</b>	: Softness

<b>SANS</b>	: Small-angle neutron scattering
<b>SAXS</b>	: Small-angle X-ray scattering
<b>ST</b>	: Starch
<b>STac</b>	: Starch acetate
<b>TEC</b>	: Thermal expansion coefficients
<b>TEM</b>	: Transmission electron microscopy
<b>TGA</b>	: Thermogravimetric Analysis
<b>XRD</b>	: X-Ray Diffraction
<b>XPS</b>	: X-ray photoelectron spectroscopy
<b>WAXD</b>	: Wide angle X-ray diffraction



## LIST OF TABLES

	<b><u>Page</u></b>
<b>Table 1.1:</b> Chemical structure of commonly used 2:1 phyllosilicates.....	6
<b>Table 1.2:</b> Classification of synthesis methods and final properties of PCNs .....	30
<b>Table 1.3:</b> Characterization techniques used to analyze PLSNs. ....	40
<b>Table 2.1:</b> Nonbonded (vdW and electrostatic) and cohesive energies and solubility parameters of studied homopolymers. ....	70
<b>Table 2.2:</b> Nonbonded (vdW and electrostatic) and cohesive energies and solubility parameters of PECs at different grafting ratios. ....	71
<b>Table 2.3:</b> Dipole moments of PEC oligomers.....	75
<b>Table 3.1:</b> Experimental and Theoretical Lattice Parameters of Pyrophyllite .....	96
<b>Table 3.2:</b> Theoretical and Experimental Vibrational Frequencies.....	96
<b>Table 3.3:</b> Theoretical and Experimental Lattice parameters of Na-MMT. ....	97
<b>Table 3.4:</b> Bond lengths and angles of optimized MMT structure.....	98
<b>Table 3.5:</b> Energy and structure comparison of cis and trans MMT .....	99
<b>Table 3.6:</b> Nucleophilic and electrophilic local centers of MMT cluster.. ....	101
<b>Table 4.1:</b> Structure of unit, supercell and CEC of clays.....	108
<b>Table 4.2:</b> The Charges of Atoms in Montmorillonite. ....	110
<b>Table 4.3:</b> Basal spacing values calculated by MD and experimental XRD. ....	114
<b>Table 5.1:</b> Mixing energies calculated for MMT and alkyl ammonium head groups. ....	143
<b>Table 5.2:</b> Calculated mixing energies for MMT cluster with PE and PEC oligomers. ....	145
<b>Table 5.3:</b> Calculated mixing energies for head groups with PE and PEC oligomers. ....	147
<b>Table 5.4:</b> Calculated positive mixing energies between PE and PEC oligomers. ....	148



## LIST OF THE FIGURES

	<u>Page</u>
<b>Figure 1.1:</b> Classification of silicates. ....	3
<b>Figure 1.2:</b> Crystalline structure of a 2:1 layered silicate, showing two tetrahedral layers and one octahedral . ....	5
<b>Figure 1.3:</b> Structure of sodium MMT . ....	7
<b>Figure 1.4:</b> Aspect ratio distribution of native sodium MMT platelets . ....	9
<b>Figure 1.5:</b> Classification of polymer clay nanocomposites with respect to clay delamination. ....	27
<b>Figure 1.6:</b> TEM of 3wt% filled polyamide nanocomposite. PS=phase separate domains; I= intercalated;E=exfoliated platelets . ....	28
<b>Figure 1.7:</b> Mechanism for intercalation of polymer chains from solution. ....	31
<b>Figure 1.8:</b> Mechanism for In Situ Intercalative Polymerization Method. ....	32
<b>Figure 1.9:</b> Mechanism for Melt Intercalation Method.....	32
<b>Figure 1.10:</b> Tortuous path model to which a gas molecule has to follow when diffusing through a PCN. ....	35
<b>Figure 1.11:</b> Spectroscopic methods used to analyze PCNs. ....	39
<b>Figure 1.12:</b> General examples XRD and TEM results for PLSN . ....	43
<b>Figure 1.13:</b> TEM of unstained and stained PP-clay nanocomposites.....	52
<b>Figure 1.14:</b> Theoretical methods used for PNCs.....	55
<b>Figure 2.1:</b> Structures of (a) PE-g-AA, (b) PE-g-GMA, (c) PE-g-IA, (d) PE-g-MA. ....	66
<b>Figure 2.2:</b> Optimized geometries and atomic charges of the modeled PEC oligomers. ....	73
<b>Figure 2.3:</b> 3D electrostatic potential surface of PECs (high ESP: yellow, low ESP: blue).....	73
<b>Figure 2.4:</b> Fukui reactivity indices of PECs. (electrophilic attack sites are yellow and nucleophilic attack sites are blue.) ....	74
<b>Figure 2.5:</b> Change in the $\chi$ interaction parameters between PE and PECs with temperature. ....	75
<b>Figure 2.6:</b> Change in the $\chi$ interaction parameters between Nylon-6 and PECs with temperature. ....	76
<b>Figure 2.7:</b> Change in the $\chi$ interaction parameters between PET and PECs with temperature. ....	77
<b>Figure 2.8:</b> Change in the $\chi$ interaction parameters between PVA and PECs with temperature. ....	78
<b>Figure 2.9:</b> Change in the $\chi$ interaction parameters between PLA and PECs with temperature. ....	79
<b>Figure 2.10:</b> Change in the $\chi$ interaction parameters between starch (ST) and PECs with temperature. ....	80
<b>Figure 2.11:</b> Change in the $\chi$ interaction parameters between starch acetate (STac) and PECs with temperature. ....	81

<b>Figure 2.12:</b>	A snapshot picture of PE-g-MA with 0.88 %w (left) and 1.7 %w (right) grafting ratios.....	82
<b>Figure 2.13:</b>	A snapshot picture of PE-g-MA with 4.4 %w (top) and 5.5 %w (bottom) grafting ratios. ....	82
<b>Figure 2.14:</b>	Change in the radius of gyration of PE-g-MA with grafting ratio MA. ....	83
<b>Figure 2.15:</b>	The snapshot picture of MA-pentamer grafted PE chain with grafting ratio of 4.4 %w. ....	83
<b>Figure 2.16:</b>	Change in the radius of gyration of PE-g-MA with polymeriaztion degree of MA. ....	84
<b>Figure 3.1:</b>	Tetrahedral-Octahedral-Tetrahedral structure of MMT layer. ....	88
<b>Figure 3.2:</b>	Stacked MMT layers with interlayer cation. ....	88
<b>Figure 3.3:</b>	Trans and cis isomers of Na-MMT layer from XRD data. ....	91
<b>Figure 3.4:</b>	Cluster model of MMT used to calculate reactive sites.....	92
<b>Figure 3.5:</b>	Structure of octahedral layer in MMT. ....	97
<b>Figure 3.6:</b>	Cis and trans Montmorillonite structure with $Mg^{+2}$ substitution.....	99
<b>Figure 3.7:</b>	a) Optimized structure of MMT structure and b) positions of $Na^{+}$ ions.....	100
<b>Figure 4.1:</b>	Mechanism of organoclay formation by cation exchange. ....	106
<b>Figure 4.2:</b>	Structure and atomic charges of DODDMA. ....	109
<b>Figure 4.3:</b>	Structure of cluster used to calculate atomic charges. ....	109
<b>Figure 4.4:</b>	Two initial geometries for the HDTMA in MMT2 clay.....	110
<b>Figure 4.5:</b>	Strucrures and symbols of cationic surfactants used in this study. ..	112
<b>Figure 4.6:</b>	Organoclay structure formed by MMT2 and ODA. ....	115
<b>Figure 4.7:</b>	The general structure of organoclay structure.....	116
<b>Figure 4.8:</b>	General layering behaviors of the organoclays. ....	117
<b>Figure 4.9:</b>	Organoclay structure based on the primary alkyl ammonium. ....	118
<b>Figure 4.10:</b>	Interlayer distribution of head groups and alkyl tails in organoclays.....	118
<b>Figure 4.11:</b>	Equilibrium positions of ammonium head groups in organoclays ...	119
<b>Figure 4.12:</b>	The head group positions of phosphonium based surfactants in organoclays.....	119
<b>Figure 4.13:</b>	The head group positions of surfactants with ring type head grups in organoclays. ....	120
<b>Figure 4.14:</b>	The concentration profiles of head group nitrogens among z-direction in MMT2.....	121
<b>Figure 4.15:</b>	The concentration profiles of head group nitrogens among z-direction in MMT3.....	122
<b>Figure 4.16:</b>	Surface coverage of ODA with increasing CEC of MMT. ....	122
<b>Figure 4.17:</b>	Concentration profile of $-CH_2$ groups for a) ODA, b) HDPy and c) 3MIMID at different CEC of clays.....	124
<b>Figure 4.18:</b>	Surface coverage of MMT2 based organoclays with ODTMA, DODDMA, TODMA.....	125
<b>Figure 4.19:</b>	Concentration profile of $-CH_2$ groups for surfactants with different number of tails. ....	126
<b>Figure 4.20:</b>	Concentration profile of $-CH_2$ groups for surfactants with increasing alkyl tail lengths.....	128
<b>Figure 4.21:</b>	Surface coverage of MMT2 based organoclays with HDTMA and HDTBP.....	129

<b>Figure 4.22:</b>	Concentration profile of $-\text{CH}_2$ groups in surfactants with increasing volume of head groups .....	130
<b>Figure 4.23:</b>	Concentration profile of $-\text{CH}_2$ groups in HDPy and HDQ surfactants .....	131
<b>Figure 5.1:</b>	Constituents of clay, organoclay and PE-organoclay nanocomposite .....	133
<b>Figure 5.2:</b>	End group saturated-MMT cluster used to determine clay-polymer and clay-surfactant interaction. ....	137
<b>Figure 5.3:</b>	Nucleophilic attacking centers and atomic charges on surfactant. ...	138
<b>Figure 5.4:</b>	Clusters used to calculate mixing energies with surfactants. ....	138
<b>Figure 5.5:</b>	Optimized geometry and atomic charges of IA grafted oligomer. ...	139
<b>Figure 5.6:</b>	Cluster used to calculate mixing energies with PE and compatibilizers .....	140
<b>Figure 5.7:</b>	Parallelly stacked structure of MMT.....	140
<b>Figure 5.8:</b>	Minimum energy conformations of PE oligomer .....	141
<b>Figure 5.9:</b>	Minimum energy conformations of H1 and MMT systems .....	141
<b>Figure 5.10:</b>	Minimum energy conformations of H2 and MMT systems.....	142
<b>Figure 5.11:</b>	Minimum energy conformations of MMT and PE oligomer. ....	143
<b>Figure 5.12:</b>	Minimum energy conformations of MMT and IA grafted PE oligomer.....	144
<b>Figure 5.13:</b>	Minimum energy conformations of MMT and MA grafted PE oligomer.....	144
<b>Figure 5.14:</b>	Experimentally proposed structures of MMT with MA grafted PE oligomer. ....	145
<b>Figure 5.15:</b>	Minimum energy structures of IA grafted PE oligomer with H1 ....	146
<b>Figure 5.16:</b>	Minimum energy structures of IA and MA compatibilizers with PE oligomers.....	147
<b>Figure 5.17:</b>	Minimum energy structures of compatibilizers interacting with end group atoms of MMT.....	148
<b>Figure 5.18:</b>	Minimum energy structures of MMT with H1 .....	149
<b>Figure 6.1:</b>	Structures used in the MD simulations.....	153
<b>Figure 6.2:</b>	Initial structures of PE and IA grafted PE oligomers for MD simulations. ....	153
<b>Figure 6.3:</b>	Different organoclays used to model PE-organoclay nanocomposites. ....	154
<b>Figure 6.4:</b>	Initial structure of the nanocomposite formed by MMT2, ODA, PE and PE-g-IA (side view). ....	155
<b>Figure 6.5:</b>	PE-organoclay nanocomposites before equilibration.....	158
<b>Figure 6.6:</b>	PE-organoclay nanocomposites after equilibration .....	158
<b>Figure 6.7:</b>	Nanocomposite formation. ....	159
<b>Figure 6.8:</b>	Snapshot picture showing the interactions of IA, ammonium and MMT surface at equilibrium.....	160
<b>Figure 6.9:</b>	The concentration profile of $-\text{OH}$ groups in IA for DDA surfactants with different CEC clays.....	161
<b>Figure 6.10:</b>	The concentration profile of $-\text{OH}$ groups in IA for MMT3 with different surfactants.....	161
<b>Figure 6.11:</b>	Snapshot picture showing the interactions of IA, quarternary ammonium and MMT surface. ....	162
<b>Figure 6.12:</b>	Snapshot picture showing the interactions of IA, quarternary ammonium and MMT surface. ....	162

<b>Figure 6.13:</b>	The concentration profiles of –OH in imidazolium based organoclays among the z-direction. ....	163
<b>Figure 6.14:</b>	Snapshot picture showing the interactions of IA, HDTBP head group and MMT1 surface.....	164
<b>Figure 6.15:</b>	Snapshot picture showing the interactions of IA, HDTBP head group and MMT3 surface.....	164
<b>Figure 6.16:</b>	The concentration profile of –OH atom in HDTBP based organoclays with high CEC.....	165
<b>Figure 6.17:</b>	Snapshot picture showing the MA group adsorbed on the MMT surface. ....	166
<b>Figure 6.18:</b>	Snapshot picture showing the interactions of MA, ammonium head group and MMT surface. ....	166
<b>Figure 6.19:</b>	Snapshot picture showing the interactions of MA, ring shaped surfactants and MMT surface.....	167
<b>Figure 6.20:</b>	Snapshot picture showing the interactions of MA, imidazolium groups and MMT surface. ....	167
<b>Figure 6.21:</b>	Snapshot picture showing the interactions of MA, HDTBP and MMT surface. ....	168
<b>Figure 6.22:</b>	The concentration profile of –OH in high amount of IA groups .....	169
<b>Figure 6.23:</b>	The concentration profile of –OH in TODMA based organoclay with high CEC. ....	170
<b>Figure 6.24:</b>	Snapshot picture showing the interactions of TODMA and IA groups in MMT3.....	170
<b>Figure 6.25:</b>	The concentration profile of –CH <sub>2</sub> in ODTMA, DODDMA and TODMA based organoclays. ....	171
<b>Figure 6.26:</b>	The concentration profile of –CH <sub>2</sub> in ODTMA based organoclays with low and high CEC. ....	172
<b>Figure 6.27:</b>	The binary interaction energies in nanocomposites formed by MMT2, pristine PE and different surfactants. ....	173
<b>Figure 6.28:</b>	The binary interaction energies in nanocomposites formed by MMT1, pristine PE and different surfactants. ....	174
<b>Figure 6.29:</b>	The binary interaction energies in nanocomposites formed by MMT3, pristine PE and different surfactants. ....	175
<b>Figure 6.30:</b>	The binary interaction energies in nanocomposites formed by MMT3, PE-g-IA and different surfactants. ....	176
<b>Figure 6.31:</b>	The binary interaction energies in nanocomposites formed by MMT2 and PE-g-IA with ODTMA and TODMA surfactants. ....	177
<b>Figure 6.32:</b>	The binary interaction energies in nanocomposites formed by MMT2 and ODTMA with different compatibilizers.....	178
<b>Figure 6.33:</b>	Type of pairwise interactions in PE-organoclay nanocomposites....	179

# **MOLECULAR DYNAMICS SIMULATIONS ON THE STRUCTURE AND INTERFACIAL INTERACTIONS OF POLYETHYLENE-ORGANOCLAY NANOCOMPOSITES**

## **SUMMARY**

Understanding structure and interfacial interactions between polyethylene (PE) chains, clay, compatibilizers, and surfactants in PE-montmorillonite clay nanocomposites plays a key role in controlling mechanical and physical properties of the material. These interfacial interactions were studied quantitatively at experimental temperature and concentration ratios by employing quantum mechanical, molecular dynamics and Monte Carlo methods. The effect of the type and the ratio of the polar group grafted onto the PE compatibilizer, the structure of the head group and the length of the tail group of the surfactant, the electrostatic potential surface of the clay on the stability of the nanocomposite material were analyzed.

First montmorillonite clay and the organoclay then the nanocomposite which was formed by the penetration of the PE chains into the interlayer region, were modeled. It was shown computationally that the intercalation of the clay which is necessary to synthesize such a nanocomposite material were dependent on the chemical nature and the volume of the cationic head group and the length of alkyl tail group of the surfactant, the charges on the surface atoms of the clay layer and the cation exchange capacity of the clay. The major interaction between the polymer and compatibilizer was shown to be dipole-dipole and H-bond interactions. It was demonstrated that the most reactive sites were mainly concentrated on the polar functional groups of the compatibilizer and they showed better performance at low grafting ratios. The interaction energy between the PE and the montmorillonite layer determined by the periodic nanocomposite simulations was seen to be inversely proportional to the volume of the surfactant due to the decreased electrostatic interactions between the compatibilizer and the hydrophilic clay surface and head group of the surfactant. However, the vdW type interactions between alkyl chains and the PE chains were decreased when the tail of the surfactant was shortened. This shielding effect of the surfactants become more pronounced at high loadings or when the head groups were large or when the clay with high cation exchange capacity were used. All these factors increasing shielding, on the other hand, made the vdW interactions between alkyl tails and PE chains more attractive and resulted in larger basal spacing. We showed that there existed fine balance between electrostatic and vdW type forces on the stability and the enhanced properties of the PE-organoclay nanocomposite structure. Itaconic acid (IA) and maleic anhydride (MA) were found to be the most eligible polar groups in the PE compatibilizers and IA would be a better alternative to the frequently used MA due to its biodegradability. The high correlation observed between the experimentally measured mechanical properties and polymer-clay binding energies calculated proved that the modeling and the methods employed here were successful. This study is of great significance since it enables to estimate the

optimum ratios of constituents to prepare a nanocomposite with desired properties and it can be instructive for experimentalists to synthesize materials with enhanced properties.



# **POLİETİLEN-ORGANOKİL NANOKOMPOZİTLERİNİN YAPISAL ÖZELLİKLERİNİN VE ARAYÜZEY ETKİLEŞİMLERİNİN MOLEKÜLER DİNAMİK SİMÜLASYON YÖNTEMLERİYLE İNCELENMESİ**

## **ÖZET**

Polietilen-kil nanokompozitleri oluşturan polietilen (PE), kil, uyumlaştırıcı ve yüzey aktif moleküller arasındaki etkileşimlerin anlaşılması, malzemenin mekanik ve fiziksel özelliklerinin kontrol edilmesi konusunda çok önemli bir rol oynamaktadır. Bu bileşenler arasındaki arayüz etkileşimleri nicel olarak deneysel sıcaklık ve yapılar temel alınarak kuantum mekanik, moleküler dinamik ve Monte Carlo yöntemleri kullanılarak belirlenmiştir. Polietilen uyumlaştırıcıya aşıl原因 polar grubun cinsinin ve oranının, yüzey aktif bileşiklerin baş grup yapısının ve kuyruk uzunluğunun, kilin elektrostatik potansiyel yüzeyinin nanokompozit malzemenin kararlılığına olan etkileri araştırılmıştır.

Önce kil olarak seçilen montmorillonit ve kilin organik olarak değiştirilmesiyle oluşan organokil sonra kil katmanının arasına polietilenin girmesiyle oluşan nanokompozit malzeme modellenmiştir. Yapılan hesaplamalarla deneysel olarak böyle bir malzemenin oluşabilmesi için gerekli olan kil katmanları arasındaki mesafenin açılmasının yüzey aktif bileşiğin katyonik baş grubunun yapısına ve hacmine, alkil kuyruk sayısına ve uzunluğuna, kil katmanını oluşturan atomların yüklerine ve kilin katyon değiştirme kapasitesine bağlı olduğu gösterilmiştir. Uyumlaştırıcı ile polimer zinciri arasındaki en temel etkileşimin dipol-dipol ve H-bağı etkileşimleri olduğu gösterilmiştir. Polietilen uyumlaştırıcılarındaki en reaktif bölgenin sadece polar fonksiyonel grup üzerinde bulunduğu ve bunların düşük aşıl原因ma yüzdelğinde daha iyi performans gösterdikleri tespit edilmiştir. Periyodik nanokompozit simülasyonlarıyla polietilen ile kil katmanı arasındaki bağlanma enerjisinin yüzey aktif bileşiğin hacmi ile ters orantılı olarak değiştiği gösterilmiştir. Bunun nedeninin uyumlaştırıcı ile hidrofilik kil yüzeyi ve yüzey aktif maddenin baş grubu arasındaki elektrostatik etkileşimlerin, yüzey aktif bileşiğin hacmi ile ters orantılı olarak artması olduğu gösterilmiştir. Ancak yüzey aktif moleküllerin kuyrukları kısalduğunda alkil zincirleri ile polietilen zincirleri arasındaki vdW tipi etkileşimler de azalmaktadır. Bu şekilde yüzey aktif molekülün neden olduğu perdeleme etkisi büyük hacimli yüzey aktifler kullanıldığında ve yüksek katyon değiştirme kapasiteli kil kullanıldığında daha fazla etkin olmuştur. Bu perdeleme etkisinin polietilen-kil arasındaki istenmeyen etkileşimleri azaltmak ve kil katmalarının arasının daha fazla açılmasını sağlamak gibi bir etkisi de vardır. Kararlı ve özellikleri saf PE ile hazırlanmış olana göre daha fazla gelişmiş bir PE-organokil nanokompozit yapısının hazırlanmasının vdW ve elektrostatik etkileşimler arasındaki dengeye bağlı olduğu gösterilmiştir. İtakonik asit ve maleik anhidritin en iyi uyumlaştırıcı polar grup oldukları ve itakonik asitin biyo bozunur olması nedeniyle, sıklıkla kullanılan maleik anhidritin iyi bir alternatifi olacağı gösterilmiştir. Deneysel olarak ölçülen mekanik özelliklerle hesaplanan polimer-kil bağlanma enerjileri arasındaki korelasyonun yüksek olması hem modellemelerin hem de kullanılan yöntemlerin doğruluğunu göstermiştir. Bu hesapsal çalışma polimer-kil

nanokompozitleri oluřturan bileřenlerin en iyi oranlarının tahmin edilmesi aėısından büyük nem tařımaktadır ve daha iyi zellikteki malzemelerin sentezlenmesi yolunda yapılacak alıřmalar ncesinde deneycilere yol gsterici olacaktır.

## 1. INTRODUCTION

### 1.1 Nanocomposites

The word composite is generally used to define any material that consists of more than one component. In IUPAC definitions, composite is “a multicomponent material comprising multiple different non-gaseous phase domains in which at least one type of phase domain is in a continuous phase [1].” Depending on the matrix nature, composite materials can be broadly classified into three categories such as polymeric, metallic, and ceramic [2]. The structural unit is on the micrometer ( $10^{-6}$  m) length scale and is used mostly to improve the mechanical properties of matrix material in most of the commercially available composite materials. Nowadays, one dimension of the structural building block can be at the nanometer ( $10^{-9}$  m) scale, the resulting composite material is called a nanocomposite. Nanocomposite is defined as a system “in which at least one of the phases has at least one dimension of the order of nanometers” by IUPAC [3].

Nanoscale materials, a new branch of materials research, are attracting a great deal of attention because of their potential applications in general areas such as electronics, materials research, optics, catalysis, ceramics [4]. Nanostructured material researches are part of a new field of a popular area of current researches in chemistry researches called nanotechnology includes also specific and target studies mostly on advanced materials such as polymer-based biomaterials, nanoparticle drug delivery, imprint lithography, miniemulsion particles, fuel cell electrodes, polymer bound catalysts, electrospun nanofibers, magnetic data storage, layer-by-layer self-assembled polymer films, polymer blends and nanocomposites [5-7]. The unique properties and the improved performances of nanomaterials are determined by their sizes, surface structure and interconstituent interactions. If these composite hybrid materials formed from a polymeric matrix and another phase in nanometer range, it is called polymer nanocomposite (PNC). This definition can be narrowed by considering this nanocomposites are nanoparticles in a polymeric matrixes [8].

## 1.2 Nanofillers

Over the last few years, various types of nanofillers are in development such as layered silicates, metal oxide nanoparticles, nanocrystalline metals, inorganic nanotubes, expandable graphite, layered titanate, cellulose nanowhiskers, polyhedral oligomeric silsesquioxanes (POSS) and etc [4,8-11]. Also polymer blends and block copolymers can have phase separations which can be in the nanoscale dimensions can form nanocomposites [12]. In reality, it has been decades since the mixing of nanoparticles with polymers has been practiced such as one of the first commercialized the clay reinforced resin was introduced in the early 1900s called as, Bakelite. At early times, isodimensional spherical carbon black nanoparticles was used for reinforcement of rubber and polymer filled with SiO<sub>2</sub> networks as well as naturally occurring fibers were synthesized decades ago [13].

Spherical particles such as silica and metal nanoparticles, one dimensional fibril particles such as carbon nanotubes, and bidimensional particles which are usually lamellar such as clays are used as nanofillers. Nanofillers used in polymer-layered silicate nanocomposites (PLSN) has at least one dimension larger than 100 nm in dimensional classification [14]. The phase domain morphologies can be diverse with respect to architecture and interfacial strength. Carbon nanotubes, carbon nanofibers, exfoliated graphite (graphene) are popular nanoparticles used with several modifications [15,16].

In polymer-silicate nanocomposites, containing natural minerals emerging with interesting properties, that the common ones composed of amorphous silicates, such as quartz, silica, feldspar, gypsum, albite, anorthite, orthoclase, apatite, halite, calcite dolomite, sodium carbonate, siderite, biotite, muscovite, chlorite, stilbite, pyrite, montmorillonite (MMT), kaolinite, hematite, and many others [17-19] are common fillers. In structural applications, the only nanosized particles of industrial interest are layered, natural or synthetic ones called 2:1-phyllsilicates such as smectite clays (e.g., MMT, bentonite, nontronite, beidellite, hectorite), synthetic clays (e.g., hectorite), layered silicic acids (e.g., kanemite, makatite), other clays (e.g., micas, vermiculite, illite), mineral layered hydroxides, layered double hydroxides, layered aluminophosphates [20-22].

### 1.3 Clays

Nowadays, clays, zeolites, graphene sheets, and carbon nanotubes are popular types of non-standard nanofillers which are currently part of the most research interest rather than classical fillers [23,24]. Clays have differentiated from these nanoparticles by having a great diversity with respect to composition because they have an extremely large family with respect to their large compositional differences that can be classified by crystal unit cells, layering behavior and atomic composition in nature.

Clay minerals are very small minerals smaller than 10 micrometer. They belong to the phyllosilicates group (from the Greek “phylon”: leaf, and from the Latin “silic”: flint). They can be observed with electron microscope and their detailed structure can be analyzed by XRD techniques (Figure 1.1). XRD determines distances between atomic planes of crystals [25].

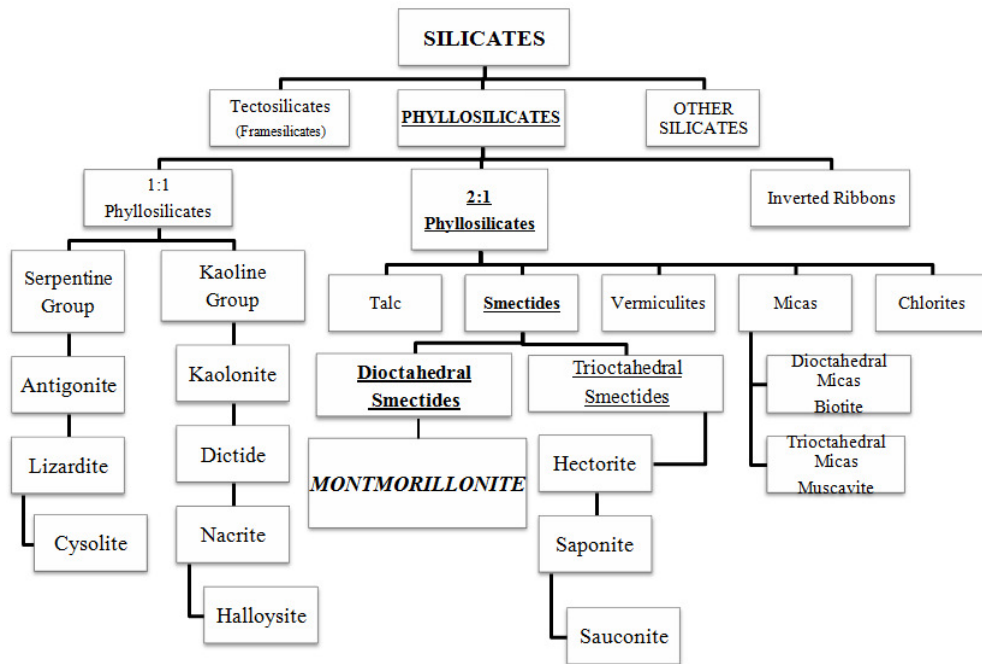


**Figure 1.1:** Classification of silicates.

Clay sheets are not necessarily electrically neutral. The layer charge is not constant and varies from layer to layer. It is considered as an average value over the total clay structure. Ionic substitutions in the crystal lattice can induce a deficit of positive or negative charge, reflected by a net negative charge. Electrical neutrality is then

neutralized by exchanging cations between the sheets, which may be anhydrous cations or anions such as  $K^+$ , as in the micas [26].

Layered silicates is divided to two types of main constituents that are tetrahedrally substituted and octahedrally substituted layers. In the tetrahedrally substituted layered silicates, the negative charge is located on the surface of silicate tetrahedral layers and, hence, in octahedrally substituted material like MMT the polymer matrices interact more readily since they are not directly face with the charge [27]. From a mineralogical point of view, the structure formed by binding an octahedral layer to a tetrahedral layer is called a 1:1 sheet, and it has thickness about 0.7 nm. By binding a tetrahedral layer on either side of an octahedral layer, one obtains a 2:1 sheet. In its natural state, this clay exists as stacks of many platelets. Thus, each primary particle contains approximately 16 platelets in average.

The crystal structures of all phyllosilicates based on three types of layers [28]:

- a) 1:1 layers in which one tetrahedral sheet is bonded to one octahedral sheet. Kaolinite is the example used in the PLSN several times.
- b) 2:1 layer in which one octahedral sheet is sandwiched between two tetrahedral sheets which is the most important class industrially.(Figure 1.2).
- c) 2:1 inverted ribbon type clays, which have two continuous tetrahedral sheets and discontinuous octahedral sheets.

### **1.3.1 2:1Phyllosilicates**

From electron microscopy, it is known that phyllosilicates have aggregated structure of platelets. Each family of phyllosilicates has a specific structural, morphological, crystal and layering characteristics. Smectite group which includes dioctahedral smectites such as MMT and trioctahedral smectites for example saponite. The general formula for these clays is  $Al_4[Si_4O_{10}](OH)_2$ . Most of the silicates used in nanocomposites belong to the family of these 2:1 phyllosilicates where the structure is formed by the stacking of platelets composed of two silicate tetrahedral sheets and a central octahedral sheet, attached to the tetrahedral sheets by oxygen atoms in common between them as shown in Figure 1.2 [29].

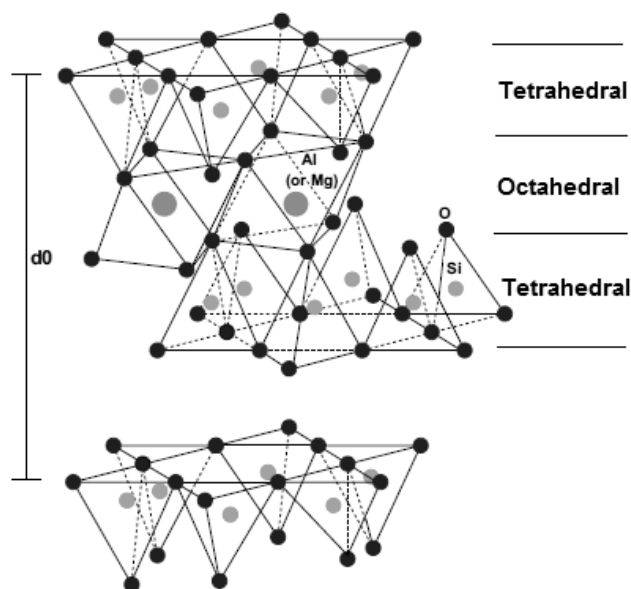


**Figure 1.2:** Crystalline structure of a 2:1 layered silicate, showing two tetrahedral layers and one octahedral [30].

Layered silicates are composed of two-dimensional layers that are stacked together face to face with a regular van der Waals gap [31]. The crystal structure of one unit layer consists of tetrahedral silica sheets combined with sheets of octahedral layers. The layers may be electrostatically neutral or possess negative electrostatic charge due to the isomorphous substitution of the cations (in either the tetrahedral or octahedral sheets) with low valence.

Smectite, vermiculate and mica are the most important clay types of 2:1 structures. The apical oxygen atoms of the tetrahedral sheet are all shared with the octahedral sheet. Such layers extend continuously in the plane constituted by the  $x$  and  $y$  axes and are stacked up in the  $z$ -axis direction, thus forming the crystal structure in the 3 dimensions. Among the three major groups, smectite types are the most commonly used layered silicates for the synthesis of PLSNs due to their high abundance. Two tetrahedral layers linked with one central octahedral alumina or magnesia layer creates a 2:1 layer smectides. Smectite clays, such as MMT all belong to the structural family of 2:1 phyllosilicates [32]. Smectites has a 2:1 layer structure consisting of two fused silica tetrahedral sheets sandwiching an edge-shared octahedral sheet of alumina. This basic structural element of phyllosilicates can be imagined as a hexagonally ordered layer of octahedra sandwiched between two tetrahedral siloxane layers, commonly referred to as a TOT layer. Various

isomorphic substitutions in the octahedral and tetrahedral layers of the clay minerals result in a permanent structural charge of the TOT unit (Table 1.1).

**Table 1.1:** Chemical structure of commonly used 2:1 phyllosilicates [33].

2:1 Phyllosilicates	General formula
Montmorillonite	$M_x(Al_{4-x}Mg_x)Si_8O_{20}(OH)_4$
Hectorite	$M_x(Mg_{6-x}Li_x)Si_8O_{20}(OH)_4$
Saponite	$M_xMg_6(Si_{8-x}Al_x)O_{20}(OH)_4$

Like other crystal structures, phyllosilicates are represented by a unit cell. Layered silicates play an important role in the synthesis and processing of PLSN, biodegradable hybrid materials, and cosmetics. To achieve better compatibility with hydrophobic organic matrices, superficial alkali cations in hydrophilic minerals such as muscovite, mica and MMT can be exchanged to transform the surface polarity from hydrophilic to hydrophobic [34].

The large hydration energy of these free cations allows water to enter the interlayer space, causing intracrystalline swelling, and this makes them easy to exchange with other metallic or organic cations [33-35]. This swelling may proceed to very wide separation distances due to repulsive forces of entropic origin when the compensating cations form a double diffuse layer around the particles (osmotic swelling). Each 2:1 sheet has an extremely large lateral extension in comparison to this thickness. It can reach as much as 1  $\mu m$ , which corresponds to an aspect ratio of 103. As a free platelet, the sheets are extremely flexible, although this flexibility decreases when they are stuck together by hydrated interlayer cations.

The distance between the layers depend on the size and orientation of the organic molecules that are swelled into the gallery. Their amount as well as on the ion density of the filler are other important factors in organophilization by swelling. The ion density is dependent on the exchange capacity of layered silicates changes in a wide range from 65 meq/100 g for hectorite to 250 meq/100 g for biotite [36].

### 1.3.2 Montmorillonite

The most common representatives of the smectite family known as the MMTs, which have the trade name of Bentonite for a certain minimal level of purity, and the hectorites, for which a commercially produced synthetic similar form is Laponite.



The name of MMT named after Montmorillon, France where the first deposit was discovered in 1847, firstly identified by Knight in 1896, but is found in many places worldwide like Wyoming USA and Reşadiye Turkey in very large amounts (Figure 1.3) [37].

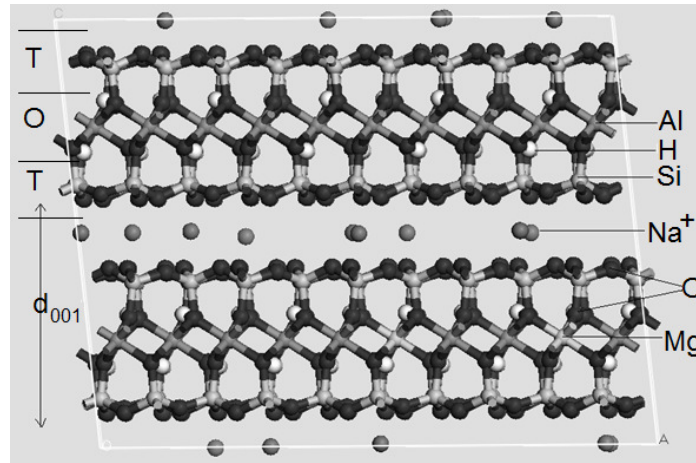


**Figure 1.3:** Structure of sodium MMT.

Isomorphic substitution occurs when some atoms in the crystal structure are replaced with other atoms with different valence without any change in the sketch of the crystal structure. For instance, when there is an isomorphic substitution of  $\text{Mg}^{+2}$  for  $\text{Al}^{+3}$  in the octahedral lattice, a negative charge of minus one -1 is generated, which is normally counterbalanced by cations adsorbed from the ambient solution. Different isomorphic substitutions can take place also in both octahedral and tetrahedral lattices at less amounts. Such as a portion of  $\text{Si}^{+4}$  in tetrahedral sheets can be replaced with  $\text{Al}^{+3}$ , and a part of  $\text{Al}^{+3}$  in octahedral sheets can be substituted with  $\text{Mg}^{+2}$ ,  $\text{Fe}^{+2}$  or  $\text{Zn}^{+2}$ . Since they can exchange with cation ions in aqueous suspension and bulk solution; these are called exchangeable ions. Trivalent cations which are not replaced by bivalent cations in the two thirds of the octahedral sites of MMTs.

Sodium and calcium MMTs are the most common smectide clay found in the earth. The experimental structural formula of MMT is  $\text{Na}_{0.38}\text{K}_{0.04}(\text{Ca}_{0.12}\text{Mg}_{0.50}\text{Fe}^{3+}_{0.41}\text{Al}_{2.90}\text{Ti}_{0.01}\text{Mn}_{0.01})(\text{Si}_8)\text{O}_{20}(\text{OH})_4$  which is also depending on the source [38].

The basal spacing (d-spacing) of completely dry sodium MMT which is the mostly used one in PLSNs is 0.96 nm while the platelet itself is about 0.94 nm thick. The platelets are attached by the Van der Waals forces leaving an interlayer space (or

gallery) between them on the order of 0.2 nm [16, 39]. In this space, usually inorganic cations typically sodium ions counterbalance the negative charge from the surface of the platelets. A negative charge formed on the surface as a result of isomorphous replacement of aluminium atoms by low valence magnesiums in the octahedral layer, and thus each layer surface possesses 0.25–1.2 units of negative charge per unit cell, which must be compensated by the adsorption of exchangeable cations in the spacings between MMT platelets. The total amount of cations in one layer of unit cell expressed in miliequivalents per hundred grams or mol of dry clay, is called the cation exchange capacity (CEC). MMT is typically known to have average CEC values of 81-124 meq/100 g [40]. The modulus of each MMT sheet is around 170 GPa. The idealized chemical formula in theoretical calculations for MMT is  $M_x(Al_{4-x}Mg_x)Si_8O_{20}(OH)_4$  [41].

The clay platelet stacks are usually called tactoids. In clay minerals, these tactoids form random polycrystalline aggregates, which should be broken to produce nanocomposites. The height of the stacked platelets is 80–100 Å with a changeable diameter and the thickness of platelet causes very large surface area by this way. Each platelet is 1 nm thick and its lateral dimensions range from 30 nm to a few micrometres [42].

Although MMT has a soft and plate-shaped structure with 1 µm sheets spaced by 1–2 nm distances, the xy dimensions of the platelets are usually exaggerated in the lateral size of dimensions to the order of microns or even to tens of microns due to the stacking of platelets. They depend on how the platelets grew from solution and the source where in the geological process that formed them. Nowadays, thickness of MMT platelets are defined well with accurate crystallographic dimensions. A commonly used MMT was accurately understood at last years by depositing platelets on a mica surface from a very dilute suspension and then measuring the lateral dimensions by atomic force microscopy. Since the platelets are not uniform or regular in lateral size or shape, the platelet area,  $A$ , was measured and its square-root was normalized by platelet thickness,  $l$ , ( $\sqrt{A}/l$ ) to calculate an aspect ratio which is determined to be layer thickness on the order of 1 nm, and aspect ratios changes from 10 to 1000 and they are usually around 100-200 (Figure 1.4) [43].

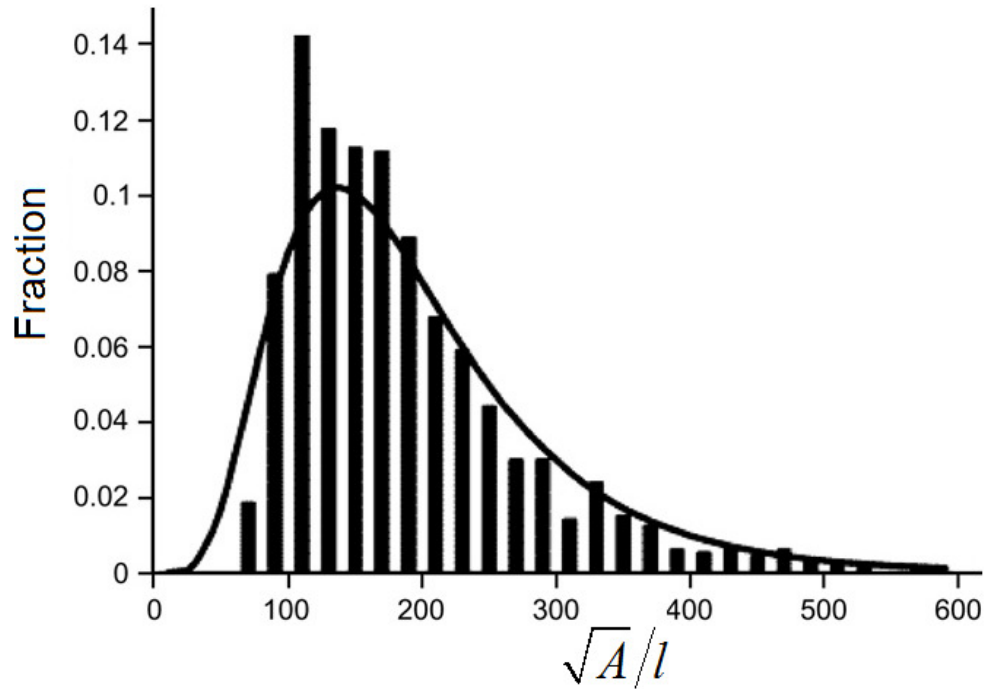


**Figure 1.4:** Aspect ratio distribution of native sodium MMT platelets [44].

Unlike clay minerals such as talc, whiting etc. that have been used as fillers for years, MMT clays can be delaminated and dispersed into individual layers of minimum 1 nm in thickness of single platelet. The result is a radical increase in the surface area-to-volume ratio with a maximized surface area. That is the reason that special attention was paid to its high surface area of about 800 m<sup>2</sup>/g [45]. It has ability to swell like other layered silicates. It swells upon absorption of water into the spaces between its aluminosilicate layers. Hydration of the sodium ions causes the galleries to expand and the clay to swell; indeed, these platelets can be fully dispersed in water. Their large surface area and swelling properties are responsible for a number of unique physical and chemical properties such as cation exchange, and pH-dependent sorption of MMTs.

MMT, an environmentally friendly, low-cost nanofiller and has been applied in various industrial fields. For example, it can be used as desiccant, catalyzer, semipermeable membrane in the disposal process of organic and radioactive wastes, component of drilling agent because its high capability to absorb water, and a popular component in many nanocomposites [46]. In the polymer engineering area, most of the studies is currently focused on PLSN synthesized by using the MMT clay, as it is possible to achieve impressive enhancements of properties when

compared with virgin polymer. These improvements can include high moduli, increased strength and heat resistance, decreased gas permeability and flammability, and increased degradability of biodegradable polymers [47]. The main disadvantage of the MMT are its non-uniform composition depending on the deposit origin, processing and numerous contaminants, which are hard to eliminate.

#### 1.4 Theoretical Studies on Clay Structures

The structure and electrostatic properties of 2:1 clays have been modeled several times. The results of calculations used for explaining experimental data for the structures. In the field of mineralogy, the first ab initio calculations based on density functional theory were performed on cordierite (magnesium aluminum silicate;  $\text{Mg}_2\text{Al}_4\text{Si}_5\text{O}_{18}$ ) by Winkler et al. The DFT methods based on local density approximation (LDA) have been performed for hydrated Mg end-member clays to elucidate the location, orientation, and total energy of hydration in the ground state [48]. The calculations showed the energetically most stable orientations in the layers. It was shown that the symmetry-constrained model is able to reproduce basic structural characteristic of clays. Quantum mechanical calculations of this kind was performed later by Teppen et al. by studying several aluminum and silicon oxide clusters using density functional theory calculation to investigate the structure and charge distribution of these model systems representing smectite clays [49]. These electronic methods are, however, very much concentrated on gaining insight into understanding XRD datas and the role of clays as catalysts except the study of Minisini and Saint-Diaz who optimized the whole periodic cell of Na-MMT by DFT methods [41,50,51].

Study on the absorption of surface water molecules and the hydrate of interlayer counterions in MMT is important for understanding of its swelling and polymer-clay nanocomposite formation. Traditional experiment has certain limitations in understanding the micro interactions in MMT layers. When there is a need to understand the experimental results on minerals, molecular simulation has become an instrument in the study of the MMT-cations-water system for the understanding the swelling properties of MMT. Skipper *et al.* have established model systems on natural Li,Na and K smectites and have used Monte Carlo (MC) computer simulation to study water molecules confined between the layers of 2:1 clay minerals [52]. They

calculated the densities and average potential energies of the interlayer water molecules, and then analyzed and compared the interlayer structures in the two systems. The interlayer cations in Mg-smectites lie in the central plane between the layers, whereas the interlayer cations in Na-smectites have a tendency to bind to the clay surface. Chang *et al.* have investigated the interlayer structures of one, two, and three layer Li-Wyoming and K-MMT hydrates by MC and MD [53]. Sposito *et al.* uses MD methods to simulate K-MMT at room temperature to determine the structure and kinetic properties of interlayer water molecules and cations ions. Further discussions were made on the impact of temperatures on the properties [54].

Bivalent metal counterions has very important effect in the organization of water molecules in the interlayer of hydrated clay minerals. Greathouse *et al.* have investigated water diffusion and concentration profiles in Mg-clay hydrates, by MC and MD simulation [55]. All these studies on the hydrated MMT contained only counterions in the platelet layers have fully demonstrated the significance of MC and MD. They also found that the differences in size and hydration energy of counterions have strong implications for the structure and the internal energy of interlayer water. The MMT interlayer cation interacts solvents, monomers and even with explosives and radioactive elements systems were simulated and swelling patterns of MMT that have different interlayer counterions were investigated. The structures and movements of interlayer species have been studied further and the underlying reasons for variations in the diffusion modes of  $\text{Na}^+$  and  $\text{Mg}^{2+}$  have been investigated by mean square displacement analyses after MD simulations.

## 1.5 Organoclays

Layered natural inorganic structures as MMT, hectorite, vermiculite, saponin, kaolin, etc. have been used for preparation of organoclays based nanocomposites. Their crystal structure consists of two silica tetrahedral sheets sandwiching an edge-shared octahedral sheet of either alumina or magnesia. Stacking of the layers leads to a regular Van der Waals gap called gallery or interlayer between the layers.

Isomorphous substitution of  $\text{Si}^{4+}$  for  $\text{Al}^{3+}$  in the tetrahedral lattice, and of  $\text{Al}^{3+}$  for  $\text{Mg}^{2+}$  in the octahedral sheet generates excess of negative charges that are normally counterbalanced by cations ( $\text{Na}^+$  or  $\text{K}^+$ ) residing in the interlayers. The charge in the naturally occurring clay is balanced, typically, by a sodium cation which lies

between the layers in what is called the gallery space. This is the key point that the sodium is replaced with much larger organic surfactants, the gallery expands and the X-ray d-spacing may increase by as much as 2 to 3-fold by this way [56]. The sodium ions exchanged with organic cations, such as that from an onium salt, to form an organomodified relatively hydrophobic clays called organoclays. This modification of the hydrophilic surface of clays decreases poor compatibility of clays with the polymer matrix. The extent of exchanging the cation charge of the clay is characterized by the cation exchange capacity (CEC).

Different surfactants such as ammonium, phosphonium, imidazolium, and stibonium compounds called oniums are most often used for modification of the clays by exchanging of intergallery cations [57-59]. The onium cation may have long hydrocarbon tails and polar head groups attached make it to amphiphilic nature and called as surfactant for this reason. The high CEC and swelling properties makes MMT recognized as an appropriate choice for preparing high performance polymer/clay nanocomposites [60]. The organo-modification of MMT is an important step in the preparation of polymer-layered silicate nanocomposites (PLSNs). In fact, the layer separation and therefore, the achievement of exfoliated morphologies depend on the establishment of favourable interactions between the polymer and the clay surface. Hydrophilic silica surfaces can become organophilic with the inclusion of alkylammonium cations, which improve the wetting characteristics of the polymer matrix. In fact, the molecular level interactions of organic compounds, either natural or synthetic, with clay surfaces are at the heart of fields of study as diverse as nanocomposites fabrication.

### **1.5.1 Synthesis of organoclays**

The intergallery distance of  $d_{001}$  plane of the clay which has not been organically modified, is relatively small, and the intergallery environment is hydrophilic. This hydrophilic nature of the clay surfaces limits homogeneous dispersion in the organic polymer phase. To overcome this problem, it is usually necessary to change the surface to organophilic prior to its use in nanocomposite formation [61]. Several methods have been used to modify the MMT clays such as directly modify the clay layers by using ion exchange processes, organic coupling agents, such as silane coupling agents or using supramolecules to complex the clay cations. The most popular way to prepare organoclay for polymeric nanocomposite precursor is

exchanging cations ions in the interlayer with organic cations, such as those from an ammonium salt, to form an organoclay [62].

The preparation of an organically-modified clay simply involves ion exchange of the sodium cation for the ammonium cation that accomplished by dispersing the inorganic clay in water by using swelling property and also adding the ammonium ion. An ion exchange process is utilized to displays the inorganic cations (e.g. sodium) with organic cations, thus improving the compatibility of the organosilicate with relatively hydrophobic organic environment. Modification and organophilization of 2:1 clay minerals can be accomplished by using liquids (water, alcohols, glycols, crown ethers, monomer solutions), organic cations, oligomers, polymers or copolymers, and their solutions [63].

The ammonium cation has shown to be one of the most suitable cations, it has hydrocarbon tails and cationic head groups attached and is called as a ‘‘surfactant’’ owing to its amphiphilic nature. The combination of the hydrophobic nature of the amphiphilic surfactants and the stable layered structures of the clays has unique physicochemical properties refereed as organoclay or organophilic-clay.

The extent cation exchange of the clay is characterized by the cation exchange capacity which determines how many organic cations placed in the interlayer and it can be determined X-ray d-spacing analysis [64]. The increase of spacing is depending on the CEC and also the size of organic surfactants as a volume determines the gallery expands. The organically modified clays (organoclay) are mostly prepared by the exchanging the long chain aliphatic quarternary ammonium or phosponium, imidazolium and pyridium cations with interlayer cations. When mixed into the host polymer, exfoliation, breaking apart of the layered material can be accomplished in nanocomposites whereby the silicate sheets lose their attraction from each other.



Intercalation of organic surfactant between layers of clays can not only greatly increase the basal spacing of the layers, but also change the surface properties from hydrophilic to hydrophobic. Since the newly formed clay will not soluble due to hydrophobicity, it precipitates and can be filtered. Organically modified clays with

surfactants have potential to be well dispersed in polymer matrix and interact better with polymer's chain. A very large increase in surface area occurs, if the chemistry between the polymer chains and clay sheets properly designed. A hybrid inorganic-organic materials can be synthesized with altered properties depending on the level of dispersion, the organic cation, the layered silicate, CEC and the host polymer.

### **1.5.2 Properties of organoclays**

The ability of the clay to improve the properties of the polymer is primarily determined by the extent of its dispersion in the polymer matrix, which, in turn, depends on particle size of the clay. The interfacial adhesion between the organic and inorganic phases of the nanocomposite plays a role of primary importance [65]. Therefore, the role of the organic compound in the OMMT is to reduce the surface energy of the MMT and to improve the interaction characteristics with the polymer or monomer. In addition, it increases interlayer spacing, reduces the interlayer binding forces and helps the movement and accommodation of the monomers or polymers [66].

The successful formation of a hybrid material is, to a large extent, determined by the mixing capabilities of individual components of the system. The cationic exchange leads to organically modified clays, which, however, may contain unreacted organic compounds and residues which must be washed for the better properties of the final product. When the interlayer cations of smectite are replaced by amphiphilic compounds, the hydrophilic surfaces of the smectites are substantially modified to become strongly organophilic. These organically modified smectites accommodate non-ionic dyes by hydrophobic interactions. The states of the intercalated dyes can be controlled by changing the length of alkyl chain of the amphiphilic compounds, the amount of the adsorbed amphiphilic compounds, and the temperature. Ion exchange reaction with a cationic dye and interlayer cation of smectite is a way of constructing a photofunctional material with ordered structure by host-guest interactions [67].

Organoclays are widely used for many industrial and technological applications in polymer science, electric materials and in general organic-inorganic nanocomposite materials. Since the first introduction of organoclays, a substantial industry has been established to utilize these organically modified smectite clays. The effect of



organoclays is very high. So that the mechanical properties such as the modulus of composites prepared from alkylammonium based nanoscale organoclays increases ten times more than composites based on clay that acts like a noninteracting microscale filler. Organoclays supply also some advantages in synthesis that they compounded almost three times more rapidly than fiberglass or pure montmorillonite microcomposites [68].

The majority of their applications involve the rheological behavior of organoclays in various solvent systems. Some studies have showed that replacing the inorganic exchange cations of clay minerals with organic cations can result in greatly enhanced capacity of the materials to remove organic contaminants from contaminated sites. They serve as adsorbates for removing organic pollutants from water, herbicides, humic acids, various pollutants and aromatic compounds as well as radioactive substances from the soil.

They also have potential applications in painting, industrial grease, cosmetics and personal care products, chromatographic stationary phase, rheological control agents, reinforcing fillers for plastics and electric materials. Additionally, the alkylammonium or alkylphosphonium cations can provide functional groups that can react with the polymer matrix or in some cases initiate the polymerization of monomers to improve the strength of the interface between the inorganic and the polymer matrix [68].

Thermal stabilities are very important in industrial processes. Lee et al. showed the importance of the thermal stability of the organoclays by using two organoclays that are modified with different alkylammonium cations [69]. After melt compounding, the organoclays modified with alkylammonium cations of poorer thermal stability causes a reduction in their interlayer spacings, which is explained by the release of organic molecules by thermal desorption of organic ion, as well as the thermal decomposition of the organic molecule itself. In addition, the cleavage of organic ions from clay surface may make the surface of the organoclay less organophilic, causing poorer compatibility with polymers. Imidazolium and phosphonium based organoclays have shown to be more stable thermally [70,71].

### 1.5.3 Characterisation of organoclays

Detailed structure, morphology, interlayer arrangement and the atomic local environment is very hard to determine from experimental measurements due to the fine particle, the low crystallizability, and the complicated and diverse chemical components of clays in organoclay. Nevertheless, the structural properties of self-assembled alkyl onium surfactants on MMT surfaces such as head group-surface interactions, gallery spacing, interlayer density, chain conformation, and thermal transitions have been tried to understood several times with X-ray, FTIR, NMR, DSC, TGA, and TEM [72,73]. XRD and FTIR are the most widely used techniques to determine the layered structure and orientation of intercalated surfactants, which is based on the basal spacing and the assumption that all the surfactant chains have all-trans conformations. The surfactant distribution within the resultant organoclays were investigated by X-ray photoelectron spectroscopy (XPS) in combination with XRD and high resolution thermogravimetry (HRTG). On the basis of IR shifts and the basal spacings measured by the XRD results and the length of the alkyl chains, various arrangement models have been proposed for the intercalated surfactants, including lateral-monolayer, lateral-bilayer, pseudo-trilayer, paraffin-monolayer and paraffin-bilayer [74].

Traditional structural characterisation to determine the orientation and arrangement of the alkyl chain involved primarily the use of wide angle X-ray diffraction (WAXD). Thus, the wide angle X-ray scan of the polymer composite is expected to look essentially the same as that obtained for the organoclay powder; there is no shifting of the X-ray d-spacing. Generally, such scans are made over a low range of angles, such that any peaks from a crystalline polymer matrix are not seen since they occur at higher angles. For completely exfoliated organoclay, no wide angle X-ray peak is expected for the nanocomposite since there is no regular spacing of the platelets and the distances between platelets would, in any case, be larger than what wide angle X-ray scattering can detect.

Depending on the packing density, temperature and alkyl chain length, the chains were thought to lie either parallel to the silicate layers forming mono or bilayers, or radiate away from the silicate layers forming mono or bimolecular arrangements. Results showed that short intercalated organic molecules lay parallel with the silicate layers [75]. With increasing chain length and coverage they occupy more space and

above a critical value two parallel chains will be found between the layers. At high ion density the free area around one ion is small, the organic molecules will be tilted or oriented vertically to the surface. Depending on the amount of surfactant used, these may be adsorbed in the silicate galleries in one or more layers. The thickness of one aliphatic chain with 18 carbon atoms is known to be between 0.35 and 0.46 nm. The length of the chains can be calculated in a similar way [76].

Vaia et al. studied the structure of dioctadecyldimethylammonium films on MMT with varying mean charge density by X-ray diffraction (XRD), fourier transform infrared spectroscopy (FTIR), and differential scanning calorimetry (DSC) and showed that the alkyl chains assume an ordered state [77]. It is found that monoalkylammonium cations build a self-assembled monolayer on the mineral surface.

The idealized structural models based on the assumption that the intercalated surfactants have all-trans conformations after intercalation were shown to be wrong by Vaia et al. by using Fourier transform infrared spectroscopy (FTIR) [78]. Vaia and Giannelis have shown that alkyl chains can vary from liquid-like to solid-like, with the liquid-like structure dominating as the interlayer density or chain length decreases, or as the temperature increases. They used FTIR, because of the relatively small energy differences between the trans and gauche conformers from the frequency shifts of methylene on alkyl chains. The FTIR results showed the substantial existence of gauche conformation even though the trans conformation is still predominant in most conditions. In addition, for the longer chain length surfactants, the surfactants in the layered silicate can show thermal transition to melting or liquid-crystalline to liquid like transitions upon heating. Nevertheless, FTIR provides little information on the dynamics of molecular chains.

Then, it is found that coexistence of gauche and all-trans conformers from low to high packing density present together shown by  $^{13}\text{C}$  NMR. Additionally, the room temperature dynamics of the alkyl chains in the pristine organo modified MMT have been examined by NMR. In view of this, nuclear magnetic resonance (NMR) spectroscopy has been proven to be one of the most powerful techniques for probing structure and conformation, as well as dynamics of surfactants at surfaces and confined between two solid surfaces [79]. In fact, recent NMR studies on intercalated surfactants in layered solids further clarified the coexistence of ordered trans and

disordered gauche conformations. At very high charge densities, large surfactant ions can adopt lipid bilayer orientations in the clay galleries. Also, most results support the concept that for an intercalant with a relatively low dielectric constant the cationic head group stays in close proximity to the aluminosilicate surface and the isomorphic substitution defect in the lattice. To complement these structural investigations, recent efforts have begun to quantify the dynamics within the organically modified montmorillonites (OMMTs) interlayer. Although various structural models have been proposed for the intercalated surfactants, they do not directly reveal the significant structural characteristics of the surfactants at molecular levels.

#### **1.5.4 Organic compounds used to prepare organoclays**

Organoclays are synthesized via the exchange of hydrated cations by organic ones such as alkylammonium or alkylphosphonium on the clay surfaces. The use of these OMMTs as nanofillers for polymers has motivated extensive recent efforts to elucidate the factors that dictate the structure of the organic surfactant within the interlayer gallery and thus to understand better the underlying factors determining their compatibility and interfacial properties with various polymers. Surface energy, basal spacing and thermal stability of these organoclays depend strongly on the chemical structure, packing density and the type of cation head included in the surfactant. By exchanging of sodium or calcium cations for organic cations, the surface energy of MMT decreases and the basal spacing expands with respect to both clay and surfactant chemistry.

The first generation of MMT-based organoclays employed ammonium surfactants. The most common cationic surfactants that are used to modify clay for the preparation of PLSNs are primary, secondary, tertiary, and quaternary alkylammonium cations. The alkyl chain length and molecular structure of the alkylammonium modifiers have been found to have important effects on the morphology of the nanocomposites. Reichert et al. have experimentally showed the influence of the alkyl chain length of protonated alkyl-substituted primary amines on the exfoliation behavior of synthetic clay [80]. It was determined that alkyl chains that are longer than eight carbon atoms are needed for the clay modification to be effective. This is because only a limited expansion of interlayer space for chain lengths fewer than 8 tend to give smaller basal spacing which can not let the polymer

chains move into the interlayer gallery. D-spacing is found to increase significantly for longer alkyl tail chains. Kim and White have also found that organoclays modified with quaternary ammoniums tend to have relatively better compatibility with non polar polyolefins (POs) in comparison to their primary, secondary, or tertiary counterparts [81]. Quaternary ammonium salts that contain more than one long alkyl chains can result in a larger organic surface and interlayer spacing in the clay galleries, which helps to the penetration of polymer chains into the clay layers. Ammonium surfactants used in commercially available organoclays usually incorporate short aliphatic chains and benzyl and sometimes hydroxyl groups [82]. They also contain at least one long aliphatic chain (C12–C18) to cause expansion of the distance between the layers. Other MMT modifiers include alkyl amines, alkyl carbazol, poly(dimethylsiloxane), and pyridinium and derivatives. Other ammonium surfactants are more complex molecules, oligomers and reactive groups.

Systematic studies on MMT's organic modification have been widely reported. For primary alkyl-amines (ammoniums) modified MMTs, the intergallery distances increase with the increases of the carbon numbers of the main chains. When the carbon numbers of the main chains are the same, the increases of the intergallery distances of OMMT modified by quaternary ammoniums are larger than that of OMMT modified by primary alkyl ammoniums [78].

Short-chain alkylammonium ions are arranged in monolayer and long chain alkylammonium ions in bilayer with their alkyl chains parallel to the silicate sheets. The monolayer type gives a basal spacing of ca. 1,4 nm, and the bilayer type gives a spacing of ca. 1,7 nm. Since the monolayer rearranged into a bilayer if the area of the flat-lying alkylammonium ions becomes larger than the equivalent area, the monolayer/bilayer transition with increasing the alkyl-chain length can be used as a measure of the layer charge [83].

The type of alkylammonium surfactants affects the dispersion of the organoclay through not only decreasing surface energy by covering it and interlayer spacing, but also increasing the thermal stability of the organoclay, since the melt compounding of POs usually proceeds at temperatures above 150 C. The low thermal stability of ammonium surfactants presents a problem for melt compounding and processing of PLSN, where high processing temperatures exceeding 200 °C are commonly encountered. Thermal degradation during processing could initiate/catalyze polymer

degradation, in addition to causing a variety of undesirable effects during processing and in the final product. Decomposition products have undesirable color, odor and taste, and also degrade the properties of the composite. However, in matrices requiring higher processing temperatures, such as polyethylene terephthalate, polyamides, or thermosetting resins, the thermal degradation of the intercalating agent could become a critical parameter, rendering the use of highly thermally stable organoclays mandatory [84].

In this case, dialkyl imidazolium modified MMTs, in particular, might provide an interesting alternative to commercial dialkyl ammonium modified clays, since they exhibit a similar basal distance and a much higher thermal stability. Imidazolium cation has better thermal stability than the alkylammonium and pyridinium cations synthesized C12, C16, and C18, three new thermally stable. OMMT, prepared using new cationic imidazolium surfactants having a polymerizable group, showed a greater thermal stability as compared with a standard alkylammonium cation [85].

Patel et al. tried the preparation of organo-montmorillonites with the intercalation of quaternary phosphonium cations that give higher thermal stability organoclays than the ones prepared with quaternary alkylammonium salts [70]. The tetrabutylphosphonium (TBP) and tetraphenylphosphonium (TPP) modified MMTs showed enhanced thermal stability (300–400 °C) and may be potentially useful materials for melt processing of nanocomposites. MMTs modified with quaternary phosphonium ions have a greater thermal stability than their quaternary ammonium-modified counterparts, in accordance with the findings by Xie et al [73]. The thermal stability of organically modified MMTs (organoclays) has been investigated using differential thermal analysis, differential scanning calorimetry, and thermogravimetry also in comparison with X-ray diffractometry for different surfactants show a decrease in the TBP≈TPP>TMA order. Because of their relatively high thermal stability, organoclays containing phosphonium surfactants would be more suitable to preparing clay-PO nanocomposites by melt extrusion with respect to ammonium based organoclays. Results showed that efforts have been made to synthesize organoclays based on phosphonium, imidazolium, pyridinium and other onium surfactants can have higher thermal stabilities in addition to enhancing flame retardancy in the final nanocomposite material.

These materials are mostly known with their trade names. Cloisite Na<sup>+</sup>, Somasif, Dellite, Nanofil787 are a natural industrial unmodified MMTs. Cloisite is the mostly used organoclays in PLSN have several types. For example, Cloisite 15A and 20A are natural MMT modified with a quaternary ammonium salt and Cloisite 30B is a natural MMT modified with with a quaternary ammonium bis-2-hydroxyethyl head groups. Cloisite 25A is a natural MMT modified with 2-ethylhexyl quaternary ammonium head group and so on.

### 1.5.5 Theoretical studies on organoclays

The experimental results may not picture the exact state for the molecular arrangements and layering behaviour and it is difficult to quantify them without observing the microcosmos. The MD and MC simulations are useful techniques to observe systems at microscopic level and to obtain results comparable with experimental ones.

In the organoclays for low surfactant concentrations, the surfactant cations mainly occupy the clay interlayer with lateral arrangements (lateral monolayer, lateral bilayer and pseudotrilayer) [87]. However, when the surfactant concentrations are higher, the surfactants occupy both the clay interlayer space and the interparticle pores, and paraffin type arrangements of surfactants (paraffin monolayer and paraffin bilayer) are adopted in the clay interlayer spaces [88]. More recent modeling experiments has provided further insights into the packing orientations of the alkyl chains in organically modified layered silicates. MD simulations were used to study the static and dynamic properties of 2:1 layered silicates (CEC = 0.8, 1.0 and 1.5 meq/g for two MMT clays and a hectorite, respectively) intercalated with alkyl-ammonium ion, having 6 to 18 -CH<sub>2</sub> groups to understand molecular properties such as density profiles, normal forces, chain configurations and trans-gauche conformer ratios. For the mono-, bi- and psuedo-trilayers with respective *d*-spacings of monolayers 13.2, bilayers 18.0 and trilayer 22.7 Å° for ODTMA, a disordered liquid-like arrangement of chains was preferred in the gallery [75]. Clay layers was kept fixed during all these simulations. In the disordered arrangement the chains do not remain flat, but instead, overlap and co-mingle with onium ions in opposing layers within the galleries. The authors postulated molecular arrangements varying from solidlike to liquidlike and in intermediate cases liquid crystalline, depending on the packing density and chain length. However, it is not clear how a monolayer of

tethered alkyl chains can adopt a liquid crystalline order, neither nematic nor smectic. No liquid crystalline phase has been yet reported in alkanes of similar chain lengths, presumably due to the relatively small energy differences between the trans and gauche conformers in these chains. Results show that the primary, secondary, and tertiary ammonium organoclays showed relatively poor compatibility with the polymers compared with quaternary ammonium organoclays [89]. Moreover, penetration of polymer chains between the gallery of silicate layers of the quaternary ammonium organoclay are better than that of the primary, secondary, and tertiary ammonium organoclays, probably due to increased basal spacing or higher surface coverage. This means, only the highest polarity polymers such as polyethyleneoxide can form nanocomposite with pure clays and primary ammonium organoclays.

The interactions of the amino acid lysine with sodium MMT were studied using theoretical molecular modeling methods. The molecular level interactions of amino acids, either natural or non-natural, with clay surfaces are at the heart of fields of study as diverse as nanocomposites fabrication, drug delivery, bio-remediation of soils and catalysis of biological polymers, to name a few [90]. These systems and the potential uses to which they could be put suggests the necessity of a deeper understanding of the interplay of bonds, conformations, and configurations between the molecules and the hosts.

The structural and dynamic properties of dioctadecyldimethylammoniums (DODDMA) intercalated into 2:1 layered clays are investigated using isothermal-isobaric (NPT) molecular dynamics (MD) simulations [75]. The simulated results are in reasonably good agreement with the available experimental measurements, such as X-ray diffraction (XRD), atomic force microscopy (AFM), Fourier transform infrared (FTIR), and nuclear magnetic resonance (NMR) spectroscopies. Again using classical MD, Pospisil et al. compared the interlayer structure of organoammonium surfactants with cetyl pyridinium and cetyltrimethyl ammonium headgroups [91, 92]. Zeng et al. examine the interlayer structure and dynamics of a range of organo-ammonium surfactants in the interlayer of MMT [93]. In direct comparison with experimental work, Heinz et al. used MD simulations to gain insight into the phase transitions observed in alkylammonium mica, gaining good quantitative agreement [94].



## 1.6 Polymer Layered Silicate Nanocomposites

Polymer-layered silicate nanocomposites (PLSN) have received a great deal of attention during the past decade in today's materials research, as it is possible to achieve impressive enhancements of properties when compared with virgin polymer. The reason is that the combination of a few percents of inorganic-layered silicates (or clays) with polymers can produce a final composite with improved physical and mechanical properties and with final economical advantages [95].

By exploiting synergies between materials inorganic and organic components, layered silicate-based PLSN have demonstrated a significant potential to become the basis for development of the next generation of high performance polymer compounds. These materials exhibit unique property enhancements in relation to the virgin polymer and to conventional polymer composites. Incorporation of low loadings of layered silicates (<5%) of properly treated, well-dispersed/exfoliated organoclay into the base polymer results in a compound with a substantial improvement in thermal, mechanical, flame retardancy as well as other physical properties over those of the base polymer compared to neat polymers or conventional micro- and macrocomposites.

Any physical mixture of a polymer and layered silicate, however, does not form a nanocomposite. This situation is analogous to polymer blends, and in most cases separation into discrete phases normally takes place. In immiscible systems, which typically correspond to the more conventionally filled polymers, the poor physical interaction between the organic and the inorganic components leads to poor mechanical and thermal properties. In contrast, the strong interactions between the polymer and the layered silicate in PLSNs leads to the organic and inorganic phases being dispersed at the nanometer level. Besides, in contrast to conventional composites, a much lower filler loading is required. So, to obtain better properties of a material, it is of crucial importance to make a fine dispersion of silicate layers in the polymer matrix. The main reason for these improved properties in nanocomposites is the interfacial interaction between the matrix and layered silicate, as opposed to conventional composites. A few weight percent of layered silicate particles that are properly dispersed throughout the matrix can thus create a much larger surface area for polymer filler interactions than do conventional composites [96].

The first polymer/clay nanocomposite was successfully synthesized with a polymer containing a polar group because the polar group allowed the clay to disperse readily in Toyota [97]. Since the Toyota group developed a nylon6/MMT nanocomposite with excellent mechanical properties, there has been considerable academic, government, and industrial interests in the investigation on various polymer system based nanocomposites. Polymer-layered silicate nanocomposites represent a large group of nanocomposites materials that has developed in the last 15 year. Publications in this field started appearing in around year 1995, increased up to 50 in 2000, was about 200 in 2005 and over 1000 in 2010. Most publications still concentrate on the importance of the chemistry used to modify the surface of the clay.

### **1.6.1 Polymers used in PLSN**

Started in 1990s by the Toyota group in Japan, property enhancement of a wide range of polymers containing only a few volume percent of nanofiller in polymer-layered silicate nanocomposites have generated significant interest in literature and industry. Very large variety of polymers (almost all known polymers) can be used for the PLSN. But most attention has been given to rubber-based nanocomposites at first times [98]. Such rubber–clay nanocomposites prepared by earlier workers from our laboratory have demonstrated good results, which depends on the kind of rubber, the solvent used for casting, the nature of the clay, and other factors. Among the thermoplastic nanocomposites, those based on nylon 6 have experienced the most dramatic development due to their greater compatibility with the inorganic silicates and are today entering commercial markets. A review of nylon 66 nanocomposites has been presented by Goettler and Recktenwald, since nylon 6 have experienced the most dramatic development due to their greater compatibility with the layered silicates and is the first one in the thermoplastic nanocomposites in markets [99]. Early work with nylon polymers documented in the reviews and books involved MMT clays modified with several surfactants from amino acids to onium types either an amino acid or a hydrocarbon functionality. Amino acids was used in-situ polymerization that was chemically reacted with caprolactam by serving as the catalyst for the ring opening polymerization. Various alkylorganoclays have been melt blended into nylon 6 and nylon 66 [100].

Pristine layered silicates in nature usually contain hydrated  $\text{Na}^+$  or  $\text{Ca}^+$  ions. Obviously, in this pristine state layered silicates are only compatible with hydrophilic polymers, such as polyethylene oxide (PEO), polyvinyl alcohol (PVA) etc [100]. To render layered silicates compatible with other polymer matrices, one must convert the normally hydrophilic silicate surface to organophilic, which makes the intercalation of many engineering polymers possible.

Thermoplastics like PE, polypropylene (PP), polyamides, polystyrene, etc., thermosets like epoxy etc., and elastomers like polyurethanes, polydimethylsiloxane, etc. were frequently used to synthesize PLSN. Matrix polymers such as: polyetherimide (PEI), polybenzoxazines, polymethyl methacrylate (PMMA), poly( $\epsilon$ -caprolactone) (PCL), polylactides, polycarbonates, styrene-acrylonitrile copolymer (SAN), acrylonitrile-butadiene-styrene copolymer (ABS) and liquid crystalline polymers (LCP) were other important polymers used to prepare PLSN in the literature after the processing with organoclays [30,84].

Polyolefin nanocomposites can be prepared by an in situ polymerization of the proper monomers around dispersed inorganic layers [101,102]. There is a rich literature on polyethylene (PE) nanocomposites; however, in most cases the reported results are not consistent. Most of the studies report exfoliation of the silicate structure, when maleic anhydride functionalized PE is used either as a compatibilizer or as the polymer, especially for high ratios of compatibilizer to organoclay [103]. Exfoliation or intercalation is reported depending on the degree of functionalization of the maleic anhydride and the chain length of the organic modifier.

Thermoplastic elastomers or block copolymers has been get less attention during development of nanocomposites. Krishnamoorti and co-workers synthesized block copolymer based nanocomposites [104]. Recently, various types of block or segmented copolymers have attracted much attention as nanomaterials on their own because of nanoscale phase separation between different blocks. Due to the self-assembly characteristics of the block copolymers, many interesting phenomena like imprinting and thin film applications are expected [105].

### **1.6.2 Definitions**

Nanocomposites have physicochemical properties can often be defined due to nanometer-level inter-phase morphologies formed due to interactions and quantum

effects. One have to know some definitions first related to PLSN prior to study on this subject. The formation of the polymer-clay nanocomposite entails extensive delamination of the layered clay structure or complete dispersion of the clay platelets throughout the polymer matrix. The definitions of PLSN are mostly related to this delamination phenomena (Figure 1.5).

Depending on the nature of the components used (type of MMT, organic modifier (surfactant) of the clay surface, polymer matrix, and additives) and the method of preparation, three main types of composites may be obtained: microcomposites and intercalated or exfoliated nanocomposites. However, these are the ideal cases, mixed structures usually formed in the nanocomposites (Figure 1.5).

Intercalant, surfactant or organic modifier is the material placed between platelets that binds with their surfaces to form an intercalate. Often the intercalant is an onium salt that bonds ionically with platelet anion. When the polymer is unable to enter the spaces between the clay layers, and the clay still remains in the form of large stacks known as tactoids, a phase-separated microcomposite results. The properties of such composites remain in the same range as conventional microcomposites. The term intercalated describes the case where a small amount of polymer moves into the gallery spacing between clay platelets, but causes less than 3 nm separation between the platelets. Thus, intercalated nanocomposites correspond to these well-ordered multilayered structures where the polymer chains are inserted into the spacing between the silicate layers. When the single polymer chains are inserted into the spaces between the clay layers, an intercalated nanocomposite is obtained. The separation between the individual layers called spacing or basal spacing ( $d_{001}$ ) is often increased due to the presence of the polymer that is sandwiched between the clay layers.

Flocculated nanocomposites is another morphology conceptually this is the same as with intercalated nanocomposites, however, silicate layers are sometimes flocculated due to hydroxylated edge-edge interaction of the silicate layers.

Exfoliation or delamination occurs when polymer further separates the clay platelets e.g. by 8-10 nm or more where delaminated platelets distributed homogeneously in the polymer. The platelets can be oriented, forming stacks or tactoids [106]. As a rule, a strong interaction between polymer and clay is required for the preparation of exfoliated nanocomposites which the individual silicate layers are separated within

the polymer matrix and are no longer close enough to interact with the gallery cations. With extensive penetration of the polymer chains into the clay galleries, the clay can be completely delaminated into individual nanometer-thick layers. Exfoliation is this process where converting intercalated turns into exfoliated. Usually, the clay content of an exfoliated nanocomposite is much lower than that of an intercalated nanocomposites.

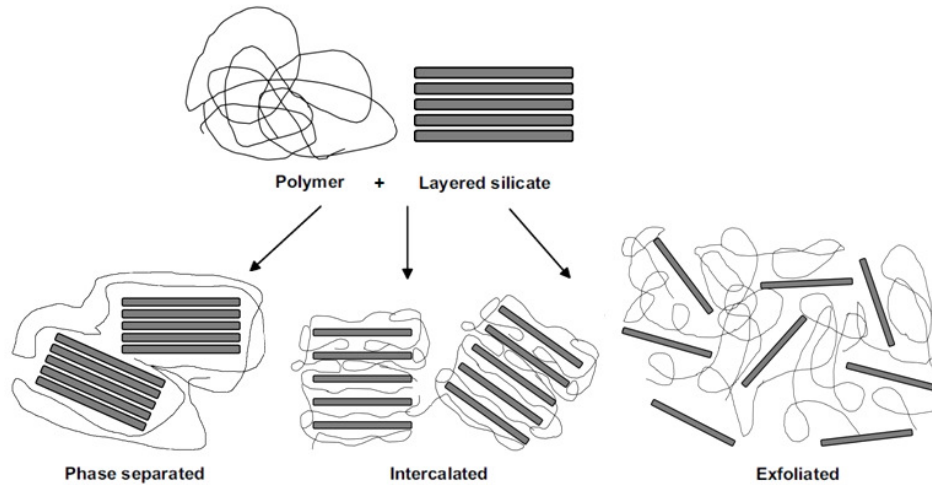


**Figure 1.5:** Classification of polymer clay nanocomposites with respect to clay delamination.

The nanocomposites are obtained when the sheets of the clay unit cells are more or less intercalated in the polymers. In the case of no intercalation, the clay and the polymer are phase-separated and no composite is obtained. At an intermediate level of the polymer intercalation, the clay sheets distance is increased compared to the original distance without the polymer. In the opposite limit, the clay sheets are delaminated from each other that a complete exfoliation occurs [107].

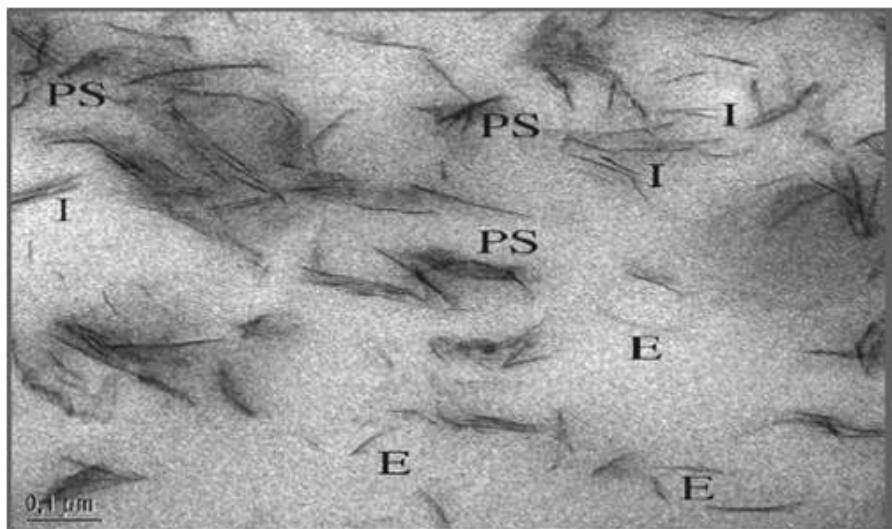


**Figure 1.6:** TEM analysis of 3% filled polyamide nanocomposite. PS is phase separated domains; I is intercalated; and E is for exfoliated platelets [108].

Different morphologies like intercalated, mixed intercalated and exfoliated, ordered exfoliated and disordered exfoliated, have been observed, in this sequence as the concentration of silicate decreases (Figure 1.6). Even for unmodified PE, there are conflicting reports on intercalation besides those reporting immiscible systems [109]. It has been possible to achieve exfoliation for specific systems; however, widely applicable and cost effective approaches to exfoliate layered silicates in common hydrophobic and polar polymer matrices remain of great significance for automotive, aerospace, packaging, and commodity applications [110]. In spite of theoretical studies on clay minerals and polymers, difficulties to achieve exfoliation in polymers using existing techniques are still linked to limited understanding of dispersion and self-assembly processes.

### 1.6.3 Preparation of polymer nanocomposites

A major challenge in PLSN synthesis is the exfoliation of the silicate layers in polymer matrices to create a bulk material of interfaces as opposed to intercalation or agglomeration of the layered silicates in the matrix. In many cases intercalation of organic components into the cavities is difficult because of diffusion limits. Several porous or layered inorganic materials have already been used to prepare hybrid materials and nanocomposites. Probably the most studied materials, class in this respect is that of two-dimensional (2-D) layered inorganic materials that can

intercalate organic molecules and if polymerization between the layers occurs even exfoliate, producing nanocomposites. Three main approaches have been developed to for the formation of polymer–clay nanocomposites can be used:

1. Direct intercalation of polymer chains from solution
2. Intercalation of monomers followed by *in situ* polymerization
3. Polymer melt intercalation

PLSNs have been obtained successfully through these strategies in a large variety of polymer systems with layered silicates (Table 1.2). However, synthesis of PE/layered silicate nanocomposites remains a scientific challenge because of the weak interaction between nonpolar PE chains and hydrophilic clay surfaces [111]. Many approaches have been explored to achieve exfoliation, including the use of different minerals, variation in cation exchange capacity (CEC), surfactant architecture and chemistry, *in situ* polymerization of polymer precursors under addition of organically modified minerals, reactions between modified minerals and polymer precursors followed by polymerization, and various extrusion techniques of silicate-filled polymer melts [112]. Two methods are most commonly used to synthesize PE/layered silicate nanocomposites according to the starting components and processing techniques are melt intercalation method and *in situ* intercalative polymerization. Other possibilities less chosen are exfoliation-adsorption, template synthesis, the sol–gel process and monomer-polymer grafting to clay layers.

**Table 1.2:** Classification of synthesis methods and final properties PCNs.

Method	Energetic Factor	Advantages	Disadvantages	Application
Melt intercalation	Both enthalpic and entropic contributions of the polymer-organoclay interactions.	Environmentally clean; No residues or solvent; extrusion and molding technology can be used, high amounts of materials can be prepared.	Non guaranteed intercalation, high temperatures require thermal stability.	PE, nylon 6, polystyrene, Polypropylene polyethylene terephthalate, Polyesters, Polyurethanes
Solution exfoliation	Entropy from by Solvent diffusion, decreased of intercalated polymers.	Soluble polymers.	Expensive solutions, solvent residues, Intercalated residues, Less amounts of resulting material	epoxy, polyimide, polyethylene (PE), polymethylmethacrylate.
<i>In-situ</i> Polymerization between clay layers	Intercalation and interaction between monomer and MMT surface; Enthalpic Factors.	Appropriate for low soluble polymers; Guaranteed intercalation	Clay exfoliation depends on swelling of monomers. incomplete polymerization.	epoxy, polystyrene, nylon6, PE, polyethylene oxide,

Intercalation of polymer chains from solution is based on a solvent system also called pre-polymer from solution method in which polymer or pre-polymer is soluble and the silicate layers are swellable. The electrostatic forces holding the layers together are relatively weak. As a result, the stacks swell in water and the layers can be easily exfoliated on shearing. The layered silicate is first swollen in a solvent, such as water, chloroform or toluene. Layered clays are exfoliated into single platelets using a solvent in which the polymer is soluble. The polymer is then mixed with the clay suspension and adsorbed onto the platelets [113]. The solvent is finally eliminated from the clay polymer complex through evaporation. When the polymer and layered silicate solutions are mixed, the polymer chains intercalate and displace the solvent within the interlayer of the silicate (Figure 1.7).



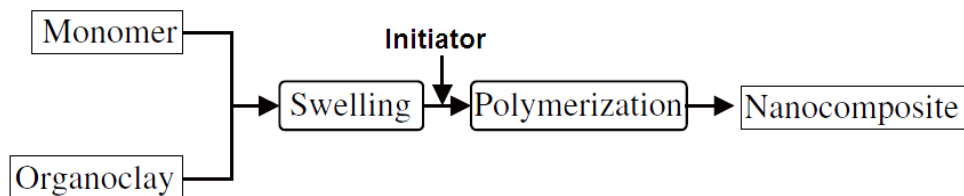


**Figure 1.7:** Mechanism for intercalation of polymer chains from solution.

In situ intercalative polymerization method, the organoclay is swollen within the liquid monomer or a monomer solution so that the polymer formation can occur in between the intercalated sheets. In *in-situ* polymerization method, monomers are intercalated into layered clays easily and then polymerized within the gallery via heat, radiation, pre-intercalated initiators or catalysts (Figure 1.8). The patent of Okada et al. from Toyota explained the procedure for *in situ* polymerization of a Nylon6/clay nanocomposite. They provide a description of resultant product properties but do not include the role of processing or give details of the compounding setup. In-situ interlayer polymerization relies on swelling of the organoclay by the monomer, followed by in-situ polymerization initiated thermally or by the addition of a suitable compound. The chain growth in the clay galleries accelerates clay exfoliation and nanocomposite formation. This technique of in situ interlayer polymerization is also particularly attractive due to its versatility and compatibility with reactive monomers and used for commercial applications. The in situ intercalation method relies on the swelling of the organoclay due to by the monomer, followed by in situ polymerization initiated thermally or by the addition of a suitable compound [114]. Thus, an advantage of the in situ method is the preparation of polymer hybrids without physical or chemical interactions between the organic polymer and the inorganic material.

Mostly styrene, methyl methacrylate, amides as well as some olefins were polymerized by in situ polymerization in a one step reactions which can also be called ship-in-the-bottle polymerization. Easy dispersion of clay particles can be accomplished after formation of the polymer chains if new new hydrogen bonds in the presence of various organoclay.

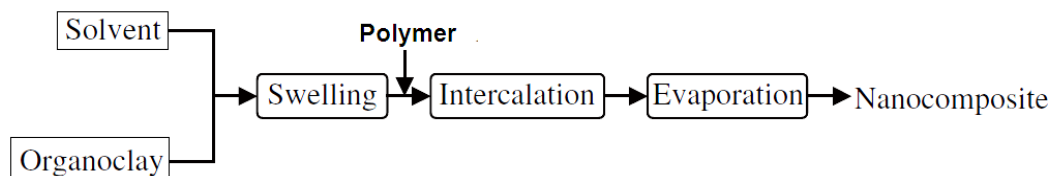


**Figure 1.8:** Mechanism for in-situ intercalative polymerization method.

In last decade, the melt intercalation technique became the standard for the synthesis of PLSNs. The melt intercalation technique first reported by Vaia et al. in 1993 has been widely used to prepare PLSNs, since this method makes an environment-friendly and economically viable alternative for application in industry (Figure 1.9) [115]. During melt process, the layered silicate and polymer matrix are mixed in the molten state, the polymer then dragged into the interlayer space and forms either an intercalated or an exfoliated nanocomposite. It is accomplished by organic polymer pellets and treated clay are directly mixed in the extruder machine and are then melt-extruded together to prepare the nanocomposite on a large scale to obtain the exfoliated layers. Formation of nanocomposites via melt intercalation primarily depended on the surface energies of the polymer and silicates. Direct melt intercalation method offers convenient techniques for preparation of hybrids, which involve mixing the layered silicates with the polymer matrix above its softening point.

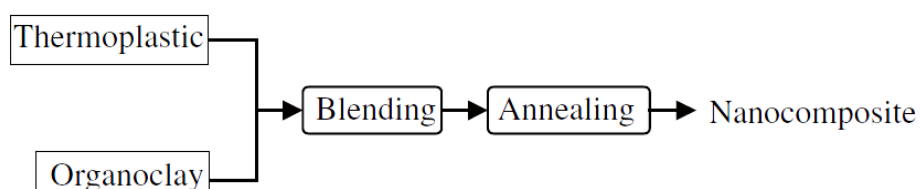


**Figure 1.9:** Mechanism for melt intercalation method.

In the process of melt intercalation, If the silicate surfaces are sufficiently compatible with the chosen polymer when it is mixed with a molten polymer matrix, then the polymer can enter the interlayer space and form an intercalated or an exfoliated nanocomposite. A wide range of polar thermoplastics, such as polyimide, poly(methyl methacrylate), poly(butylenes terephthalate), and poly(ethylene-co-vinyl acetate) (EVA), have been successfully prepared by this method; however, PE has so far only been successfully intercalated to a limited extent since it has no polar groups in the chain [116].

Melt blending of nonpolar polymers is very difficult and almost always results in the formation of immiscible systems, unless a compatibilizer is used. For a polymer such as PP or PE, the usual compatibilizer is maleic anhydride. It is impossible to directly intercalate PE chains into silicate galleries. Also PET-MMT nanocomposites are incapable of being prepared via such technology because of easy degradation at softening temperatures [117]. Melt intercalation of inorganic clay mineral consisting of layered silicates with polymers is still used over either in situ intercalative polymerization or polymer solution intercalation, as it is environmentally friendly since it does not involve any solvent. Moreover, it is compatible with current industrial processes, such as extrusion and injection molding with high efficiency makes this method more economical, more flexible for formulation for commercial practice. For most purposes, complete exfoliation of the clay platelets, i.e., separation of platelets from one another and dispersed individually in the polymer matrix, is the desired goal of the formation process [118]. However, this ideal morphology is frequently not achieved and varying degrees of dispersion are more common.

Polymer intercalation of the layered silicates directly from a polymer melt or the dispersion of clays into the final nanocomposite composition can be accomplished in various types of polymer compounding equipment, including batch mixers and single or twin-screw extruders, to provide both distributive and dispersive mixing. The nature of the extruder and the screw configuration are important to achieve good organoclay dispersion also longer residence times and shear in the extruder resulted in better dispersion. The single screw extruder has been found significantly less effective [119].

In some cases, having a higher melt viscosity is helpful in achieving dispersion apparently because of the higher stresses that can be imposed on the clay particles; however, this effect is not universally observed. The location of where the organoclay is introduced into the extruder has also been shown to be important [120]. The effects of the dispersive mixing process on the final state of reinforcement size, or aspect ratio, and dispersion depend on the characteristics of both the reinforcement and the matrix, as well as the parameters of the mixing process.

#### **1.6.4 Properties and applications of PLSN**

Due to the dimensional characteristics and interlamellar behaviour of chains, nanocomposites possess superior properties to conventional composites, since they maximize the interfacial adhesion very large inorganic surface. These properties make them extremely interesting in the field of design and creation of new materials. PLSN has enhanced important material properties compared with pure polymer or conventional composites include, improved mechanical properties (strength, stiffness, high moduli), increased thermal stability, increased transparency, electric insulation properties, remarkable decrease of gas, water and hydrocarbon permeability, increased biodegradability for biodegradable polymers, heat resistance, increased transparency, flame retardancy and less smoke emission, weight reduction, improved chemical resistance and surface appearance [121-124].

The mechanical and thermal properties of all polymers are generally improved by the addition of inorganic layered silicates. Since the organic polymer matrix is not relatively compatible with the MMT, improvements in the interfacial adhesion between the polymer matrix and the reinforcing material become a challenge in this area of high-performance polymer clay nanocomposite materials. A better interfacial bonding can highly enhance properties of a PNC if only improved attraction between MMT and the polymer matrix gives physico-mechanical, thermal, morphological, and optical properties due to a better particulate dispersion in the entire nanocomposite. However, the rules for better nanocomposite formation is not clear if there is an upper bound on the modulus for these nanocomposites. In fact, the process of melt blending is that it was found to increase up to twice for nylon nanocomposite in injection moldings and three times in blown film.

Nanocomposites made from POs, styrenics, and other polymers that lead to lower degrees of exfoliation reveal particles much thicker than single clay platelets as expected. As the polymer-organoclay affinity is increased by adding a compatibilizer, e.g., PP-g-MA or PE-g-MA, or increasing the content of a polar comonomer, e.g., vinyl acetate, the clay particles not only become thinner (fewer platelets in the stack) but also become shorter [125]. However, generally the particle thickness decreases more rapidly than the length such that the aspect ratio increases; this generally improves performance.

PLSN are promising as a coating materials as significantly enhance the properties or can introduce new functionalities like low permeability in the final coating products. To take full advantage of the reinforcement or tortuosity clay platelets or particles can provide to mechanical and thermal or barrier properties of nanocomposites, they must be oriented in the appropriate direction. Tortuous pathway caused by dispersed silicate platelets penetration of gas molecules and decreased permeability which is very important in packaging industry (Figure 1.10) [126]. They also strongly enhance the stiffness of nanocomposites, when oriented in the load direction. In spite of their potential to display advanced properties, these improved properties are achieved at a small clay loading (e.g. 3–5 wt.%). Generally, Nielson labyrinth tortuous path model explains barrier effects best which is accomplished for fully exfoliated clay layers oriented in parallel within resulted in the diffusing species to diffuse a longer way around the impermeable clay platelets in PLSN [127].

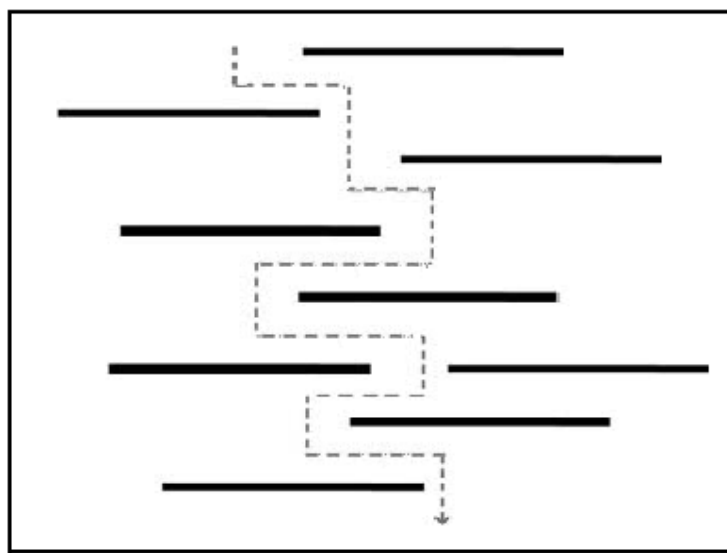


**Figure 1.10:** Tortuous path model to which a gas molecule has to follow when diffusing through a PCN.

The alignment of particles is affected by the type of processing used to form the test specimen, extrusion, injection molding, etc [128]. This is a separate issue from the degree of dispersion or exfoliation which is usually determined in the mixing process. Techniques like compression molding usually do not lead to good alignment or straightening of the high aspect ratio particles, and measurements made on such specimens often underestimate the potential performance. TEM can be used to assess and even quantify particle orientation and curvature and this information can, in

principle, be factored into appropriate models to ascertain their effect on performance.

The amount of fully exfoliated clays used for manufacturing polymeric nanocomposites is in the range from 5 ppm to 15 wt% of clay. Additionally, modified clays in the polymer matrices can act as fire retardants by the reduction of heat release rate through char formation. Reduced flammability behavior was observed in PLSN such as PP with 2% nanoclay loading, obtained from decrease heat release rates (HRR) [129]. Another example is PS-clay nanocomposites 10% organoclay loading show flame retardancy effect is evaluated by 21 % decrease in the HRR compared with the pristine polymer [130]. The most impressive example for this effect is the 40% decrease in the HRR for %5 organoclay loaded nylon6-clay nanocomposite [131]. The char formation that prevents flames is the reason for reduced flammability which forms from the burning of organic materials and clay layers.

A common reason for adding fillers to polymers is to increase the modulus or stiffness via reinforcement mechanisms described by several theories for composites like Mori-Tanaka and Halpin-Tsai numerical methods. Properly dispersed and aligned clay platelets have proven to be very effective for increasing stiffness. By comparing the increase in the tensile modulus,  $E$ , of injection molded composites based on polymers, relative to the modulus of the pure polyamide matrix,  $E_m$ , when the filler is an organoclay versus filler. In one of this example, three times more mass of glass fibers than that of MMT needed for increasing the modulus by a factor of two relative to that of nylon6 approximately. The degree of exfoliation for the reinforcement is critical for both mechanical properties and strength development, with respect the generation of high aspect ratio and for the elimination of stress concentrations [132]. Nanoscale layered silicates and accompany molecules on them behave as agents that promote dispersion during normal mixing operations, while possibly also contributing to improved bonding to the matrix. In the case of polyolefin-MMT based nanocomposites, surfactant coating pre-applied to the clay walls are important as dispersion agents.

The high thermal expansion coefficients (TEC) of neat thermoplastics cause some problems during molding and as the temperature changes that are unacceptable in some industrial application like automotive parts. Fillers can be frequently added to

plastics to lower the TEC. For low aspect ratio filler particles, like spherical particle fillers the reduction in TEC follows a simple additive rule that is the linear TEC changes are similar in all three coordinate directions [133]. However, when high aspect ratio fillers, like nanotube fibers or clay layers, are added, the effects can be much larger; in these cases, the TEC in the three coordinate directions may be very different.

The fibers or MMT layers typically have a higher strength and a lower TEC than the polymer matrix. As the temperature of the material changes, the matrix extend or contract as normally; however, the fibers or platelets prevented this change creating opposing stresses in the two different phases. When the filler to matrix modulus is large, the restraint to dimensional change can be quite significant within the direction of alignment. Clay layers causes their pressure in two directions, when appropriately oriented, while fibers can only do so in one direction.

Optically transparent hybrid materials can also be synthesized by using the organic–inorganic nanocomposites which MMT clays as layered silicates can be considered to be good candidates for the preparation that they can be broken down into nanoscale building blocks [134].

It is claimed that biodegradation mechanism of polymer matrices were caused by catalytic role of the organoclay. First reported biodegradable clay based nanocomposite which is poly( $\epsilon$ -caprolactone) (PCL) and poly(lactic acid) (PLA) with OMMT as filler, have proven to gain improved biodegradability [135].

PLSN accompany with other structures such as granular-activated charcoal, reverse osmosis, and air strippers used in water treatment unit processes which become common in industry to extract oil, grease, or humic acid. Nanoclays have a great potential as drug vehicle can be used in medicinal application for controlled release which is one of the fascinating and competitive area of biosciences. Polar organic compounds can be accommodate between layered silicate layers and form a variety of intercalated compounds whose release rate can be controlled by chemical factors[136].

## 1.7 Characterization of PLSN

All the high technology properties of PLSN are similar to other composites, but with smaller ratio of filler loading. Although scientific and industrial developments have been made in the nanocomposites over the past decades, it is widely known that design of PLNS for the best possible performance remains as a still very challenging task. A major reason is the lack of fundamental characterization on this type of nanostructured composite materials. The main reason for the improved properties in nanocomposites is the interfacial interaction between the matrix and layered silicate, as opposed to conventional composites. In practice, many of the properties have been enhanced only for special cases, because they depend on a good compatibility between the polymer and the clay, which is not easy to be achieved. To understand and try to increase this compatibility, it is very important to understand and characterize the structure of clay quantitatively.

PLSNs can be characterized by X-ray diffraction (XRD) and transmission electron microscopy (TEM) [137,138]. X-ray diffraction (XRD) patterns and transmission electron microscopic observations showed that silicate layers were either intercalated or exfoliated. XRD is the most straightforward way to evaluate the spacing between the silicate layers, reflecting the relationship of the clay layers with themselves. However, one should be careful with the interpretation of the XRD results, because it can only detect the periodically stacked silicate layers, the degree of exfoliation and how well the clay dispersed can not be assessed by X-ray analysis because delaminated layers cannot be detected not give information on is throughout the polymer (Figure 1.11).

Schematic illustration for microscopy and scattering methods resolutions in the literature is taken from Jinnai [139]. Abbreviations are OM (optical microscopy), LSCM (laser scanning confocal microscopy), X-ray CT (X-ray computerized tomography), SEM (scanning electron microscope), TEMT (transmission electron microtomography), AFM (atomic force microscopy), WAXS (wide-angle X-ray scattering), SAXS (small-angle X-ray scattering), LS (light scattering), USAXS (ultrasmall-angle X-ray scattering), SANS (small-angle neutron scattering), and USANS (ultrasmall-angle neutron scattering). 3D microscopy techniques were shown in bold.



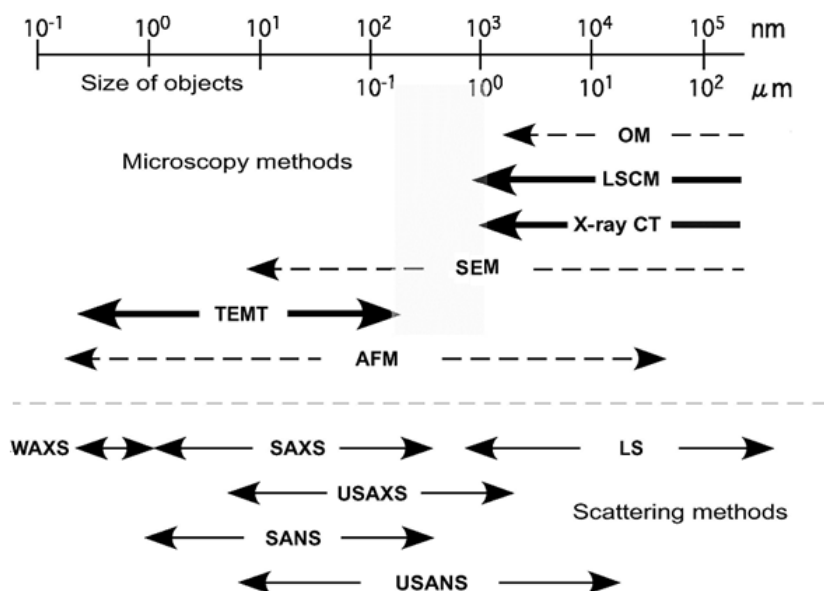


**Figure 1.11:** Spectroscopic methods used to analyze PCNs [139].

Vaia made XRD measurements on hybrids during in-situ annealing [140]. Manias and coworkers used ex-situ sample during annealing for XRD and other measurements. The ex-situ method has several advantages over the in-situ method like lower polymer chain decomposition and give opportunity to investigate the same side/surface of the pellet sample by XRD [141]. Manias made several researches by using in-situ small-angle neutron scattering (SANS) and intermediate-angle neutron scattering (IANS) to monitor the behavior of polymer chains, *i.e.*  $R_g$ , and also to follow the changes in the single chain scattering function during intercalation. SANS and IANS studies directly reflects the motion inside the 2 nm slit pore of the polymer chains during intercalation so the the silicate gallery expansion. The results suggested that the confined film adopts a layered structure normal to the solid surfaces, with the polar phenyls dominating the PS chains interacted with the clay polar surfacess, and the aliphatic groups PS predominantly in the center of the interlamellar cavity.

$^1\text{H}$ - $^{29}\text{Si}$  cross-polarized nuclear magnetic resonance (NMR) measurements revealed a existence of both ultra-fast and solid-like slow chain dynamics throughout a wide temperature range, below and above  $T_g$ , for both the styrene phenyl and the backbone carbons. Fast dynamics occur in the lower density regions like the center of the spacing, whereas slower dynamics occur in high-segment density regions close to the surface causes inhomogeneity in the direction normal to the clay oxygens.

Common characterization techniques and expected results for clay-based PLSN given in Table 1.3.

**Table 1.3:** Characterization techniques used to analyze PLSNs.

	Property
XRD/WAXRD	Dispersion degree of clay platelets Clay delamination: intercalated or exfoliated intercalation process
SEM	Surface properties and morphology Dispersion of clay
TEM/HRTEM	Morphology dispersion (intercalated or exfoliated) Distribution of platelets Structural heterogeneities Defect structure and atomic arrangement
AFM	Crystallization behavior of polymer Surface roughness Particle size and distribution Morphology and microstructure (intercalated vs exfoliated)
FTIR	Component identification and analysis Interfacial interactions Crystallization and orientation of polymer
NMR	Local behaviours of polymer chains Morphology and dispersion of clay particles Surface chemistry
SAXS	Dispersion of nanoscale clay platelets Morphology (intercalated, exfoliated or mixed) and its development Phase behavior and structure evolution Lamellar texture and thickness
TGA	Thermal stability
DSC	Melting and crystallization behavior Local dynamics of polymer chains
Cone calorimetry	Flame retardancy, Coal formation Thermal stability
Rheometry Mechanical Test	Nanorheology Modulus Tensile strength Elongation at break Viscoelastic properties

An important issue is to relate the performance of nanocomposites to their morphological structure; experimental evaluation of performance is certainly easier than characterization of their morphology. Wide angle X-ray scattering, WAXS, is frequently used because such analyses are relatively simple to do. In some cases, the

WAXS scan may reveal a shift in the peak location relative to that of the neat organoclay [142]. The peak may shift to lower angles, or larger d-spacing, and is generally taken as evidence of intercalation of polymers (or perhaps other species) into the galleries. However, an opposite shift may also occur, and this is usually attributed to loss of unbound surfactant from the gallery or to surfactant degradation. All of these processes may simultaneously render uncertainty in the interpretation. However, such analyses can be misleading and are not quantitative enough. The organoclay has a characteristic peak indicative of the platelet separation or d-spacing; other peaks may be seen resulting from multiple reflections as predicted by Bragg's law. The presence of the same peak in the nanocomposite is irrefutable evidence that the nanocomposite contains organoclay tactoids. However, the absence of such a peak is not conclusive evidence for a highly exfoliated structure as has been repeatedly pointed out; many factors must be considered to interpret WAXS scans. If the sensitivity or counting time of the scan is low, then an existing peak may not be seen [143].

Small angle X-ray scattering, SAXS, is referred more informative and quantitative by some authors [144]. However, this technique has not been widely used except in a few laboratories probably because most laboratories do not have SAXS facilities or experience in interpreting the results.

Scanning electron micrographs revealed efficient for mixing of the polymers in the presence of organically modified layered silicate [145]. A far more direct way of visualizing nanocomposite morphology is via transmission electron microscopy, TEM [146]. This approach requires considerable skill and patience but can be quantitative, photographic and allows us qualitative understanding of the internal structure, spatial distribution of the various phases, and defect structure through direct visualization. TEM is a necessary complement for evaluating nanocomposite structure, since it allows a qualitative understanding of the internal structure, spatial distribution of the various phases, and observations of the defect structure through direct visualization [147]. It can be utilized to obtain this information from the permeation properties of the composites, which correlate well with the aspect ratio of the inclusions and consequently with the degree of exfoliation.

Use of TEM is often criticized because it reveals the morphology in such a small region. However, this can be overcome by taking images at different magnifications

and from different locations and orientations until a representative picture of the morphology is established. The major obstacle in obtaining good TEM images is not in the operation of the microscope but in microtoming sections that are thin and uniform enough to reveal the morphology [148]. Fortunately, the elemental composition of the clay compared to that of the polymer matrix is such that no staining is required. When exfoliation is essentially complete, as in the case of nylon 6, one can see the 1 nm thick clay platelets as dark lines when the microtome cut is perpendicular to the platelets. Image analysis can be used to quantify the distribution of platelet lengths, but meaningful statistics require analyzing several hundred particles. Another serious drawback of TEM is the fact that it projects three-dimensional (3D)-body on to two-dimensional (2D) plane. The information along the direction of thickness of the sample is only shown on one direction and this actually leads to the wrong conclusion about the degree of dispersion of silicate layers in the polymer matrix (Figure 1.12).

To avoid the misunderstanding and to get accurate information about the dispersion of MMT layers in the polymer matrix, electron tomography technique is applied recently. Three dimensional analysis of MMT dispersion in the poly[(butylene succinate)-co-adipate] matrix was characterized by using FIB-tomography technique [150]. However, this technique is very time consuming and special care is needed during sample preparation. Next, the volume for analysis is small and it is therefore very difficult to see the general picture of clay particles distribution in the polymer matrix. Other techniques like solid-state NMR have also been used on a limited basis to explore clay dispersion.

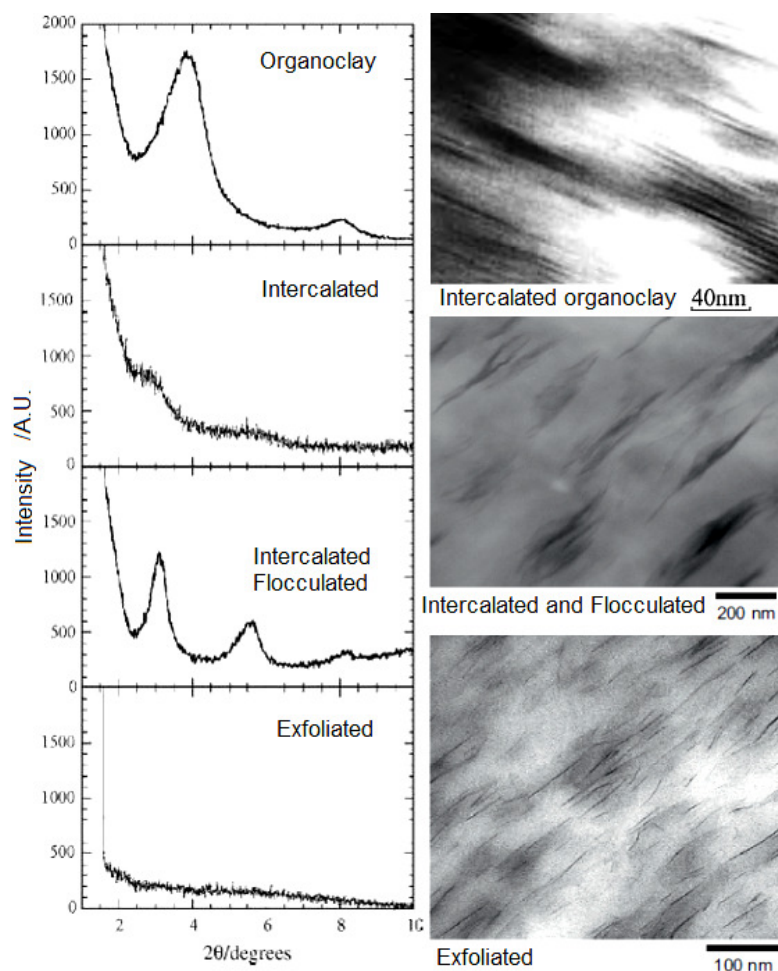


**Figure 1.12:** General examples XRD and TEM results for PLSN [149].

## 1.8 Polyolefin Nanocomposites

The microstructure and the resulting properties of a PLSN depend on the type of polymer matrix and nanoclay used and the interactions between them. The interactions in turn depend on the hydrophobicity of the polymer constituent [151]. The most effective configuration corresponds to that where the silicate layers are individually and homogeneously dispersed in the polymer matrix (exfoliated structure). Previous studies on polar polymers showed that polarity of the matrix polymer is of fundamental importance in controlling the nanoscale structure. It is difficult to obtain this type of morphology in the presence of POs, due to their non-polar structure. Dispersion of the hydrophilic silicates in a hydrophobic matrix like PE is a real challenge. Preparing the organoclay is crucial step especially for the formation of polyolefin-layered silicate nanocomposites where converting the

normally hydrophilic silicate surface to an organophilic surface has more importance due to polarity.

The most common way as introduced is the ion exchange functionalization with quaternary ammonium salts, which lower the surface energy and the hydrophilic character of the nanoclays, and make them more compatible with nonpolar POs. As a result, it is possible to increase the interlayer distance of the platelets and to allow better interactions with the polyolefin matrix. The morphology of the clay in the matrix, indeed, plays an important role on the final properties of the nanocomposite material, such as its mechanical behavior and thermal resistance. The higher thermal stability experimentally verified for PLSN have similar microstructural reason with the barrier properties that dispersed clay layers form tortuous path for the diffusion of the hot gases and aid the formation of char.

For the preparation of PO–organoclay nanocomposites, two approaches have been applied; in situ intercalative polymerization and melt-compounding. Although the first offers more homogeneous composites with a better dispersion of the silicate layers, the second is usually preferred because the in situ polymerization leads to polymers of low molecular weight. The dispersion attained by the in situ polymerization method is also thermodynamically unstable.

To promote the dispersion of clays in POs, the addition of functionalized polar groups on the chains in small quantities has been proposed. The functional group is expected to anchor to the clay surface and the polymer chain provides a favourable enthalpy and entropy of mixing with the polymer matrix. Simulation studies also showed that increased polymer-filler attractive interactions (functionalized polymer matrix) may create bridges between adjacent silicate layers [152]. Grafting of polar functional groups like maleic anhydride (MA) onto polymer chains has been suggested to improve the mechanical and rheological properties in PE and PP clay nanocomposites. The fraction of bound maleic anhydride in the compatibilizer is important for both exfoliation and good interaction [153]. The degree of interaction between polymer and nanolayers also affects the stability of morphology. The compatibilizer and organoclays help to lower the surface energy of the POs and clays, improve the wetting characteristics of the PP matrix, as well as facilitate the intercalation of hydrophobic polymers such as PO chains into the clay galleries.

The high degrees of exfoliation are promised by an alternative way that is compatibilizing POs for clay intercalation is based on the block copolymerization where one block of the copolymer is compatible with the layered silicate and the other with the PO matrix. This approach is similar to one used for compatibilization of polymer blends. A typical example for this kind of block copolymer compatibilizer must have a hydrophilic block compatible with clay and a hydrophobic block compatible to polymer.

### **1.8.1 Polyethylenes**

PE is one of the most widely used PO polymers. PE production is over 100 million tons per year worldwide as a result of its wide application. PE is the world's largest volume thermoplastic due to its attractive properties like low cost, good recycling performance, good processability, nontoxicity and biocompatibility, and finds wide use in packaging, electric insulation, consumer goods, pipes, etc [154]. Like other POs it have a low surface free energy due to its non-polar character, so the lack of miscibility with polar polymers and low value of interaction polar surfaces which causes poor mechanical properties and morphologies of its blends and weak adhesion to polar surfaces [155].

PE is only an abbreviation of different PE products at these days. That is, PE belongs to a family of products with diverse performance, such as high-density polyethylene (HDPE), linear low-density polyethylene (LLDPE), middle-density polyethylene (MDPE), linear high-density polyethylene (LHDPE), etc. If PE is divided according to its applications, there are PEs for special applications, such as PE for cable application, blown-film PE, casting-film for food package, ultra-high-molecular-weight polyethylene (UHPE) for pipelines or man-made skins etc [156]. Although it has so many applications and advantages, PE has its disadvantages, such as poor stiffness, low-temperature toughness and low melting behavior, which have left a great opportunity for investigators to improve the PE properties. Low density polyethylene (LDPE), a widely used packaging material, seems to be specially attractive for nanocomposite preparation, mostly due to the expected improvement of barrier properties [157].

Many of the properties of PE and most of its properties below the melting point depend largely on its crystalline content, which in turn depends essentially on the

number of branches rather than their length. Crystallinity in PE is primarily a function of the number of branches along the chain. As more branches are introduced, disruption becomes greater and crystallinity decreases rapidly [158]. At an extremely high degree of branching, PE would become an amorphous material. Increased crystallinity increases hardness, modulus, strength, abrasion and wear resistance, creep resistance, barrier properties, shrinkage, and density. Low crystallinity offers good processability, economical melt processing, and good thermoforming capability [159].

Probably the most important and significant single mechanical measurement to be made on PE is the determination of elastic modulus or ‘stiffness’. The stiffness of PE increases linearly with density and depends on temperature. The properties of PE are generally correlated also to density rather than crystallinity. Yield strength, tensile strength, and elongation at break are mechanical properties that are particularly important in terms of practical applications. They represent the maximum elastic strength, the ultimate strength, and the amount that the PE can be drawn, respectively. These are commonly determined from stress–strain curves. Increasing density causes an increase in tensile strength, as does an increase in molecular weight. Impact strength can be defined as the amount of energy that the PE can take up before some permanent damage is done. The area under the stress–strain curve, i.e., approximately the product of tensile strength and elongation, can be somewhat arbitrarily taken as the ‘impact strength’. The impact strength increases rapidly with molecular weight in PE.

### **1.8.2 Polyethylene compatibilizers**

Nylon6 seems to have good affinity for the silicate surface, mostly by hydrogen bonding, and as a result very high levels of exfoliation can be achieved in this matrix provided the extruding conditions and melt behaviour are properly set. On the other hand, non-polar PO segments that have not any interaction with the polar silicate surface, and in this case, increasing the number of alkyls on the onium improves dispersion of the organoclay in the PO matrix since a larger number of alkyls causes the possible unfavorable PO-silicate interaction to be lower and increases the number of more favorable PO-alkyl contacts. Even at the best of synthesis conditions exfoliation of organoclays in neat POs like polypropylene (PP) or PE is not very



good and far less than that observed in nylon, polyurethanes, and some other polar polymers [160].

One of the most important method on improving the PE polar properties is grafting functional groups on polymer to introduce intermolecular interactions (hydrogen bonding) with polar polymers and higher interaction between PE or a polar surface. This method is known as the compatibilizer precursor (CP) preparation. Compatibilizers of PEs can be prepared by the modification of POs by grafting small polar functional groups like acrylic acid (AA), glycidyl methacrylate (GMA), maleic anhydride (MA), diethyl maleate, industrial ionomers and itaconic acid (IA) as pendant units or short-chain branches [161-164]. Maleic anhydride grafted POs have been widely used as interfacial agents and more recently, the compatibilizer family suitable for POs has been enlarged by ethylene-acrylic acid copolymers, ethylene-methacrylic acid copolymer, oxidized POs have been used as compatibilizers instead of the classical maleic anhydride grafted PEs. Gaylord reported formation of single and oligomeric grafts during grafting of maleic anhydride onto POs [165]. Pesetski and Yazdani-Pedram have shown grafting of IA on PE with high grafting degree and low crosslinking [166,167].

Blending has acquired importance in improving the performance of olefin based polymeric materials. It has become an economical and versatile route to obtain polymers with a wide range of desirable properties. In order to ensure homogeneity in blends at microscopic level, it is necessary to reduce the interfacial tension, so that the characteristics of blend components are improved or at least retained. These modified polyolefins are mostly used for improving miscibility of the components of the blends, stronger interfacial adhesion, decreased surface tension between the phases [168,169]. As a result, better compatibility of components enhancing the adhesion of PE to high energy surfaces, preparation of special structures like being core materials in sandwich structures, in addition to enhanced wettability, and the hydrophilicity are achieved.

The blends of PE and other thermoplastics, such different type PE, polypropylene (PP), polylactide (PLA), polyamide-6 (PA-6), rubber, and other commodity polymers reported several times, but the blend of PE and its functionalized counterpart has not been systematically studied [170-172]. These studies have demonstrated that the addition of CPs functionalized with maleic anhydride into the PE/PA blends greatly

improves the blends properties by strongly enhancing the dispersion of the minor phase droplets, and improving interfacial adhesion.

Compatibility and mechanical properties of a PE/chitosan composite were improved by using PE-g-AA in place of PE. The blending of PE-g-AA with chitosan leads to the formation of an ester carbonyl and an imide functional group not present in PE/chitosan. It is showed that high-density polyethylene (HDPE) modified with glycidyl methacrylate (GMA) enhanced the miscibility of HDPE/starch blends. PE-g-GMA decreased the MFI values and increased the tensile strength in all blends, indicating an improved interfacial interaction between the phases of the blends [173,174]. Maleic anhydride grafted LDPE is among the most common compatibilizers used for the blends as mentioned above a blend of hydrophobic non polar LDPE and hydrophilic polar starch have inferior mechanical properties owing to poor adhesion between the two phases. This modified LDPE has now polar carboxylic functional groups which can effectively react with the hydroxyl groups of starch. The LDPE/starch blends compatibilized by LDPE-g-itaconic acid exhibited better mechanical properties as compared to their uncompatibilized counterparts [175]. A naturally obtained carboxylic acid, i.e., itaconic acid was grafted onto LDPE, thereby introducing a polar group on LDPE. This was used as a compatibilizer for the blends.

It is also reported that the appropriate selection of a compatibilizer can be used to create a material which exhibit a stable, fine distribution of the dispersed phase within the matrix phase by reducing the interfacial tension between the blend components. By this way, the improvement of the morphology and mechanical properties of the blends can be achieved by adding the compatibilizer. Maleic anhydride has been reported to improve adhesion of coating of steel and aluminium due to its high polarity[176].

Finer dispersion of stacked fillers in the LDPE matrix is achieved as the amount of anhydride groups in the copolymers increases a studies have shown that the addition of dry starch granules to low density polyethylene (LDPE) follows the general trend for filler effects on polymer properties. The modulus increases due to the stiffening effect of the starch granules and the elongation decreases as the starch content is increased. In pioneering work, Griffith reported on the preparation of starch-filled PE composites. It is shown that branching and high grafting ratios in PE compatibilizers

prepared by using MA can lower degree of crystallinity, in addition to the nucleation of PE-g-MA and simultaneously produced more defects in PE crystals [177].

It is successfully proved several times experimentally that, the CP synthesized by using MA, GMA, IA and AA can be used in preparation of successful PLSN [178,179]. Attractive interactions between the functional groups of polymer and organic modifier and simultaneous repulsive interactions between modifier and backbone of polymer result in conformational changes in polymer, which causes disruption of periodicity of polymer manifesting in changes in crystallinity of polymer. Only the functional groups of PCs undergo attractive interaction with the organic modifiers in PCN. The existence of an exothermic heat of mixing between the organic amine and the polymers seems to be the key to intercalation of the polymer melt. Thus, the polymer and surface experience an attractive interaction. As the polymer diffuses through the energetically favorable gallery, it maximizes contact with the two confining clay layers. It was found that PCL-clay interactions account for slightly less than half (about 2/5) of the PCL-surfactant interactions [180]. Since PCL is more polar than POs, the interaction between organic modifiers and CPs of PEs will be more important quantitatively to prepare polymer-layered silicate nanocomposites.

Maleic anhydride grafted PP (PP-g-MA) is ascertained to mix well with certain organoclays to form nanocomposites. In addition to the architecture of the alkylammonium surfactants, the loading of the surfactants in the organoclays has also been found to exert an important influence on the clay dispersion in the PP matrix. The most common way used is preparing a masterbatch of the graft copolymer, PP-g-MA, with the OMMT and then combining this with the virgin polymer so that the maleic anhydride content is not too high.

Despite the fact that experimental results were not precise enough to permit a quantitative comparison they accounted for the improvement of the interaction energy in the presence of maleic anhydride interact with organic modifier strongly bonded to the clay surface. With increasing content of PE-g-MA and anhydride functionality, enhanced exfoliation and intercalation was achieved. However, PE-g-MA is usually of low molar mass because the free radical grafting process is often accompanied by chain scission and some of the added compatibilizers are oligomers. The grafted maleic units also lead to reduced crystallinity. At high maleic anhydride

content, it was determined that the miscibility between PP-g-MA and PP is also no more granted. Hence, the addition of large quantities of PP-g-MA has consequences for the crystallinity and mechanical properties of the polymer.

### **1.8.3 Synthesis and properties of polyethylene nanocomposites**

Most of the investigations on PE nanocomposites focused on the synthesis, morphology, and mechanical properties of the composites. There are several studies have examined the feasibility of melt intercalation for preparing better exfoliated PP-clay nanocomposites with various compatibilizers and characterizes their resulting physical properties. By contrast, little research has focused on the melt intercalation of PE-clay because of the relative difficulty of preparing nanocomposites using this method.

PP nanocomposites mostly prepared by using organo-MMTs and maleic anhydride-grafted PP as compatibilizers [181]. These organoclay based nanocomposites were prepared by melt mixing of PP of different molecular weights and modified PP grafted with different percentages compatibilizers.

Alternatively, the solution method has been applied to PE-clay nanocomposites. With regard to the PE-clay system, Jeon et al. employed a solution-mixing technique to prepare a nanocomposite with OMMT partially intercalated in the PE matrix [182]. PE-clay nanocomposites showed a fully exfoliated morphology only in-situ polymerization was performed. However, the solution method usually needs a large amount of solvent, which causes manufacturing difficulties as well as environmental problems.

Initial attempts to create the nonpolar polymer-clay nanocomposites by melt intercalation were based on the introduction of a modified oligomer to mediate the polarity between the clay surface and polymer. A partially intercalated-exfoliated PE-clay nanocomposite was successfully synthesized using the melt-intercalation method with PE-g-MA compatibilizer and a swelling agent. The XRD analysis and TEM observations depicted partially intercalated-exfoliated, well dispersed nanoclays in the nanocomposite.

Zhang and Wilkie also synthesized a PE-clay nanocomposite by melt intercalation using with and without PE-g-MA as a compatibilizer [183]. XRD patterns and TEM studies revealed that all hybrids had a mixed immiscible–intercalated structure and

there was better intercalation when PE-g-MA was combined with LDPE. Their results indicated that the clay in the composite was barely intercalated.

The clay exfoliation was achieved in LLDPE based system when the clay was properly chemically modified and maleic anhydride group content in compatibilizers was larger than 0.1 wt.%. Some increase of crystallization and melting temperatures together with the decrease of crystallinity were found in those nanocomposites.

The effectiveness of nanoclay exfoliation in LDPE based nanocomposite was determined to be lower than in HDPE based system because of more difficult penetration of branched LDPE macromolecules into clay galleries. The polarity and reactivity of polar groups give as a result better interfacial adhesion and subsequent mechanical performance. Intercalated HDPE-organoclay nanocomposite has been obtained successfully via a novel compounding process, namely, one-step melt intercalation, which directly starts from Na-MMT by a melt intercalation technique, using hexadecyl trimethyl ammonium bromide as a reactive compatibilizer. The melt-mixed nanocomposite was usually intercalated because of the PE to behave independently from the filler addition. Other works on melt-mixed PE and other nanocomposites based on nonpolar polymers have confirmed the poor dispersion of the clay and lack of exfoliation of the clay in these systems.

Wang et al. studied the preparation of LLDPE-clay nanocomposites using melt blending found that exfoliation of the clay in nanocomposites was promoted when the organic modifier on the clay had more than 16 methyl groups and the maleation level was higher than 0.1 wt%. Osman et al. conducted studies on high-density PE nanocomposites and suggested that complete coverage of the surface of the clay by the surfactant leading to high *d*-spacings also favored exfoliation [184]. Hotta and Paul also found better dispersion in nanocomposites of LLDPE with surfactants with two alkyl tails rather than with surfactants with a single alkyl tail because of the larger *d*-spacing in the clay caused by the bulkier surfactant [185]. They studied the influence of PE-g-MA addition on the mechanical and permeation properties of linear low density PE composites with octadecyl- and dioctadecyl-organoclays. The exfoliation, tensile modulus and yield strength were enhanced with increasing ratio of compatibilizer to organoclays. The dioctadecyl organoclay composites showed better dispersion and mechanical properties than those of the octadecyl-organoclays. Several other studies also indicated the beneficial effect of maleated PE and PP on

the exfoliation of the clay in PEs. It is then of great interest to improve the understanding of the role of the compatibilizers on these properties.

The gas permeability was also decreased by ca. 40% in the dioctadecyl-organoclays nanocomposites at 0.069 inorganic weight fraction and 13 wt% PE-g-MA. A good combination of properties, mechanical and barrier, was obtained with the metallocene-based functionalized PE polymers as compatibilizers. When MA grafted polymers were used as compatibilizers, better exfoliation and thus nanocomposite properties were expected when the molar mass was low and the MA content was adequate. This correlation does not necessarily hold in the case of metallocene-based functionalized PE compatibilizers. For these, other structural features such as the comonomer distribution, molar mass distribution, crystallinity, and crystalline structure could also be influencing the final nanocomposite properties.

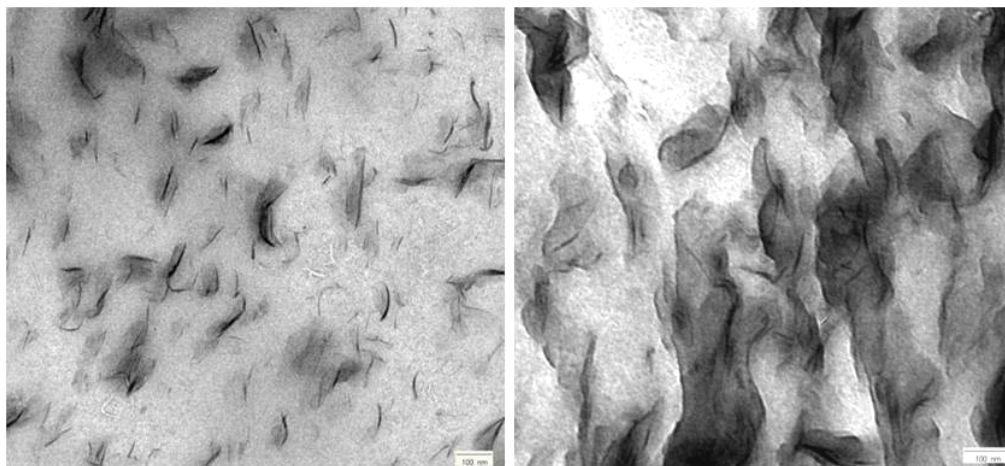


**Figure 1.13:** TEM of unstained and stained PP-clay nanocomposites [186].

It has been recently shown that by enhancing the contrast between the phases osmium tetra-oxide,  $\text{OsO}_4$  for staining, Compatibilizer-organoclay interface was enhanced in PP nanocomposites has been revealed by TEM images. This result is important which means that compatibilizer mostly placed on the organoclay surface since  $\text{OsO}_4$  is only react with maleic anhydride groups [186]. It is shown that up to the ratio of compatibilizer:organoclay 4:1; the compatibilizer polar groups preferentially placed on the surfaces of MMT platelets and there is a phase separation between bulk PP and compatibilizer (Figure 1.13).

However, for the PE-clay system, the relationship between the properties, in particular mechanical properties, and morphology is rather complicated and

inconsistent in open literature. Kato et al. reported that the addition of clay to LLDPE-PE-g-MA generally enhances yield strength and elastic modulus but slightly diminishes the ductility. They showed that the elongation at break of the hybrids was significantly decreased when clay loading reached 6% [187]. In studies on LLDPE, PE-g-MA and clay system, the effect of PE-g-MA was found to be significant for the clay exfoliation at low clay loadings.

The effects of the addition of polyethylene glycol as a compatibilizer have been investigated for HDPE-clay nanocomposites. The results indicate that the addition of polyethylene glycol has remarkably improved the dispersion of clay in the matrix and has enhanced the thermal stability of the compatibilized materials. Ethylene-glycidyl methacrylate copolymer (EGMA) has been employed as a compatibilizer for LDPE-clay and HDPE-clay nanocomposites. It has been demonstrated that the microhardness and flame retardant properties of the compatibilized LDPE and HDPE composites are significantly improved [188]. Zanetti and Costa prepared the LDPE-layered silicate nanocomposites in the presence of EVA, the resulting XRD patterns and TEM images indicated the effectiveness of EVA as a compatibilizer to facilitate the formation of intercalated nanocomposites [189].

The tensile properties of PE have been found to be improved when nanocomposites are formed with silicates, particularly the tensile modulus. Several studies reported the mechanical properties of PE-clay nanocomposites as a function of clay content and PE-g-MA compatibilizer. Zhai et al. studied the thermal degradation characterization of HDPE-organoclays and HDPE-g-MA nanocomposites [190]. The TGA results revealed that the onset of the degradation temperature for HDPE-organoclays nanocomposites with organoclays content of 1–5 wt% was increased from 426.5 to above 453.4 °C for HDPE.

Nanocomposites films made of POs and nanostructure fillers show great potential as packaging materials, for their increased barrier properties by reducing the oxygen-permeability rate at least by 10%, as compared to values obtained for neat POs, while still they are transparent. The capacity to act barrier for oxygen gas and humidity is clearly a function of both the concentration and the type of organoclay used. Next, just as in other PLSN, the efficiency of the system to work as a good barrier is directly related to the orientation and dispersion of nanofiller in the polymeric matrix. If the filler dispersion accomplished preferentially as single layers or



individual particles, it will promote a significant increase of the obstacles against the permeate gas, yielding a significative improvement in the barrier property.

Incomplete dispersion by forming agglomerates or tactoides of clay platelets is responsible for reduction in the barrier, thermal, and mechanical properties. Jacquelot found a reduction of approximately 10% in the oxygen-permeability coefficient for LLDPE-g-MA with the addition of 5 wt % nanoclay, proving to be efficient in enhancing the permeated-gas barrier property after its exfoliation [191]. Hotta and Paul found similar results in a study done by showing the improvement of the oxygen barrier property for LLDPE-g-MA and organoclay-compounds films. As POs are made of nonpolar methyl chains, as LLDPE, they are highly hydrophobic and can act as a good barrier for water vapour. However, Dumont et al. reported a high decrease in barrier properties against water vapor for a PO nanocomposite with maleic anhydride containing organoclay [192]. The addition of small amounts of maleic anhydride in the PO matrices could be a good strategy to enhance their hydrophilicity and interaction with the inorganic fillers, improving the compatibility of the PO-based system.

## **1.9 Theoretical Studies on PLSN**

In practice, many of the improved PLSN properties have been observed only in special cases, because they depend on a good compatibility between the polymer, surfactant and the clay, which is not easy to be achieved. There has been considerable interest in theory and simulations towards the synthesis and properties of PLSN, and they are also considered to be wonderful model systems to study the structure and dynamics of polymers with the new terms such as reinforcement, surface polymer interaction or behaviours in the confined environments theoretically (Figure 1.14).



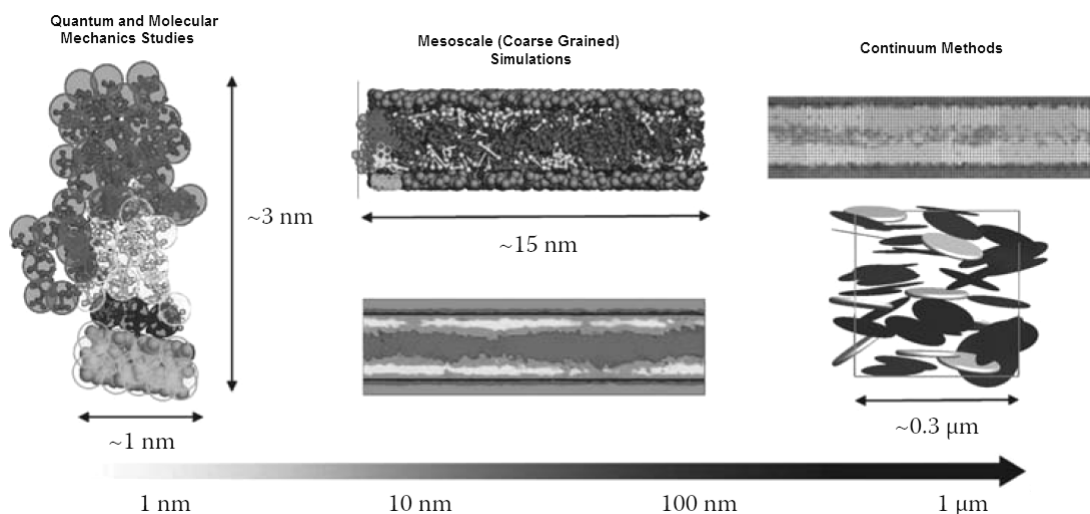


**Figure 1.14:** Theoretical methods used for PNCs [193,194].

(i) Fully atomistic simulations, which span length scales of the order of a few nanometers and time scales of the orders of a few nanoseconds, and include validated methods such as molecular dynamics (MD) and Monte Carlo (MC) techniques [195,196];

(ii) Mesoscale level simulations, in which the length scale is extended up to hundreds of nanometers and the time scale may reach up to hundreds of microseconds. These recent computational techniques substantially include Brownian dynamics (BD), dissipative particle dynamics (DPD), and mean-field density functional theory (MFDFT) [197,198];

(iii) Micromechanical simulations, which basically refer to the well known micromechanical and finite-element method calculations. The most popular technique so far employed in PCN characterization is finite element method, which is a general numerical method for obtaining approximate solutions in space to initial-value and boundary-value problems, including time-dependent processes. It uses preprocessed mesh generation, which enables the model to fully capture the spatial discontinuities of highly inhomogeneous materials, and also to incorporate nonlinear tensile relationships into analysis.

Theoretical studies were conducted especially in last years to solve micro interactions, dynamical, structural questions asked by experimentalists. Vaia and coworkers started these calculations by a meanfield statistical lattice model for the evaluation of the effects of various aspects of polymer and clay-organoclay on

nanocomposite formation [199]. Calculations based on the mean field theory agree well with experimental results that entropy losses associated with the confinement of a polymer melt during nanocomposite formation; this process is allowed because there is an entropy gain associated with the layer separation, resulting in a net entropy change near to zero. Thus, from the theoretical model, the outcome of nanocomposite formation via polymer melt intercalation depends primarily on energetic factors, which may be determined from the surface energies of the polymer and organoclay. Based on the Vaia and coworkers general guidelines can be established for selecting potentially compatible polymer-organoclay systems.

Balazs used self-consistent field theory for addressing the thermodynamic and architectural requirement for intercalated and exfoliated nanostructures; by relating the particle-polymer interaction to free energy. She found that increasing the interaction strength decreases free energy and coupling the conformation of polymer and that of surfactants in organoclay and miscibility of the polymer increases with the increase in grafting density of the polymer, as well as with decrease in the length of the polymer chain [200,201].

Coarse-grained calculations showed that the intercalation process and interlayer swelling of clay require a moderate polymer-surface affinity. Increasing polymer-surface affinity slows down the flow of polymer into the interlayer space; and increasing polymer molecular length leads to the decrease of flow rate. As far as the PLSN technology is concerned MD and MC simulations have been used to understand binding energy between various components and to investigate the thermodynamic behavior of PLSN [202]. Mathematical and statistical mechanical modeling of organoclays and PLSNs has been used to describe the thermodynamics, structure energetics of organic molecules in the 2:1 layered silicates.

Micromechanical model for the prediction of the mechanical properties of PLSN have been developed several times. Micromechanical models like Halpin-Tsai functions based on the “effective clay particle” were then employed to calculate the overall elastic modulus of the nanocomposites [203]. Sheng used quantitative geometric dimensions of nanoparticles extracted from experimental measurements and stiffness from MD simulations, provide a basis for microscale modeling for mechanical properties of the clay particles [204].

### 1.9.1 Molecular Dynamics and Monte Carlo studies

MC and MD simulations were used to study the static, dynamic properties of PLSNs to hybrid formation and of intercalation of small molecules in layered materials are being conducted to provide additional insights into the mechanisms and important factors associated with intercalation. These methods improve our understanding of the microscopic environment of the interlayer. Vacatello carried out MC simulations on spherical nanoparticles for dense polymer melts [205]. The model incorporated off-lattice approximation and conformational distribution of the simulated chains, similar to that of real polymers.

Manias and coworkers also studied molecular dynamic simulation by firstly using to create initial polymer conformations of PS oligomers by rotational-isomeric-state (RIS) model. Conformations that fit in the interlayer gallery were taken, and the PS chains were equilibrated by an off-lattice Monte Carlo scheme that employed small random displacements of the backbone atoms and orientational biased Monte Carlo rotations of the phenyl rings; at the same time, the surfactants were equilibrated in coexistence with the polymer chains [206]. After equilibrium, MD simulations were analyzed to obtain the structure and density profiles of the intercalated polymer/surfactant films.

Lee and coworkers have presented an investigation of the molecular mechanism of polymer melt intercalation using molecular dynamics simulations [207]. They tried to find out the motion of polymer chains from a bulk melt into a confined volume.

Minisini et al. found that for functionalized PPs based PLSN, interaction of PP increases in the presence of specific functional groups in polymer [208]. They examined interactions between octadecyldimethyl 2-ethylhexyl ammonium MMT and PP using classical MD and showed the effect of maleic anhydride presence.

Fermeglia found similar trends as those identified by Minisini that with the increase in concentration of as the volume fraction of surfactant was increased, the binding energy decreases between polymer and clay and and increases between ammonium surfactant–clay and polymer–ammonium surfactant [209]. Luo et al. developed a model of exfoliated and intercalated PLSN by MD for predicting the modulus of the nanocomposites [210]. The effect of surfactant tail length on the morphology of PLSN was studied. Sinsawat et al. investigated the influence of parameters such as

temperature, polymer architecture, etc. on the morphology of PLSN by coarse grained MD simulations [211]. Using MD simulation, Gardebien et al. studied structural characteristics of poly( $\epsilon$ -caprolactone)-based PLSNs with varying densities of interlayer polymer chains to observed that the behaviour of the polymer and molecular organizations of PLSN [212]. The structure and energetics of the biodegradable PCL-organoclay composites have been simulated by Katti and co-workers [213]. Similar results were noted for the energetics of caprolactam in 12-aminolauric acid modified MMT by Sikdar et al. The organic modifier was found to lie parallel to the clay sheet, and strong non-bonded interactions occurred between the modifier and the polymer [90,214].

Recently, molecular dynamics simulation studies have shown that the dynamics of the polymer chains show radical changes at the interfacial region as shown experimentally before. For example, both the chain mobility and the chain relaxation times can be slowed by three tiems near mica clay surfaces [215]. Not only that, extensive surface forces apparatus experiments report how these novel dynamics of polymers between are face with viscosity increases, two values orders of magnitude higher than the bulk values solid-like responses to imposed shear, and confinement based frictious dynamics that suggest the existence of a pinned, immobilized layer adjacent to the confining mica surface.

### 1.9.2 Thermodynamics of PLSN

Thermodynamics provide the guiding rules for the formation of PLSN. In general, an interplay of entropic and enthalpic factors determines the intercation structure. Favorable enthalpy of mixing for the polymer-organoclay is achieved when the polymer-clay interactions are more favorable compared to the surfactant-clay interactions. For most polar or polarizable polymers that is the reason for the nanocomposite formation. For the overall process, in which polymer is exchanged with the previously intercalated solvent in the gallery, a negative variation in the Gibbs free energy is required. If we consider the equilibrium free energy of mixing in a system composed of polymer, surfactant and clay. The free energy of mixing is given by,

$$\Delta G = \Delta G_{\text{polymer-clay}} + \Delta G_{\text{surfactant-clay (organoclay)}} + \Delta G_{\text{polymer-surfactant}} \quad (1.2)$$

Thermodynamics also indicates the phase to which the nanofiller will interact. The situation becomes more complex since there is also head and tail groups for surfactant and also compatibilizer of the PEs. But still, these principle can be extendable to complex cases.

A negative Gibbs free energy is reported to be required for the process of solution intercalation, in which polymer is exchanged with the previously intercalated solvent in the gallery. Thermodynamics of solution intercalation show that entropy gained by desorption of solvent molecules, which compensates for the decreased entropy of the confined, intercalated chains is the driving force for the polymer intercalation into layered silicate. Intercalation only possible for certain polymer-solvent pairs by using this method. In solution methods, the driving force for the polymer intercalation into layered silicate is the entropy gained by desorption of solvent molecules, that equilibrated for the decreased entropy of the confined, intercalated chains. Polymers with little or no polarity into layered structures which are hard to intercalate, are good candidates for this method is, and resulted material usually used for production of polymer films with oriented clay intercalated layers.

Vaia and coworkers implement meanfield statistical lattice model successfully to solve thermodynamical issue for melt intercalation [216]. Contrary to solution process where entropy is the driving force for PCN formation, enthalpic component ( $\Delta H$ ) of the Gibbs free energy ( $\Delta G$ ) controls the thermodynamics in melt intercalation. Mechanism works by compensation of the entropy loss comes from the confinement of the polymer melt within the silicate galleries by the entropy gain comes from the increase in layer separation by intercalation of onium cations and polymer chains. A net entropy change must be near zero ( $\Delta S \approx 0$ ) for melt intercalation. But still favorable enthalpy needed for exfoliation due to hydrogen-like bonds, Lewis-acid/base interactions, dipole-dipole, and van der Waals interactions between between the polymer and the organoclay.

New hybrid nanocomposites that were thermodynamically impossible can be synthesized by melt intercalation which have many advantages over solution intercalation. Because direct melt intercalation can be highly specific for the polymer since it depends critically on interaction of constituents controlled by layered silicate surface functionalization, CEC of the clay and polar groups on the polymer.

Vaia and coworkers developed general guidelines for the successful melt intercalation for specific polymers. Firstly, interlamellar structure of the organoclays must be optimized in order to maximize the layer separation to increase interaction sites. Polymers with the greater the polarizability or hydrophilicity of the polymer do not need to much interlamellar spacing and long surfactant tails by this way. Structures-phase separated, intercalated and exfoliated morphologies were explained dependent upon the variation of the free energy of mixing by enthalpic and entropic factors. All the polymer chains were accepted to be tethered to the clay surface and energetic factors were separated for this model which were the main drawbacks.

Balazs and coworkers proposed a new model based on Fleer and Scheutjens theory to overcome the limitation of Vaia model [217,218]. They used self-consistent field (SCF) calculation to model the phase behavior of PLSN. Markov chain statistics with a mean field approximation calculations involve a planar lattice as clay where polymer chain segments were represented by lattice spacing. Model calculated interactions between two surfactant-coated surfaces lie parallel to each other and a polymer melt between the surfaces in the  $z$ -direction. As the separation between the clay layers is increased, polymer from the surrounding bath intercalate to the gap between these surfaces. Surfactants on the clay surface was represented with monodispersed end-grafted chains. Balazs and coworkers did not consider electrostatic interactions between components. They found that if Flory-Huggins interaction parameter between the polymer chains and the clay layers is attractive ( $\chi_{PC} < 0$ ), diffusion of polymer through the gallery is energetically favorable, it glues the two surfaces together as it moves through the interlayer by maximizing the attraction between them. This situation resulted in intercalated polymer and layered silicate structures rather than exfoliated structures. Contrary, when  $\chi_{PC} > 0$ , the polymer can separate the layers, as the chain tries to gain its own coiled conformation entropically [219].

On the other hand, newer studies revealed phase separated structures were formed when there was no attractive forces between clay layers and polymer matrices in the melt mixing of organically modified layered silicates with polymers. Manias and coworkers studies extended by Vaia modelled polymers entering 2 nm confined galleries of layered silicates as a function of polymer molecular weight and polymer-surface interactions [220]. They determined that the polymer-surface affinity is the

most crucial parameter for nanocomposite formation. Variation of the polymer-surface interaction was accomplished by changing the organoclay structure by varying the organic coverage or grafting interacting groups onto the polymer chain. The existence of an exothermic heat of solution between the organic ammonium and the polymers seems to be the key to intercalation of the polymer melt. Thus, the polymer and surface experience an attractive interaction. As the polymer diffuses through the energetically favorable gallery, it maximizes contact with the two confining clay layers.

According to Manias et al. dispersion sufficiently favourable enthalpic contributions to overcome any entropic penalties means that although there is a decrease in the conformational entropy of the polymer chains during the intercalation, this process is allowed because entropy loss can be compensated by enthalpic interactions between the polymer matrix and the silicates. On the other hand, when an organically modified MMT is dispersed in a polymer, two conditions may, in theory, compensate this entropic penalty. The new one consists of an increasing in the entropic content of the system due to an improved configurational freedom of the surfactant chains.

$$\Delta S = \Delta S_{\text{polymer}} + \Delta S_{\text{surfactant}} \quad (1.3)$$

### 1.10 Purpose of the Thesis

Polymer-organoclay nanocomposites attract a great interest due to their enhanced mechanical, thermal, gas-barrier, inflammability and other properties compared to the unmodified polymers. Because of the structure and geometry of clay nanofillers, these systems have extremely high surface-to-volume ratio between filler and polymer, which is not possible when more conventional fillers are used. Before addition of polymer to the clay, surface modification of hydrophilic clays through ion-exchange reaction by alkyl ammonium cations is needed to increase the hydrophobicity of the surface and also expand the layer or basal spacing that helps polymer chains to form intercalated and exfoliated nanocomposites. It was found that, the polymer-organoclay nanocomposite system is energetically more favourable than a mixture of the polyethylene and clay.

In the case of nonpolar polymer like PE, the interaction between the hydrophobic PE and relatively hydrophilic organomodified clay surface is not as strong as desired. To overcome this limitation, some functionalized PEs are used as compatibilizers to increase the polarity of PE chains and adhesive forces between PE chains and the organoclay. Non-polar interactions by polymer backbone atoms played a significant role in nanocomposite structure. POs which have polar functionalities are intercalated into the organophilic clay galleries and then the better dispersion of silicates into the POs can be achieved.

The strong interaction between the polymer and clay makes possible to prepare exfoliated clay layers in the PE matrix. For a highly nonpolar PE, it is hard to find experimentally the appropriate organic modifier for clay and compatibilizer for PE to ensure that clay is thermodynamically compatible with the polymer matrix. In addition, it is important to link the molecular structure to the morphology of the nanocomposite (clay volume fraction, degree of exfoliation, and alignment of the at clay surface) and to the desired property enhancement. Further development of polymer-clay nanocomposites depends on the understanding of the micro and macro structures.

Due to the chemical and structural complexity of PLSN, it is experimentally hard to determine intermolecular interactions quantitatively and their effect on the structure and properties. Computer modeling and simulations are the only tool for effective design of nanocomposites because of the chemical complexity and the restrictions on experiments. Modeling studies can help to generate new scientific understandings on material properties and allow virtually any number of structures only limited by computational capacity. Since molecular level structure and interactions are critical for determining the PLSN properties, molecular scale modeling and simulation methods which include quantum mechanics, molecular dynamics (MD) and Monte Carlo (MC) methods should be employed rather than microscale numerical studies and coarse grained studies. This makes us to search new modeling and simulation strategies for dealing with those challenges for PE-based clay nanocomposites. By this way, it would be possible to explain the hierarchical characteristics of the structure and dynamics of PLSN ranging from molecular scale, microscale to mesoscale by linking the molecular structure to the morphology of the



nanocomposite as a function of clay volume fraction, degree of exfoliation, and alignment and to the desired property enhancement.

The effect of grafting of different polar groups such as acrylic acid (AA), glycidyl methacrylate (GMA), maleic anhydride (MAH) and itaconic acid (IA) on the structure and cohesive properties of polyethylene chains were studied by Molecular Dynamics simulations in the first part.

Calculations were continued on the first principle calculations to pass the optimized geometries and atomic charges to the next steps which were MD and Monte Carlo simulations. The complexity and size of the organic molecules in polymer-organoclay nanocomposite systems is required the use of ab initio methods as a first step. Functionalized PE oligomers and alkylammonium groups with different alkyl length and head groups were modelled and optimized before simulations by using DFT methods in PW91 and B3LYP/6-31g(d,p) level. In this study, different Na-MMT clays models were optimized by plane wave (PW) density functional methods (DFT). Atomic charges were determined by fitting electrostatic potentials and optimized structures were subjected for the molecular dynamics simulation methods which were employed to understand dynamics and formation of nanocomposites, and also the interfacial interaction energies in nanocomposites.

The structural optimization starts with the first energy minimization where all atoms in the silicate layers interlayer were movable without any constraints under the periodic boundary conditions. The equilibrium structures of organoclays were compared with the experimental XRD results, and interaction energies between components were related to the mechanical properties of the prepared nanocomposites. Effect of alkyl ammonium chain lengths on the interlayer interactions and basal spacing were analyzed. The most stable positions of polar alkyl ammonium heads on the clay surface were found. Molecular mechanics and classical molecular dynamics carried out by using special force fields developed for silicates. The strategy of energy minimization and crystal packer optimization were changed depending on the type of intercalation (ion exchange reaction, ion-dipole interaction) and on the choice of intercalated cations or molecules.

Finally, we have simulated several molecular models of intercalated PE-clay nanocomposites to understand the effects of composition and their interactions on the mechanical properties. Molecular dynamics simulation method was used to

determine the interaction energy between organoclay and polymer. The results were then analyzed by calculating the total potential energy of binary and ternary interactions in the system of PE, MMT and surfactant. The effect of grafting and grafting ratio, alkyl ammonium chain length, structure of head groups and clay layer atomic charges on the nanocomposite properties were investigated in different time and length scales. The enhancement in experimentally measured mechanical properties was then correlated with the increased attractive interaction energies between the small functional groups of compatibilizer and organically modified clay. The most effective interaction between the components of nanocomposites were sought on the basis of mixing energies between components.

In summary, the following steps were achieved in these thesis.

- The role of compatibilizers was investigated by using MD simulation methods.
- Different Na-MMT clay models were optimized by PWDFT methods, then reactive sites and surface properties were assigned for the next steps.
- Effect of cation exchange capacities of clays and structure of surfactants on the organoclays was studied. Head group positions on the clay surface, basal spacing and interlayer behaviour of alkyl chains were analyzed for the equilibrium structures.
- Pairwise interaction energies and minimum energy geometries between surfactants, PE, compatibilizers and clays were found.
- MD simulations were conducted to analyze binding energies, structures of nanocomposites with respect to surfactant, clay, compatibilizer structures, and amounts.

## **2. A COMPARATIVE STUDY ON THE EFFICIENCIES OF POLYETHYLENE COMPATIBILIZERS BY USING THEORETICAL METHODS**

Polyethylene (PE) is one of the most extensively used polyolefin (PO) due to its low cost, good recycling performance, good processability, nontoxicity, high versatility and suitability for using in packaging, electric insulation, consumer goods, pipes, etc. Like other nonpolar POs, it has low surface free energy and poor miscibility with polar polymers. Its low affinity against polar surfaces give rise to weak interfacial interactions and therefore, poor mechanical properties. Besides, the syntheses of new polymer blends or composites containing PE with targeted properties become very limited [221].

The blends of PE with other thermoplastics, such as polyamide-6 (PA-6), polyethylene terephthalate (PET) and other petroleum based commodity polymers were reported several times especially for recycling processes of consumed plastic materials [222]. In some of these PE blends, ethylene vinyl acetate (EVA) was used as a polar counterpart. Recently, instead of petroleum based polymers, poly(lactic acid) (PLA) is used to prepare PE blends since PLA is a renewable natural thermoplastic used in drug delivery devices, food packaging due to its high biocompatibility, processability, good mechanical properties, and its transparency [223].

Since PE is a high molecular weight polymer, highly hydrophobic and have lack of functional groups recognizable by microbial enzymes and therefore have low susceptibility against biological attacks. In some of its composites, starch is used to make the resulting material more biodegradable. Usually, before blending with PE, starch is esterified to prepare starch acetate and phthalate to make it more hydrophobic, thermoplastic, crystalline and stable than unmodified starch.

The most versatile method for improving the polarity of PEs is grafting with functional groups which enable polymer to interact more with polar polymers or surfaces in PE based composites. The modified PEs (so called compatibilizers) are used to increase interfacial adhesion, decrease surface tension between the

interacting chains. PE compatibilizers can be prepared by grafting small polar functional groups like acrylic acid (AA), glycidyl methacrylate (GMA), maleic anhydride (MA), industrial ionomers and itaconic acid (IA) as pendant units or short-chain branches (Figure 2.1). Among the polar groups, MA has been widely used to prepare PE compatibilizer.

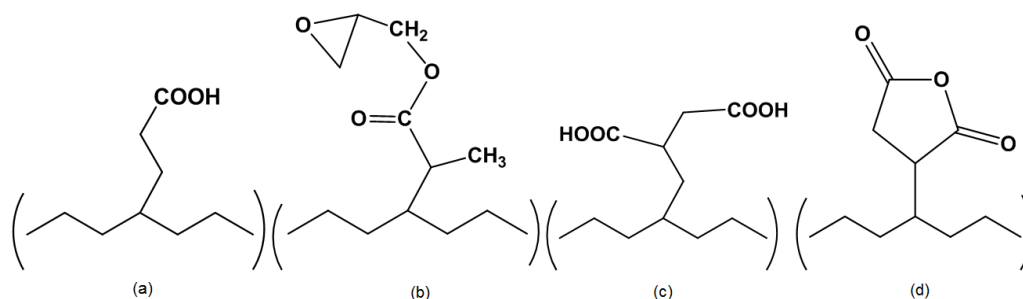


**Figure 2.1:** Structures of (a) PE-g-AA, (b) PE-g-GMA, (c) PE-g-IA, (d) PE-g-MA.

Gaylord reported the grafting of MA in the form of monomer and oligomer onto the PE backbone chain. PE-g-GMA decreased the melt-flow-index (MFI) values and increased the tensile strength in all blends of PE, indicating an improved interfacial interaction between the phases of the blends [224]. Microstructure analysis of the GMA grafted linear low density polyethylene (LLDPE) showed that grafting of a single molecule or short oligomers are possible. It is shown that the grafting of IA on PE with high grafting degree and low crosslinking is also possible. PE-starch blends have been prepared by using ethylene acrylic acid as a compatibilizer. Although there are enormous amount of experimental study on the preparation and properties of PECs as, the theoretical calculations are rather scarce. Until now, to our best knowledge, the miscibility behaviors of PECs with respect to pristine PE and their effects on composite properties has not been systematically studied.

Functionalization of polyethylene chains by grafting of polar groups onto backbones is the most versatile way for preparing polyethylene based compatibilizers (PECs). In this chapter, a series of theoretical studies were performed to analyze the structure, adhesion and mixing behaviors of PECs. The calculations on the blends of PECs with starch monomer (ST), starch acetate (STac), polyethylene terephthalate (PET), polyamide6 (Nylon6), polyvinyl acetate (PVA) and (PLA) were performed to understand the structural factors on the properties of polymer blends and composites at the molecular level. The effect of grafting of different polar groups such as acrylic

acid (AA), glycidyl methacrylate (GMA), maleic anhydride (MAH) and itaconic acid (IA) on the structure and cohesive properties of polyethylene chains were studied by Molecular Dynamics simulations (Figure 2.1). The mixing behavior of polyethylene with PET, Nylon6, PVA and biodegradable polymer PLA, ST and STac were investigated quantitatively by determining accurate interaction parameters using the extended Flory-Huggins Theory [225].

## 2.1 Theoretical Calculations

### 2.1.1 Simulations of polymer chains in amorphous cell

Amorphous cells were constructed for all of the pristine PE, PECs, and chosen polar polymers using the Materials Studio 5.0 software package [226]. Each cell contained four oligomer chains having 250 atoms, at the experimental densities. 20 different cells with 1000 atoms for each polymer type were prepared and minimized first for 5000 time steps by employing Molecular Mechanical techniques. COMPASS (Condensed-phase Optimized Molecular Potentials for Atomistic Simulation Studies) force field which is consistent and ab initio parameterized using extensive data for molecules in the condensed phase was used in all simulation studies [227]. Then, canonical (NVT) molecular dynamics simulations for 200 ps by using Ewald summation method for the long-range interactions were conducted and temperature was kept constant at room temperature using the Nose thermostat. Last 50 ps of the trajectories was stored at every 5 ps for the further analyses of nonbonded and cohesive energies from which the solubility parameters were calculated.

### 2.1.2 Determination interaction parameters and reactivities

According to Flory-Huggins (FH) Theory, the free energy ( $\Delta G$ ) of mixing for polymer chains per mole is given by the Eqn.1. In this equation it is assumed that the segments are randomly distributed and all lattice sites are occupied,  $\Delta G_{\text{mix}}$  per mole of lattice sites is calculated by using the volume fractions of the components ( $\Phi_i$ ) and the degree of polymerization of component i ( $n_i$ ).

$$\frac{\Delta G}{RT} = \frac{\Phi_i}{n_i} \ln \Phi_i + \frac{\Phi_j}{n_j} \ln \Phi_j + \chi \Phi_i \Phi_j \quad (2.1)$$

The first two terms represent the combinatorial entropy. This contribution is always negative, hence favoring a mixed state over the pure components. The last term is the free energy due to interaction. The mixing behavior of the oligomers was studied by calculating the  $\chi$  (chi) thermodynamic interaction parameter. If the FH interaction parameter ( $\chi$ ) is positive, this term favors microphase separated state.

In this work, mixing energy values were predicted directly from the chemical structures and charges of the studied systems by using a off lattice method which combined the extended Flory-Huggins (FH) model and molecular simulation techniques employing the force field based atomistic simulation methods which require accurate atomic charges implemented in the Materials Studio 5.0.

The geometries of the oligomers with 50-60 atoms and end groups saturated by methyl groups were optimized by the Density Functional Theory method at B3LYP/6-31G(d,p) level of theory and the electrostatic potentials (ESP), charges, dipole moments and the Fukui reactivity indices were calculated by the CHELPG method implemented in Gaussian 2003 software package [228].

Monte Carlo type minimizations of a large set of clusters composed of above units were carried out to obtain the number of nearest neighbor numbers (coordination numbers) of each unit pairs. The coordination numbers  $Z$  are not necessarily integer numbers. Head and tail atoms are choosen to be noncontacted to mimic the real polymer chain.  $10^7$  configurations were generated for the blends of PE, PE-g-AA, PE-g-MA, PE-g-GMA and PE-g-IA chains with polar counterparts to calculate the binding energy,  $E_{ij}$  which can be obtained from Boltzmann averages of structures for each pair as given in equation 2.2.

$$\langle E_{ij} \rangle_T = \frac{\int dE EP_{ij}(E) e^{-E/RT}}{\int dE P_{ij}(E) e^{-E/RT}} \quad (2.2)$$

The average energy of mixing and then  $\chi$  were obtained from  $E$  and  $Z$  values as shown in equation 2.3 and 2.4 [229].

$$E_{mix} = \frac{1}{2} \left( Z_{ij} \langle E_{ij} \rangle_T + Z_{ji} \langle E_{ji} \rangle_T - Z_{ii} \langle E_{ii} \rangle_T - Z_{jj} \langle E_{jj} \rangle_T \right) \quad (2.3)$$

$$\chi = \frac{E_{mix}}{RT} \quad (2.4)$$

### 2.1.3 Structural Properties of polyethylene compatibilizers

PE chains composed of 400 repeating units (800 backbone carbons) were modeled and they were brought to equilibrium in 2 ns at T=400 K employing molecular dynamics simulation technique using same force field explained above in canonical (NVT) ensemble without imposing periodic boundary conditions. Nose thermostat was used to keep the temperature constant. A simulation time step of 1 fs was used. The cut-off radius for nonbonded atom based interactions was 12.5 Å. The trajectories of the atoms were stored for every 5 ps at last 100 ps. The coiling tendency of the polymer chains were analyzed by calculating the radius of gyration ( $R_g$ ) as a function of the grafting ratios.

## 2.2 Results and Discussion

### 2.2.1 Simulations of polymers in amorphous cell

Nonbonded energies are the sum of the van der Waals (vdW) and electrostatic energies which are represented by the Lennard-Jones (9-6) and Coulomb potentials for the interacting chains. Cohesive energy ( $E_{coh}$ ) is defined as the increase in energy per mole of a material if all intermolecular nonbonded forces are eliminated in atomistic simulations given by Eqn. 2.5 and Solubility parameter ( $\delta$ ) is defined as the square root of the cohesive energy density ( $e_{coh}$ ) given in Eqn. 2.6.

$$E_{coh} = E_{isolated}^{nb} - E_{periodic}^{nb} \quad (2.5)$$

$$\delta = \sqrt{\frac{E_{coh}}{V}} = \sqrt{e_{coh}} \quad (2.6)$$

The nonbonded energies, cohesive energies as well as solubility parameters and their vdW and electrostatic components were given in Table 1. The good agreement between the theoretical and experimental solubility parameters observed for Nylon6, PVA, PET and PLA homo polymers and enabled us to calculate the solubility parameters of the PECs in the same manner.

Chemical compatibility between i and j chains is depends on the square of difference between solubility parameters,  $(\delta_i - \delta_j)^2$  as proposed by Hildebrand [230]. The relatively high difference between the solubility parameters of Nylon6, PET, PLA and PE and PE makes their mixing impossible. Hansen suggested the solubility parameters can also be splitted into parts representing dispersion, polar and hydrogen-bond interactions. Dispersion is represented by vdW solubility parameter ( $\delta_{vdW}$ ), polar and hydrogen-bond interactions by electrostatic solubility parameter ( $\delta_{elec}$ ). Both parameters are calculated using the corresponding energy components of the nonbonded energies. We have seen from Table 2.1 that the weak interactions between the nonpolar polymers were reflected in the calculated solubility parameters. The main contribution to the total solubility parameter of PE comes from the vdW ( $\delta_{vdW}$ ) part of the nonbonded energies and very small  $\delta_{elec}$  was obtained. The composites or blends of PE with incompatible polymer chains was characterized by the coarse morphology with large voids, fractured surfaces and poor adhesion between the phases in SEM analyses [231]. In addition, no interaction between phases in thermogravimetric responses in TGA and no change in  $T_g$  values in DSC were observed. The decrease of the elongation at break and impact strength were observed for the brittle PE composites where polar chains behave as defects inside the PE matrix.

**Table 2.1:** Nonbonded (vdW and electrostatic) and cohesive energies and solubility parameters of studied homopolymers.

Polymer	$E_{nonbonded}$ (kcal/mol)	$E_{vdw}$ (kcal/mol)	$E_{electrostatic}$ (kcal/mol)	$E_{Coh}$ (J/cm <sup>3</sup> )	$\delta_{vdW}$ (J/cm <sup>3</sup> ) <sup>1/2</sup>	$\delta_{electrostatic}$ (J/cm <sup>3</sup> ) <sup>1/2</sup>	$\delta$ (J/cm <sup>3</sup> ) <sup>1/2</sup>	$\delta$ (exp.) (J/cm <sup>3</sup> ) <sup>1/2</sup>
PE	-492.8	-492.1	-0.7	330.8	18.17	0.75	18.19	-
Nylon6	-666.1	-493.6	-172.5	512.9	19.50	11.52	22.64	24.25
PVA	-551.5	-498.0	-53.4	343.3	17.37	6.44	18.52	18.35
PET	-707.6	-651.7	-55.8	480.3	21.36	6.11	22.22	21.88
PLLA	-648.2	-584.3	-63.8	421.6	19.49	6.44	20.53	20.20
ST	-713.7	-272.3	-441.4	439.8	12.70	16.68	20.54	-
STac	-218.7	-153.1	-63.6	87.6	7.83	5.13	9.36	-

PVA have nonbonded, cohesive energies and also solubility parameter which are closest to that of PE's among the studied polar polymers. For this reason, ethylene



vinyl acetates (EVA) with different VA contents have been successfully used as compatibilizers in the composites and blends of PEs.

Starch has three hydroxyl (-OH) groups in its repeat unit (glucose) and naturally it has a high H-bond making capacity. This is why we observed the most negative nonbonded energy which is mostly due to the strong electrostatic interactions or H-bond interactions for starch. This also explains why the solubility of starch in polar solvents with high solubility parameter is high. When starch is transformed into the plasticized starch (STac), all of the nonbonded interactions decrease. The energies become less negative and electrostatic energy component approaches to that of the PE's indicating that the compatibility between STac and PE is enhanced.

**Table 2.2:** Nonbonded (vdW and electrostatic) and cohesive energies and solubility parameters of PECs at different grafting ratios.

Grafted PE	$E_{\text{nonbond}}$ (kcal/mol)	$E_{\text{vdw}}$ (kcal/mol)	$E_{\text{elec}}$ (kcal/mol)	$E_{\text{COH}}$ (J/cm <sup>3</sup> )	$\delta_{\text{vdW}}$ (J/cm <sup>3</sup> ) <sup>1/2</sup>	$\delta_{\text{elec}}$ (J/cm <sup>3</sup> ) <sup>1/2</sup>	$\Delta$ (J/cm <sup>3</sup> ) <sup>1/2</sup>
PE-(AA)	-414.4	-403.9	-10.5	289.7	16.80	2.70	17.02
PE-2(AA)	-439.8	-401.9	-37.7	282.7	16.08	4.92	16.81
PE-3(AA)	-449.8	-386.7	-63.0	272.8	15.32	6.18	16.52
PE-(GMA)	-428.7	-425.8	-2.9	282.1	16.74	1.36	16.80
PE-2(GMA)	-437.1	-433.46	-3.7	251.6	15.80	1.44	15.86
PE-3(GMA)	-490.5	-478.4	-12.6	255.3	15.78	2.49	15.98
PE-(MA)	-460.8	-456.7	-4.1	314.9	17.67	1.66	17.74
PE-2(MA)	-447.8	-437.9	-10.0	276.0	16.43	2.47	16.61
PE-2(MA) <sub>2</sub>	-471.6	-456.6	-15.0	251.2	15.60	2.83	15.85
PE-2(MA) <sub>3</sub>	-522.0	-486.8	-35.2	244.9	15.11	4.06	15.65
PE-3(MA)	-512.2	-488.6	-23.6	292.7	16.71	3.67	17.11
PE-(IA)	-406.5	-376.2	-30.3	270.2	15.81	4.49	16.44
PE-2(IA)	-479.2	-396.0	-83.2	280.9	15.24	6.98	16.76
PE-3(IA)	-537.9	-416.8	-121.2	287.0	14.91	8.03	16.94

The same properties are given for the PECs in Table 2.2. Degree of grafting of polar groups (AA, GMA, MA and IA) is increased from 1 to 3, and also the polymerization degree of grafted MA is increased from 1 to 3. Decrease in vdW energies and increase in the electrostatic energies of all PECs were observed when compared to ungrafted PE. The enhancement of the electrostatic interactions and  $\delta_{\text{elec}}$  becomes more pronounced when more polar groups are incorporated into the PE

backbone. The same trend is also observed when the polymerization degree was increased. IA acts as a most powerful polar groups grafted which makes the whole PEC more polar due to the two carboxylic acid groups. AA has one carboxylic acid group and it is the second effective polar group. PE-g-IA and PE-g-AA make more hydrogen bonds when interacting with the functional groups of the other chains and additionally dipole-dipole interactions of these groups are larger than that of the MA and GMA. The compatibilization mechanism of IA and AA are mostly dependent on the physical nonbonded interactions whereas GMA and MA are chemically more reactive species due to the ring opening possibility during the interaction.

### 2.2.2 Determination interaction parameters and reactivities

Solubility parameters and intermolecular energies can give idea about the possibility of mixing. However, these parameters only contain interactions between same components ( $E_{ii}$ ,  $E_{jj}$ ). Exact mixing of PE and PECs with polar polymers can be characterized by Flory-Huggins interaction parameter,  $\chi$  which is determined from the nonbonded energies between different counterparts ( $E_{ij}$ ) and coordination numbers. Prior to the calculations, the geometries of PEC oligomers were optimized and the atomic charges were calculated at B3LYP/6-31g(d,p) level. The optimized geometries and atomic charges of the modeled PEC oligomers are given in Figure 2.2. All charges are localized onto the functional group atoms. The charge values of the PE backbone atoms are very small and show no difference when the grafted functional polar group changes. However, bending of the PE skeleton by 10-20° points out some changes in the crystalline behavior of PE would be expected upon grafting.

The delocalization of charge on the functional groups is of structural importance and has some consequences as it will be discussed later. The 3D electrostatic potential energy surfaces of the PECs are given in Figure 2.3. The regions with high potentials are shown in yellow and with low potentials are shown in blue. High potentials like atomic charges are concentrated on the functional groups. MA having more continuous electrostatic potential is more susceptible to the interaction with other polar polymers and surfaces.

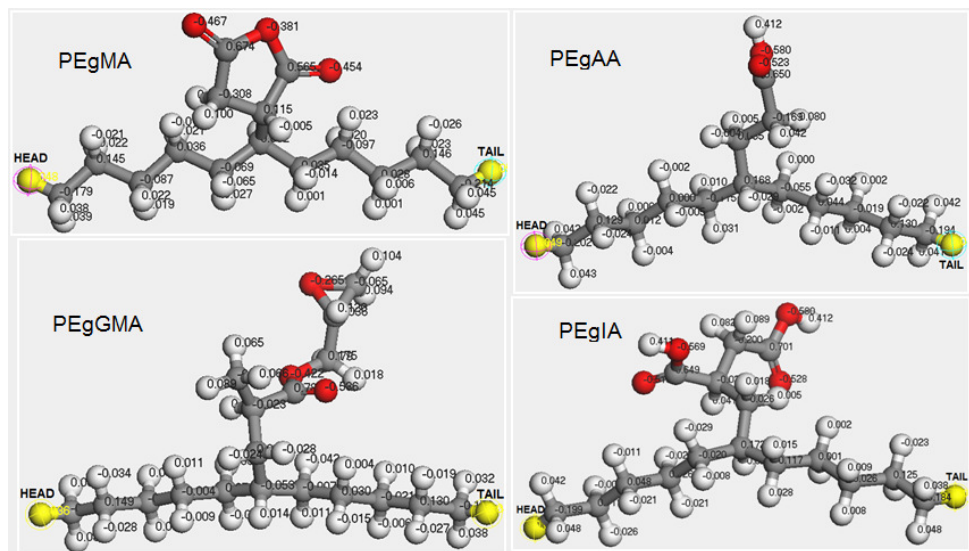


**Figure 2.2:** Optimized geometries and atomic charges of the modeled PEC oligomers.

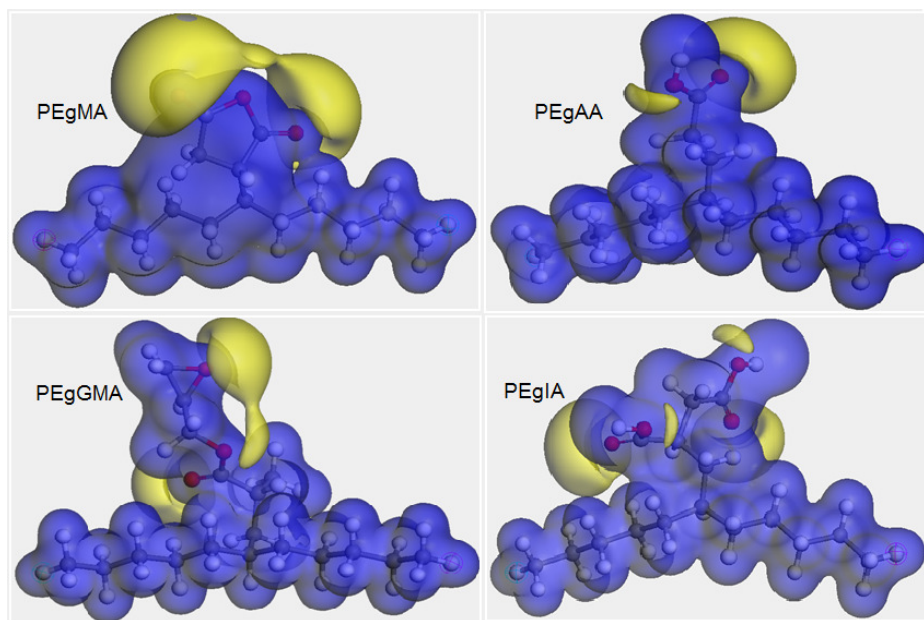


**Figure 2.3:** 3D electrostatic potential surface of PECs (high ESP: yellow, low ESP: blue)

Chemical reactivities of the PECs were studied by calculating the Fukui indices [236] which were clearly shown in Figure 2.4 where susceptible sites for electrophilic attacks are colored in yellow for the nucleophilic attacks are colored in blue. High susceptible group for the electrophilic attack was observed to be the epoxy group of PE-g-GMA with the value 0.350 which was confirmed by the experiments reporting that GMA grafted polymers are reactive compatibilizers in polyester blends. It is

believed that the epoxy groups react with hydroxyl and carboxyl end groups which behave as nucleophiles. The reactivity of IA and AA is mainly due to the carboxyl groups resulted in enhanced MFI as shown experimentally.

The reactivity of MA against  $\text{-NH}_2$  end groups of nylon was higher than that of AA. This fact is also shown by our results which find the Fukui indices for the susceptible sites for nucleophilic attack are 0.567 and 0.450 for MA and AA, respectively. Other reason for MA has higher reactivity than AA is the possibility for its easy transformation to an acid by hydration. In our calculations, the solubility parameters and the Fukui reactivity indices indicated that IA and AA mostly accomplish their compatibilizing role by electrostatic interactions and hydrogen bonding, whereas GMA and MA serve more as reactive compatibilizers.

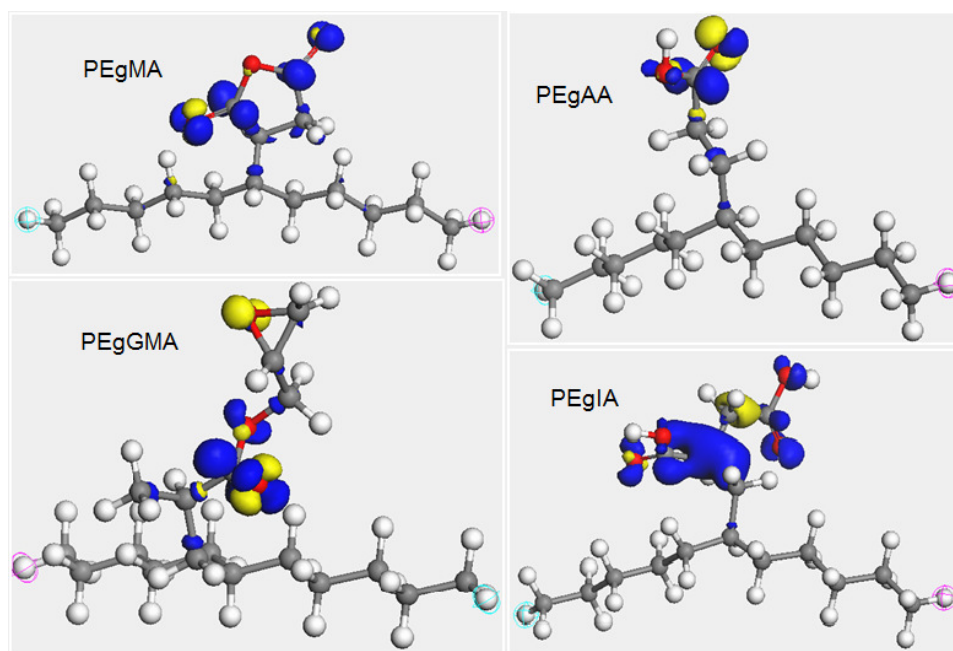


**Figure 2.4:** Fukui reactivity indices of PECs. (electrophilic attack sites are yellow and nucleophilic attack sites are blue in color.)

The mixing behavior of PEC containing PEs with Nylon-6, PET, PVA, PLA, ST, and STac were studied quantitatively by determining the interaction parameters,  $\chi$ . Although only the  $\chi$  values above 400 K are more meaningful for experimentalists since the processing of PE is accomplished at high temperatures above its melting temperature, in our calculations, the temperature is changed from 250 K to 500 K.

In Figure 2.5, we observed that all  $\chi$  values are positive, i.e., favoring the phase separation and they become less positive with increasing the temperature, favoring

mixing at some extent. The differences in the  $\chi$  parameter depending on the functional group in PECs are more prominent at room temperature and slowly disappear and  $\chi$  values approach to comparable values at higher temperatures. Heating favors the mixing state and phase behaviors of PE/PEC blends are expected to be similar at elevated temperatures. IA and MA containing PECs have higher  $\chi$  value than AA and GMA containing PECs. This result can be correlated with the polarity of the functional groups as seen in the calculated dipole moments in Table 2.3. The highest interaction parameter of PE-g-IA with PE chains can be related with its bifunctionality with more conformational freedom than cyclic MA group and its larger molar volume.

**Table 2.3:** Dipole moments of PEC oligomers.

	PE	PE-g-GMA	PE-g-AA	PE-g-MA	PE-g-IA
Dipole Moments (Debye)	0.05	0.90	1.80	4.76	2.43

Due to the incompatibility of the chains at room temperature, it can be expected that the functional groups reside more on the surface rather than present in the bulk and become available for interaction with polar groups at the interfaces as will be proven later.

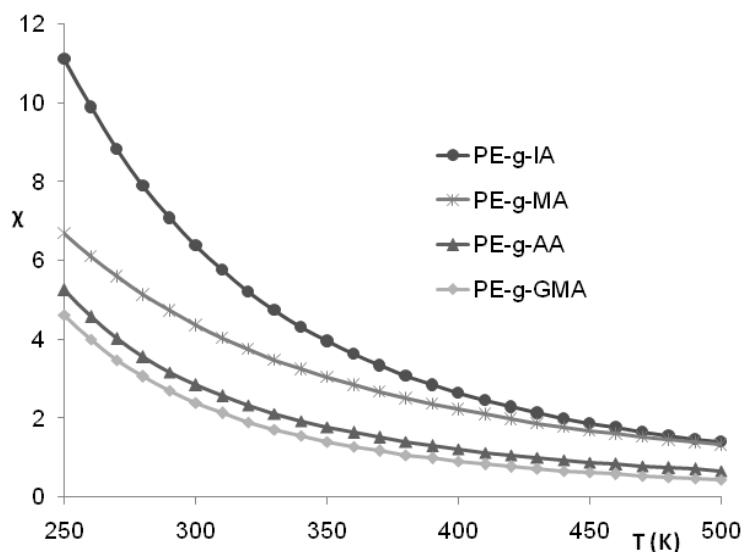


**Figure 2.5:** Change in the  $\chi$  interaction parameters between PE and PECs with temperature.

$\chi$  parameters for the Nylon-6 with PE and PECs are given in Figure 2.6. The interactions get stronger if the PE is grafted. The highest compatibility is observed between the Nylon-6 and PE-g-MA chains even at low temperatures and the  $\chi$  parameter for this interaction seems to be unaffected by the temperature. The compatibilizing role of PE-g-IA and PE-g-AA approaches to that of PE-g-MA at high temperatures. Generally, mixing of PE with polyamides was studied several times experimentally. The decrease in the disperse phase area in the SEM images due to the adhesion of the interacting chains and improvement in the mechanical properties were reported for Nylon-6/PE blends containing PECs. In a recent study, PE-g-GMA, PE-g-AA and PE-g-MA were used to prepare Nylon6-LDPE blend and an improvement in the mechanical properties by adhesion between phases observed by SEM analysis for all compatibilizers. As our calculations showed, PE-g-AA and PE-g-MA was found to give better results than PE-g-GMA. It was also found that PE-g-MA serves as a best compatibilizer among industrial compatibilizers by reducing the interfacial tension and decrease of the dimension of the dispersed particles drastically [232]. By taking the advantage of shear, temperature, reactivity of MA groups and the low interaction parameter between PE-g-MA/Nylon-6, it is possible to prepare well mixed nylon-PE blends with enhanced mechanical properties.

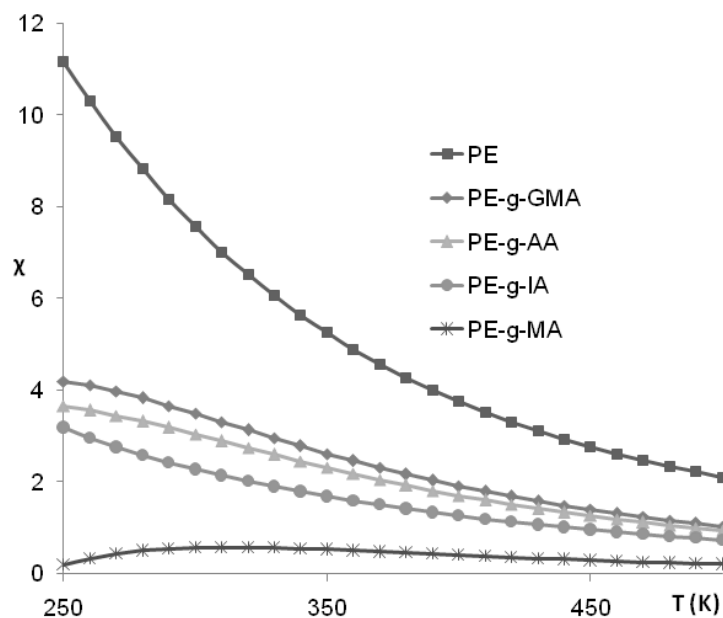


**Figure 2.6:** Change in the  $\chi$  interaction parameters between Nylon-6 and PECs with temperature.

The PET and pristine PE interaction has the highest  $\chi$  parameter at all temperatures and the interaction gets stronger when PECs are added. At above 400 K, all PECs except PE-g-MA have similar performance. The PE-g-MA enhances the interaction slightly more than the others (Figure 2.7).

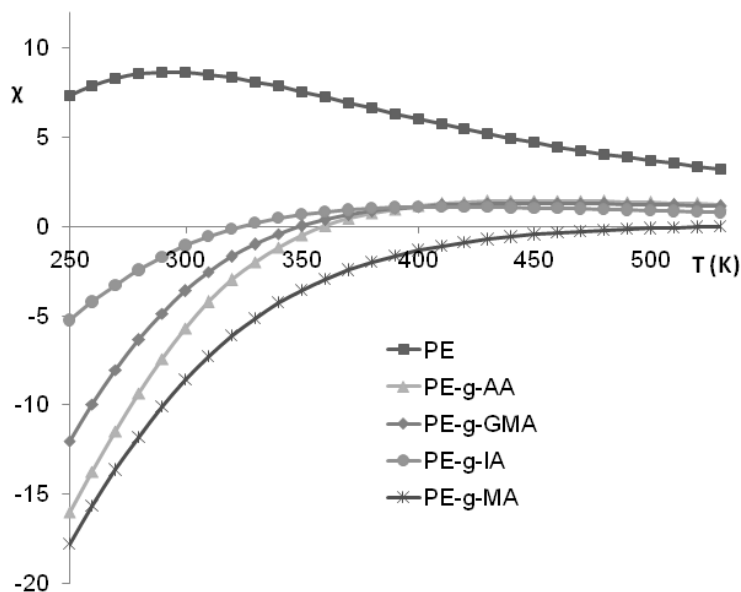


**Figure 2.7:** Change in the  $\chi$  interaction parameters between PET and PECs with temperature.

A decrease in the melt viscosity of EVA/LLDPE systems was observed experimentally due to the separation between the polar EVA and the nonpolar LLDPE phases at the interface. Upon compatibilization by PE-g-MA, the viscosity was increased and the dispersed domain size was reduced which indicated an increase in interfacial interaction. Similar result that pure PE has the highest  $\chi$  parameter or least interaction with PVA and addition of compatibilizers lowers the  $\chi$  parameter was obtained and shown in Figure 2.8. Although the performances of PECs are close to one another at high temperatures, they follow the order: MA>IA>AA>GMA. PE-g-MA compatibilized PE can mix with PVA at all temperatures and can be used synergically with EVA for the PE blends with polar polymers.

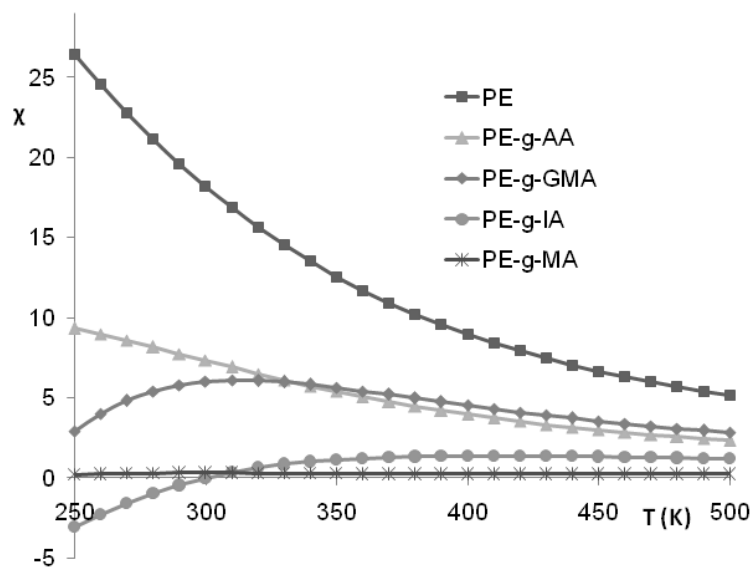


**Figure 2.8:** Change in the  $\chi$  interaction parameters between PVA and PECs with temperature.

Poly lactide is most studied biological lactic acid based thermoplastic and it is found to be immiscible with PE due high  $\chi$  parameter at room temperature (Figure 2.9). This was supported by the SEM results which showed clear and sharp boundary between the PLA and LLDPE phases and proved weak interfacial adhesion between them [233]. Mixing of PE and PLA phases can be achieved over melting temperatures. We found that the temperature at which the phase separation starts, is 350 K. Although the  $\chi$  parameter increased with temperature, the all PEC added PE/PLA blends are miscible at all temperatures and the minima at around 250-300 K have no physical meaning. Our calculations demonstrated that PE-g-IA with higher interaction parameter would be a better alternative to the traditionally used PE-g-MA compatibilizer since it has as same functional group as PLA.

PE-g-AA showed second enhanced interaction and better than PE-g-MA and PE-g-GMA. PE-g-GMA causes decreased interfacial adhesion due to reactive compatibilization shown also experimentally. Our results are consistent with the experimental FTIR results that indicated a shift due to hydrogen bonding in the carbonyl group after adding PE-g-MA compatibilizer as well as some interactions observed by DSC analysis. All compatibilizers ensured negative interaction parameter make us to claim PE-PLA blend or ternary blends of them can replace PE composite blends of PET and polyamides in the future.



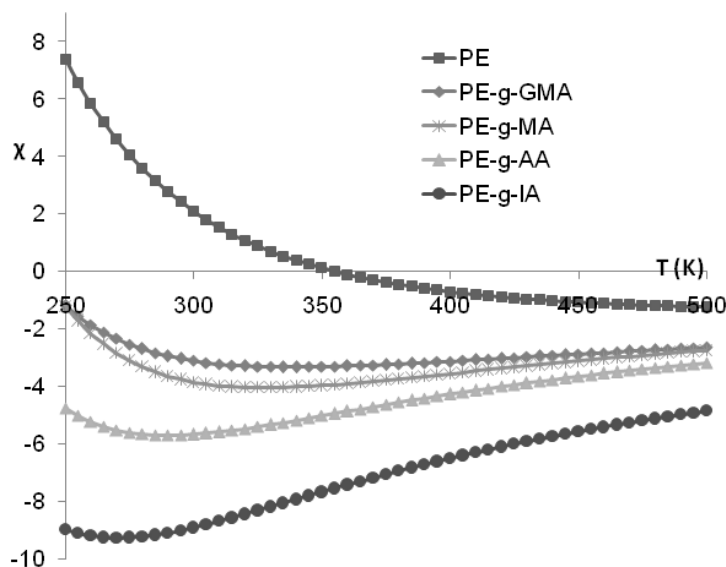


**Figure 2.9:** Change in the  $\chi$  interaction parameters between PLA and PECs with temperature.

Starch having with highly polar hydroxyl groups is known as a immiscible filler with polyolefins and naturally have positive  $\chi$  parameters as shown in Figure 10. SEM images of the same system showed poor interaction and large interfacial tension in their composites.

All compatibilizers except PE-g-IA have significantly low  $\chi$  parameters which are very close to zero and not changing with temperature. Although the interaction increases between PE-g-IA containing PE and ST with temperature, its value is still higher than the other PECs. Due to the strong interaction between the functional groups of compatibilizers and the hydroxyl groups of starch, the compatibilized blends showed better interfacial adhesion between the polymer and starch phases and thus better mechanical properties. The improvement in the modulus and tensile strength for PE-g-MA compatilizer can not be explained only by lowering of interaction parameter.

Starch particles not only placed between the interface but also embedded into the PE matrix that can be explained by high reactivity of MA resulted in a reaction between the anhydride groups of PE-g-MA and the hydroxyl groups of starch. It is also showed that high-density polyethylene (HDPE) modified with glycidyl methacrylate (GMA) enhanced the miscibility of HDPE/starch blends. PE-g-GMA decreased the

MFI values and increased the tensile strength in all blends, indicating an improved interfacial interaction between the phases of the blends as shown in Figure 2.10.

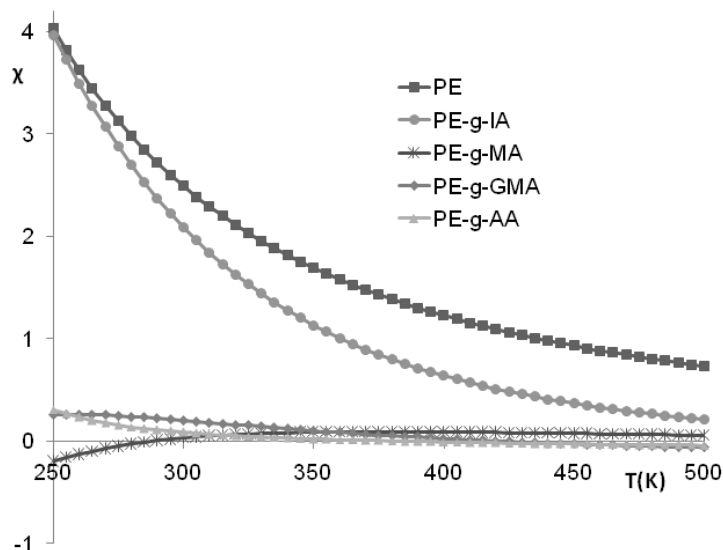


**Figure 2.10:** Change in the  $\chi$  interaction parameters between starch (ST) and PECs with temperature.

Native starch granules can be used as a filler for PEs, but real blends with more increased mechanical properties is only possible by using gelatinized starch to decrease water adsorption and thermoplastic starch like one treated with glycerol and esterified starch like STac. STac showed better mixing and degradation behaviour from the pure starch [234]. For PE-g-MA compatibilized systems, the interaction parameters are below zero at all temperatures referring to the mixed state. When PE-g-IA was used, the mixing starts at around room temperature. The mixing tendency of PE-g-AA and PE-g-GMA is slightly better than pristine PE but their interaction parameters are still positive. Our results indicated that esterified starch and PE blends by using MA and IA compatibilizers have enhanced properties due to negative interaction parameters between components (Figure 2.11).

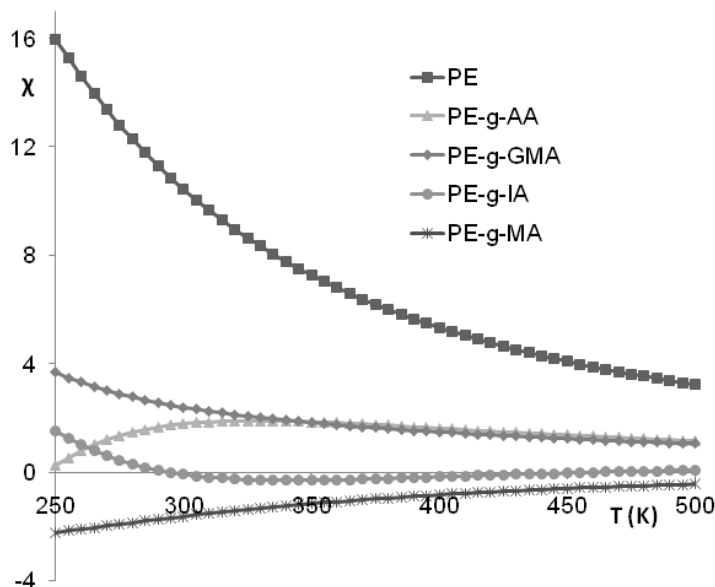


**Figure 2.11:** Change in the  $\chi$  interaction parameters between starch acetate (STac) and PECs with temperature.

### 2.2.3 Structural properties of PECs

The results given here are only for commercially used MA compatibilizer since the structural properties of the other compatibilizers almost have the same trends. The snapshots pictures taken from the simulation box for the equilibrium structures of only 1 and 2 MA grafted PE backbone composed of 800 carbon atoms are given in Figure 2.12. The bending behavior of the PE chains at the carbon atom to which polar group is attached observed in the optimized structure of the short chains is also seen in the snapshots given in Figure 2.12.

The grafting ratio in single and double MA containing PECs corresponds to 0.88 and 1.7 %w, respectively. The analyses of many equilibrium structures demonstrated that the functional groups are mostly on the surface of the polymer coil due to the repulsive interaction between PE and PECs as shown in Figure 2.5, even if at such a low grafting ratios. It was reported that the low amounts of PECs are enough for a successful preparation of PE-blends, PE-clay nanocomposites and metal surface coatings. The reason for this success is mainly stemmed from the moving of functional groups to the surface without any damage in the crystal structure. However high grafting ratios can have some structural drawbacks such as nucleation of PE-g-MA, appearing of defects on the grafted sites, reduced degree of crystallinity and fractured morphology as shown by experimental studies.

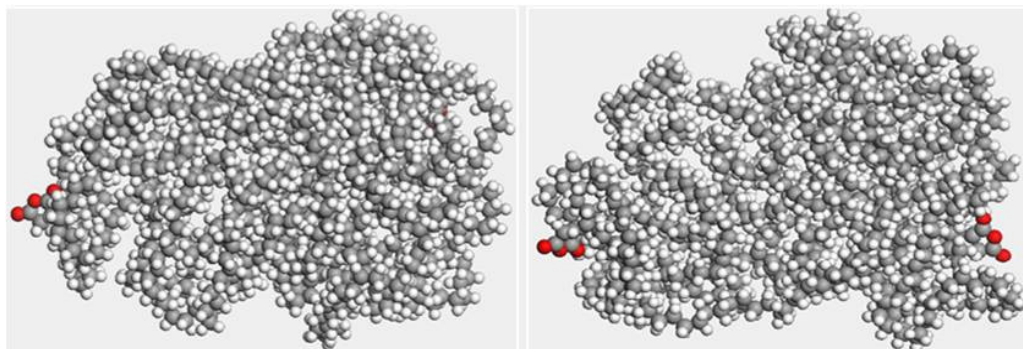


**Figure 2.12:** A snapshot picture of PE-g-MA with 0.88 %w (left) and 1.7 %w (right) grafting ratios.

In the SEM images for the 5 % w MA grafted blends, very rough surfaces with irregular shapes were observed. Our results for the equilibrium structures having high grafting ratios (4.4 and 5.5 %w) given in Figure 2.13 showed that the MA groups are either present on the polymer surface or inside the cavity created within the polymer coil, called defects, due to the polarity mismatch between the polar functional group and the nonpolar PE chains. The structure given in the Figure 2.12 and 2.13 are quite consistent with the experimental results. The presence of the defects increases the radius of gyration and also volume of a polymer coil as given in Figure 2.14.

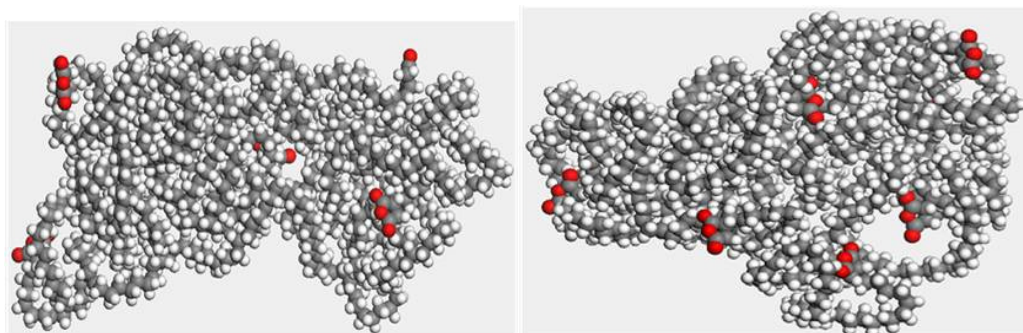


**Figure 2.13:** A snapshot picture of PE-g-MA with 4.4 %w (top) and 5.5 %w (bottom) grafting ratios.

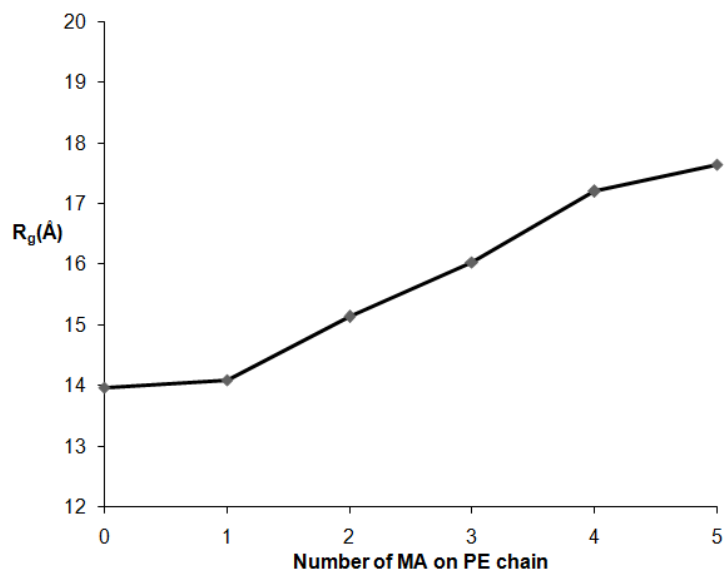


**Figure 2.14:** Change in the radius of gyration of PE-g-MA with grafting ratio MA.

Another factor affecting the grafting ratio and hence the structure of PEC is the polymerization of the functional group on the PE chain. This factor lowers the efficiency of compatibilizing role of polar group since it causes less interacting sites at interface and also lowers the crystalline phase due to the deformed structure and formed cavities. The cavity around the polar group in the equilibrium structure of pentamer of MA grafted PE chain is seen in the Figure 2.15.

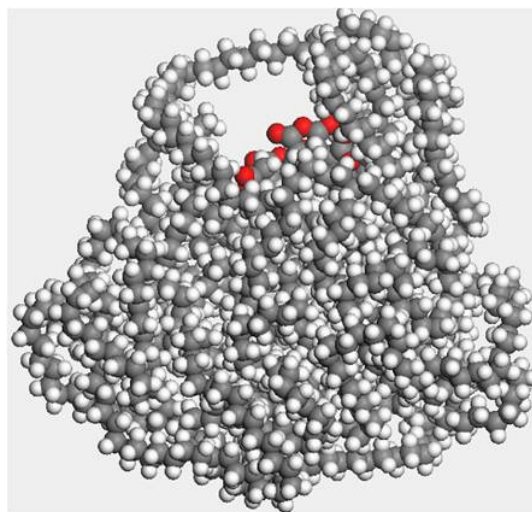


**Figure 2.15:** The snapshot picture of MA-pentamer grafted PE chain with grafting ratio of 4.4 %w.

Packing of chains is hindered as a result of oligomerization of polar groups as observed experimentally for MA. Cavity formation is the reason for rough surfaces and could be followed by the increase in the radius of gyration as a function of the chain length of MA, as given in Figure 2.16.

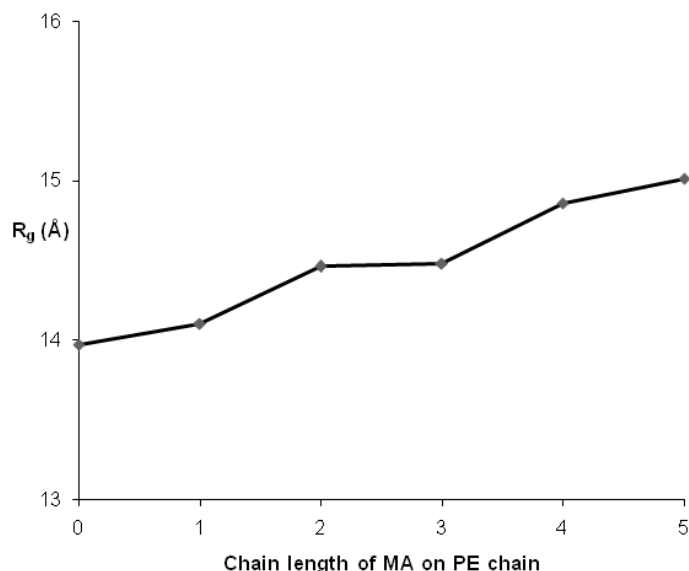


**Figure 2.16:** Change in the radius of gyration of PE-g-MA with polymerization degree of MA.

The incorporation of a polar functional group onto the PE backbone has led to improvement in the morphology and mechanical properties of the overall system. This improvement is due to the stronger interactions between nonpolar PE and polar polymer and it was proven quantitatively by the calculated interaction parameters. We showed that the compatibilizers achieved their function by physical and/or chemical interactions which included mostly dipole-dipole and hydrogen bond type interactions. By calculating the Fukui reactivity indices, we demonstrated that the most reactive sites undergoing chemical reactions were the polar groups. The best compatibilizing performance of PECs can be achieved at low grafting ratios.

The increase in the grafting ratios has negative effects on the structure and it is not desired. Polar functional groups escape from the nonpolar PE chains and reside on the surface or at the interfacial region. In our structural analyses, we have observed that in some cases, especially at relatively higher grafting ratios, functional groups can be present in the bulk phase inside the cavity created by them due to repulsive

interaction with the PE environment. These cavities are called defects and observed experimentally. Among the others discussed here, MA and IA serve as the best PE compatibilizers and the latter can be used as an alternative to MA due to its biodegradability.





### 3. DETERMINATION OF STRUCTURES AND ELECTRONIC PROPERTIES OF MONTMORILLONITE CLAY

Clays are layered aluminosilicates with several physicochemical properties such as swelling, adsorption, surface acidity, ion exchange, etc. They are natural minerals based on a two-dimensional layer of stacks made of inorganic layers. The layers are formed from both tetrahedral sheets of  $\text{SiO}_4$  motifs and octahedral sheets of metal oxide and hydroxides. The basic structural element of phyllosilicates are hexagonally organized layer of octahedra sandwiched between two tetrahedral siloxane layers, called as TOT layers such as pyrophyllite, montmorillonite, hectorite and beidellite. Smectites are one of the 2:1 dioctahedral structurally layered silicate, has three sheets; one octahedral sheet is sandwiched between two tetrahedral sheets. 66% of the octahedral sites are formed by aluminum atoms, and silicon atoms are situated in the tetrahedral sites. The tetrahedral groups formed by silica are arranged to form a hexagonal network, which is repeated indefinitely to form a sheet of composition  $\text{Si}_4\text{O}_6(\text{OH})_4$ . The octahedral sheet includes of double sheets of packed oxygen and hydroxyl groups where aluminum or magnesium atoms. These atoms are placed in octahedral coordination. Silicon atoms in tetrahedral coordination have equal distance from four oxygen atoms or hydroxyls. Octahedral metal atoms have equal distances from six oxygen atoms or hydroxyls.

Pyrophyllite that have unit cell formula  $\text{Al}_2[\text{Si}_4\text{O}_{10}](\text{OH})_2$ , is the simplest structure for 2:1 dioctahedral phyllosilicates. Since pyrophyllite has not any permanent electric charge in the TOT layer, it can be used to study structural properties of the clays not related to the charge or interlayer cations as a simple model. So, the pyrophyllite is chosen for our study as an initial model (Figure 3.1).

Some substitutions in the octahedral and tetrahedral layers of the clay minerals result in a structural and charge varieties in the 2:1 layer. This charge is equilibrated by counter alkali ions in the basal interlayer. The examples for most common substitutions are Si by Al in the tetrahedral layer and Al by Mg or Fe in octahedral layer causes the formation of beidellites and montmorillonites respectively.

Montmorillonite mineral are smectite type of clays that are characterized by main substitution of  $\text{Mg}^{2+}$  for  $\text{Al}^{3+}$  within the octahedral sheets. The low valence  $\text{Mg}^{+2}$  substitutions create negative charge for each substitution that compensated by interlayer cations. That is the main difference of pyrophyllite with MMT (Figure 3.1).

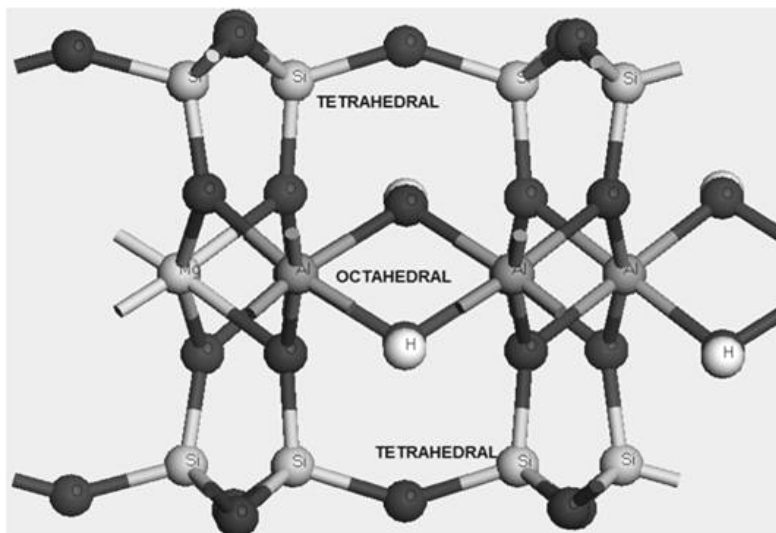


**Figure 3.1:** Tetrahedral-Octahedral-Tetrahedral structure of MMT layer.

Montmorillonites are lamellar silicates, i.e., consists of layers stacked one above the other. Stacking between the layers is stemmed from the weak electrostatic and van der Waals interactions. Stacking of MMT layers is generally related by interlayer cation, solvation nature of ion if water exists, structural character of the mineral, the average crystallite size, and the interlayer cation organizations (Figure 3.2). MMT structure and reactivity are investigated by using DFT methods in this chapter.

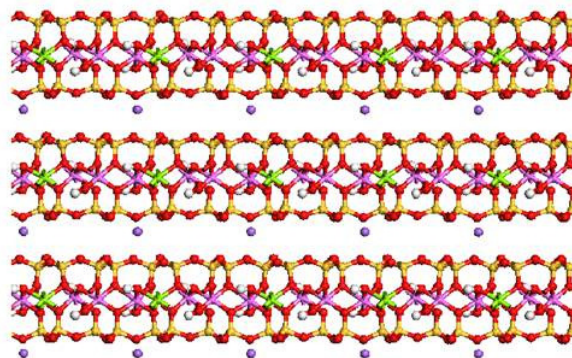


**Figure 3.2:** Stacked MMT layers with interlayer cation.

### 3.1 Theoretical Methods in the Clay Research

Since it is hard to determine properties of clays by classical simulations; electronic structure methods is usually used for calculations for the properties of clays where the distribution of electrons using wavefunctions and molecular orbitals calculated by approximate solutions to the Schrödinger equation. Hartree–Fock, DFT or hybrid DFT are the most common ab initio methods used to derive minimized structures.

Electronic structure methods can also be used to evaluate electron density, electrostatic potentials, thermodynamics, spectroscopic data, reaction mechanisms, and other properties. Contrary to standard HF methods that based on the wavefunction, DFT based on the density of electrons and includes electron correlation by correcting for the local distortion of an orbital in the vicinity of another electron. DFT uses advanced numerical methods such as local density approximation (LDA) or more sophisticated generalized gradient approximation (GGA) to calculate for electron correlation. Plane-wave DFT (PW-DFT) methods are another important method used for solid state structures such as layered clays. It accounts by a plane-wave expansion that is implemented only for the valence electrons of the atoms.

Although there are exciting development in the sophisticated quantum chemistry softwares and supercomputers, electronic structure calculations even DFT methods are very limited to about tens of atoms usually only one layer of the clay layers. There have been a significant increase in the use of electronic structure calculations for the calculations of layered clays.

First studies of electronic structure methods modeled relatively simple cluster models such as only tetrahedral layers, octahedral layers or representing binding environments associated with bridging oxygens (Si–O–Si(Al)) in layered aluminosilicate clays. Most of the first studies based on a standard Hartree–Fock or perturbed HF methods to correct for electron correlation. These methods then evolved with in theory and the availability of new software that let users to the energy determination and geometry optimization of periodic structures by PW-DFT. This periodic plane-wave pseudopotential DFT method was used in comparison of optimized talc ( $\text{Mg}_3\text{Si}_4\text{O}_{10}(\text{OH})_2$ ) and pyrophyllite ( $\text{Al}_2\text{Si}_4\text{O}_{10}(\text{OH})_2$ ) structures.

The highest occupied molecular orbitals were determined for the optimized structures of the layered material for reactivity and selectivity, especially related to the solvent adsorption and surface catalyze effects.

DFT based methods such as recent studies by Sainz-Diaz used simulation studies used to search dehydroxylation and hydroxylation mechanisms in dioctahedral phases [44]. Moreover, DFT based methods was used to calculate the relative stabilities of various cation substitutions and their organisation in the clay sheets, the reactivity and positions of hydroxyl groups in the clay structure and vibrational spectra. Next, molecular dynamics methods can be used synergically with electronic structure calculations to get more accurate force field parameters for clays.

Quantum chemical methods have been applied to calculate the structure of the montmorillonite several times. An important research on the structure and the electrostatic reactivity of the basal surface in montmorillonite as well as configurational disorder on the electrostatic properties was conducted. The DFT method has been used by Minisini to optimize the atomic positions and to perform a Mulliken population analysis of different models [50].

DFT studies was the best method for the prediction of crystal structure parameters where experimental XRD data was complicated or absent. Stackhouse and other researchers performed DFT calculations on pyrophyllite to get an optimized geometry to be used as a first step for 2:1 clay minerals such as montmorillonite [235].

## **3.2 Theoretical Methods Used in the Study**

### **3.2.1 Determination of structures and electronic properties by DFT methods**

The unit cell formula of the montmorillonite is  $(M^+_x)(Al_{4-x}Mg_x)Si_8O_{20}(OH)_4$  where  $x$  is called layer charge, and  $M$  is  $Na^+$  used for balancing cation for this study. The structure of montmorillonite with the formula  $MSi_8Al_3MgO_{20}(OH)_4$  used in this study. It can be generated from XRD structure determined experimentally or from the structure of well-defined pyrophyllite clay which do not have any substitution in the octahedral layer.

- i. As a first step, the method is tested by modeling basic pyrophyllite clay having the unit cell formula  $Si_8Al_4O_{20}(OH)_4$  was optimized by using PW-DFT methods. The

software package CASTEP (Cambridge Serial Total Energy Package) was used for the calculations. CASTEP is a pseudo-potential total energy code that employs Perdew Wang 91 (PW91) exchange-correlation functional, super cells and special point integration over the Brillouin zone and a plane wave basis set for the expansion of the wave functions. The ultrasoft pseudo-potentials were constructed from the CASTEP database. The effects of core electrons were calculated by using local density approximation (LDA), while the valence electrons energies were calculated by GGA method. Calculations were performed on a unit cell with automatically assigned  $k$ -point in the the Brillouin zone. High cut off energy was used during calculations. The unit cell was moved freely without any constraint during the optimization of cell parameters and atomic coordinates.

ii. Montmorillonite have more complex dioctahedral clay structure, since substitution of  $Mg^{+2}$  takes place. An important study by Tsipursky and Drits to model structure of montmorillonite in terms of octahedral site vacancies showed that there can be two configurations within montmorillonite [236]. Two sites are named cis and trans depending on the position of the hydroxyl group. Drits et al. have determined that only one of these configuration is present in one sheet. Having trans-vacant or or cis-vacant strongly influences the physical properties (Figure 3.3).

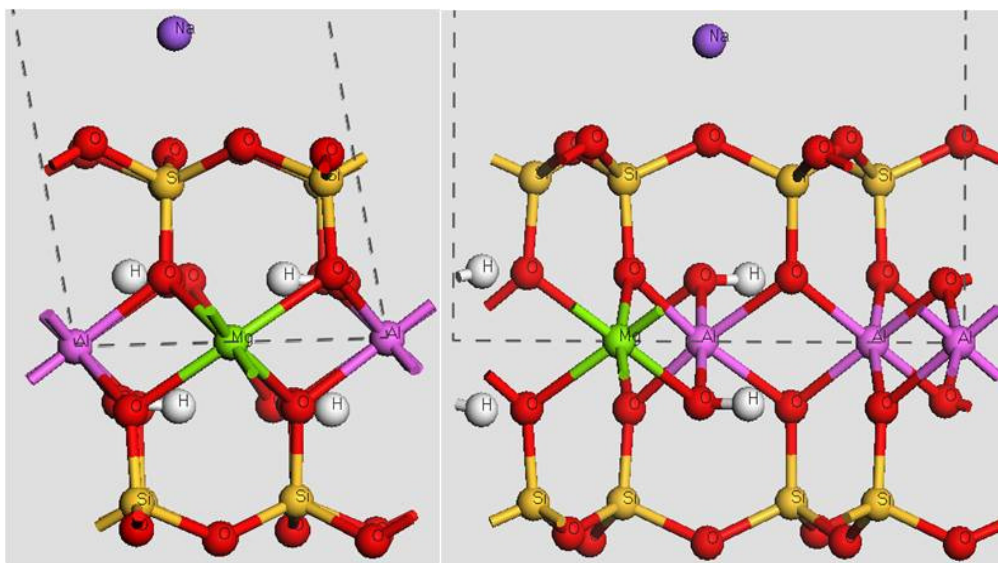


**Figure 3.3:** Trans and cis isomers of Na-MMT layer from XRD data.

Two different (cis and trans) periodic models of montmorillonite with unit cell formula  $[\text{Si}_8][\text{Al}_3\text{Mg}]\text{O}_{20}(\text{OH})_4$ , where one aluminum atom was substituted by a magnesium atom corresponding to a high cation exchange capacity have been constructed. Both of the structures were modeled by atomic positions determined experimental XRD datas from a montmorillonite sample by Tsipursky and Drits [237]. One of the MMT structure is called TV (trans-vacant) configuration other called CV (cis-vacant). The counter  $\text{Na}^+$  ion was positioned at the middle of basal spacing (fractional coordinates= 0.5 0.5 0.5). The plane-wave pseudopotential density functional theory code CASTEP implemented in Material Studio 5.0 were used to perform GGA calculations by using Perdew-Wang91 functional. Ultra-soft Vanderbilt potentials available in the CASTEP database with energy cutoff of 370 eV was used. Hellmann–Feynmann theory were used to calculate the forces on the  $\text{Na}^+$  ions and Broyden-Fletcher-Goldfarb-Shanno (BFGS) algorithm were implemented during the optimization.

### 3.2.2 Hard-soft acid base principle

To use the DFT calculations, a MMT clusters were taken from the optimized montmorillonite structure.  $\text{MgAlSi}_{10}\text{O}_{31}(\text{OH})_2$  and 14 hydrogen atoms for end group saturation were used to build a cluster (Figure 3.4).

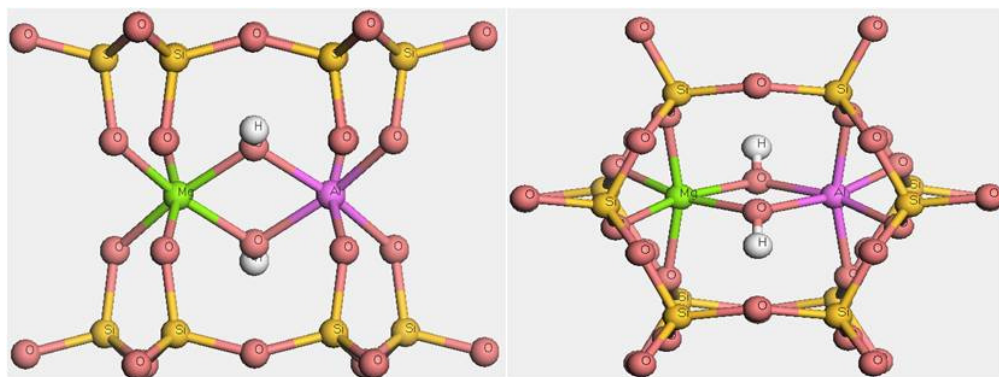


**Figure 3.4:** Cluster model of MMT used to calculate reactive sites.

Firstly, B3LYP is hybrid of Hartree–Fock and density-functional exchange-correlation terms was used in Gaussian09 to optimize hydrogen atoms added for saturation, which employs the Becke GGA exchange term B; Becke88 means mixing with the nonlocal HF exchange in the ratio of 0.5HF+0.5B and the Lee–Yang–Parr (LYP) is the part of GGA correlation term.

Then, Hard-Soft acid base principle (HSAB) was used to calculate reactivity with DFT using the DMOL3 implemented in Materials Studio 5.0. HSAB uses computational advantages of DFT, that is source used by chemists to calculate several properties such as the electronegativity, hardness and softness and Fukui's frontier molecular orbital reactivity index. This area of DFT was termed by R. G. Parr as "conceptual DFT" based on the principle of electronegativity equalization and HSAB named by Pearson [238,239]. A gradient corrected functional PW91 and DNP basis set (quality level: 6-31g\*\*) was used throughout the calculation.

The concepts have been developed based on Density Functional Theory (DFT) and HSAB are electronic chemical potential,  $\mu$ , global chemical hardness,  $\eta$ , chemical softness,  $S$  and the Fukui function,  $f(r)$  which is defined as response of the system to the electron movements in the system. Single point energy calculations on the cation and anion cluster at the optimized geometry of the neutral molecule were also conducted to calculate Fukui functions, global and local softness. Two types of parameters are possible; global for describing reactivity as a whole cluster and local for atomic reactivities such as local Fukui functions and local softness.

In this study, global reactivity of the MMT cluster is represented by using the softness. The softness can be defined as

$$S = \frac{1}{IP - EA} \quad (3.1)$$

Where IP and EA are ionization potential and electron affinity defined as;

$$IP = E(N-1) - E(N) \quad (3.1)$$

$$EA = E(N) - E(N+1)$$

These are all approximations based on the Koopmans theorem, where E is the energy, N is the number of electrons of the systems. In reality global softness is defined as

$$S = \left( \frac{\partial N}{\partial \mu} \right)_{v(r)} \quad (3.4)$$

Where  $\mu$  is the chemical potential and  $v(r)$  is the potential, which is identified with the negative of electronegativity shown by  $\chi$ .

$$\mu = \left( \frac{\partial E}{\partial N} \right)_{v(r)} = -\chi \quad (3.5)$$

The local softness is defined as

$$S = \int s(r) dr \quad (3.6)$$

or

$$s(r) = \left( \frac{\partial \rho(r)}{\partial \mu} \right)_{v(r)} \quad (3.7)$$

$\rho(r)$  is the electron density at the atom placed at  $r$ . The local softness  $s(r)$  can also be identified as

$$s(r) = \left( \frac{\partial \rho}{\partial N} \right)_{v(r)} * \left( \frac{\partial N}{\partial \mu} \right)_{v(r)} = f(r) * S \quad (3.8)$$

by using the  $f(r)$  which is the local Fukui function.

Fukui functions,  $f_H^+$  and  $f_H^-$ , are calculated to locate the possible sites for nucleophilic and electrophilic attacks, confirmed several times experimentally accurate trends of reactivity to solve molecular interactions in solids.

Local Fukui functiona of an A atom in a cluster with  $N$  electrons at constant external potential,  $v(\vec{r})$  is defined as;

$$f_A^+ = \frac{1}{\Delta N} [\rho_A(N_0 + \Delta N) - \rho_A(N_0)] \text{ (for nucleophilic attack )} \quad (3.9)$$

$$f_A^- = \frac{1}{\Delta N} [\rho_A(N_0) - \rho_A(N_0 - \Delta N)] \text{ (for electrophilic attack)} \quad (3.10)$$

where  $\rho_H(N_0)$ ,  $\rho_H(N_0 + \Delta N)$  and  $\rho_H(N_0 - \Delta N)$  are electronic densities on atom A and  $N_0$ ,  $N_0 + \Delta N$  and  $N_0 - \Delta N$  are the number of electrons in the systems.



The local Fukui functions are calculated for MMT clusters by the formula given below since it is not possible to calculate charge density for small electron density charges so 1.0 is used for  $\Delta N$  and formula turns into;

$$\begin{aligned} f_A^+ &= q_A(N+1) - q_A(N) \\ f_A^- &= q_A(N) - q_A(N-1) \end{aligned} \quad (3.11)$$

or

$$\begin{aligned} f_A^+ &= q_A^{anion} - q_A \\ f_A^- &= q_A - q_A^{cation} \end{aligned} \quad (3.12)$$

Where  $q_A(M)$  is the atomic number of electron at atom A ( neutral system  $M=N$ , the cation  $M=N-1$ , or the anion  $M=N+1$ . As a result, the local softness can be shown by;

$$\begin{aligned} s_k^+ &= f_k^+ * S && \text{for a nucleophilic attack, and} \\ s_k^- &= f_k^- * S && \text{for a electrophylic attack.} \end{aligned} \quad (3.12)$$

### 3.3 Results and Discussions

#### 3.3.1 Determination of structures and electronic properties by DFT methods

Pyrophyllite is very basic and well known clay contains only two tetrahedral silicate and one octahedral alumina layers. So, pyrophyllite has very similar structure with MMT. The only difference is between substitution at the octahedral layer that causes a negative charge in MMT layer. As shown in Table 3.1, the cell parameter were well predicted by PWDFT method. Bulk and slab geometry optimizations of both pyrophyllite were performed at DFT level, the interatomic distances from optimizations were very close to those obtained in bulk optimizations. In the case of pyrophyllite, the tetrahedral and octahedral sheets were distorted with respect to the ideal hexagonal symmetry as seen from the cell parameters. Calculated cell parameters reproduced the previous theoretical and experimental studies.

**Table 3.1:** Experimental and Theoretical Lattice Parameters of Pyrophyllite.

	a-b-c	$\alpha - \beta - \gamma$
MacKenzie et al. [239]	5.20-9.15-9.45	92-98.8-89
Lee and Guggenheim [240]	5.16-8.97-9.34	91.18-100.46-89.64
Wardley [241]	5.16-8.96-9.35	91.03-100.37-89.75
This Study	5.21-8.89-9.25	94.2-105.3-91.7

When the IR frequencies were calculated after scaling due to theoretical errors, both the absolute frequency values for pyrophyllite clay were comparable with the experimental data (Table 3.2). The well known –OH stretching is found with an error smaller than 1%. By this way, we validated our methods for the most basic and well-known 2:1 clay.

**Table 3.2:** Theoretical and Experimental Vibrational Frequencies.

BOND	Experimental	This Study
Si-O-Si	1038-1026	1062
Si-O	1115-1090	1150
Si-O-Al	695	710
Al-O-H	796, 896, 915	940
O-H	3690	3710

After confirmation of method for the well known structure, the similar DFT calculations by using the same method for MMT models were conducted.

Lattice parameters obtained from the PW-DFT optimizations were listed in Table 3.3. Computationally determined crystallographic lattice parameters were compared with the calculated results and average results of available experiments. Although, there is a little negative effect observed for the a and b lattice parameters of unit cell, an increased c parameter of unit cell size is observed with respect to unsubstituted because of the interlayer cation ( $\text{Na}^+$  in our case). Similar distortions from the ideal symmetries also observed for MMT clay layers.

**Table 3.3:** Theoretical and Experimental Lattice parameters of Na-MMT.

	Na- MMT		
	Our results	Sainz-Diaz et al.[242]	Experiment
$a$ (Å)	5.22	5.23	5.18
$b$ (Å)	9.13	8.9	8.97
$c$ (Å)	11.12	10.22	9-15
$\alpha$ (°)	92.1	—	—
$\beta$ (°)	103.8	105.7	100.4
$\gamma$ (°)	91.1	—	—

The calculated lattice parameters for MMT-Na were 1-3 % larger than the experimental results for the montmorillonite sample. We have to bear in mind that the general formulas and substitutions were used in our calculations. Spectroscopic methods for MMT samples showed that it has the chemical composition with several substitutions:  $(\text{Ca}_{0.12}\text{K}_{0.18}\text{Na}_{0.34})(\text{Si}_{7.96}\text{Al}_{0.04})[\text{Al}_{2.76}\text{Fe(III)}_{0.28}\text{Mg}_{0.96}]\text{O}_{20}(\text{OH})_4$ .

Ab initio calculations is a necessary tool to investigate the molecular structure and the effects of isomorphous substitutions of the tetrahedral and octahedral metals, since it is impossible to observe this structural effects by XRD or other spectroscopic tools. The effect of layer charge by the octahedral substitution of  $\text{Mg}^{2+}$  for  $\text{Al}^{3+}$  as well as the effect of interlayer cation were observed in terms of differences in the structural angles as given in Figure 3.5.

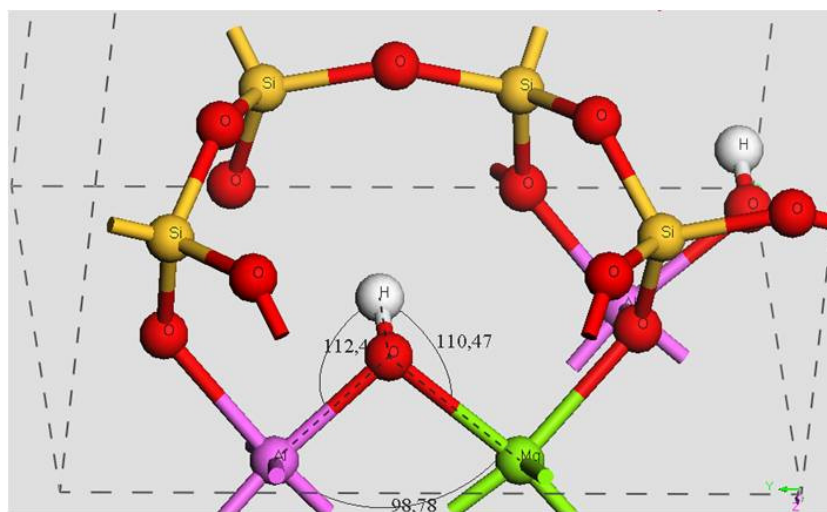


**Figure 3.5:** Structure of octahedral layer in MMT.

The internal coordinate calculated for MMT with structural formula  $\text{MSi}_8\text{Al}_3\text{MgO}_{20}(\text{OH})_4$  supported by with the available experimental values. The symmetrical angle Al-O-Al is distorted for Al-O-Mg angle after substitution. The silicons in the hexagonal cavity were all equivalent with same Si-O and Si-O-Si angle. The geometrical parameters show that the distortions from ideal geometries of  $\text{AlO}_6$  and  $\text{SiO}_4$  were due to the Al-O-Al bridges, Al-O-Si bridges and Al-O-H bridges. The bridge between octahedral and tetrahedral layers causes this distortions in MMT. This results therefore show that there must be also a relation between the energy and geometry of these clusters. The oxygen-hydrogen bond lengths (O-H) were the same with ideal distances (Table 3.4).

**Table 3.4:** Bond lengths and angles of optimized MMT structure.

	Distances (Å)		Angles (°)
Si-O	1.59	Al-O-H	112.4
O-H	0.97	O-Al-O	92.4
Al-Al	2.92	Si-O-Mg	112
Al-Mg	2.95	Si-O-Al	128.4
Al-O	1.88	Mg-O-H	110.47

Another important structural feature of clay with a systematic layer charge and interlayer cation dependence is the structural OH angle with respect to *ab* plane ( $\angle_{ab}\text{OH}$ ). It is a measure of the proximity between the hydrogen and the surface is to measure the (ab)-(OH) angle. The hydrogen positions were important because they could have effectson the electrostatic potential of the hexagonal cavities on the surface. The corresponding angles and optimized orientations of these structural OH were determined. The average angle of this structural OH angle is determined as  $\sim 5^\circ$  for pyrophyllite and, while it is  $9\text{-}13^\circ$  for MMT. Stackhouse et al. also calculated the OH angle with respect to the *ab* plane in their DFT study of MMT. They obtained an average angle of  $-22.31^\circ$ . However, the MMT structure used by them have an additional proton counterion attached to the siloxane surface of the tetrahedral sheet, that changes the orientation of the structural OH significantly.

When there is not any interlayer  $\text{Na}^+$  cation, the structural OH groups in the octahedral layer look toward the interlayer space. However when there is a  $\text{Na}^+$  ion in the gallery, this angle increases due to the polarization of tetrahedral oxygens. The

polarization of tetrahedral oxygens that form hexagonal cavities on the surface causes more interaction with hydrogen atom of the –OH group and increase in the (ab)-(OH) angle.

Another result from MMT optimization showed that, (ab)-(OH) angles of the cis-vacant configurations were higher than those of the trans-vacant configurations. There were two main reasons for these difference. One is the repulsive interactions between hydrogens and the other is the higher -OH interaction with the bridge oxygen between tetrahedral and octahedral layer for cis-vacant MMT that decreases the angle (Figure 3.6). (AlOAl)-H and (AlOMg)-H bond distances were also found to be higher for trans MMT due to less steric effects.

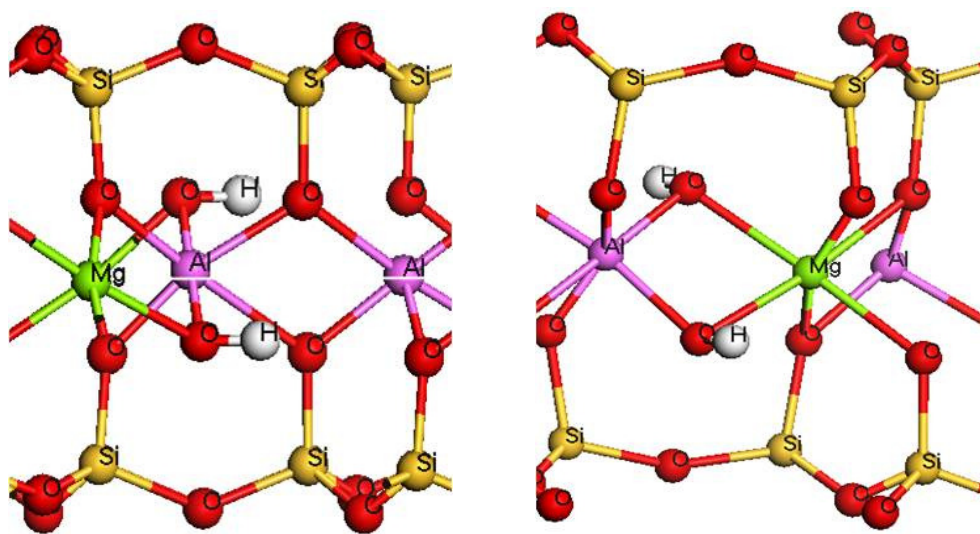


**Figure 3.6:** Optimized cis and trans MMT structure with  $Mg^{+2}$  substitution.

We found that the trans structure of MMT is more stable than cis MMT . The energetical difference between two isomer is at 0.1% level that both cis and trans vacant MMT can be found in the nature at about equal amounts dependent on the source of the clay (Table 3.5).

**Table 3.5:** Energy and structure comparison of cis and trans MMT.

	Total Energy (eV)	(AlOAl)-H bond length	(AlOMg)-H bond length	$\angle_{ab}OH$
cis	-1.397E+004	0.970- 0.977	0.973- 0.974	9
trans	-1.398E+004	0.977- 0.978	0.974- 0.975	13

The position of the interlayer  $\text{Na}^+$  cation determined as a result of PW-DFT calculations. It is found that hexagonal cavity is the most favorable position for sodium cations in our calculations. We found that the  $\text{SiO} \cdots \text{Na}$  distance is between 2.0-3.6 Å. The high range of this distance is because of the coordination of  $\text{Na}^+$  two oxygen atoms. It is claimed by the previous studies that the only lithium ion is small enough to move into the hexagonal cavity on the clay surface. Another result on Cs-MMT and K-MMT indicated the cesium and potassium cation placed in the middle of the cavity.  $\text{Na}^+$  cations were determined to be adsorbed to the corners of siloxane cavity and stay at about equal distance from top and bottom clay layers. It has still enough distance to push back hydrogen atoms in the octahedral layer.

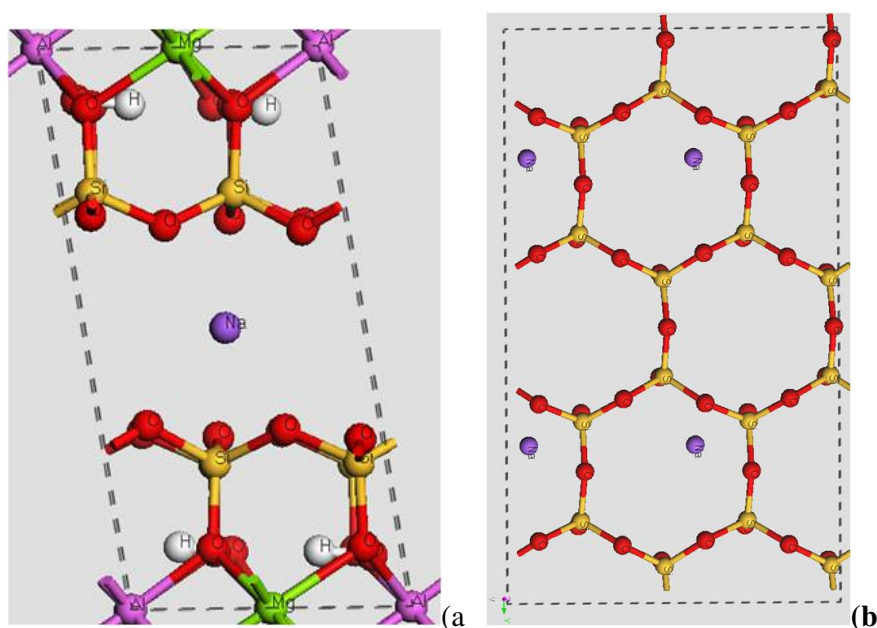


**Figure 3.7:** a) Optimized structure of MMT structure and b) positions of  $\text{Na}^+$  ions

### 3.3.2 Hard-soft acid base principle

The total softness of the MMT cluster was calculated as 1.98 that indicated the soft base property. Since the cationic surfactant-clay and acidic compatibilizer-clay interactions were important for the PE-organoclay nanocomposites formation, the determination of susceptible sites for both nucleophilic attack and electrophilic attacks are important. These values are local softness ( $s$ ) and local Fukui functions ( $f$ ) of the atoms on the clay cluster calculated by using atomic charges and global softness by DFT calculations.

Generally, we found that the most important nucleophilic center for our cluster is the hydroxyl hydrogen in the octahedral layer as shown in Table 3.6. Although interlayer  $\text{Na}^+$  cations are more reactive, they will be removed during the organoclay preparation by cation exchange. -OH groups can have important roles on adsorption or intercalation with small organic structures by their reactivity and H-bonding ability. However the surfactants and PE compatibilizers are very large to interact with -OH groups. The end group hydrogens formed by the saturation of the cluster have higher reactivity as a nucleophilic center and seems to interact at first with electrophilic sites since other nucleophilic centers are sterically hindered by stacking of clay layers as well as the basal surface oxygens. We can conclude that the most important nucleophilic center for the polymer-organoclay nanocomposites is the edge -OH groups that have properties show chemical similarities to the behavior of Si oxides and Al hydroxides.

**Table 3.6:** Nucleophilic and electrophilic local centers of MMT cluster.

	$\mathbf{f}^+$	$\mathbf{s}^+$
<b>Si</b>	0.061	0.121
<b>Mg</b>	0.125	0.248
<b>Al</b>	0.114	0.226
<b>O<sub>hyd</sub>, O<sub>bridge</sub>, O<sub>surface</sub></b>	0.234, 0.111, 0.224	0.468, 0.220, 0.448
<b>H (hydroxyl)</b>	0.276	0.546
<b>H (end group saturation)</b>	0.356	0.707
	$\mathbf{f}^-$	$\mathbf{s}^-$
<b>Si</b>	0.122	0.241
<b>Mg</b>	0.112	0.221
<b>Al</b>	0.119	0.235
<b>O<sub>hyd</sub>, O<sub>bridge</sub>, O<sub>surface</sub></b>	0.264, 0.231, 0.244	0.523, 0.457, 0.483
<b>H (hydroxyl)</b>	0.111	0.217
<b>H (end group saturation)</b>	0.105	0.208

All compatibilizers and surfactants used in these study have acidic hydrogen atoms susceptible to interact with nucleophilic atoms. These nucleophilic atoms are

electrophilic centers. The most important electrophilic centers were found as oxygen atoms. Although the oxygen in the –OH group is more reactive, it is hard to interact with surfactants and polar groups of PECs. The number and reactivity of the surface oxygens in the tetrahedral SiO<sub>4</sub> layer were the highest. If the clay layers intercalated, hexagonal cavities of these oxygen atoms form an electrophilic zone for the acidic hydrogens of ammonium and compatibilizers. Since metal atoms in the cluster were polarizable they have average reactivities with respect to both electrophilic and nucleophilic sites.

In conclusion, Plane Wave DFT calculations were performed to optimize MMT cell. These quantum mechanical calculations on periodic MMT clay and the cluster structure showed that the hydroxyl hydrogen in the octahedral layer have mostly trans configuration and acts as a nucleophilic center, whereas oxygen atoms in the tetrahedral layer and basal surface were electrophilic centers. The high atomic charge and reactivity of the oxygen atoms and octahedral hydrogen atoms clarify the hydrophilic activity of montmorillonite as observed from the DFT calculation. The counter ion position depends on its size and –OH position depends on the cis and trans structure as well as the interaction with the counterion. The positions of Na<sup>+</sup> ion coordinated in the hexagonal cavity. The edge hydrogen groups were very reactive and can catalyze the intercalation by catching nucleophiles around clay stack.



#### **4. MOLECULAR DYNAMICS SIMULATION STUDY ON THE BASAL SPACING AND LAYERING BEHAVIOUR OF CATIONIC SURFACTANTS IN ORGANOCLAYS**

Montmorillonite (MMT) is a highly hydrophilic clay and its surface modification is needed to achieve good interfacial adhesion, for industrial usage and increase adsorption capacity. For this purpose, cationic surfactants with alkyl tail can be exchanged with the small metal cations called exchangeable cations present in clay structure. These cationic chains help to increase the spacing between the clay layers, increase processability and thermal stability with respect to their chemical and structural properties. The counter ions between clay layers exchanged with organic cations called surfactants, such as that from an onium salt, to form an organomodified relatively hydrophobic clays. This family of organomodified clays (organoclays) with hydrophobic surfaces, synthesized by modifying swelling clays with various surfactants.

During the last decades, organoclays have attracted great interest in a number of applications, such as adsorbents for organic pollutants, rheological control agents, precursors for preparing mesoporous materials and reinforcing fillers for plastics and clay-based nanocomposites. Especially polymer-clay nanocomposites has emerged as a new class of materials where organoclays used due to their increased mechanical, thermal, gas-barrier, inflammability properties. Prior to addition of polymer, surface modification of hydrophilic clays to form organoclays is needed by ion exchange reactions of organophilic cations for sodium ions to achieve good interfacial adhesion.

The ability of the clay to improve the properties of the nanocomposites is primarily determined by the extent of its dispersion in the polymer matrix, which, in turn, depends on the clay particle intercalation and basal spacing. The interfacial adhesion between the organic and inorganic phases of the nanocomposite plays a role of another importance. Therefore, the role of the organic compound in the organomodified montmorillonite (OMMT) is to reduce the surface energy of the

MMT and improving the interaction characteristics with the polymer or monomer by this way in addition to the increased interlayer space. It has many additional advantages such as reducing the interlayer binding forces and helps the movement and accommodation of the monomers or polymers.

Alkyl ammoniums are the most commonly employed clays for polymer nanocomposites preparation because of their commercial availability. Except the primary alkyl ammonium molecules, which presumably have linear conformations over the silicate surface, we cannot estimate the exact conformation of the secondary, tertiary, and quaternary organic ammonium molecules between silicate layers. Kwolek et al. employed a homologue series of alkyl benzyl dimethylammonium bromides,  $[C_6H_5CH_2N(CH_3)_2R]Br$ , to obtain organoclay [243]. The quaternary ammonium with one or more alkyl tails which are also mostly used commercially for nanocomposite preparation are particularly susceptible to decomposition near the processing temperature of polymer extrusion, which is about 200 °C or less for polyethylene.

Other alternative cationic surfactants, such as phosphonium, pyridinium and imidazolium have also been used due to their higher thermal stability. Thermal characteristics of montmorillonites modified with quaternary phosphonium and ammonium surfactants were investigated at last years using thermo-analytical techniques and X-ray diffractometry. Patel et al. reported the preparation of organo-montmorillonites with the intercalation of quaternary phosphonium cations that show higher thermal stability than those prepared with quaternary alkylammonium salts [70]. Quaternary phosphonium cations (hexadecyl tributylphosphonium; tetradecyl tributylphosphonium; tetraphenylphosphonium; methyl triphenylphosphonium; ethyl triphenylphosphonium and propyl triphenylphosphonium) were intercalated into montmorillonite MMT rich bentonite. MMTs modified with quaternary phosphonium ions have a greater thermal stability than their quaternary ammonium-modified counterparts, in accordance with the findings by Xie et al [73].

Chigwada et al. introduced the pyridine groups and quinoline derivatives of it on the hexadecylammonium cation and obtained quinolinium and pyridinium salts, that was used to prepare organo-montmorillonites [244]. These small changes in the surfactant head groups by replacing pyridine by quinoline resulted in significant changes in the organoclays properties. An individual even amino acid like structures (12-

aminolauric ammonium) molecule was used to modify clays. 1-vinyl hexadecyl imidazolium, 1-vinyl octadecyl imidazolium, dihexadecyl imidazolium, dioctadecyl imidazolium has shown to be good alternatives for thermoplastic polymer nanocomposites.

Due to the nanosized particle size, the low crystallizability, and the complicated chemical structures of clays, detailed information about the interlayer structure and the atomic local environment in organoclay is rarely available from experimental measurements. XRD is the most widely used technique to determine the structure of organoclays. Organoclays obtained by cation exchange offer a great diversity of interlayer structures. On the basis of the measured basal spacings and the length of the alkyl chains, various arrangement models have been proposed for the intercalated surfactants, including lateral-monolayer, lateral-bilayer, pseudo-trilayer, paraffin-monolayer, and paraffin bilayer. These idealized models are based on the assumption that the intercalated surfactants adopted all-trans conformation after intercalation. However, XRD patterns cannot provide the detailed information about the intercalated layers, including whether they are regularly intercalated layers or not.

These idealized structural models were first shown to be unrealistic by Vaia et al. on the basis of Fourier transform infrared spectroscopy (FTIR). Vaia have proposed a more realistic description based on FTIR and XRD experiments to probe the interlayer structure and the phase structure of alkylammonium [245]. By monitoring the frequency shifts of the  $\text{-CH}_2$  stretching and scissoring vibrations as a function of interlayer packing density, chain length, and temperature, they found that the intercalated molecules exist in states with different degrees of order. In fact, recent NMR studies on intercalated surfactants in layered solids further clarified the coexistence of ordered trans and disordered gauche conformations. Unfortunately, all these experimental results only provide an average state for the molecular arrangements and layering structure and it is difficult to quantify them. General structure and formation scheme of organoclays are given in the Figure 4.1.

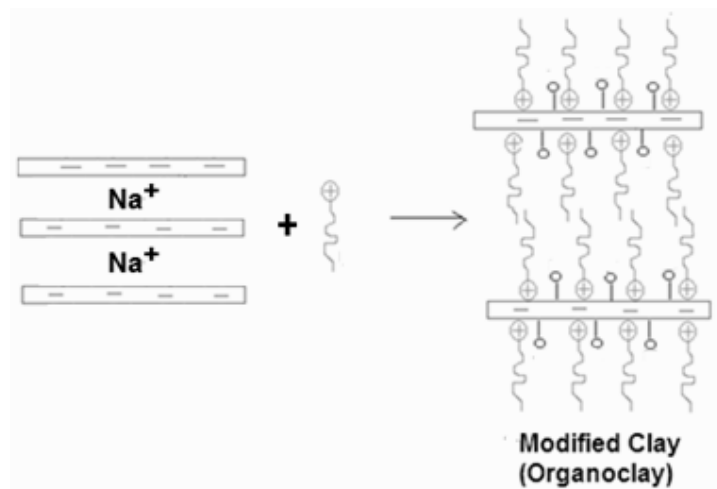


**Figure 4.1:** Mechanism of organoclay formation by cation exchange.

More recently, molecular simulation has been proved to be a powerful technique to probe the detailed information about molecular arrangements of molecules in the confined layers like clays. The simulated results provide not only the complementary evidence for the experimental results but also new insights for the microstructure of organoclay. For example, molecular simulation has demonstrated a mixed structure of paraffin-type and trilayer or quadrilayer in organoclay, which has never been discussed in experimental studies. This reflects that the real structure of organoclay is more complicated than those proposed on the basis of the experimental measurements. Molecular modeling demonstrates that in all arrangements of surfactant within the clay interlayer, the headgroups of the surfactants will be close to the clay surface due to the strong electrostatic interaction between the negative clay surface and the positive headgroups of the alkyl chains. Previous reports have shown that, in the organoclays with lower surfactant packing density, the alkyl chains within the interlayer space are parallel within the interlayer space and are individually separated. With the increase of surfactant packing density, the interchain interaction among the surfactants becomes the dominant force and the orientation of the hydrocarbon tail changes from parallel to the silicate surface within the interlayer space to parallel but at an angle to the silicate surface as shown by XRD and FT-IR results [246]. Although various structural models have been proposed for the intercalated surfactants, they do not directly reveal the significant structural characteristics of the surfactants at molecular levels.

The present work is focused on investigation of the surface modification of a montmorillonite with a series of differently structured alternative surfactants and structure analysis based on molecular simulations. The concentration of the surfactants in simulations was varied with respect to cation exchange capacity (CEC) of the clay. More detailed information on structure and characteristics of layering behaviour in organoclays will be provided. This is of great importance in the design and application of organoclay-based materials. In this study, different Na-montmorillonite clays models are optimized by plane wave (PW) density functional methods (DFT). Organoclay with onium groups with different alkyl numbers, lengths and head groups were modelled structure and its properties are determined by using molecular dynamics (MD) simulation technique.

## 4.1 Theoretical Methods

### 4.1.1 Modeling methods of organoclays

The first step in preparing the initial organoclay configuration for molecular simulation is to create a negatively charged montmorillonite framework. The clay model construction was carried out with the Crystal Builder of Material Studio package. However, complete crystal structure information is not available because of the microcrystalline and poor ordering of smectite clays. Therefore, the atomic coordinates for montmorillonite in this study are based on the optimized structure of trans vacant Na-MMT layers from the XRD data of Tsipursky and Drits. Plane-wave pseudopotential density functional theory with PW91 functional and ultra-soft Vanderbilt potentials was used to optimize unit cells of the trans-vacant MMT by using same procedure given by Minisini. Three basic types of montmorillonites (MMT1, MMT2 and MMT3) with different layer charges ( $-0.4/-0.66$  and  $-1.066$  per unit cell, respectively) are built, with their unit cell formula given by  $\text{Na}_x(\text{Al}_{4-x}\text{Mg}_x)\text{Si}_8\text{O}_{20}(\text{OH})_4$ .

Accordingly, the unit cell formulas are  $\text{Na}_{0.4}(\text{Al}_{3.6}\text{Mg}_{0.4})\text{Si}_8\text{O}_{20}(\text{OH})_4$  for MMT1,  $\text{Na}_{0.66}(\text{Al}_{3.34}\text{Mg}_{0.66})\text{Si}_8\text{O}_{20}(\text{OH})_4$  for MMT2, and  $\text{Na}_{1.066}(\text{Al}_{2.934}\text{Mg}_{1.066})\text{Si}_8\text{O}_{20}(\text{OH})_4$  for MMT3. The calculated cation exchange capacities were 56 meq/100 g for MMT1, 91 meq/100 g for MMT2 and 143 meq/100g for MMT3. All cationic surfactants was optimized by quantum mechanical methods at B3LYP/6-31+(d,p) by using Gaussian03. In our idealized clay models, we assume that all layer charge comes

from the substitution of aluminum by magnesium in the octahedral sheets. To keep the electroneutrality, the difference of charges was homogenously distributed on these atoms. By this way, cations in the 5x3 structure of 6 exchangeable cations for MMT1, 10 exchangeable cations for MMT2, 16 exchangeable cations for MMT3 are used to prepare three different type of organoclays (Table 4.1).

**Table 4.1:** Structure of unit, supercell and CEC of clays.

x	$\text{Na}_x(\text{Al}_{4-x}\text{Mg}_x)\text{Si}_8\text{O}_{20}(\text{OH})_4$	5x3x1 cell formula	CEC (meq/100 g)	Symbol
X=0.4	$\text{Na}_{0.4}(\text{Al}_{3.6}\text{Mg}_{0.4})\text{Si}_8\text{O}_{20}(\text{OH})_4$	$\text{Na}_6(\text{Al}_{54}\text{Mg}_6)\text{Si}_{120}\text{O}_{300}(\text{OH})_{60}$	56	MMT1
X=0.66	$\text{Na}_{0.66}(\text{Al}_{3.934}\text{Mg}_{0.66})\text{Si}_8\text{O}_{20}(\text{OH})_4$	$\text{Na}_{10}(\text{Al}_{50}\text{Mg}_{10})\text{Si}_{120}\text{O}_{300}(\text{OH})_{60}$	91	MMT2
X=1.066	$\text{Na}_{1.066}(\text{Al}_{2.934}\text{Mg}_{1.066})\text{Si}_8\text{O}_{20}(\text{OH})_4$	$\text{Na}_{16}(\text{Al}_{44}\text{Mg}_{16})\text{Si}_{120}\text{O}_{300}(\text{OH})_{60}$	143	MMT3

Molecular dynamics (MD) simulations were carried out to determine interfacial interactions and structures in the organoclay formed by the intercalation of onium cations of the Na-Montmorillonite clay. As a prestudy forcefield determination, COMPASS, Dreiding and Universal force fields were used. Unfortunately, the intramolecular parameters do not exist for the apical oxygen linking the tetrahedral and octahedral sheets and octahedral aluminum in montmorillonite. All the tests require the rigid MMT layer will atomic and fractional coordinates. This is due to the fact that the parameters for classical forcefields are not easy to determine for systems with ionic-covalent bonds. That is why the montmorillonite was modelled by an atomic rigid model in the previous studies. Moreover, when the electrostatic charges were given by force fields for all the atoms, all charges are localized on the head groups. For this reason, atomic charges surfactants were calculated with Merz-Kollman scheme where electrostatic potentials were pointed to the atomic centers by PW91/DNP level single point calculations on optimized geometries. The atomic charges calculated for one of the surfactant (dioctadecyl dimethyl ammonium: DODDMA) is given in Figure 4.2.

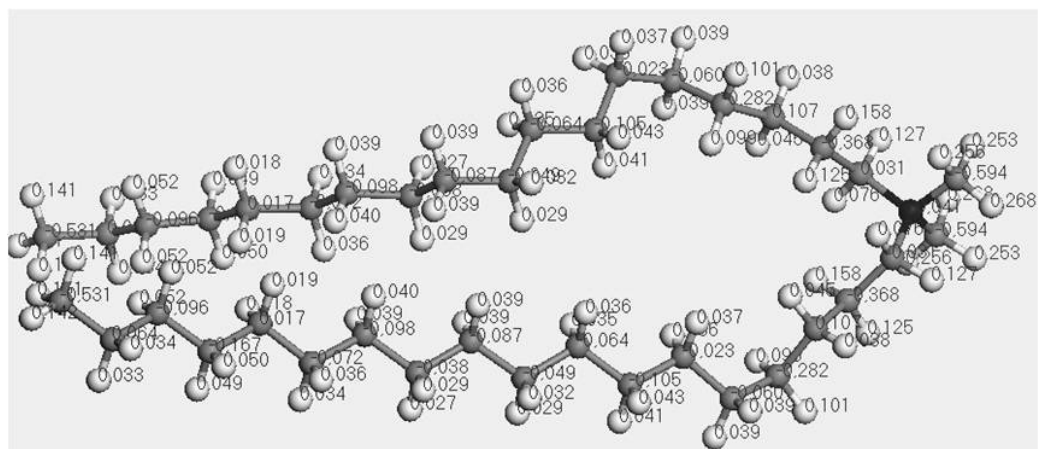


**Figure 4.2:** Structure and atomic charges of DODDMA.

The atomic charges for MMT is calculated by the same method. A cluster of MMT platelet from the optimized periodic cell is prepared with hydrogen saturated edge sites as given in the Figure 4.3 to use the same charge determination methods for the all constituents. Then, PW91/DNP level single point calculation is conducted to find electrostatic charges with Merz-Kolman algorithm.

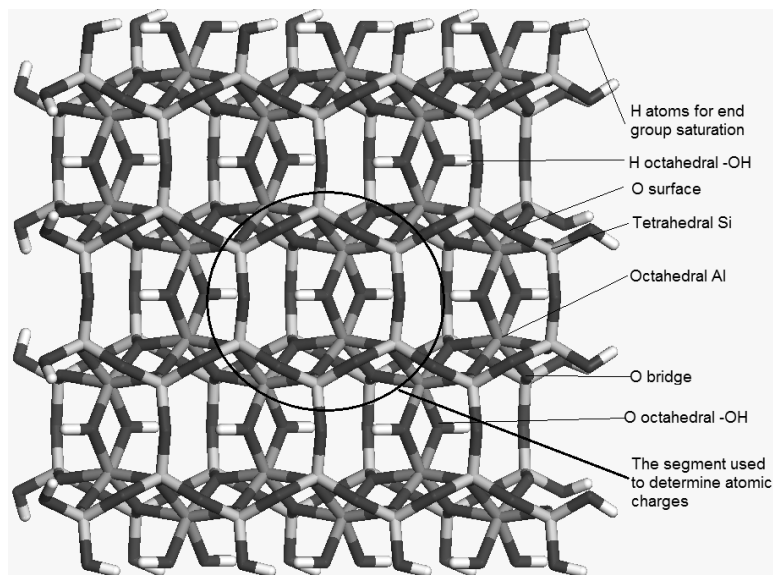


**Figure 4.3:** Structure of cluster used to calculate atomic charges.

The atoms in the middle hexagonal cavity and octahedral layer are used to find average charges for the clay layer as given in the Table 4.2.

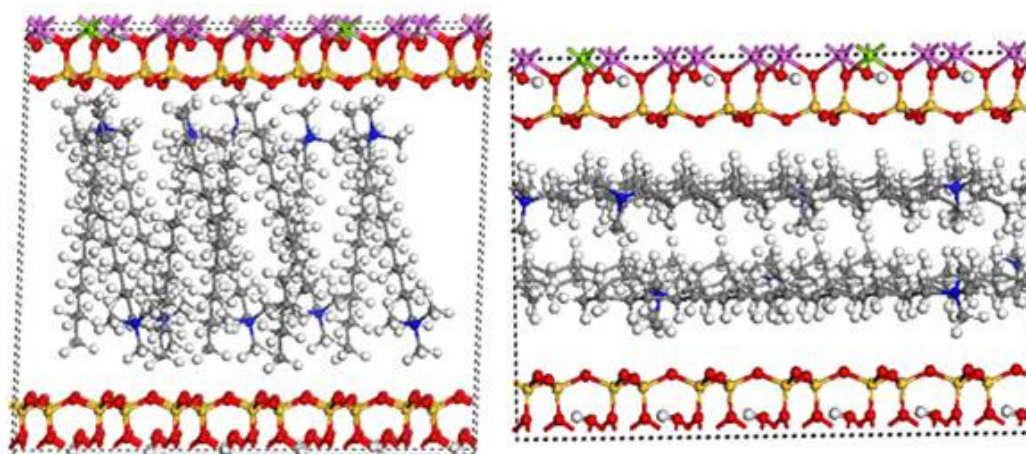
**Table 4.2:** The Charges of Atoms in Montmorillonite.

	Si	Al	Mg	Na	O <sub>bas</sub>	O(H)	H	O <sub>api</sub>
Skipper	1.2	3	2	1	-0.8	-1.424	0.424	-1.0
Heinz	1,1	1.45	1.1	1	-0.55	-0.683 -0.792 <sup>a</sup>	0.20	-0.758 -0.867 <sup>a</sup>
This study	1.3	1.45	1.1	1	-0.739	-0.683 -0.792 <sup>a</sup>	0.316	-0.758 -0.867 <sup>a</sup>

<sup>a</sup> when bonded to Mg defect

The MD simulations were carried out with the polymer consistent force field modified for silicate applications (PCFF-silicate force field) which was used successfully for organoclays several times only with difference in atomic charges of the MMT layer [247,248]. A cutoff for van der Waals interactions at 1.2 nm, and evaluation of Coulomb interactions through Ewald summation with very high accuracy  $10^{-6}$  kcal/mol.

The surfactant cations were manually placed into the montmorillonite interlayer with their longest chains oriented in a direction approximately parallel to the plane of the clay layers, similar to the method described in the literature [87]. By using two initial structure of the HDTMA<sup>+</sup>/MMT2 hybrids given in the Figure 4.4, the basal spacing and energy minimum was calculated. Second structure where the surfactants were parallel to the clay layers was found to be has %1-2 lower in energy. In addition, basal spacing found to be 17,75 Å which is more consistent with the experimental results.

**Figure 4.4:** Two initial geometries for the HDTMA in MMT2 clay.



Simulations were performed in the canonical NVT ensemble by using Nose thermostat a time step of 0.001 ps (1 fs), to let the system reach its equilibrium. Previous studies showed that, since the system is very confined at 298 K with even 100 ps of simulation time proved to be sufficient for equilibration. Our equilibration method both involves molecular mechanics minimizations and dynamics steps given below.

- I. 1000 steps of minimization with a smart algorithm followed by at least 150 ps simulations at 700 K.
- II. 5000 steps of minimization with a smart algorithm followed by at least 150 ps simulations at 500 K.
- III. A new 5000 steps of minimization with a smart algorithm followed by at least 150 ps simulations at 300 K followed by the last 5000 steps of minimization.
- IV. 100 ps simulation at 300 K where last 50 ps trajectories were saved for analysis. To save time, only the data (including coordinates, velocity, force, and statistic quantities) for the hybrid with the energy minimum are collected every 5 ps in the last 50 ps for further analysis.

During the molecular simulations, the fractional coordinates of atoms in montmorillonite layers were not fixed because the assumption that the clay layer is rigid was shown to be false at last decade. Next, basal spacing is fixed during the MD simulations and move freely in the z-axis of cell geometry during the minimization steps with respect to the organisation of the surfactants in the layer. Effect of alkyl onium chain lengths on the interlayer interactions and basal spacing were analyzed. The most stable positions of polar alkyl onium heads on the clay surface were found.

#### **4.1.2 Surfactants used in the calculations**

Most of the commercially available organoclays are produced by exchange of alkali or alkali earth cations in the interlayer space of clay minerals with alkyl ammonium salts. Organoclays are less expensive than other nanomaterials, because the basic materials come from readily available natural sources and because they are produced in existing, full-scale production facilities. Commercial suppliers include Laviosa Chemica Mineraria, Nanocor, Süd Chemie and Elementis Specialites. The well-known commercial organoclays are Cloisite from Southern Clay Products have been

used to produce polymer nanocomposites. Chemical nomenclature will be used in this study.

The list of the surfactants chosen for investigation in these study is given below in Figure 4.5.

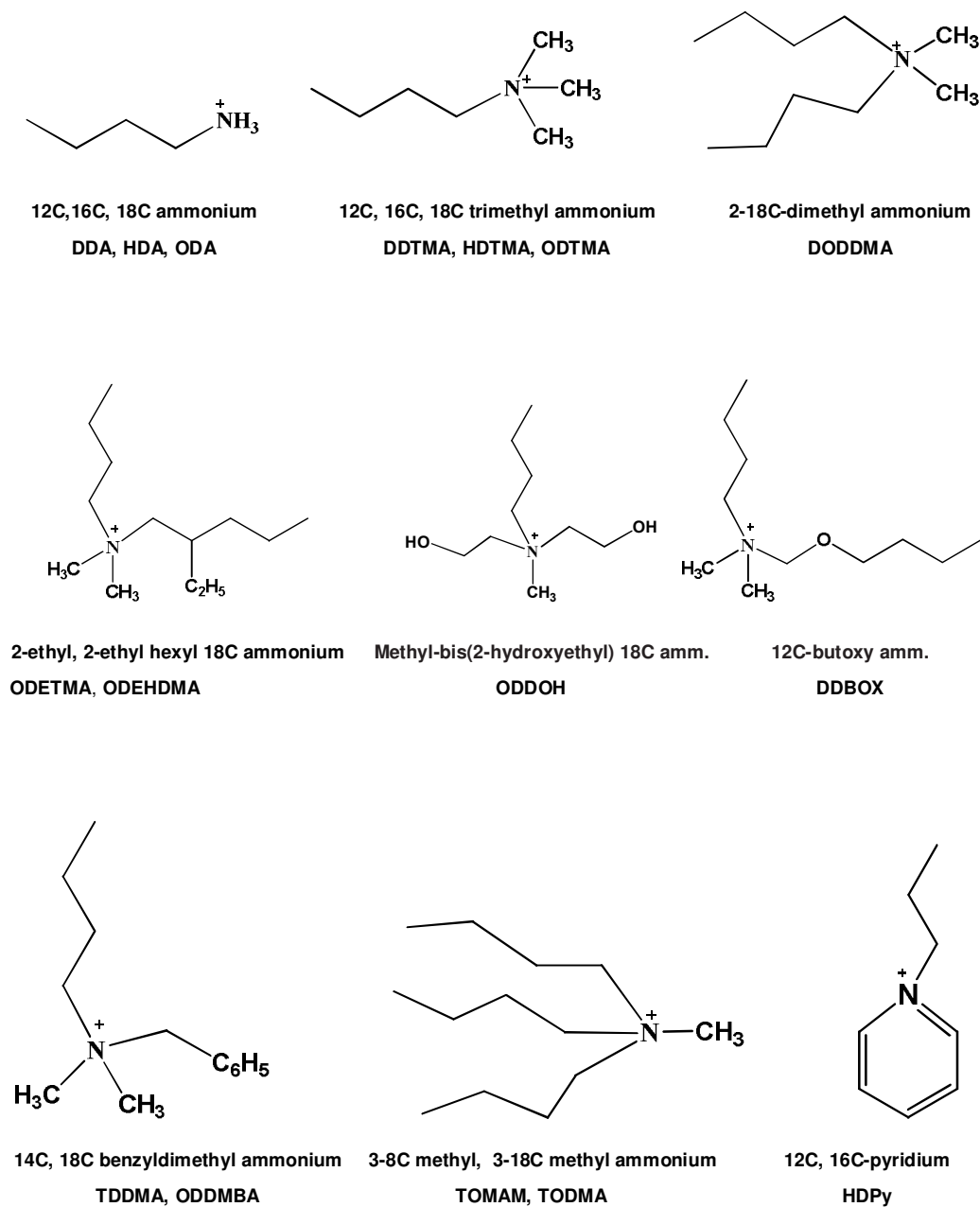
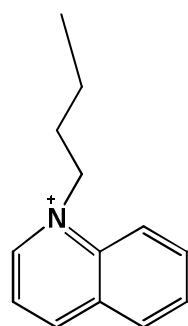
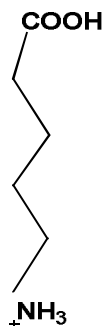


**Figure 4.5:** Structures and symbols of cationic surfactants used in this study.



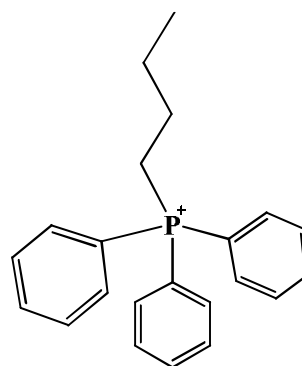
16C-quilinium

HDQ



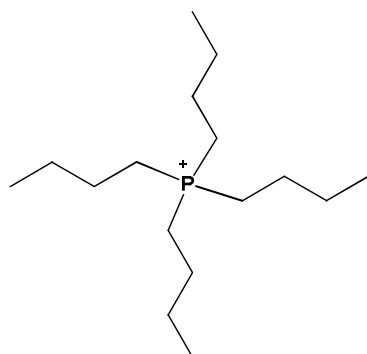
12C aminolauroic acid

12AMIN



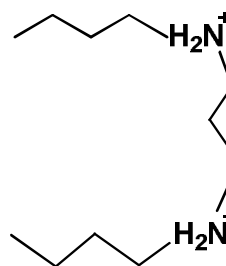
12C, 16C triphenyl phosphonium

DDTPP, HDTTP



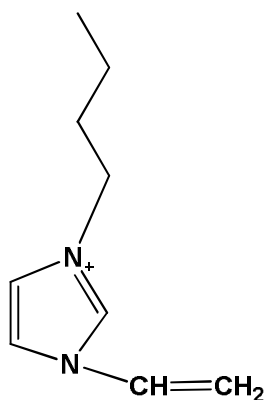
14C, 16C tributyl phosphonium

TDTBP, HDTBP



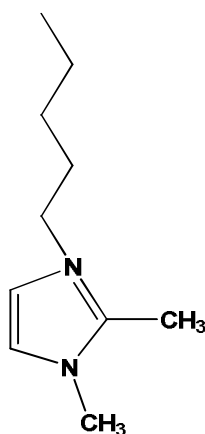
12C-4C-12C, 12C-8C-12C dimeric (gemini) ammonium

GEM4, GEM8



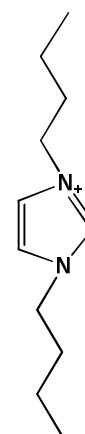
N-vinyl 16C imidazolium

IMID



12-dimethyl 16C imidazolium

12IMID



2-18C-imidazolium

2IMID

**Figure 4.5 (cont):** Structures and symbols of cationic surfactants used in this study.

## 4.2 Results and Discussions

### 4.2.1 General structure and basal spacings in organoclays at equilibrium

The basal spacing values ( $d_{001}$ ) were obtained from the end of a MMT platelet to the end of next platelet. Basal spacing increases for all the surfactant types independent from the type of head groups, number of alkyl tails and length of the carbon tails. The basal spacing between clay layers also increased for all cation exchange capacities as given in the Table 4.3.

**Table 4.3:** Basal spacing values calculated by MD and experimental XRD.

Surfactant	$d_{001}$ (MMT1)	$d_{001}$ (MMT2)	$d_{001}$ (MMT3)	Experimental[86]
12AMIN	14.01	16.79	20.05	13.5 14.0
DDA	17.73	18.00	19.28	14.0
DDTMA	14.36	17.24	22.40	18.3
HDA	14.13	18.22	22.30	
HDTMA	14.41	17.75	22.42	14/15.7/18.0 14.8/17.8/22.5 14.8/17.8/19.5 25.0, 18.0 14.8 <sup>0.5 CEC</sup> /22.2 <sup>1.0 CEC</sup>
ODA	14.66	17.47	22.63	15.7, 24.6, 21.8, 18.0
ODTMA	16.15	17.97	23.56	20.7, 20.4 17.75 <sup>0.6cec</sup> /19.03 <sup>1.0cec</sup> 20.9 <sup>1.0 cec</sup> 23.7 <sup>high CEC</sup>
ODETMA	19.20	19.39	25.39	
ODEHDMMA	19.53	22.27	28.06	20.4
TDMBA	16.69	18.33	23.42	20.78
ODDMBA	17.21	17.95	26.49	18.6, 20.7 18.3-24.4 <sup>0.5 CEC</sup> /27.6 <sup>1.0 CEC</sup> 18.4-19.2
ODDOH	19.43	20.77	26.28	18.2, 18.5, 18.4
DDBOX	18.23	20.12	23.74	14.7
DODDMA	19.35	26.77	34.74	25.7, 24.3 24.2-31.5 19.8-24.8 25.9, 24.2
TOMAM	17.57	20.91	28.62	
TODMA	24.75	31.97	42.33	35.14 <sup>low CEC</sup>
DPy	14.56	18.36	21.15	
HDPy	15.72	18.39	23.02	17.0-17.7, 17.5, 23.7
HDQ	18.81	19.23	23.99	20
İMİD	15.28	19.92	24.09	18.8, 18.1
3MIM	15.56	18.51	26.98	22
12MIM	15.70	18.32	24.73	17.7, 18.2, 21.9
2IM	18.79	25.22	32.21	24.9
DDTPP	17.64	20.12	26.13	18.2
TDTTPP	18.83	21.24	26.69	
TDTBP	18.74	21.17	27.12	21.9
HDTBP	19.13	21.51	29.27	23.2
GEM4	14.75	19.53	22.92	
GEM8	18.31	21.27	24.31	20.48

The range of the gallery increase between clay layers was diverse.

- i. The distance between clay layers were mainly dependent on the cation exchange capacities that determines the number of surfactant between MMT platelets. MMT3 based organoclays have the highest distance between clay layers as expected.
- ii. The number of alkyl groups in the tail of the surfactant is an important factor that TODMA has higher basal distance than DODDMA and DODDMA has higher basal distance than ODTMA for all clay types.
- iii. The second factor related to the surfactant structure is tail length depending on the number of carbon atoms in the alkyl tail. The order for the basal distance is ODA>HDA>DDA, ODTMA>HDTMA>DDTMA and HDTBP>TDTBP for the same CEC values.
- iv. The last important factor that determines the organoclay gallery is the structure of head group. There were several examples for this effect. The basal spacing orders such as HDTBP>HDTMA>HDA, TDTBP>TDTMA, 12IMID>3IMID, DEHDMA>ODETMA>ODTMA>ODA, HDQ>HDPy, DDBOX>DDTMA were some of the important examples for the effect of head group volume in surfactants to the basal spacing between MMT platelets.

Another important result valid for all surfactants is the coordination of all the head groups by the clay surface and lying of all alkyl tails towards the gallery. As given in Figure 4.6, MMT clay is intercalated by surfactants and interlayer gallery increases by 2 to 4 folds with respect to CEC of the clay and structure of surfactants.

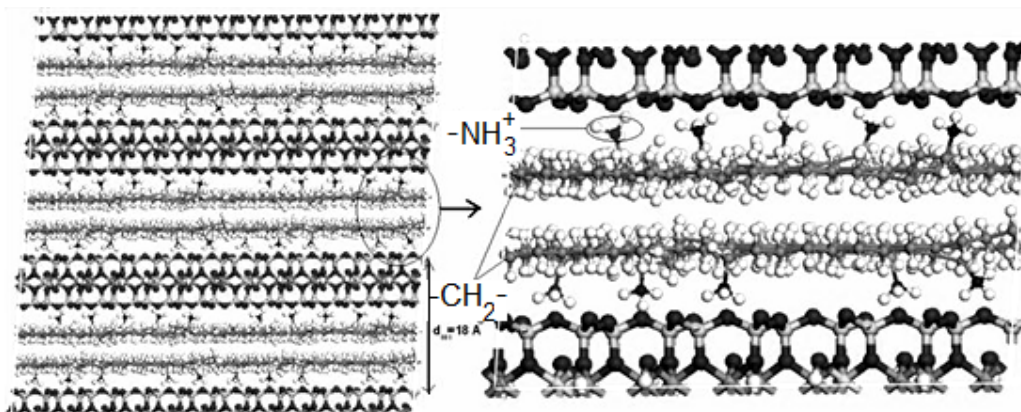


**Figure 4.6:** Organoclay structure formed by MMT2 and ODA.

This general structure causes the formation of electrostatic zone in the gallery by the ionic interactions between cationic head groups and the anionic clay layer. Alkyl tails of the surfactants resulted in the vdW zone, which is crucial for the polyethylene nanocomposite. Hydrophobic PE chains can intercalate between the galleries by relatively hydrophobic interactions only if the vdW zone exists (Figure 4.7).

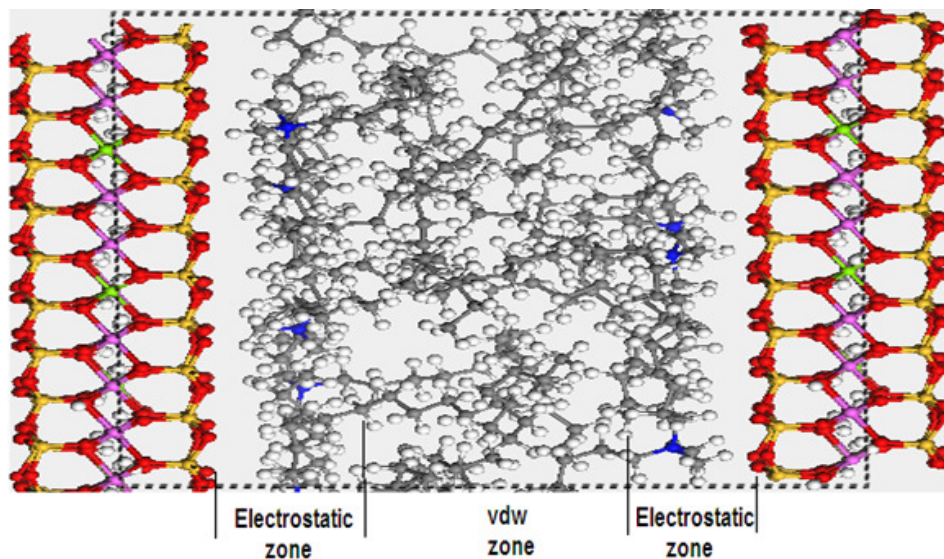


**Figure 4.7:** The general structure of organoclay structure.

The last general result observed for the organoclays is the most important one that there exists a specific layering behavior between the clay layers with respect to the packing density of the surfactants. The packing density is strongly dependent on the alkyl tail length, number of tails, CEC of the clay and structure of the head group. When the surfactant packing density is low, the monolayer which is lying parallel to the clay surface is observed. This structure is valid for DDA, HDA, ODA, 12AMIN, DDTMA and etc. Several XRD studies show that organisation of surfactant tails within the clay galleries causes formation of four main structure that were monolayer, bilayer, pseudotrilayer and paraffinlike structure [248-250]. The basal spacing the clay layers for the single layer is mostly smaller than 15 Å that means this kind of structure is not suitable for the intercalation of polyethylene chains. Since the interactions between clay surface is very strong and the interaction among the alkyl tails were weak. The increase in the alkyl tail density by increasing chain length and coverage reveals the repulsive interaction resulted in the strong layering behavior above a critical value, which is supported by the proposed structures in organoclays with various surfactant packing densities. At highest surfactant densities,

the free area in the gallery disappear and alkyl tails were tilted over each other resulted in the formation of trilayer and paraffinlike interlayer structures (Figure 4.8).

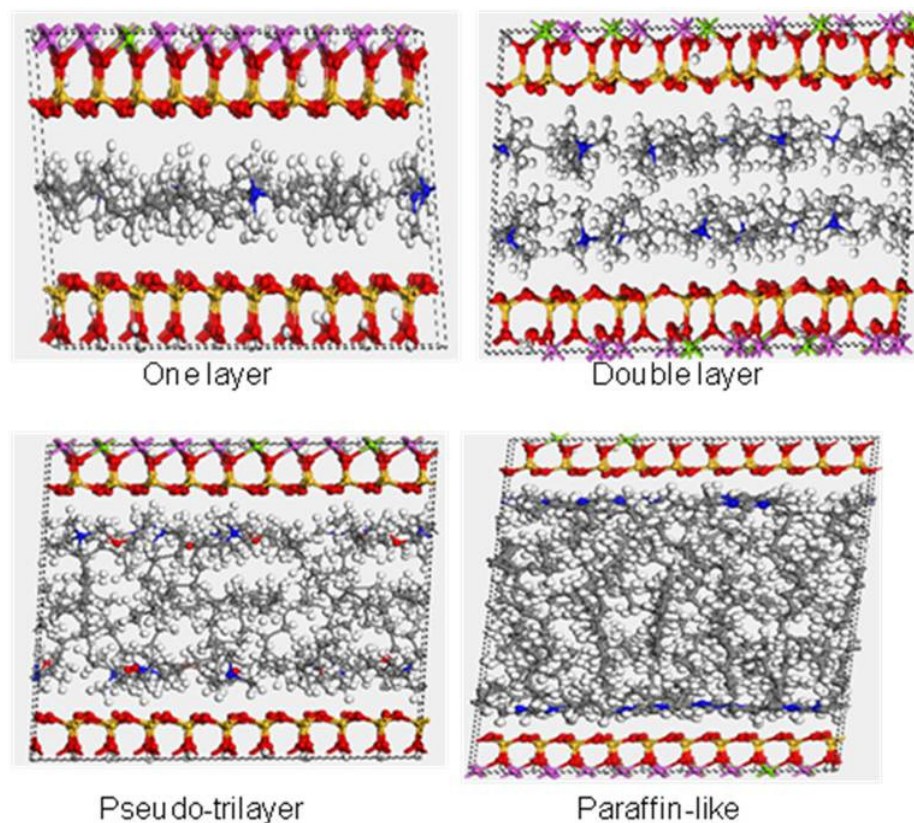


**Figure 4.8:** General layering behaviors of the organoclays.

#### 4.2.2 Interaction behaviour of head groups on the clay surface

As mentioned above, all the head groups of surfactants were coordinated by the MMT surface and form two layers in the gallery due to the two clay surface at the each gallery. The layering behaviour of alkyl tails was also diverse. The strong repulsion was observed between the electrostatic zone and vdW zone especially for the polar head groups such as primary alkyl ammoniums (Figure 4.9).



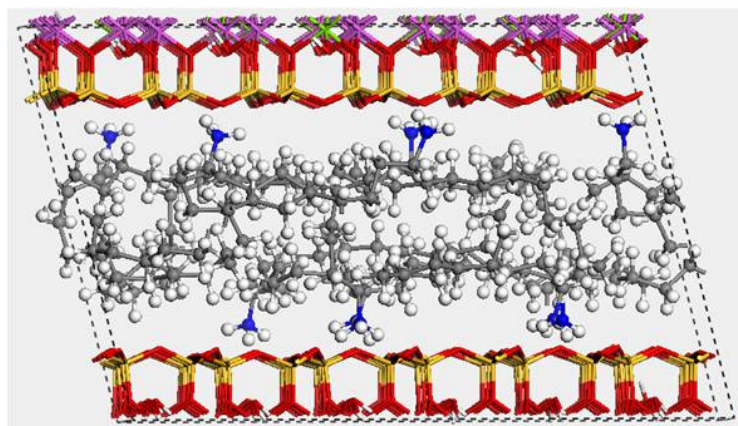


**Figure 4.9:** Organoclay structure based on the primary alkyl ammonium.

As a result of the different interaction strength between the ammonium head groups and methylene groups, the density profiles of these groups have the one for ODA surfactant in MMT2 clay is given in the Figure 4.10. Bilayered structure for both the alkyl tail is hold in the middle of the gallery and ammonium group is hold at the clay surface were observed. Different layering behaviours of alkyl tails were governed by this interlayer position of chains.

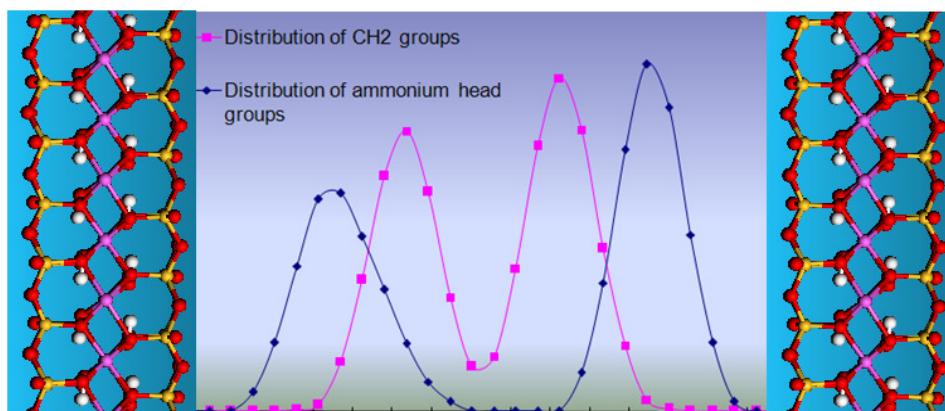


**Figure 4.10:** Interlayer distribution of head groups and alkyl tails in organoclays.

Our analyses on the structure of the ammonium head groups on MMT showed that the ammonium ( $-\text{NH}_3^+$ ) headgroups were strongly coordinated by hydrogen bonding to the cavities on the clay surface which is also supported by the experimental spectroscopy where the N-H stretching mode in IR vibrational frequency shifts to a low value in addition to the increased mobility of the tails that means pinning of head groups to the clay surface. All the ammonium based surfactant head groups have similar structure except the ones that have a hydrogen bonding capacity (Figure 4.11).



As seen from the Figure 4.11 primary alkyl ammoniums were coordinated with smaller H...O distances by the hexagonal cavities because of the stronger hydrogen bonding with respect to the tertiary alkyl ammonium. However the surface coverage is higher for these trialkyl based surfactants.

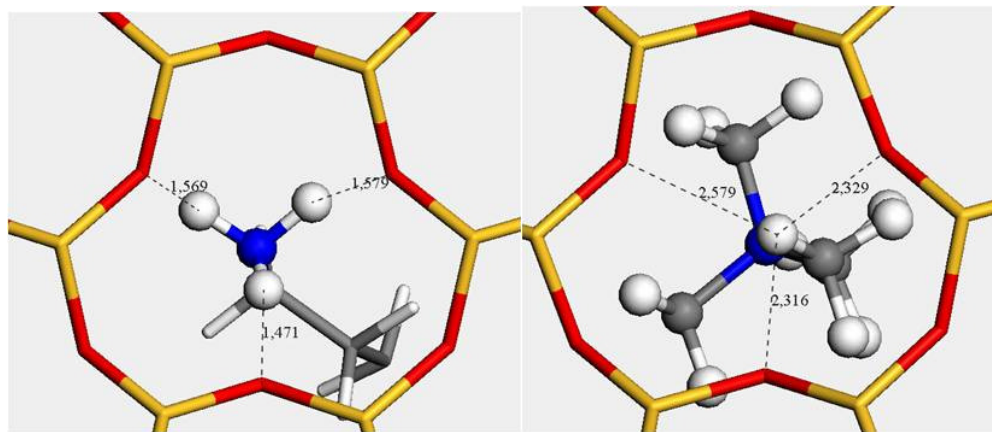


**Figure 4.11:** Equilibrium positions of ammonium head groups in organoclays.

The phosphonium based organoclays which have higher surface coverage due to the large head groups lie over the clay surface. The tributyl phosphonium is a good alternative for polyolefins and triphenyl phosphonium is a good alternative surfactant for the polystyrene based clay nanocomposites (Figure 4.12).

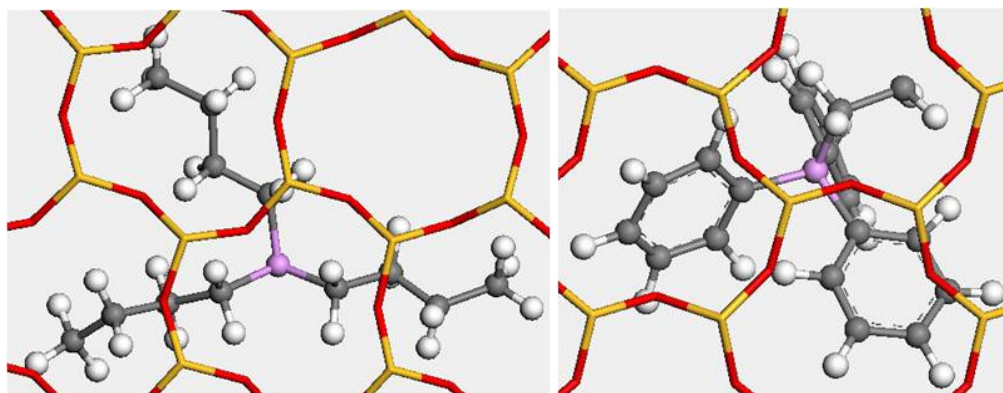


**Figure 4.12:** The head group positions of phosphonium based surfactants in organoclays.

Ring type surfactant head groups such as imidazolium, pyridium and quolinium head groups were parallel to the clay surface at equilibrium structures (Figure 4.13). Charge delocalization is more in these conjugated head groups causes more distributed and homogeneous interaction with clay surface and parallel positioning of ring type head groups. Although surface coverage of these surfactants were high and

thermal stability of organoclays were better than ammonium types, industrial usage of these surfactants were very new [70]. First experimental studies showed increased mechanical properties in polyethylene nanocomposites for these surfactants.

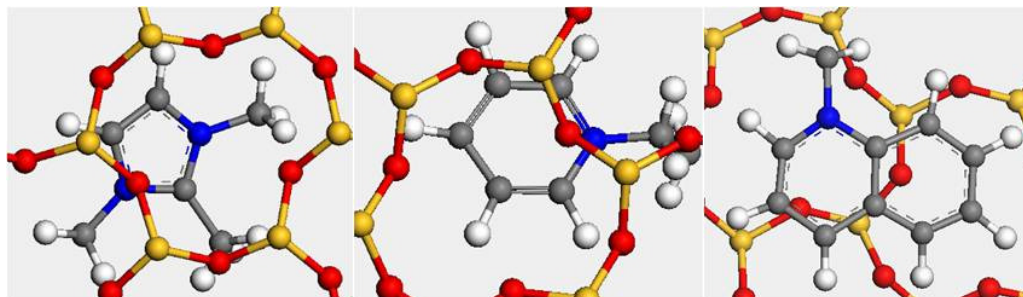


**Figure 4.13:** The head group positions of surfactants with ring type head groups in organoclays.

The atomic concentration profiles of nitrogens in z-direction from one clay layer to other for all the surfactants with octadecyl length and below that reveal bilayering behavior for MMT1 and MMT2 (Figure 4.14). Half of the head groups were close to the one MMT platelet and half to the other. This makes the concentration profile of nitrogen atoms sharp and separated. Single layer of alkyl tails have 4-5 Å thickness. If the surfactant packing density is low such as for ODTMA, the nitrogen atomic concentration displays two close peaks that can let only single layer alkyl tails between ammoniums. For higher tail densities bilayer of nitrogen occurs again this time with well-separated twin peaks such as for DODDMA and TODMA. These two well separated peaks reflect that the interlayer structure for the alkyl tails can have enough space to have bilayer or trilayer structure.

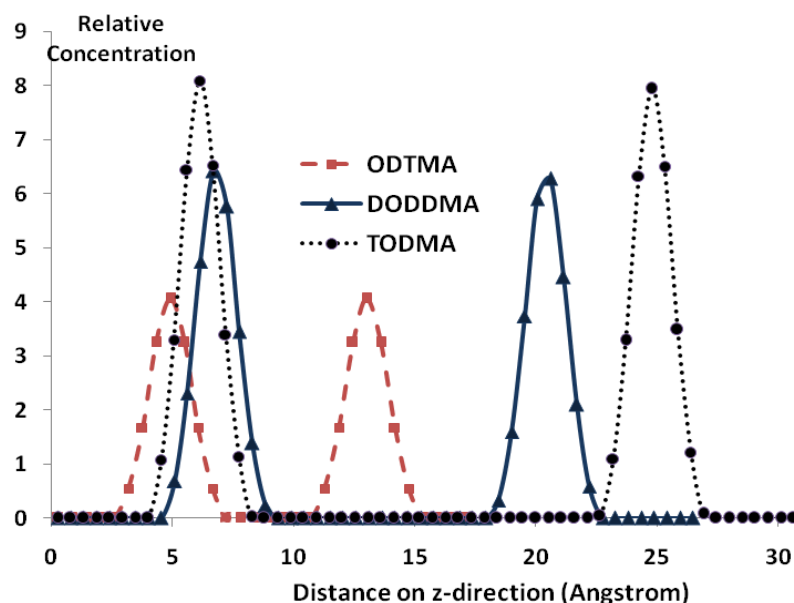


**Figure 4.14:** The concentration profiles of head group nitrogens among z-direction in MMT2.

The atomic concentration profile of ammonium nitrogens were very similar to the MMT1 and MMT2 based organoclays for MMT3 clays except the increased separation between head groups together with basal spacing. These increased basal spacing governs the alkyl tail layering behaviour will be analyzed in the next section. The nitrogens were very close and strongly bonded to the clay surface and have bilayer just like the MMT platelets that pinned with.

There is only one exception for the bilayer nitrogens near the clay surface is for the one with TODMA in MMT3 based organoclay (Figure 4.15). This model is the one with longest alkyl tail, highest CEC and highest number of alkyl tails. The highest packing density between the clay layers resulted in small concentrations of nitrogen density in the gallery due to the steric hindrance which is an unfavorable case.

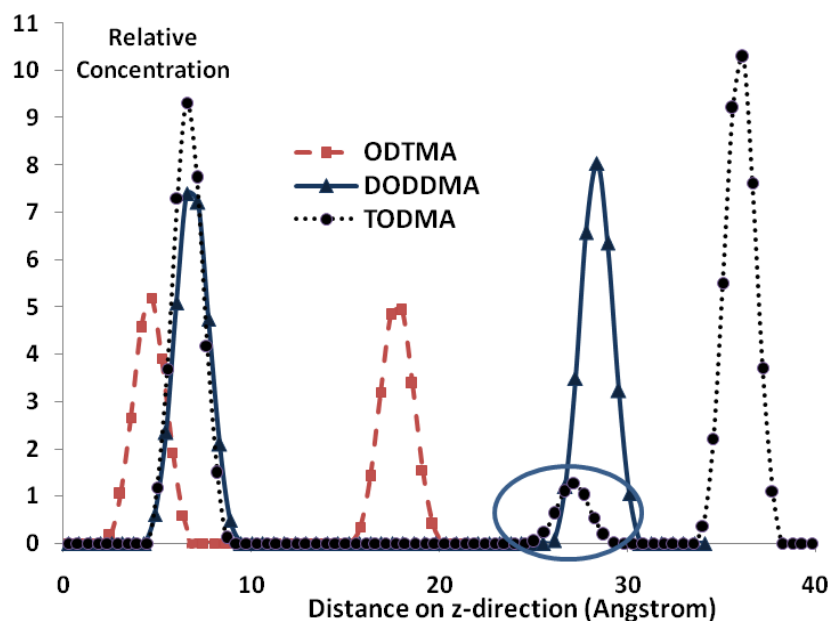


**Figure 4.15:** The concentration profiles of head group nitrogens among z-direction in MMT3.

#### 4.2.3 Effect of cation exchange capacity on the organoclay structure

Layering behavior of alkyl tails that determines the vdw region ready to interact with PE chains were strongly dependent on the clay types determined with respect to layer charge. This is because the amount of surfactant between the clay layers were determined by CEC of the MMT. The CEC of the clay not only determines the gallery distance and layering behavior but also the surface coverage as shown for ODA for MMT1, MMT2 and MMT3 respectively in Figure 4.16. Amount of surface coverage increases with respect to the number of surfactant molecules on each platelet.

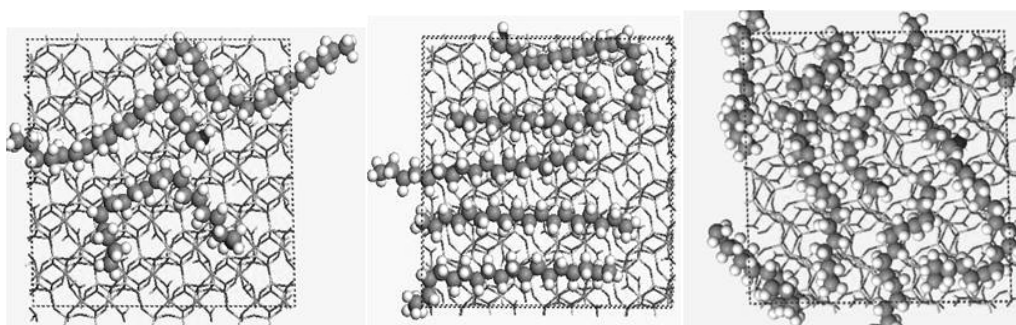
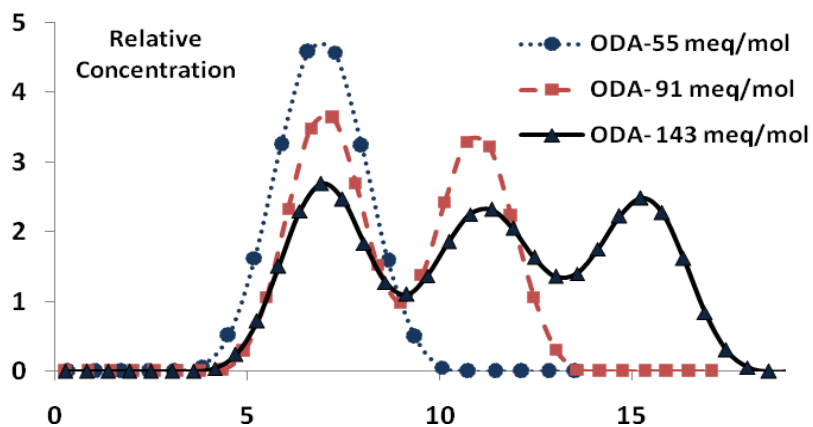


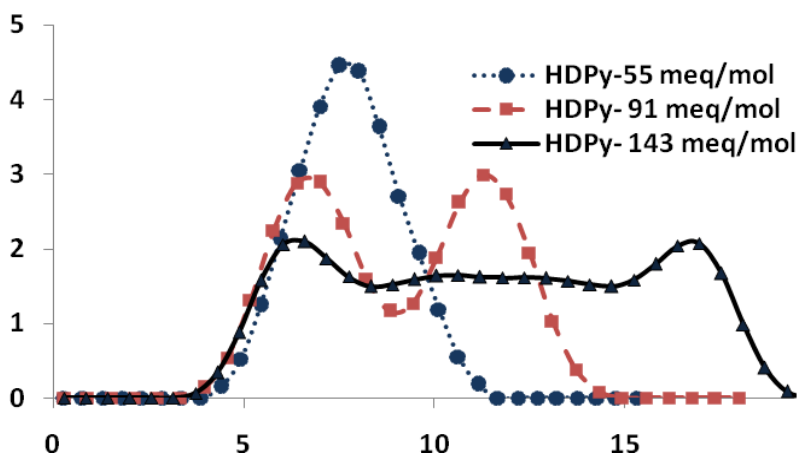
**Figure 4.16:** Surface coverage of ODA with increasing CEC of MMT.

The concentration profiles of methyl groups which determines layering behaviour of alkyl tails in the gallery were analyzed in this section for different MMT types. The concentration profile of these  $-\text{CH}_2$  groups on z-direction for ODA, HDPy and 3MIMID at different CEC of clays were given in the Figure 4.17. All the MMT1 based organoclays have single layered alkyl tails independent of the type surfactant. When we move forward to the MMT2 based organoclays bilayer structures observed with well-separated peaks. Trilayer structures of tails were observed for ODA type surfactant in MMT3. Surfactant tail groups were oriented parallel to the MMT surface in these organoclay structures. However, the disappearance of middle peaks observed for the HDPy and 3MIMID based organoclays in MMT3 type clays. This indicated the tilted or relatively vertical alkyl chains between clay layers depending on the increased packing density. Even a fourth layer can be observed for 3MIMID type organoclay with lower sharpness which indicates formation of paraffinlike alkyl layers. The surfactant packing density not only determines the gallery distance or layering behaviour but also the orientation of the chains.

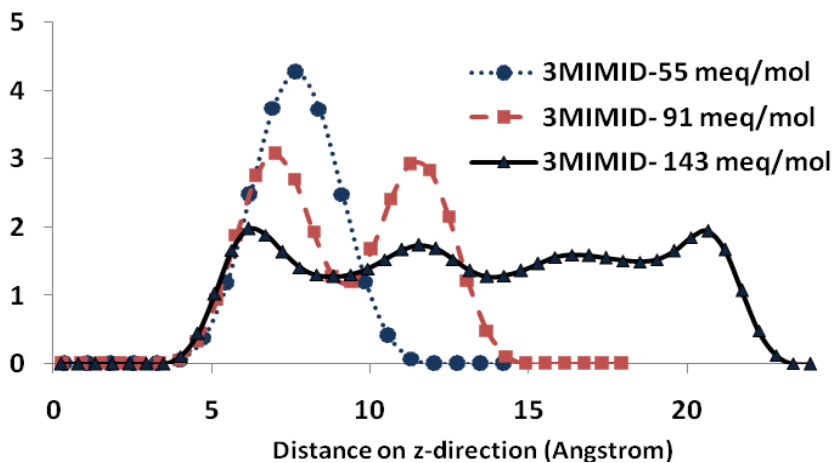
If we compare the nitrogen atomic concentration profiles with the carbon atomic concentration profiles, the separation of nitrogen atoms and distribution have more ordered layering behavior due to the stronger ionic interaction between head groups and MMT. Less organized layering behaviour of hydrocarbon tails were related to the weak vdw interactions and non existence of any strongly bonded surface. That is the reason why all nitrogen atoms in the head group can stay easily in the same distance from the MMT demonstrated by sharper peaks.



a



b



c

**Figure 4.17:** Concentration profile of  $-\text{CH}_2$  groups for a) ODA, b) HDPy and c) 3MIMID at different CEC of clays.

#### 4.2.4 Effect of number of chains in surfactants on the organoclay structure

The second important factor that increases the surfactant packing density and vdw interactions in the gallery can be controlled by number of tails in the surfactant. The surface coverage of polar MMT surface can be enhanced as it can be seen for the MMT2 based organoclays with ODTMA, DODDMA and TODMA that have mono, di and tri octadecyl alkyl tails (Figure 4.18).

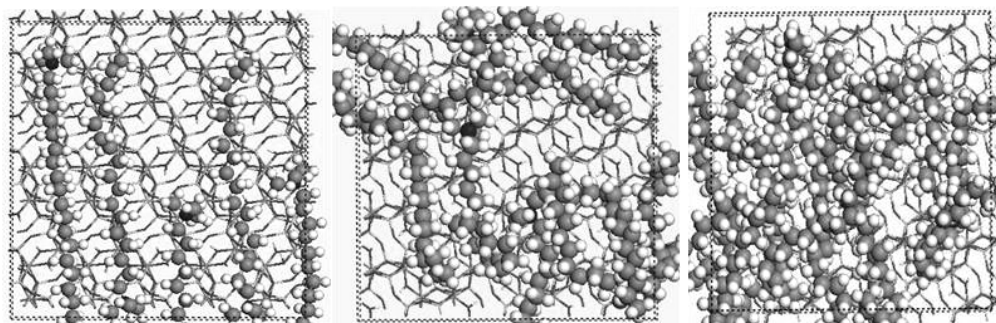


**Figure 4.18:** Surface coverage of MMT2 based organoclays with ODTMA, DODDMA, TODMA.

The methyl group concentration profile for single and double alkyl chains of imidazolium is given in the Figure 4.19a for MMT1. Also the same profile for single, double and triple alkyl chains of trimethyl ammonium surfactants were given in Figure 4.19b for the same clay. The low CEC clay, MMT1 was chosen since monolayer to bilayer transition can be seen for the alkyl tails more easily for the low CEC models. ODTMA and 3MIMID have monolayer and others have bilayered alkyl tails in the gallery. The layering behaviour strongly effects on the gallery distance as the bilayer formation happens, the gallery distance must be higher than 15 Å in the models.

For the Figure 4.19c, where the ODTMA, DODDMA and TODMA used as surfactants in MMT2 based organoclay alkyl tail layering behaviours were given. ODTMA still have monolayered alkyl tails and DODDMA have bilayered alkyl tails with increased basal distance due to the number of surfactants to compensate CEC. The TODMA based organoclays has pseudo-trilayer tails between the gallery understood from the methyl concentration profiles. It is believed that trilayer is electrostatically unstable and alkyl layer can tilt vertically to transform into the paraffinlike structure.

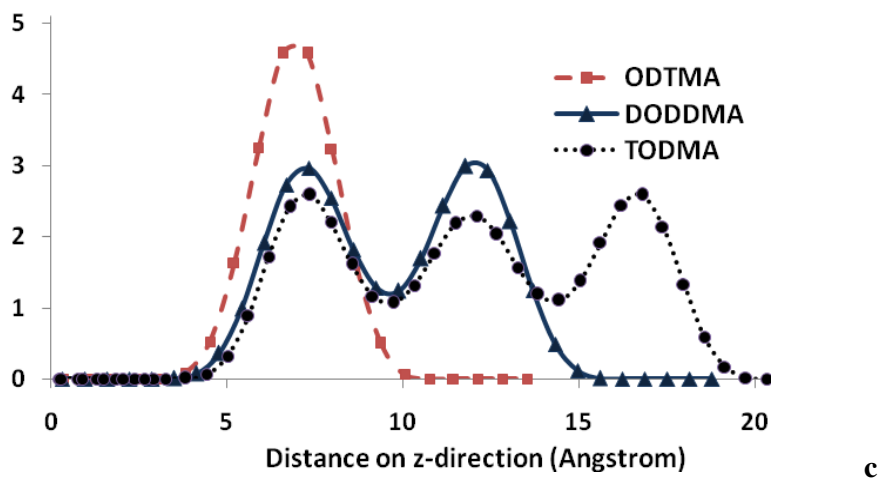
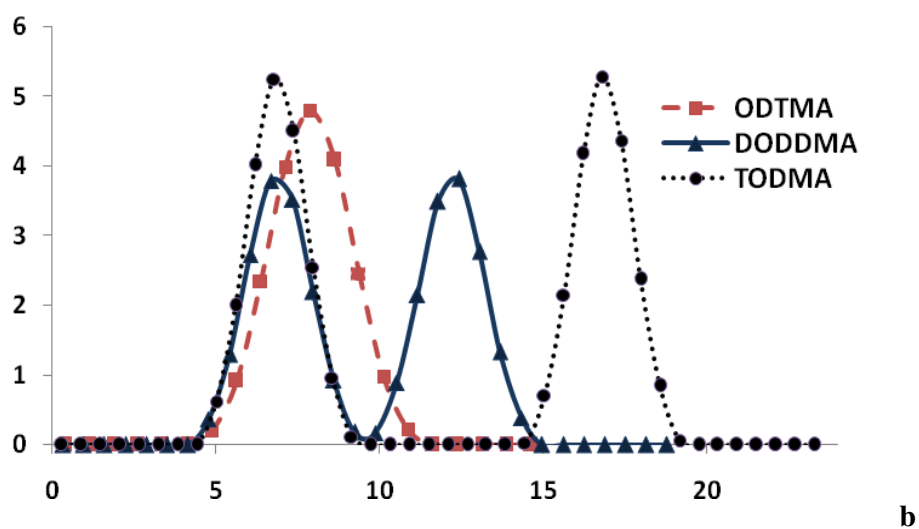
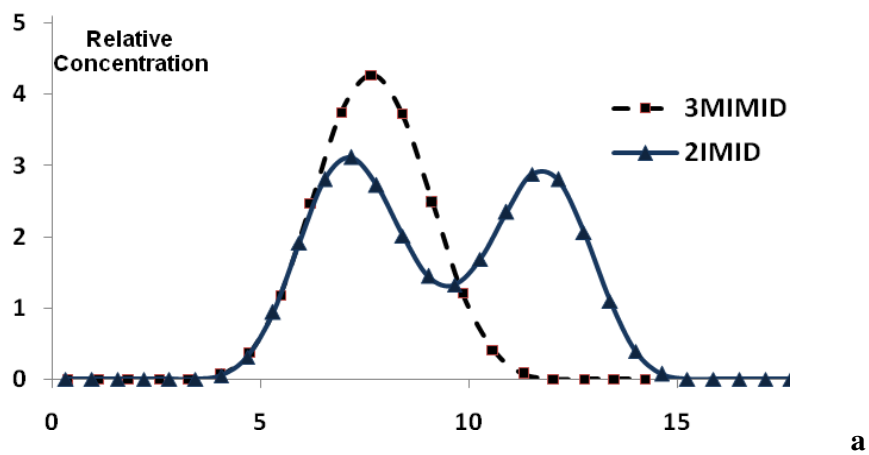


**Figure 4.19:** Concentration profile of  $-\text{CH}_2$  groups for surfactants with different number of tails.



#### 4.2.5 Effects of alkyl tail length of surfactants on the organoclay structure

For a given clay structure, an increasing trend in the alkyl tail length for the surfactants that have same head group resulted in the increased basal spacings. Some models were chosen to show how the increase in the tail lengths reflects to the basal spacing and interlayer structure in Figure 4.20.

The monolayer to pseudobilayer change in the arrangement of alkyl tails is observed in Figure 4.20a, for TDBMA and ODMBA with MMT1, low CEC clay. It is obviously seen from the end of the peak how the layering effects the increase in the basal spacing. In addition, it is demonstrated that there is a critical value for the basal spacing at around 15 Å, for the transition from monolayer to bilayer alkyl tails.

In Figure 4.20b, the bilayer to pseudotrilayer transform of the alkyl layers for MMT2 clay can be observed for DDTTP and TDTPP respectively. Although the increase in the alkyl length is only 2 methyl size, the critical value of the packing density is reached and causes a jump to the next layer between the gallery.

In Figure 4.20c, another bilayer to trilayer transition was observed for the TOMAM to TODMA in MMT2 clay. The basal spacing change from 20 Å to 25 Å also occurs with bilayer to trilayer transition at the same time.

Although there is no any exact border for the layer transitions, the monolayer structures have basal spacing lower than 15 Å. The bilayer was observed when the intergallery distance is above 15 Å. The pseudo-trilayer and trilayer alkyl structures were observed after 23 Å. Increases in the chain length were found to have less importance than cation exchange capacities and number of tails.

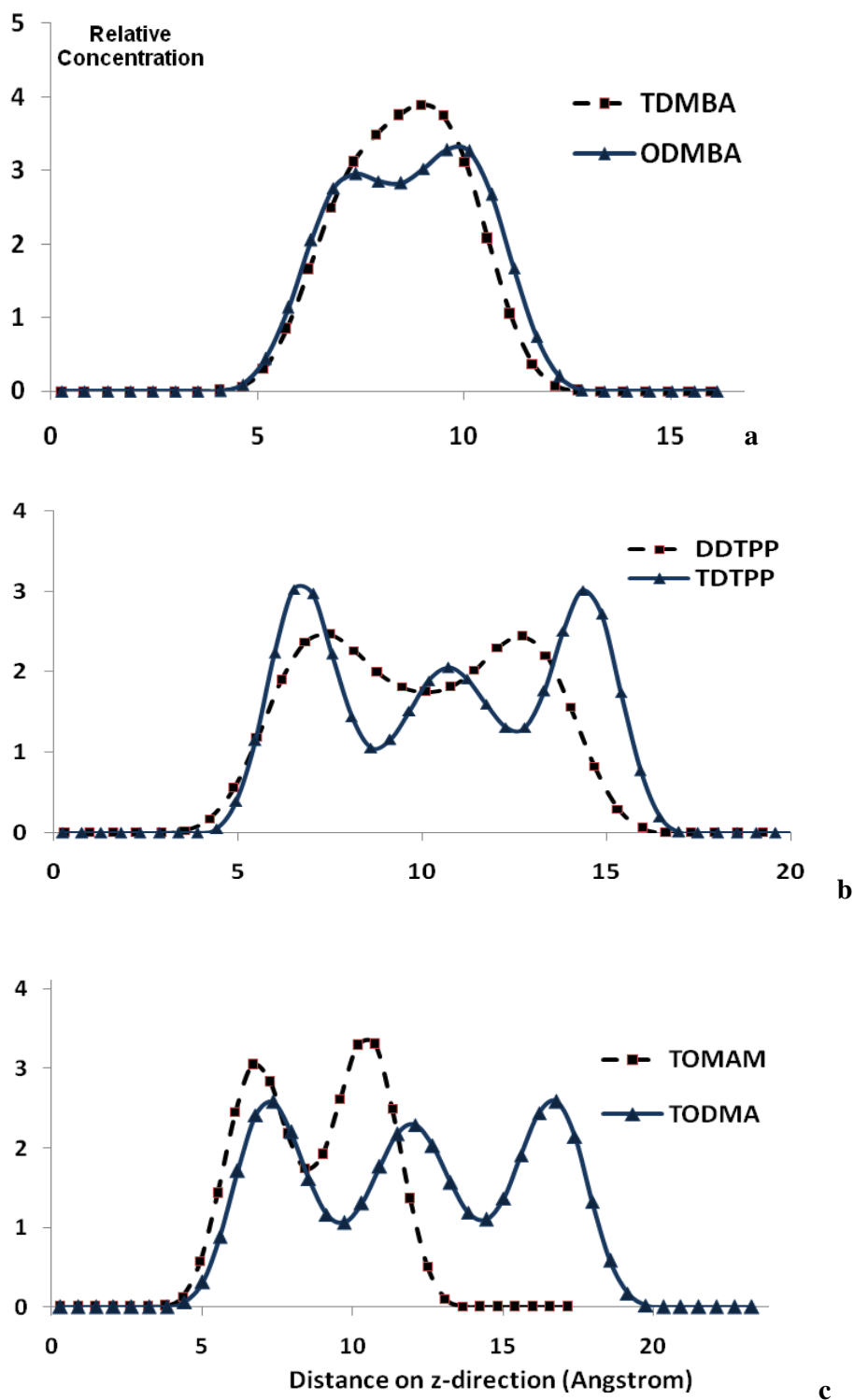


**Figure 4.20:** Concentration profile of  $-\text{CH}_2$  groups for surfactants with increasing alkyl tail lengths.

#### 4.2.6 Effect of head group volume of surfactants on the organoclay structure

Our calculations showed that when the number of methylene groups in the alkyl tails are same in the surfactants, the intergallery distances of the organoclays are higher for the ones with the larger head groups. The surface coverage for MMT2 based organoclays by HDTBP is 80% higher than the one prepared using HDTMA surfactant as seen in the Figure 4.21.

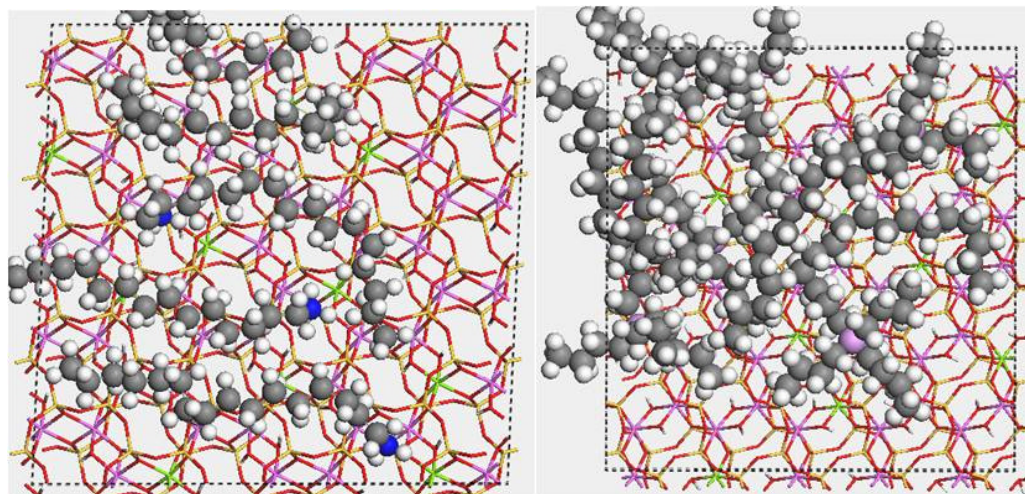


**Figure 4.21:** Surface coverage of MMT2 based organoclays with HDTMA and HDTBP.

The layering behaviors of  $-\text{CH}_2$  between the MMT3 clay can be seen for 3 alkyl chain lengths. The head group volume is changed for each alkyl length and layering of alkyl chains in the gallery is analyzed. The monolayer to bilayer transition can be seen for the 12 carbon atom tailed models in Figure 4.22a by increasing the head group volume. The transition rather than stepwise gradual from monolayer to bilayer was observed when the size of the head group is enhanced.

The bilayer to trilayer transition can be seen for the surfactants with hexadecyl and octadecyl tails. The only factor changes in Figure 4.22 b and c is the head group volume. In all cases firstly the bilayer becomes more obvious with well separated and sharper peaks. As the depth of bilayer peaks increases, the basal spacing increases at the same time. Then the most obvious enhancement in the basal spacing in response to third layer formation takes place when the depth of the bilayer reaches to its maximum.

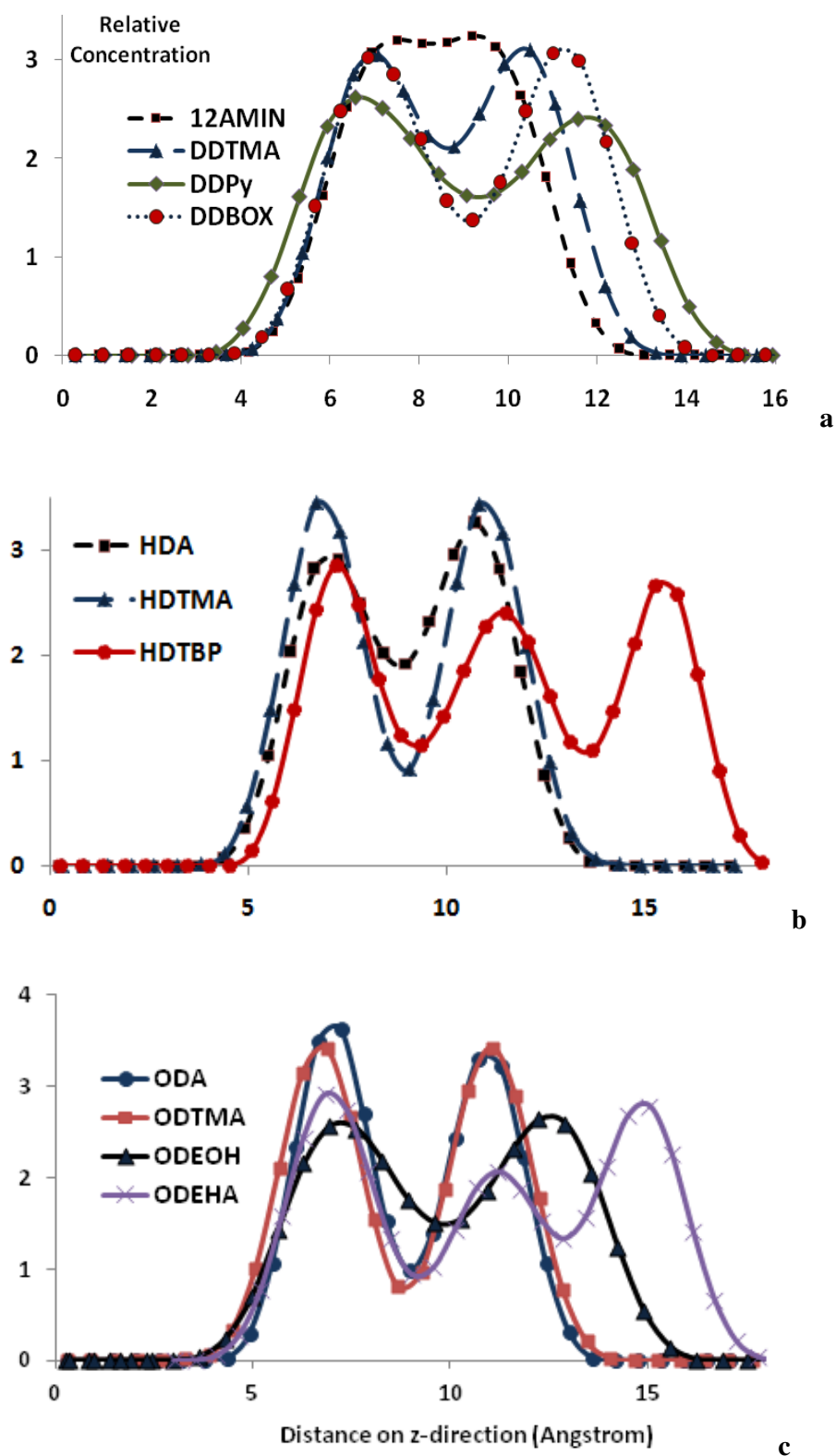


**Figure 4.22:** Concentration profile of  $-CH_2$  groups in surfactants with increasing volume of head groups.

Alkyl layers in the MMT gallery is very sensitive to the head group structure especially if the monolayer or bilayer reaches the limit of the packing density permitted to exist. As seen in the Figure 4.23, when an additional benzene ring added to the pyridinium ring, the third layer started to form in the middle of the gallery.

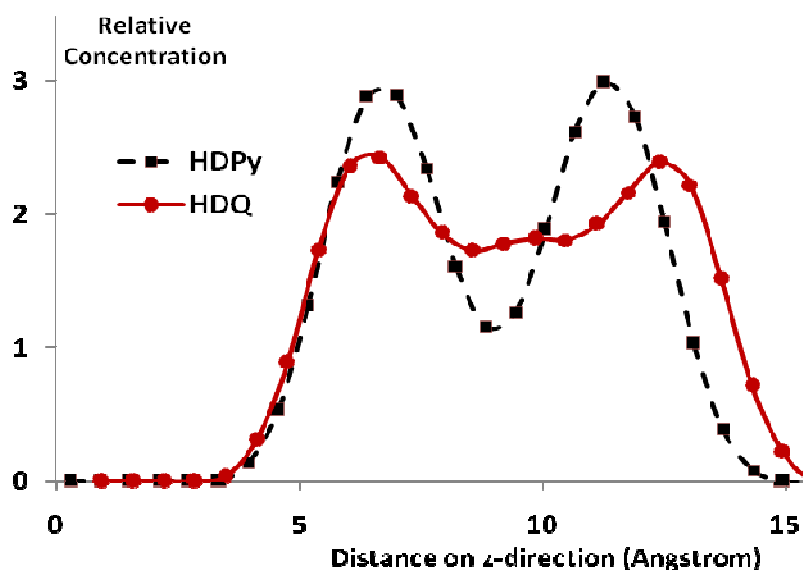


**Figure 4.23:** Concentration profile of  $-\text{CH}_2$  groups in HDPy and HDQ surfactants.

These results are consistent with the experimental results strongly suggests that there exists transition structures between monolayer to bilayer and bilayer to trilayer structures [249]. Monolayer and trilayer structures are definite structures, however trilayer structure is also a transition structure between bilayer and paraffinlike arrangement of surfactants.

In conclusion, organic layer shields the strong polar interactions between clay layers very effectively. Alkyl tails not only increases the layer spacing but also causes a nonpolar zone ready to interact with non polar polyethylene. Intercalation of organic surfactant between layers of clays increased the basal spacing, reduced the interaction of the clay surfaces and changed the surface properties from hydrophilic to hydrophobic. It is expected that these two factors together make the penetration of a hydrophobic polymers into the interlayer galleries possible.

Basal spacing (bs) can be controlled by using an appropriate surfactant. It increases by the surfactants with high CEC, by the number of alkyl tails, by the length of the alkyl tails and by the size of the head group at different extents.

These results are consistent with the experimental results which suggest that there exists more structures than mono-, bi-, and trilayers. These experimentally not well defined structures were observed in our MD simulations.

## 5. BINARY INTERACTIONS IN POLETHYLENE-ORGANOCLAY NANOCOMPOSITES

In this chapter, molecular simulation techniques together with statistical mechanical methods and Flory-Huggins Theory were employed to calculate mixing energies by using binary binding energies and coordination numbers. Since polyethylene-clay nanocomposites consist of several parts such as montmorillonite (MMT), polyethylene, polyethylene compatibilizers and different alkylammonium ions used as surfactants (Figure 5.1); binary interactions is very important for final morphology and organisation in nanocomposite structure. It is known experimentally that the head group of surfactant must have strong interaction with the clay surface for intercalation of surfactants and formation of organoclays. In addition, the PE and PE compatibilizers that constitutes interlayer polymer phase must have strong interaction with organoclay for better mechanical properties of nanocomposites.

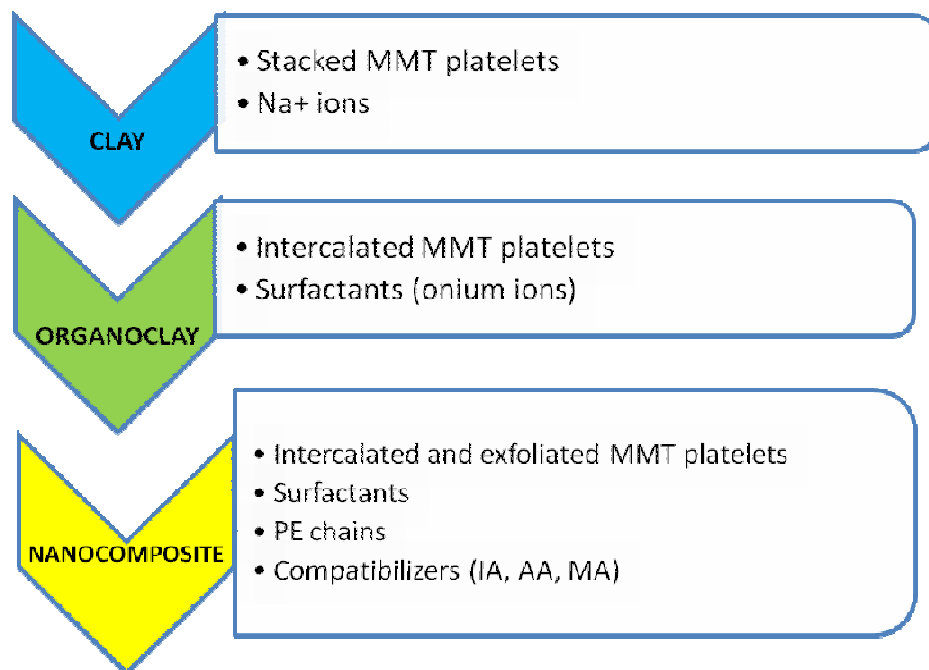


**Figure 5.1:** Constituents of clay, organoclay and PE-organoclay nanocomposite.

These enhanced mechanical properties in polyethylene-organoclay nanocomposites are direct result of exfoliation in melt blending. The compatibilizer increases the

interaction that shown to be necessary in melt blending and causes exfoliation that enhances the physical and mechanical properties of the polymer nanocomposite. The calculation of mixing energies accurately between counterparts of PE-organoclay nanocomposites is very important for the formation, morphology and properties of nanocomposites.

### 5.1 Theoretical Methods Used to Calculate Binary Mixing Energies

Mixing energies of blends or composites are the most important parameters for phase behaviours in blends and composites as shown by the Flory–Huggins Theory.

According to FH theory, the free energy of mixing ( $\Delta G_{\text{mix}}$ ) for polymer chains per mole is given in equation 5.1.

$$\frac{\Delta G}{RT} = \frac{\Phi_i}{n_i} \ln \Phi_i + \frac{\Phi_j}{n_j} \ln \Phi_j + \chi \Phi_i \Phi_j \quad (5.1)$$

In this equation, it is assumed that the segments are randomly distributed and all lattice sites are occupied,  $\Delta G_{\text{mix}}$  per mole of lattice sites is calculated by using the volume fractions of the components ( $\Phi_i$ ) and the degree of polymerization of component i ( $n_i$ ). It is known that the miscibility of the polymeric side groups with the rigid backbone has a great impact on the morphology. The mixing behavior of the polymer chains was studied here by calculating the  $\chi_{ij}$  (chi) thermodynamical parameter. The first two terms in the equation represents the combinatorial entropy. This contribution is always negative, hence favoring a mixed state over the pure components. The last term is the free energy due to interaction between monomers. If the interaction parameter,  $\chi$ , is positive, this term disfavors a mixed state. The balance between the two contributions gives us to various phase diagrams.

The miscibility behavior of binary mixtures are simply represented by  $\chi$  parameter or  $E_{\text{mix}}$  which are thermodynamical parameters and can be calculated by several methods. Firstly, if all constituents are polymer chains,  $\chi$  can be directly calculated directly by using solubility parameters which were calculated from group contribution methods or quantitative structure property relationships given in eqn where  $V_{\text{avg}}$  is average volume of polymer A and B.



$$\chi = \frac{V_{avg} (\delta_A - \delta_B)^2}{RT} \quad (5.2)$$

Secondly, solubility parameters can be calculated from cohesive energy per mole represented by  $E_{coh}$  is the obtained from the non-bond energy difference between the molecule in isolated chain state ( $E_{isolated}$ ) and in amorphous periodic state ( $E_{periodic}$ ) given in Eqn by using simulations.

$$E_{coh} = E_{isolated}^{nb} - E_{periodic}^{nb} \quad (5.3)$$

After calculating the  $E_{coh}$ , mixing energies and Flory–Huggins  $\chi$  parameters for a polymer system with components A and B, by using the cohesive energies of A, B and a mixed AB system of the two; mixing energies can be calculated by using volume (V), cohesive energies ( $E_{coh}$ ) and volume fractions ( $\phi$ ) in the mixture.

$$\Delta E_{mix} = \phi_A \left( \frac{E_{coh}}{V} \right)_A + \phi_B \left( \frac{E_{coh}}{V} \right)_B - \left( \frac{E_{coh}}{V} \right)_{AB} \quad (5.4)$$

In addition, solubility parameters can be calculated to use in the first method by using  $E_{coh}$  and volume.

$$\delta = \sqrt{\frac{E_{coh}}{V}} \quad (5.5)$$

Third method, which is used in our study based on Flory-Huggins (FH) theory, assumes the polymer consisted of a series of connected segments, each of which occupied one lattice site whose coordination number is given by the parameter Z. The interaction parameter,  $\chi$  and  $E_{mix}$  is calculated from these equation and it is the central quantity in these extended FH theory.

In this study, the  $\Delta E_{mix}(T)$  was predicted from the chemical structures of the studied systems by using a Monte Carlo method which combines a extended Flory-Huggins (FH) model and Molecular Simulation. The mixing energies ( $E_{mix}$ ) were calculated by using a method, which combined Flory-Huggins model and molecular simulation techniques. The COMPASS forcefield implemented in the Material Studio 5.0, was chosen as a force field in simulation studies. Prior to atomistic simulations, the

geometries of the segments were optimized by the Density Functional Theory method at B3LYP/6-31G(d,p) level of theory and the electrostatic potential charges (ESP) charges were calculated by the CHELP method implemented in Gaussian 2003 software package [45].

By conducting this off-lattice calculation, meaning that molecules are not arranged in a regular lattice as in the original Flory-Huggins theory, the coordination number  $Z_{ij}$  is explicitly calculated for each of the possible molecular pairs using molecular simulations. The coordination number  $Z_{ij}$  is defined as the number of molecules of component  $j$  that can be packed around a single molecule of component  $i$  within the excluded-volume constraints. One molecule of component  $i$  and  $Z_{ij}$  molecules of component  $j$  together is called a *cluster*. We treated segments as a series of connected repeating units and their coordination numbers were calculated for each of the possible molecular pairs by using randomly generated  $10^5$  clusters. In these clusters, nearest neighbors were packed around the central molecule until the entire volume is occupied and no volume left for additional packing. The terminal atoms of each unit were not taken into account during the calculations and left free to represent continuous polymer chain. Then, the temperature averaged binding energy,  $E_{ij}$  was calculated as an ensemble average of  $10^7$  configurations by weighting the distribution with the Boltzmann factor,  $\exp(-E_{ij}/RT)$ . The average binding energy between  $i$  and  $j$  at temperature  $T$  was the average of the weighted distribution function,  $P_{ij}$  as given in equation 5.6 similar to the Monte Carlo calculations.

$$\langle E_{ij} \rangle_T = \frac{\int E P_{ij}(E) e^{-E/RT} dE}{\int P_{ij}(E) e^{-E/RT} dE} \quad (5.6)$$

Once the binding energies and the coordination numbers have been established, We determined the temperature-dependent mixing energy,  $E_{\text{mix}}(T)$  is equals to the mixing energies which is defined as the difference in free energy due to interaction in the mixed and the pure states according to the equation 5.7.

$$E_{\text{mix}} = \frac{1}{2} \left( Z_{ij} \langle E_{ij} \rangle_T + Z_{ji} \langle E_{ji} \rangle_T - Z_{jj} \langle E_{jj} \rangle_T - Z_{ii} \langle E_{ii} \rangle_T \right) \quad (5.7)$$

## 5.2 Structures Used in Calculations of Binary Mixing Energies

Montmorillonite clays were modeled with respect to experimental initial optimized XRD geometries given in previous chapters. Since the MMT clay have 100 nm length of basal surface and 1 nm width, the problem of infinitely high basal surface exists for the calculations of binary mixing energies. This modeling problem was solved by saturation of end groups by  $-OH$  groups just as present in the nature (**Figure 5.2**). This  $-OH$  have zero charge and nonbond parameters to not to let any interaction with polymer and surfactant and imitate very large basal surface of montmorillonite during the calculations.

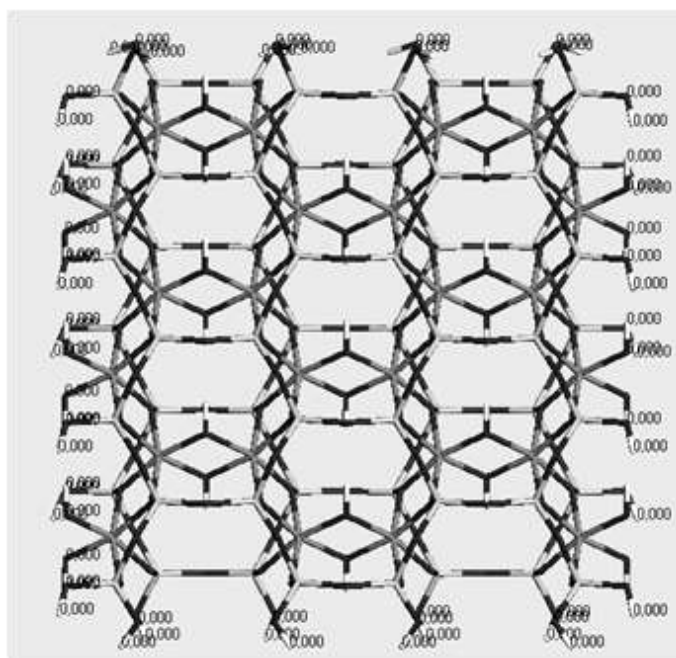


**Figure 5.2:** End group saturated-MMT cluster used to determine clay-polymer and clay-surfactant interaction.

Surfactants are cationic structures that have charged onium ions on their head groups. Reactivity of surfactants against anionic molecules such as clay layer and charge groups are concentrated on the head groups and carbon atoms near cationic head groups due to charge transfer as seen in the Figure 5.3. Calculated Fukui indices for the electrophilic attack showed that the head group is the most susceptible site to interact with the polar clay surface (Figure 5.3).

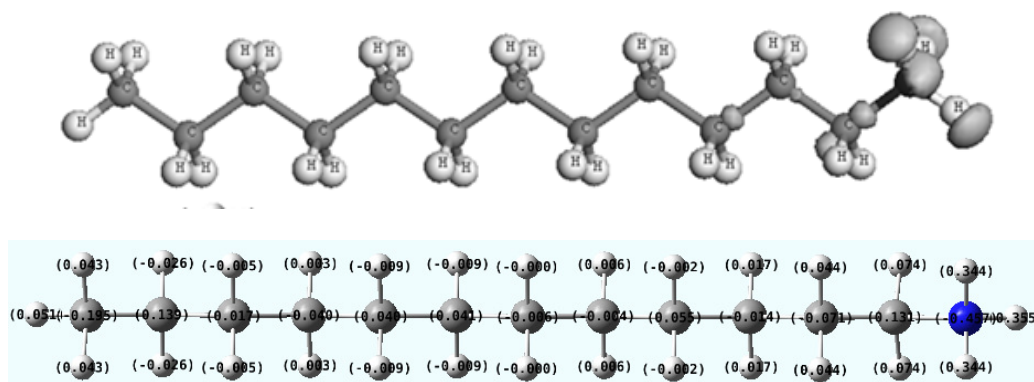


**Figure 5.3:** Nucleophilic attacking centers and atomic charges on surfactant.

Two different types of surfactants were used in calculations. Primary and quarternary alkyl ammonium models was used in calculations by dividing structures into head and tail groups as given in the Figure 5.4. T is the tail of the alkyl ammonium, H1 is the head of the alkyl ammonium, and H2 is head group of trimethyl ammonium.

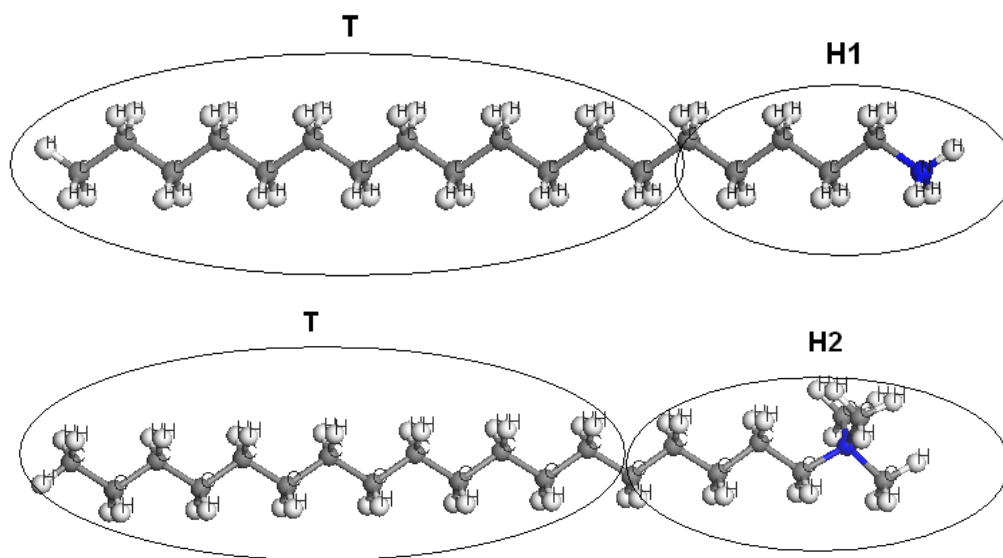


**Figure 5.4:** Clusters used to calculate mixing energies with surfactants.

The tail of the surfactant groups have the same chemical structure with each other and with pristine PE chains. The main difference is with infinitely long polyethylene chains. This problem was solved by making the end groups of PE chains and compatibilizers non-contact with other groups during the calculations.

Optimized structures and atomic charges are required for the molecular simulation methods which are used to calculate mixing energies and formation of nanocomposites such as one given for IA grafted oligomer (Figure 5.5). Polyethylene

oligomers functionalized by itaconic acid (IA), maleic anhydrid (MA) and acrylic acid (AA) groups and alkylammonium groups with different alkyl lengths and head groups were modelled and optimized by using Density Functional Theory method B3LYP with 6-31(d,p) basis set. Atomic charges were determined by pointing electrostatic potentials (ESP) onto the atoms.

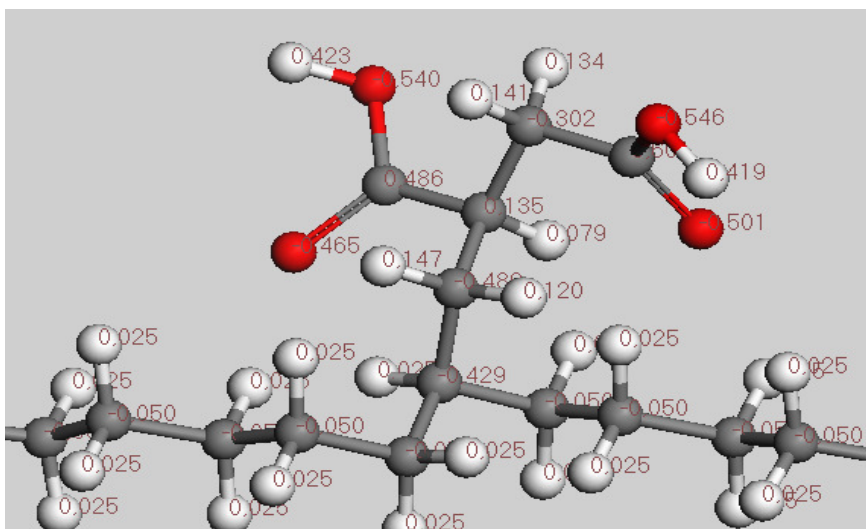


**Figure 5.5:** Optimized geometry and atomic charges of IA grafted oligomer.

The Flory-Huggins theory together with molecular simulation techniques were used to determine the mixing between the interacting pairs. The size of the interacting pair that constitutes nanocomposites must be chosen carefully to have reliable interaction energies. PE chains with 11 carbon atoms were chosen for the calculations. Similar length of compatibilizer structures are prepared by modeling polyethylene oligomers functionalized by itaconic acid (IA), maleic anhydrid (MA) and acrylic acid (AA) groups grafted from the middle oxygen atom given in the Figure 5.6.

After finishing all these calculations with these structures, additional calculations are conducted to explore the effects edge groups of MMT clays. The effects of tangling -OH groups at the end groups are investigated by calculating mixing energies with charged end groups and nonbond parameters for the small MMT cluster.

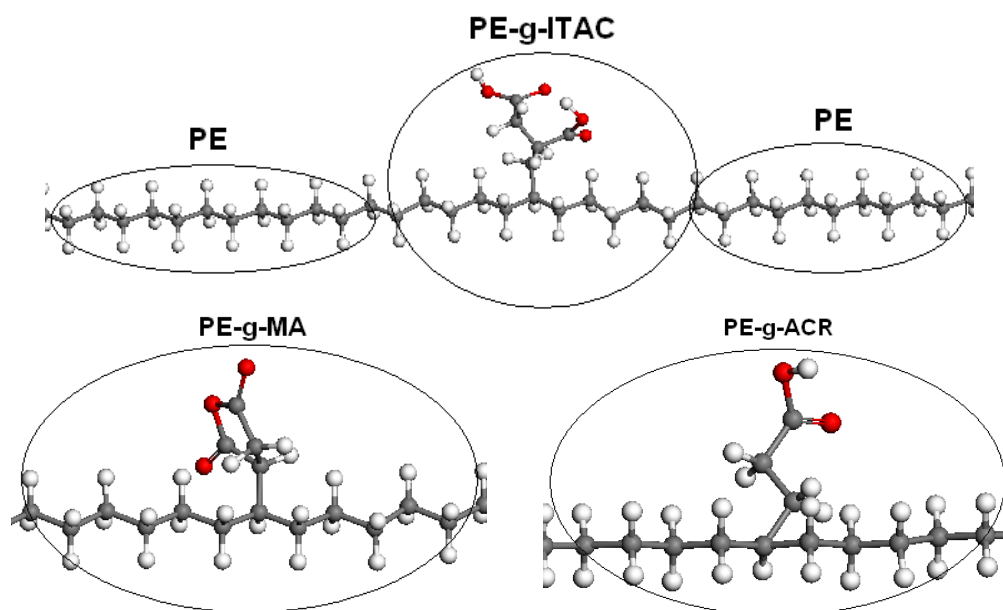


**Figure 5.6:** Cluster used to calculate mixing energies with PE and compatibilizers.

## 5.3 Results and Discussions

### 5.3.1 Validation of the method

The initial step for the results is the confirmation of our calculation procedure. This was accomplished by determining the minimum energy structure for MMT-MMT binary interaction. It is known that the MMT platelets are stacked platelets with the basal spacing from beginning of one layer to other have 10-15 Å distance. From our calculations, it is calculated as 10.05 Å which makes us to move forward to the next step for the other structures for the other pairwise interactions (Figure 5.7).

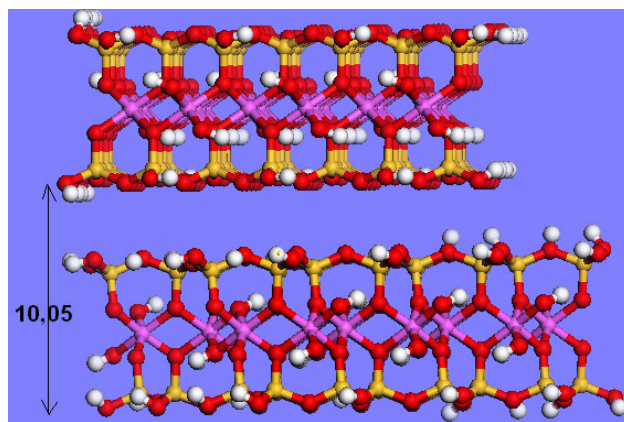


**Figure 5.7:** Parallely stacked structure of MMT.

Another important validation of the method is the pristine polyethylene binary interactions. It is known that without any branching the PE oligomers must have a parallel conformation for most of the chains. This is also confirmed by the minimum energy structure given below from the  $10^7$  different configurations with noncontacted end groups to imitate PE chains with infinite length (Figure 5.8).

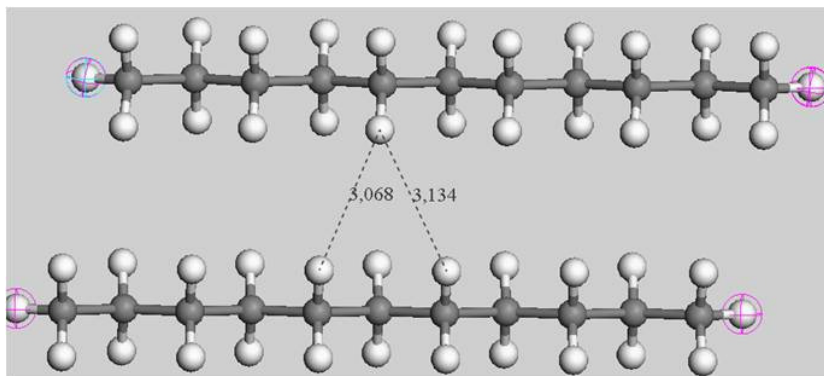


**Figure 5.8:** Minimum energy conformations of PE oligomer.

### 5.3.2 Binary mixing energies and minimum energy structures

Minimum energy structures for the head groups of primary alkyl ammonium and MMT platelet is given in the Figure 5.9. The distance between -H atoms of alkyl ammonium head and surface oxygen atoms of MMT surface is in the hydrogen bond ranges. The ammonium group reside over the hexagonal cavity of the oxygen framework where its hydrogens were directed to the oxygens. The results are very similar to the structures calculated in third chapter even there is not any initial imposed structure and the structures are calculated from very large number of randomly formed configurations. The difference is in the N-H...O-Si distance caused by the nonoptimized or minimized structures here.

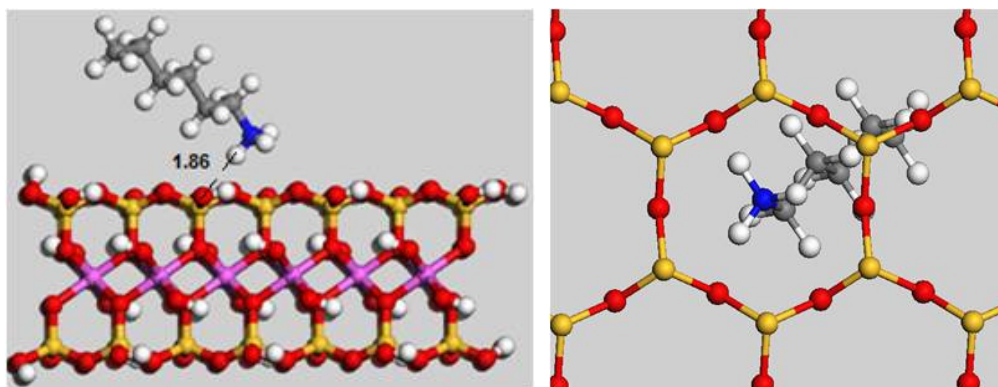


**Figure 5.9:** Minimum energy conformations of H1 and MMT systems.

The head groups of quarternary trimethyl ammoniums also directed to the hexagonal cavities. The distance with the clay platelet is higher than primary alkyl ammonium due to the absence of hydrogen bonding (Figure 5.10). However, surface coverage which is very important factor for the formation of olefinic polymer-clay nanocomposites accomplished at higher amounts for quarternary alkyl amounts. Since over 90% of nanocomposite consists of nonpolar PE chains, the less interaction between PE with clay must be reached by covering the surface of hydrophilic clay.

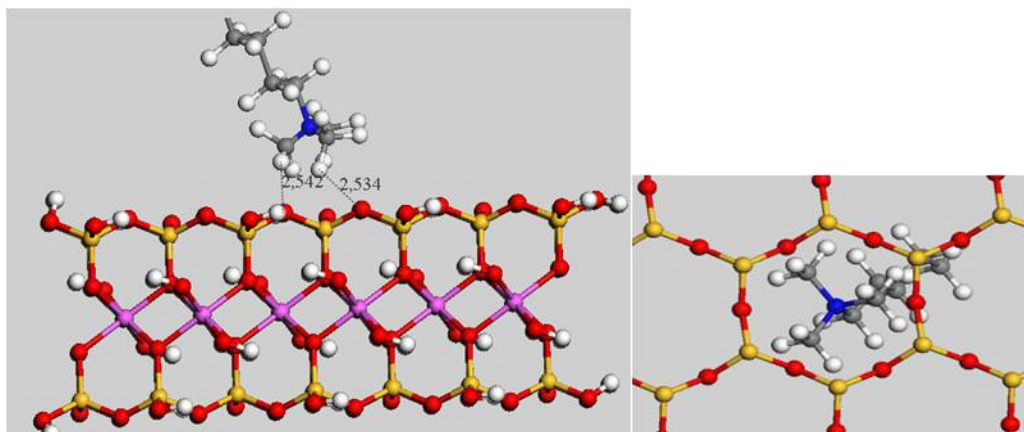


**Figure 5.10:** Minimum energy conformations of H2 and MMT systems.

Large negative mixing energies between MMT and surfactant head groups means strong binding between polar MMT surface and ammonium groups was observed. It is expected due to the ionic interaction between negatively charged MMT platelet and positively charged ammonium ion. Due to the hydrogen bonding between with primary alkyl ammonium the interaction is higher. The amount of mixing energy explains the stability of organoclays commercially available. In addition, the vibrational frequency shift for the N-H stretching to a lower value on the clay surface in the experiments supported our results [251,252]. In addition, higher mobility for alkyl tails of surfactants observed experimentally also indicating the orientation of tails freely towards the gallery between clay layers.

From the distance and mixing energies, it seems that the larger volume of the surfactant causes the lower interaction between clay surface and surfactant head group. However, for the nonpolar polymers like polyethylene, coverage of hydrophilic MMT surface and number methylene groups are other important factors for the attractive vdw interactions between PE chains and alkyl tails (Table 5.1).



**Table 5.1:** Mixing energies calculated for MMT and alkyl ammonium head groups.

	Emix (kcal/mol)
MMT- $\text{NH}_3^+$ (H1)	-2120
MMT- $\text{N}(\text{CH}_3)_3^+$ (H2)	-1813

The minimum energy structure over very large number of configurations with quantum mechanical charges and consistent parameters have shown that PE oligomers arranged parallel over the clay platelet with very high distances because of the hydrophobicity of the PE oligomers (Figure 5.11). Experimental SAXS studies have also determined the increased crystal layer of PE chains near the MMT platelets [253].

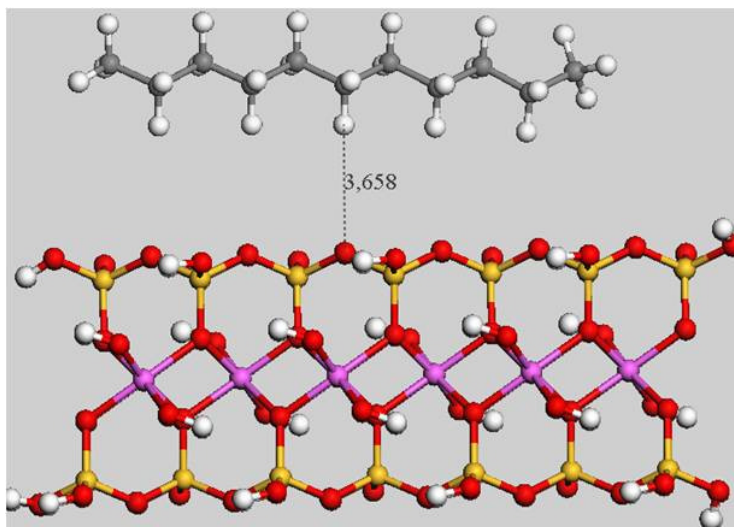


**Figure 5.11:** Minimum energy conformations of MMT and PE oligomer.

PE compatibilizers which have carboxylic acid groups in their structure such as PE-g-AA and PE-g-IA have acidic -H atoms interacted with the clay surface. Minimum energy structures given in the Figure 5.12 demonstrated the interaction of functional groups with the surface oxygens as well as orientation of the PE backbones away from the MMT surface. The interaction of these acidic groups is hydrogen bonding with the one or more oxygen atoms of the basal surface.

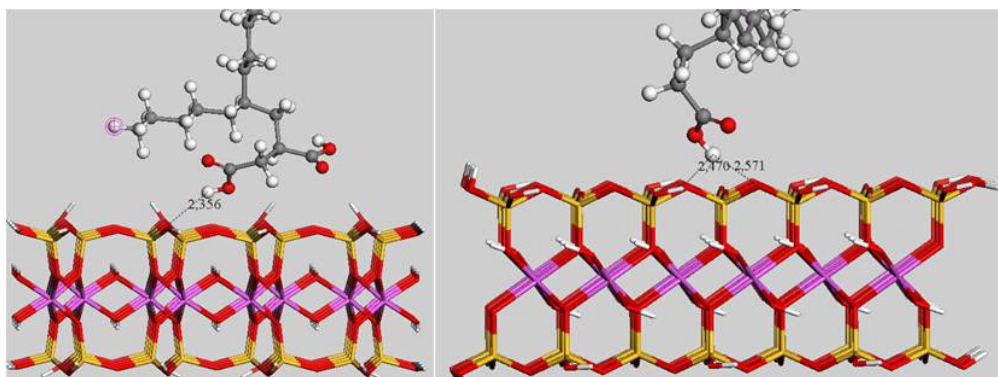


**Figure 5.12:** Minimum energy conformations of MMT and IA grafted PE oligomer.

The minimum energy structure of MMT with PE-g-MA is very similar to the other compatibilizers except the type of the interactions. PE backbone stay away from the surface and MA functional group placed over the hexagonal cavity of the clay surface (Figure 5.13). However, different from functional groups of IA and AA, there is not any hydrogen bonding, but the interaction is between the hydrogen atom of the  $sp^3$  hybridized carbon atom in anhydride group and hexagonal oxygen atoms bonded to silicon atoms of the clay surface. Another interaction observed for the first time in minimum energy structures is between the  $sp$  hybridized oxygen atoms of MA group and Si atoms of the tetrahedral layer in MMT platelet.

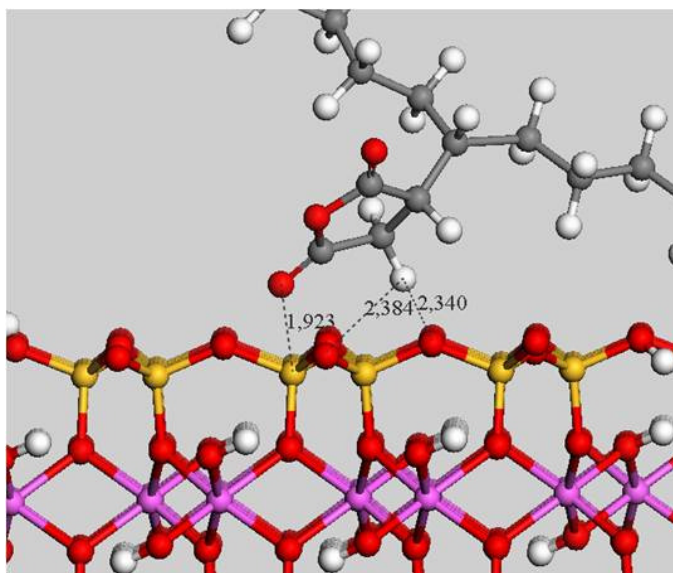


**Figure 5.13:** Minimum energy conformations of MMT and MA grafted PE oligomer.

Experimentalist proposed a model for the compatibilizing role of MA on MMT surface where an attractive interaction due to hydrogen bonding between oxygen

atoms of maleic anhydride and hydrogen atoms exist in –OH groups of octahedral layer as shown in Figure 5.14 [254]. This structure is found as one of the accepted possible structure but the not one with the minimum energy and highest probability.

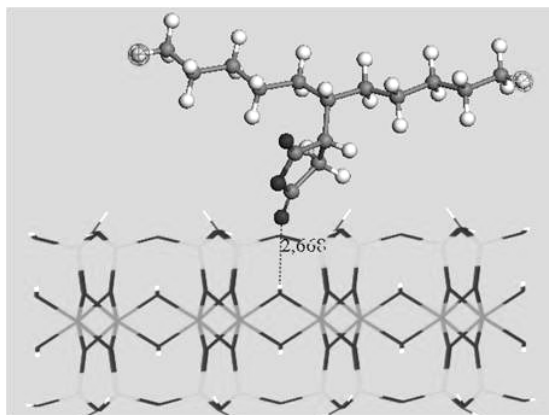


**Figure 5.14:** Experimentally proposed structures of MMT with MA grafted PE oligomer.

The interactions observed for the structures can also be seen for the mixing energies. All the functional groups grafted onto the PE chains increases the interaction and resulted in the more negative mixing energies (Table 5.2). PECs reside on the clay surface and supply enough attraction for the incorporation of PE chains to the clay layers. PE-g-IA have mixing energies with MMT which is very close to the commercially used PE-g-MA compatibilizer. The negative mixing energy of the PE with MMT is resulted from the hydrogens of hydrocarbon chain with the surface oxygens is higher than expected amount. It is originated from charge localization due to the limited sizes of the PE oligomers that calculations permitted. For infinitely large polymers over the clay platelet, PE chains will fell more repulsive interactions.

**Table 5.2:** Calculated mixing energies for MMT cluster with PE and PEC oligomers.

	Emix (kcal/mol)
MMT—PE	-32,75
MMT—PE-g-AA	-82,05
MMT—PE-g-MA	-175,83
MMT—PE-g-IA	-174,90

Another function of compatibilizers that causes the formation of stable PE-organoclay nanocomposites with enhanced properties can be seen in Figure 5.15.

There are two hydrogen bonding between head groups of ammonium groups and carboxyl group of itaconic acid. Similar hydrogen bondings was observed between the head groups with MA and AA based compatibilizers. Since the strongest interaction is between ammonium groups and clay surface, the attractive interaction of compatibilizers and head groups will also lead to the increased interaction of polyethylene chains with clay surface.

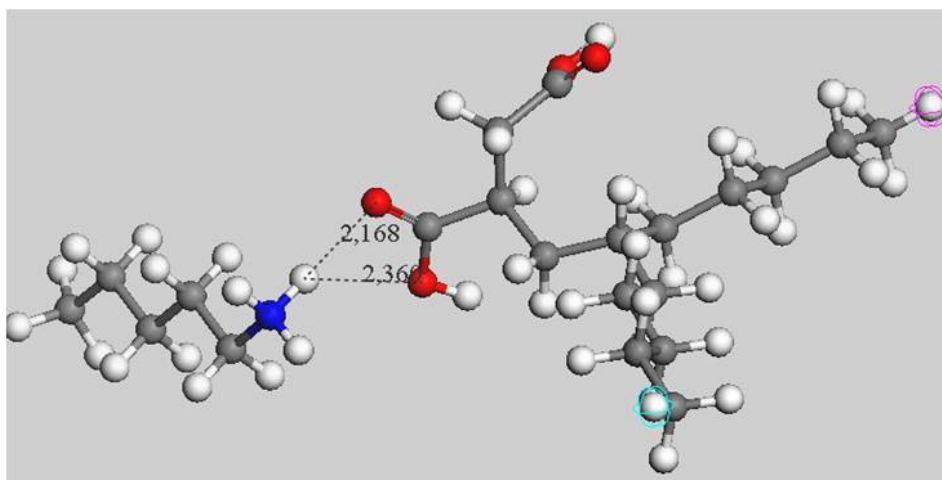


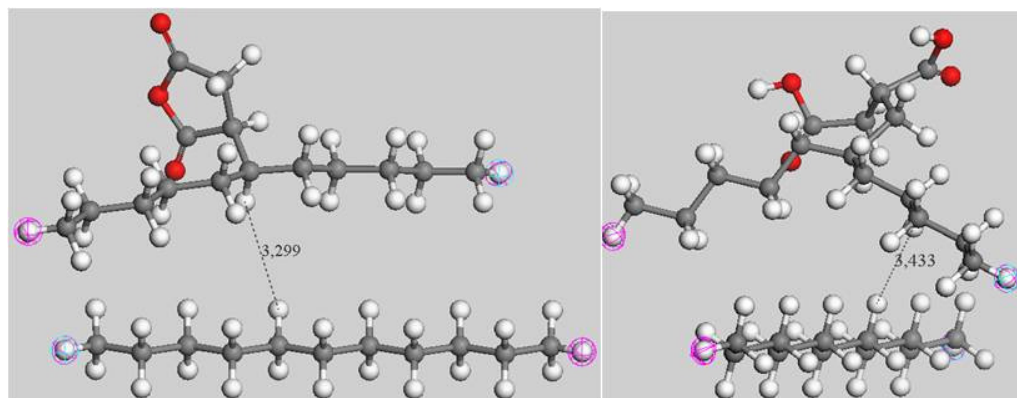
**Figure 5.15:** Minimum energy structures of IA grafted PE oligomer with H1.

More negative mixing energies showed that all compatibilizers enhances the attraction between head groups and PE chains. IA have most attractive mixing energy with both primary and tertiary ammonium head groups as given in Table 5.3. MA have the second best performances and successfully used in commercial PE nanocomposites with both primary and quarternary alkyl ammonium based organoclays. Another result stemmed from this part is that clay modification with onium ions not only increases the basal distance, it is also increases the interaction with compatibilizers. This explains why both surfactant onium ions and compatibilizers are shown to be crucial in experiments [255].

**Table 5.3:** Calculated mixing energies for head groups with PE and PEC oligomers.

	Emix (kcal/mol)		Emix (kcal/mol)
$-\text{NH}_3^+ \text{—PE}$	-46,51	$\text{N}(\text{CH}_3)_3^+ \text{—PE}$	-45,52
$-\text{NH}_3^+ \text{—PE-g-AA}$	-74,64	$\text{N}(\text{CH}_3)_3^+ \text{—PE-g-AA}$	-55,86
$-\text{NH}_3^+ \text{—PE-g-MA}$	-83,78	$\text{N}(\text{CH}_3)_3^+ \text{—PE-g-MA}$	-67,88
$-\text{NH}_3^+ \text{—PE-g-IA}$	-104,74	$\text{N}(\text{CH}_3)_3^+ \text{—PE-g-IA}$	-76,18

The last important mixing energy calculated is also mentioned in first chapter. There must be a unfavorable interaction between PE homopolymers and compatibilizers, because of the relatively hydrophilic structures grafted on the comopatibilizer chains. As concluded in chapter 1, that is the reason why small amounts of compatibilizers can reside on the surface of the PE phase and cause great changes in the physical and mechanical properties of blends and composites. The minimum energy structures from large number of clusters for PE-g-MA and PE-g-IA with PE oligomers are given in the Figure 5.16. The PE backbones oriented away from the clay surface and grafted functional groups turn other side ready to interact with any hydrophilic surfaces or onium ions.

**Figure 5.16:** Minimum energy structures of IA and MA compatibilizers with PE oligomers.

Mixing energies of compatibilizers with PE have all positive values and decreasing from PE-g-IA, PE-g-AA and PE-g-MA respectively (Table 5.4). These mixing energies decrease with the increasing temperature. That is why cooling very slowly several times can be a good choice in melt blending that the compatibilizers can move slowly towards the clay surface for the better mechanical properties of polyolefin-organoclay nanocomposites.

**Table 5.4:** Calculated positive mixing energies between PE and PEC oligomers.

	Emix (kcal/mol) 298K	Emix (kcal/mol) 400K	Emix (kcal/mol) 600K
PE—PE-g-AA	4,14	1,41	0,53
PE—PE-g-MA	3,38	2,09	1,23
PE—PE-g-IA	6,31	3,76	1,99

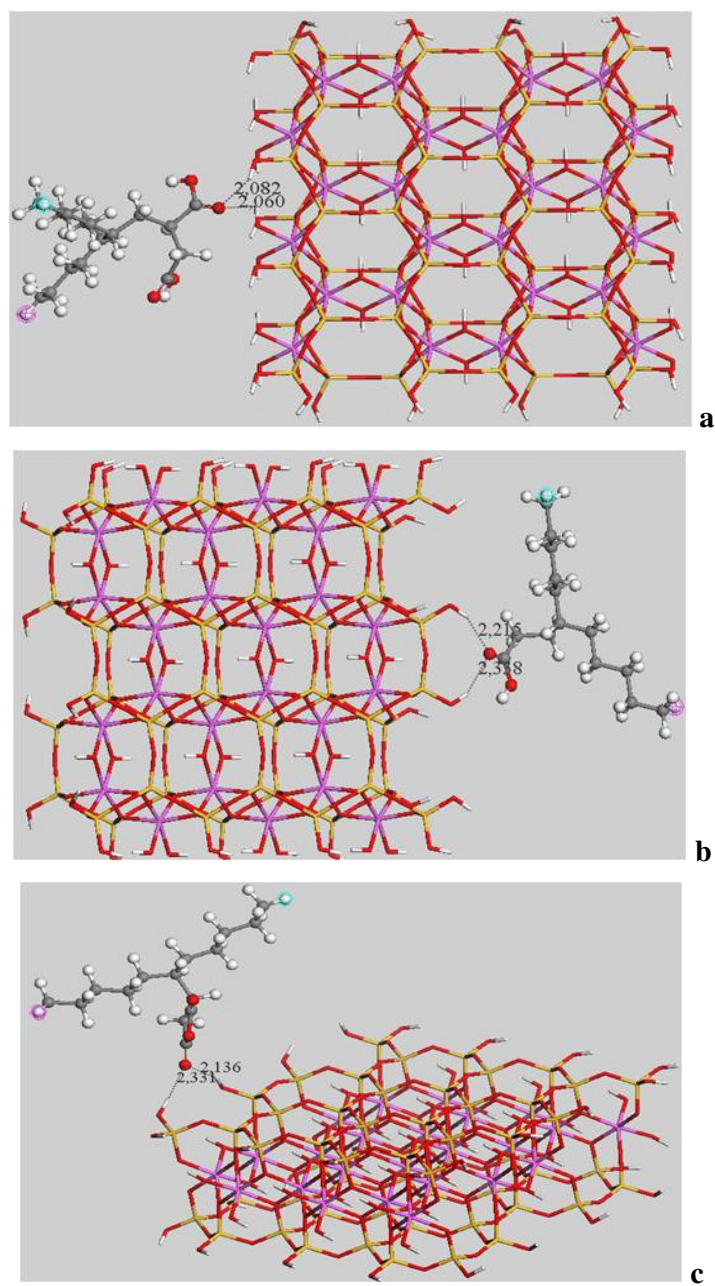


**Figure 5.17:** Minimum energy structures of compatibilizers interacting with end group atoms of MMT.



One must be bear in mind that MMT clay have 100-300 nm length and 1 nm width that means MMT platelet is a two dimensional clay and almost all the interactions are with the surface. However the strong stacking of MMT platelets causes the first contact with organic molecules with their edge groups. The –OH end group is known to be existed at the edge of the MMT clay. –OH groups have two source that one from octahedral layer bonded Al and Mg while the other bonded to the tetrahedral Si atoms. Minimum energy structures for MMT cluster with end group charges and compatibilizers showed that when the edge –OH groups taken into account, all functional groups of compatibilizers form hydrogen bonds both with the hydrogens of –OH at tetrahedral edge and octahedral edge groups (Figure 5.17).

Ammonium groups of surfactants are form hydrogen bonds if the edge sites are taken into the account as given in the Figure 5.18. Although this interaction is lower than the hexagonal coordination of ammonium head groups, it is important as a first interaction with stacked clay layers for the formation of organoclay.

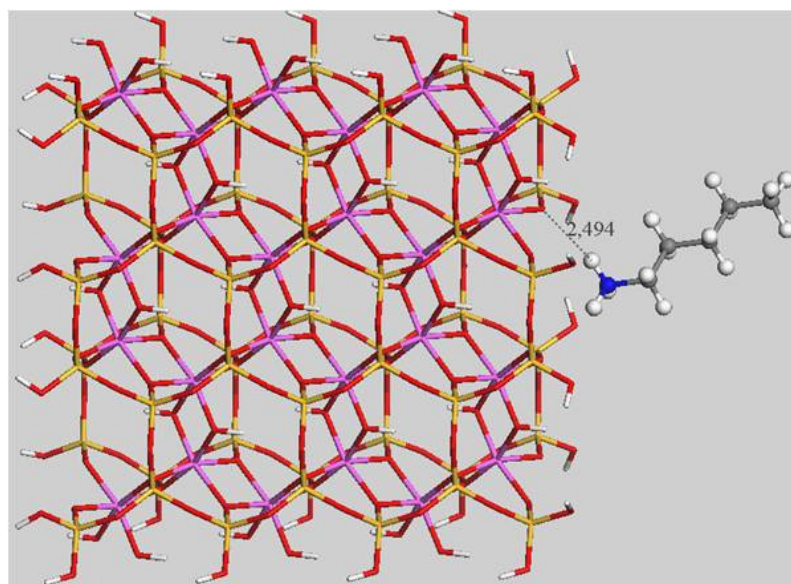


**Figure 5.18:** Minimum energy structures of MMT with H1.

A hierarchical molecular modeling procedure has been used to calculate the mixing energies quantitatively that are responsible for the formation of stable PE-organoclay nanocomposites. The molecular modeling methods have been carried out on the basis of input data obtained from lower-scale quantum mechanical optimized geometries and atomic charges. The strongest interfacial interaction was found to be between the clay surface and ammonium heads of the surfactant molecules due to the H-bonding

interactions of hydrogens (in  $\text{-NH}_3^+$ ) with the lone pairs of the framework oxygens. Among the studied compatibilizers, **IA** and **MA** were shown to be the best interacting polar groups with the organoclay constituents that are surfactant and MMT platelet by orienting their functional groups towards the clay surface. We showed that, the grafted polyethylenes (PE) interact better than PE homopolymers with the organoclay, then grafting favors the interaction between polymer and organoclay. Functional groups reside on the PE surface and enhances the transportation and incorporation of PE chains to the clay layers that yields enhanced interfacial strength with MMT than PE homopolymer. Molecular simulations procedure has been confirmed by the increased mechanical properties determined by experiments where compatibilizers were used [111]. All of the calculated interaction energies have negative values except the compatibilizer-PE one that proving that nanocomposite formation and intercalation processes are favored. This causes exfoliation during melt compounding and enhances the physical and mechanical properties of the nanocomposite material.



## **6. MOLECULAR DYNAMIS SIMULATIONS OF POLYETHYLENE ORGANOCLAY NANOCOMPOSITES**

Molecular dynamics (MD) simulation is a useful tool to predict interactions of polymers with clays, surfactants and compatibilizers that enables us to predict the energetical realities behind the formation of PNCs and to design of new nanocomposites experimentally [256].

Although the previous researches has shown some important insights to our understanding about clay–surfactant-polymer systems, there are only few comparable studies predicting the effect of interactions in nanocomposite systems.

The intercalated nanocomposite by several surfactants, compatibilizers into sodium montmorillonite clay was modeled with a detailed molecular dynamics approach in this chapter. This study is aimed at understanding the role structure and the interactions on the morphology and enhanced properties of nanocomposite.

Molecular dynamics is also helpful to understand the nature of interaction energies in a molecular system that the interaction energies within different components of organically modified montmorillonite (OMMT) and PCN can be explained if it is vdw or electrostatic sourced energy. In this chapter, clay-polymer and polymer-surfactant interactions are also studied other than the interaction of clay or organic surfactant known from previous chapters. By this way, the nature of energy contributions coming from functional groups of constituents will provide important insight into the formation of stable nanocomposite.

Previus studies have also shown that there is a strong relation between the enthalpic term from the intermolecular interactions that will be determined in this chapter, and the entropic term, associated with the intercalation of surfactants and polymers [218-220]. Some amount of this entropy loss can be compensated by increases in the basal spacing by conformational movement of surfactant molecules and the polymers in the clay layer. There must be still some enthalpic energy for stability for stability. Experimental and phase behaviour studies showed that exfoliation of silicate layers

depends on the polymer-clay interaction to get nanocomposite with completely exfoliated morphology [194, 257]. In our case, this interaction will be provided by compatibilizers.

The effect of grafting and grafting ratio, alkyl ammonium chain length and head groups, clay layer atomic charges on the nanocomposite properties are investigated in different range of time and length scales. Several molecular models of intercalated polyethylene-clay have been simulated nanocomposites to understand the effects of components ratio and their interactions on the physical properties.

## 6.1 Structures Used in MD Calculations

In this chapter, three different MMT models same as given in Chapter 3 will be used. These models (MMT1, MMT2, MMT3) have 5x3x1 supercell with the cell formulas  $\text{Na}_6(\text{Al}_{54}\text{Mg}_6)\text{Si}_{120}\text{O}_{300}(\text{OH})_{60}$ ,  $\text{Na}_{10}(\text{Al}_{50}\text{Mg}_{10})\text{Si}_{120}\text{O}_{300}(\text{OH})_{60}$  and  $\text{Na}_{16}(\text{Al}_{44}\text{Mg}_{16})\text{Si}_{120}\text{O}_{300}(\text{OH})_{60}$ .

This structures corresponds to different cation exchange capacities (56, 91, 143 meq/100g). Most of the studies here will use second model since industrial clay have CEC between 80-100 meq/100g. Since we have optimized organoclays as explained in previous chapters, we took initial models directly from there. Then, we have three different kinds of organoclays with different amounts of surfacts between clay layer with respect to CEC of the clay (6, 10 and 16 surfactants respectively). Eight well known and most used surfactants were chosen for simulations as given in the Figure 6.1. So, 24 different structures with respect to their CEC and surfactants groups were organoclays were prepared for simulations (Figure 6.1).

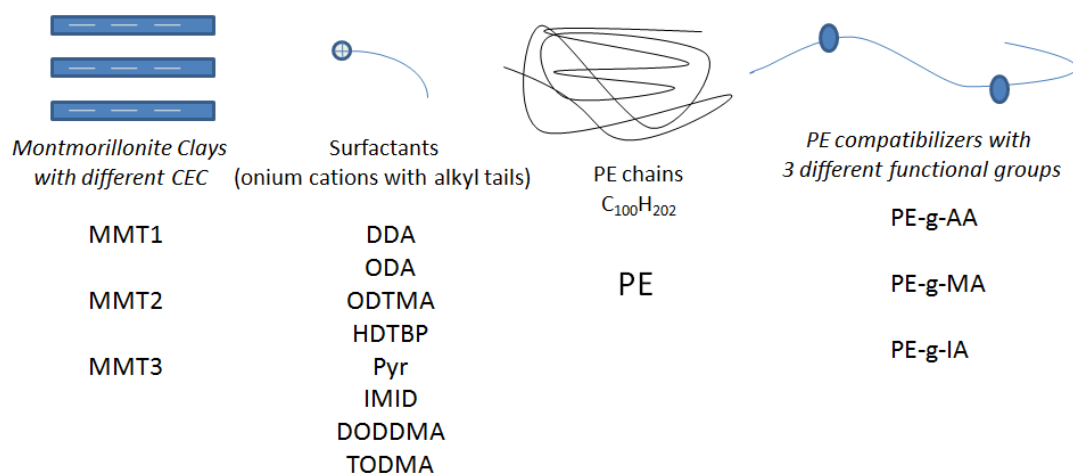


**Figure 6.1:** Structures used in the MD simulations.

Polyethylenes were modelled by building several amorphous cells by using rotational isomeric states method. They all have 100 carbon atoms in their bacbones. Same procedure were also applied to prepare compatibilizer models with 100 carbon atom in their backbones grafted with one AA, MA and IA groups to compare the effect of different functional groups in compatibilizers (Figure 6.2).

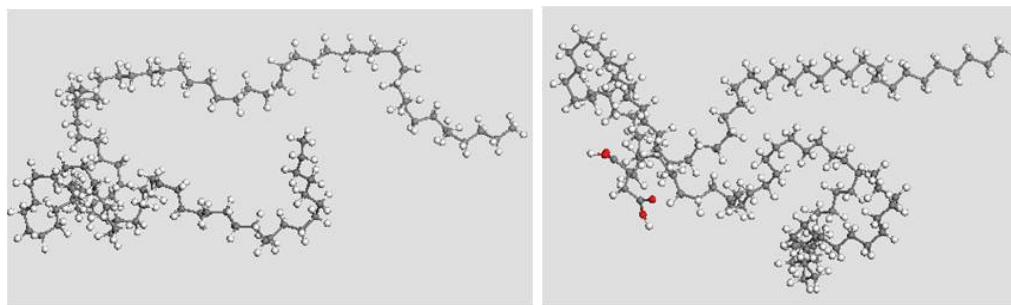


**Figure 6.2:** Initial structures of PE and IA grafted PE oligomers for MD simulations.

Three different organoclay structures with increasing CEC were prepared for different surfactants. As an example, the basal distances of organoclay were increases as shown for 3 different DDA groups to 35-55 Å to have enough basal gallery between clay layers for the addition of PE chains and compatibilizers (Figure 6.3). The distances were chosen as 1 g/mol final densities for all initial geometries of nanocomposites since we are going to compare the final energies of these structures.

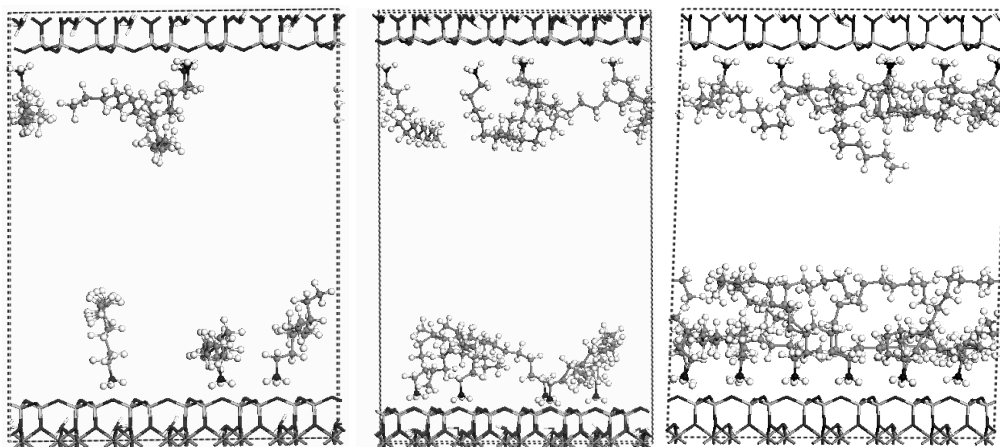


**Figure 6.3:** Different organoclays used to model PE-organoclay nanocomposites.

After modeling all the components in organoclays, the system is ready for the addition of polyethylene chains. Three polyethylene chains with different number of functional groups were added at each time. We did not impose or guarantee any initial interaction except the optimized surfactant head group-clay surface interaction at initial geometries. The functional groups of compatibilizers were also reside between the gallery to see if they are attracted to the MMT surface by any favorable or unfavorable nonbonded interactions (Figure 6.4).

At last, none of the molecules, bond lengths or distances, cell or lattice parameters kept constant or rigid during the simulations. It is the first time all parameters in clay platelets even the tangling octahedral  $\text{-OH}$  groups move freely in polymer-clay nanocomposite simulations.

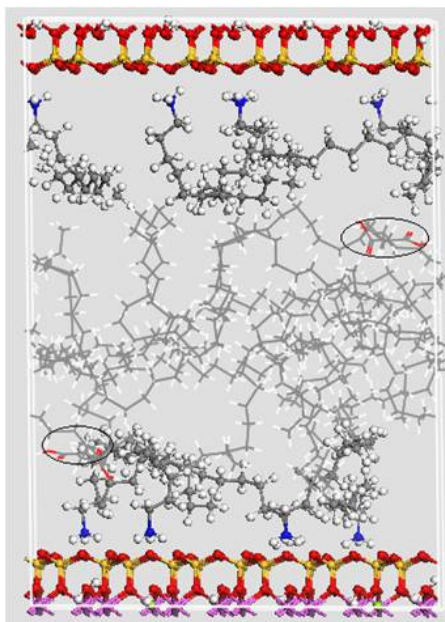


**Figure 6.4:** Initial structure of the nanocomposite formed by MMT2, ODA, PE and PE-g-IA (side view).

## 6.2 Modeling Methods and Molecular Dynamics Strategy

It must be noted that atomic charges and optimized structures were used in initial structures of all molecular dynamics simulations that will be analyzed to explain formation of nanocomposites by interaction energies and structures.

We conducted molecular simulation procedure with six steps to explore and characterize the micro scale structure and formation of nanocomposite. Three of these involve minimization and others were MD simulations. Discover MD simulation module of Materials Studio 5.0 is used in calculations. Simulations started with the initial minimization step where the 5000 steps of conjugated gradient (Fletcher-Reeves) method was used. The force criterion for convergence is  $0.005 \text{ kcal mol}^{-1} \text{ \AA}^{-1}$ , the energy difference criterion is  $10^{-5} \text{ kcal mol}^{-1}$  (RMS). This minimization method is repeated 3 times preliminary to each dynamics step with the same parameters where cell parameters are also minimized during calculations where periodic boundary conditions are used in three dimensions. The force field is polymer consistent force field modified for silicate force field (PCFF-silicate) which determined that it give consistent results in our tests and previous published studies.

After reducing the noise and potential energy by minimization, isothermal-isochoric (NVT) MD simulations are started at 600K where the integration for the equations

were repeated with a 1 fs time step. The atomic equations based on Newton motion are integrated Verlet numerical algorithm. Simulations were continued during 200 ps time length. After each MD simulation, the final structures were minimized. The second simulation is conducted with the same parameters except the temperature decreased to 400 K. The last simulation was at 300 K and continued during 100 ps. After equilibrium was achieved, the last 100 ps simulation were carried out for analysis of binding energies and atomic density distribution constituents. The energies and geometries were saved at every 5 ps of analysis part. Twenty different trajectories were used for analyses.

The concentration profiles in the z-direction (from first clay platelet to the next platelet) were analyzed for the functional groups to find out the organization and role of functional groups in compatibilizers. In addition, the carbon backbone atoms of PE chains were analyzed in the same direction to determine chain organisation in different organoclays. Then the results were analyzed by beginning to calculate the total potential energy of binary and ternary systems composed, for example, by polyethylene and compatibilizer, montmorillonite and a surfactant.

For the calculation of the interaction energy, we have to consider the total potential energy of the system that involve interaction energies [198,258].

$$E_{(PE/MMT/surf)} = E_{PE} + E_{MMT} + E_{surf} + E_{PE/MMT} + E_{PE/surf} + E_{MMT/surf (organoclay)} \quad (6.1)$$

The first three terms are the energy of MMT, PE and surfactant (consisting of both bonded and nonbonded terms), and the other terms are the interactions energies or binding energies. The interaction energy is the negative of binding energy.

$$E = \underbrace{(E_{electrostatic} + E_{vdW})}_{Nonbonded\ potential} + \underbrace{(E_{bond} + E_{angle} + E_{torsion})}_{Valence\ interaction} \quad (6.2)$$

Both the bonded and the nonbond part of the potential energies are taken into account for the calculation of interaction energies. The interaction energies constitute pairwise systems of polyethylene-organoclay nanocomposites based on polyethylene (PE) and compatibilizer, clay and different ions as surfactants.

To calculate the binding energy between the montmorillonite and the polyethylene, the surfactants were removed and the interaction energy calculated after minimization.

$$E_{bind(MMT-PE)} = E_{MMT} + E_{PE} - E_{(MMT-PE)} \quad (6.4)$$

Similar calculations were used to calculate the interactions of surfactant with PE chains and interactions of montmorillonite with surfactant molecules

$$E_{bind(PE/surf)} = E_{PE} + E_{surf} - E_{(PE/surf)} \quad (6.4)$$

$$E_{bind(MMT/surf)} = E_{MMT} + E_{surf} - E_{(MMT/surf)} \quad (6.5)$$

Since the interaction between MMT and surfactants were calculated to be very high and experiment has showed the interactions between polymers and organoclay is crucial for the stable nanocomposite formation the interaction energy of organoclay with polyethylene chains were calculated as follows.

$$E_{bind(PE)} = E_{tot} - E_{PE} - E_{MMT-surf(organoclay)} \quad (6.6)$$

## 6.3 Results and Discussions

### 6.3.1 Structure and molecular organisation in PE-organoclay nanocomposites

In all cases, the alkyl tails of the surface modifiers tends to look away from the clay surface and head groups are oriented towards to the clay surface. This result was independent from the CEC of the MMT and surfactant structure. The head groups of surfactants were positively charged and MMT surface oxygens are negatively charges, so that this interaction is always attractive. Since the alkyl tails were hydrophobic, they facilitate the increased interaction of PE chains and helps intercalation of them. Since alkyl tails of surfactant molecules sterically repulse each other, they also prevent the MMT platelets stacked together together. The alkyl tails have vdw interactions with PE chains in the gallery (Figure 6.5). However, the total coverage of 100 nm clay layer still impossible and there must be a favorable electrostatic interactions between MMT and polyethylenes.

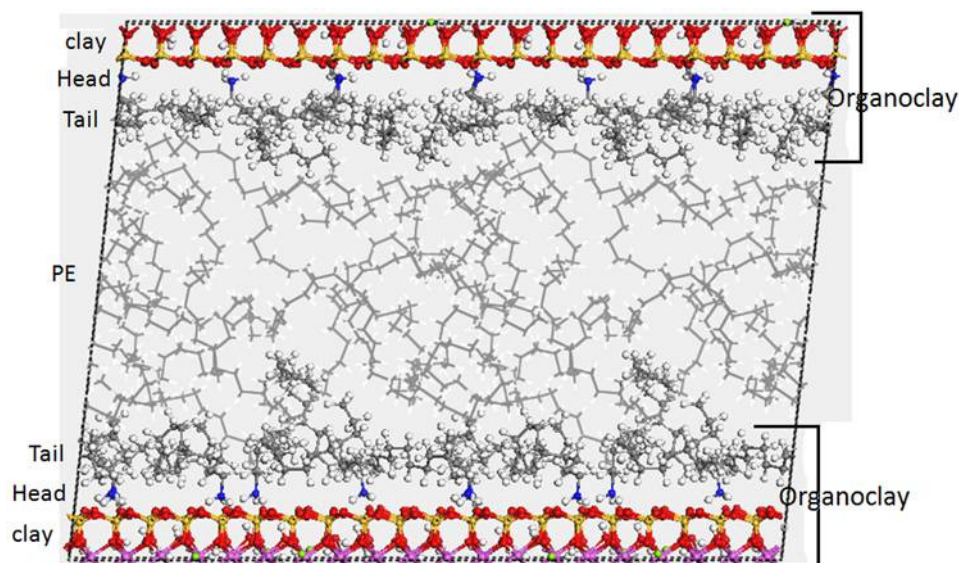


**Figure 6.5:** PE-organoclay nanocomposites before equilibration.

The favorable electrostatic interaction between polymer layers and MMT platelet was supplied by functional groups of compatibilizers. Each compatibilizer accomplished this aim by different ways. There are some ionomers or reactive compatibilizers available in the market. For our case, we found that all functional groups grafted onto the PE chains move towards the clay surface to form a bridge between inorganic hydrophilic MMT surface and organic hydrophobic PE chains (Figure 6.6).

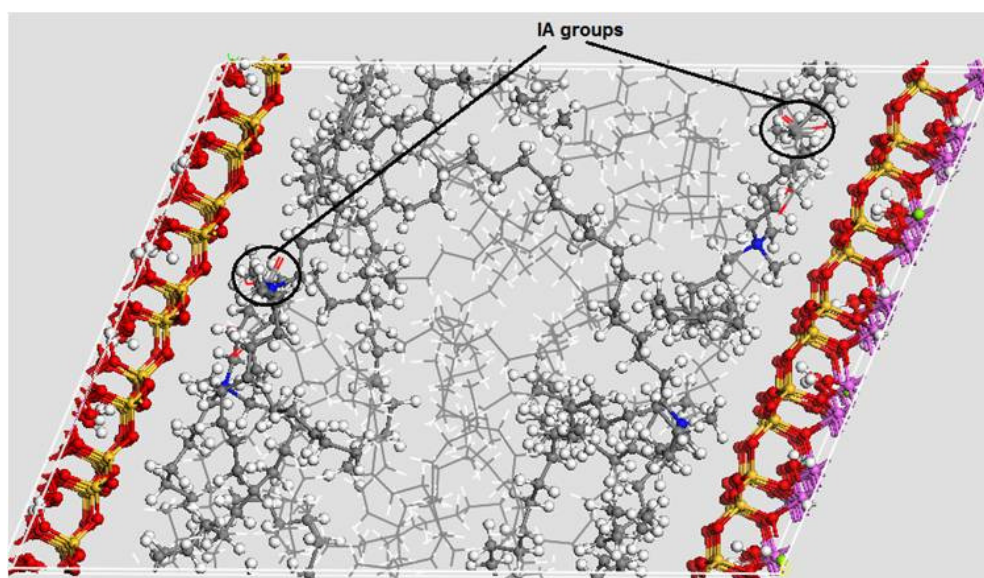


**Figure 6.6:** PE-organoclay nanocomposites after equilibration.



Until last years, it was thought that the necessary interaction for exfoliation was stemmed only from the wetting capacity of compatibilizers on the clay surface as shown below (Figure 6.7).

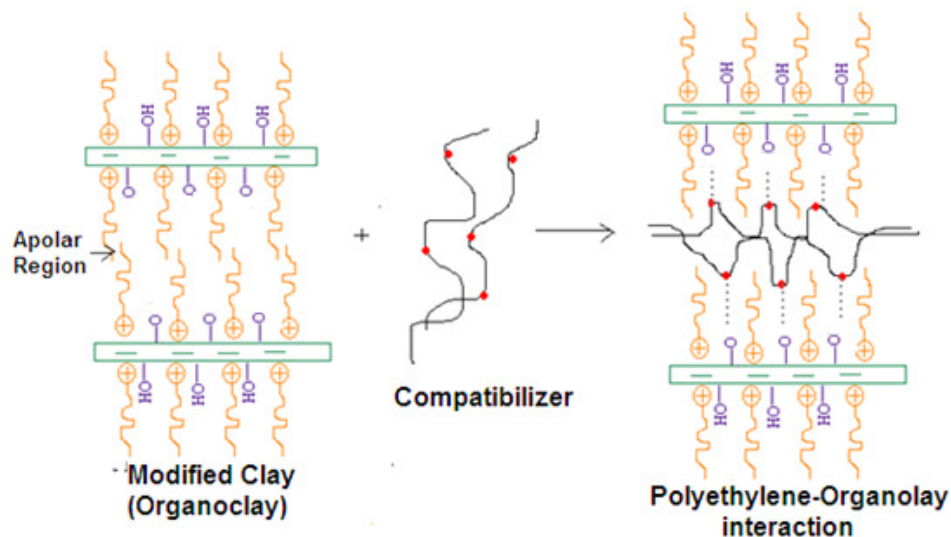


**Figure 6.7:** Nanocomposite formation.

It was determined that compatibilizers not only interact with clay surface, but also they also form hydrogen bonding between head groups of surfactant which strongly bonded to clay surface, opposite to the experimentalists view [259,260]. Both two of the interactions were found to be hydrogen bonding for AA and IA case where acidic hydrogens of compatibilizers formed hydrogen bonding with basal oxygens of negatively charged MMT and oxygens formed hydrogen bonding with hydrogens of positively charged ammonium head groups (Figure 6.8).

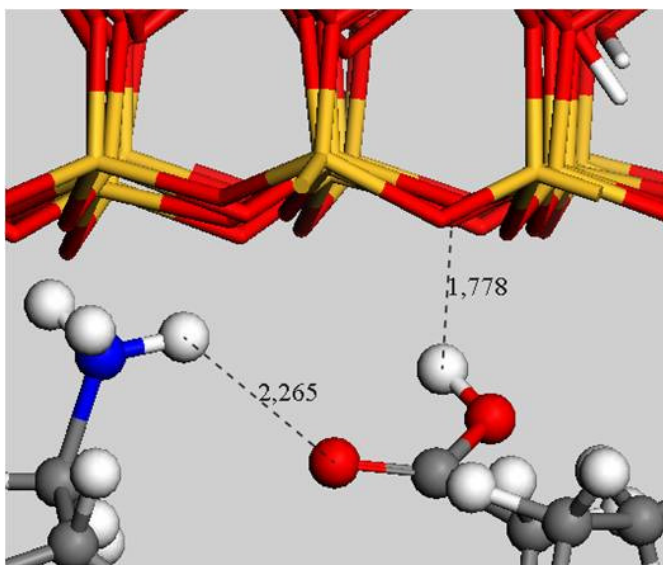


**Figure 6.8:** Snapshot picture showing the interactions of IA, ammonium and MMT surface at equilibrium.

The relative concentration profile  $-OH$  groups present in the carboxyl groups of itaconic acid for different CEC in organoclays prepared by using DDA is given in the Figure 6.9. All  $-OH$  groups are on the two surfaces of clay independent from the number of surfactant molecules. The number of surfactant molecules were effective to increase the gallery volume and increases the possibility of the interaction with compatibilizer. It seems that the  $-OH$  groups were present between first 4.5 to 10 Å distance. Since the length of the half MMT clay is 3 Å before the gallery, IA groups are 1.5-7 Å from the clay surface. Most of these functional groups are 2-4 Å far from the clay surface (peak positions).

Same results were also observed for the MMT2 based organoclays based on the DDA, ODA and ODTMA surfactants. Most of the  $-OH$  groups are found at 2-3 Å distance from the end of clay surface. As it can be seen from the Figure 6.10, small amount of signed  $-OH$  groups on the IA groups can be placed far from the clay surface during the simulation at equilibrium due to the steric hindrance and shielding ability of trimethyl ammonium at high CEC clays. In conclusion, the model of two compatibilizer functional groups layers concentrated on two clay surfaces between the gallery given in Figure 6.9 and Figure 6.10 were true for almost all the nanocomposite structures.

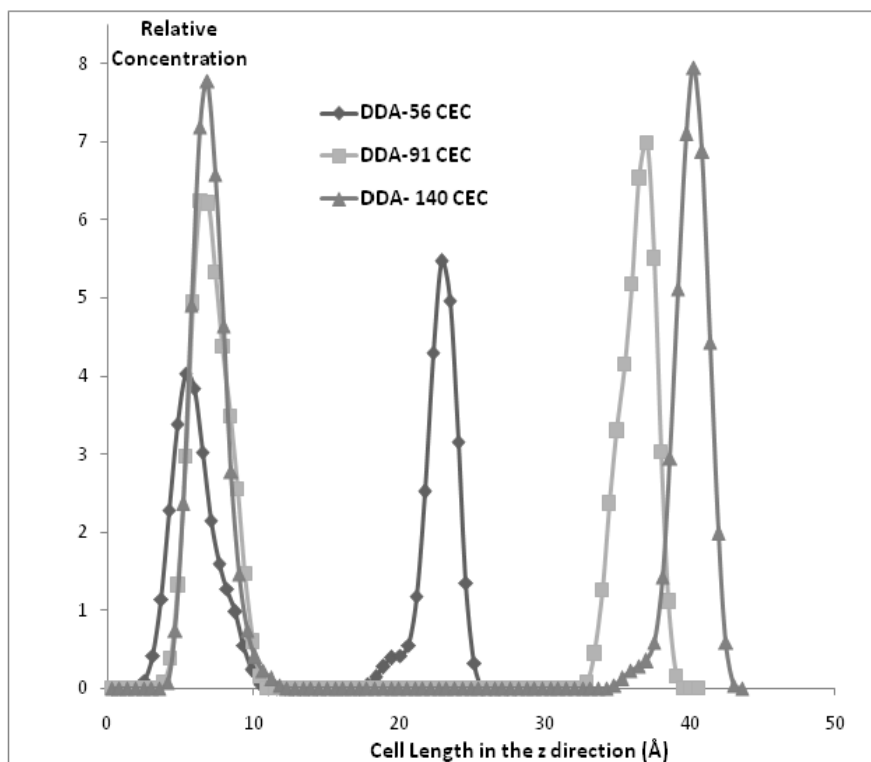


**Figure 6.9:** The concentration profile of –OH groups in IA for DDA surfactants with different CEC clays.

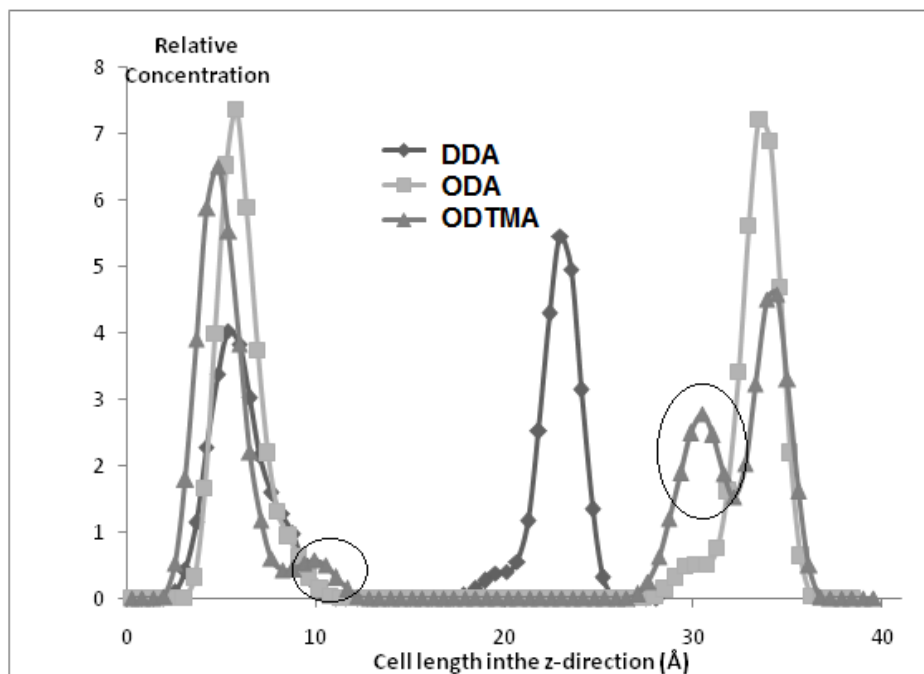


**Figure 6.10:** The concentration profile of –OH groups in IA for MMT3 with different surfactants.

For the larger head groups which were known to be resulted in nanocomposites with better mechanical properties, similar hydrogen bondings for the MMT surface oxygens with AA and IA acidic hydrogens were still in effect. As seen from the Figure 6.11, IA is a bifunctional compatibilizer and can supply enhanced interaction with clay surface. Dipole-dipole and ion-dipole interaction were effective for quarternary alkyl ammonium surfactants.

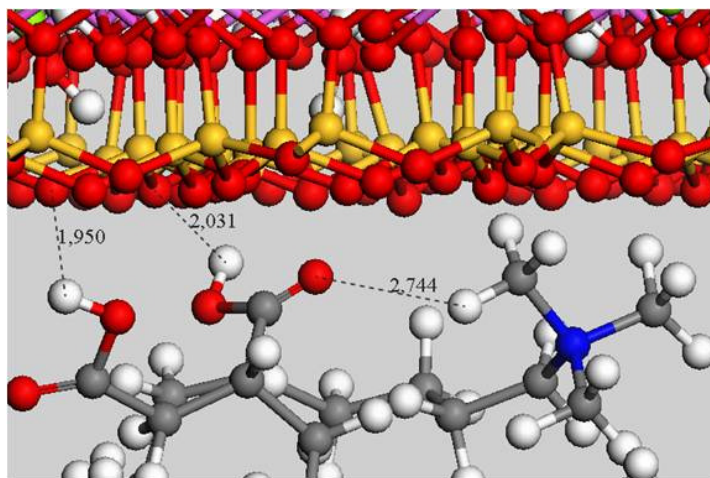


**Figure 6.11:** Snapshot picture showing the interactions of IA, quarternary ammonium and MMT surface.

Similar effects were also valid for the head groups that have ring type structure such as imidazolium and pyridium surfactants where ring structures of head groups reside parallel to the clay surface (Figure 6.12). The positive charge distributed among the rings especially on the hydrogen atoms caused the parallel configuration and better interaction with oxygen atoms of AA and IA.

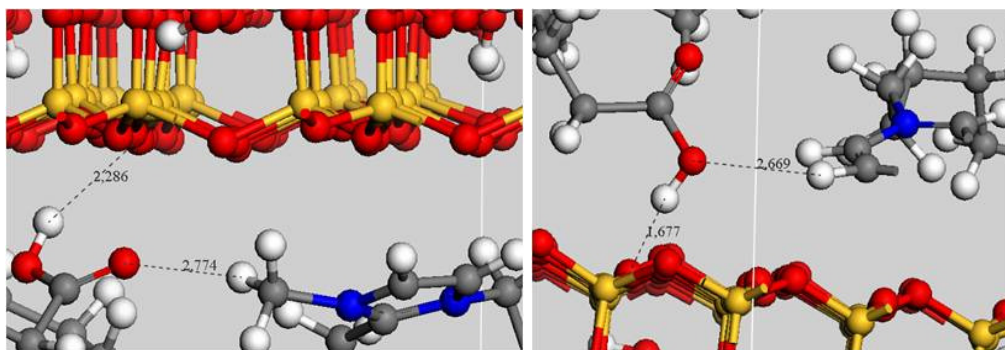


**Figure 6.12:** Snapshot picture showing the interactions of IA, quarternary ammonium and MMT surface.

The concentration profile of –OH atoms that presented only in imidazolium based organoclays in the z-direction from beginning of one clay layer to the end of next is given in Figure 6.13. For MMT1 and MMT2 where 6 and 10 imidazolium ions are present on the 5x3 clay cell, almost all the IA atoms reside on the surface of clay with the interaction given above. As the cation exchange capacity increases, all the IA groups can not reach to the surface at equilibrium and reside at 5-10 Å distance after the imidazolium groups.

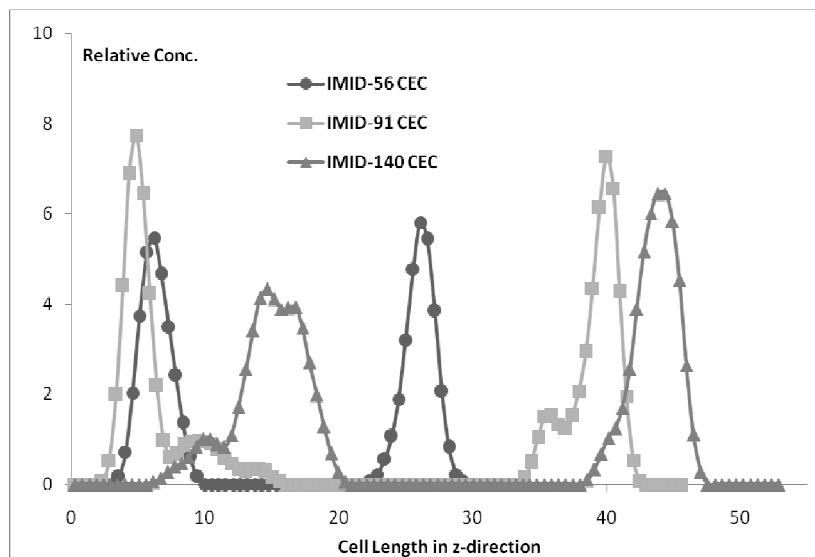


**Figure 6.13:** The concentration profiles of –OH in imidazolium based organoclays among the z-direction.

The highest distance of IA and AA with surfactants was observed for the largest head groups such as for HDTBP where all positive charges were present on the tributyl phosphonium (Figure 6.14). Moreover, phosphonium groups are softer acids than ammonium groups. Even their surface coverage are enhanced, interaction with clay surface is still sufficient and thermal stability is better than ammoniums, their interaction with the functional groups are lower due to the large volume of head groups.

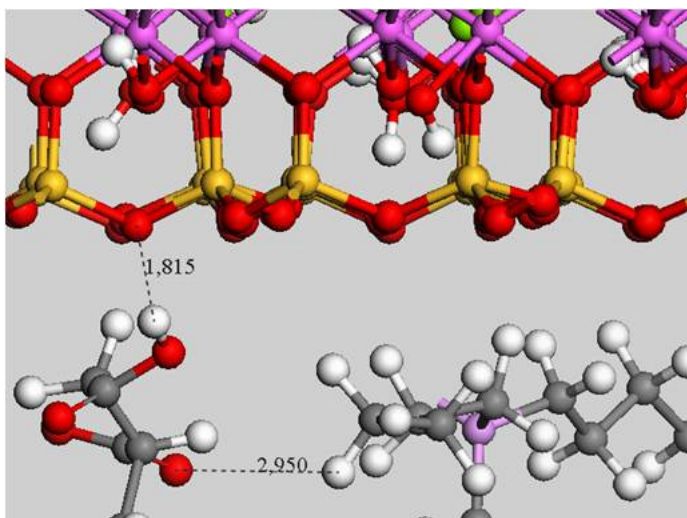


**Figure 6.14:** Snapshot picture showing the interactions of IA, HDTBP head group and MMT1 surface.

In some cases, especially for the high cation exchange capacities the large volume of surfactants such as HDTBP case, compatibilizers could not reach to the clay surface due to shielding of butyl groups (Figure 6.15). Compatibilizers still succeeded their roles by moving towards the surface and transport the PE chains to the surface.

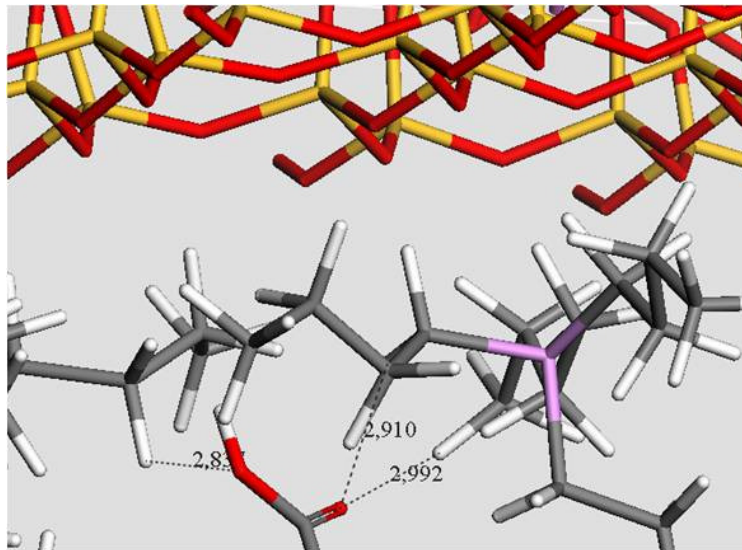


**Figure 6.15:** Snapshot picture showing the interactions of IA, HDTBP head group and MMT3 surface.

This shielding effect could be seen obviously from the distribution of  $-OH$  from carboxyl groups from IA based compatibilizers between 2 clay layers for 5x3 cell of MMT3 with 16 HDTBP ions at equilibrium in Figure 6.16. This distribution showed that due to the shielding effect of large tributyl phosphonium groups, IA groups were

confined in the gallery at the PE rich phase. The presence of hydrophilic IA groups in PE domains caused unfavorable repulsion and decline in mechanical properties of final nanocomposite. That means one should use compatibilizers carefully for high CEC and large volume surfactants where surface coverage is high.

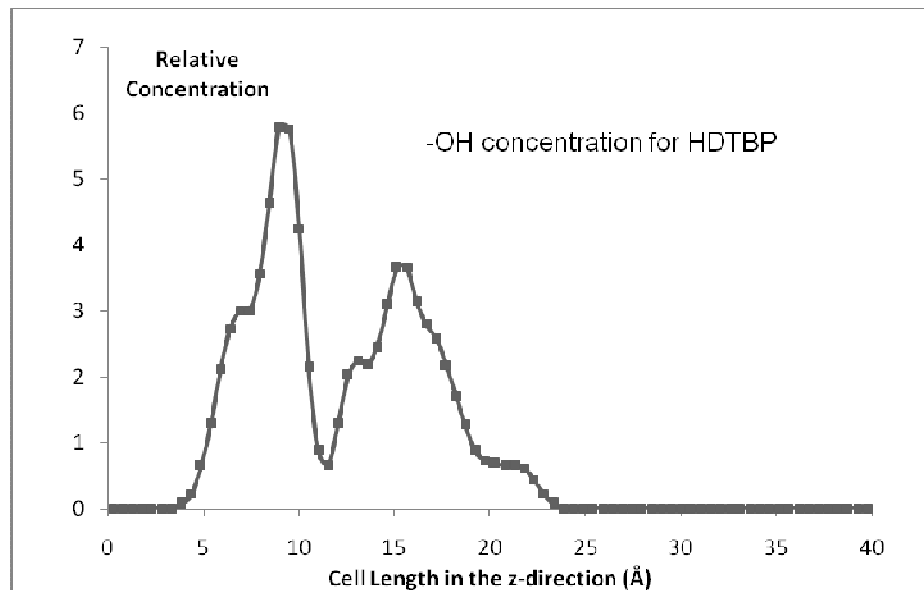


**Figure 6.16:** The concentration profile of –OH atom in HDTBP based organoclays with high CEC.

The anhydride group of MA group have different binding mechanisms with clay surface and surfactants. The average distances with clay surface given below demonstrated that all three hydrogen atoms causes dipole-dipole interactions with clay surface oxygens (Figure 6.17). MA groups placed over the hexagonal cavities. Some experimentalists speculated the presence of hydrogen bonding between octahedral –OH groups bonded to Al and Mg with oxygen atoms of maleic anhydride groups or opening of anhydride ring into maleic or succinic acid [111,259]. First case can not be possible because of the relatively upwards conformation of MA rings. The angle with the clay surface is found 25°.



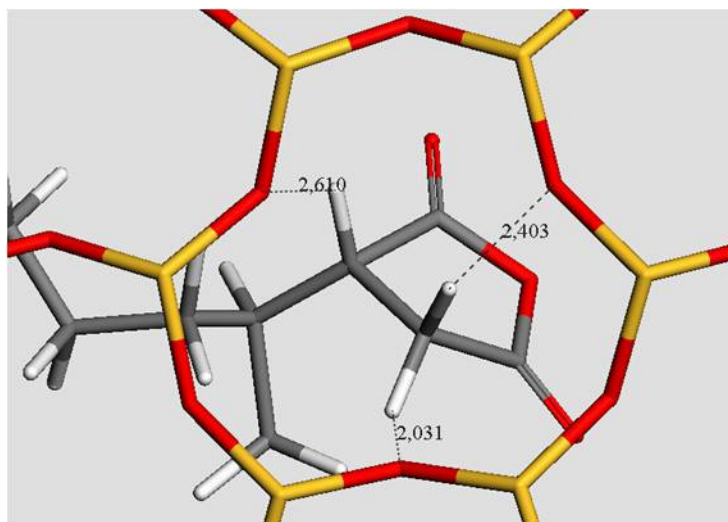


**Figure 6.17:** Snapshot picture showing the MA group adsorbed on the MMT surface.

The interaction of primary alkyl ammoniums with maleic anhydride is hydrogen bonding with –H atoms of cationic ammonium head groups. Ion-dipole interaction was found to exist with quarternary alkyl ammoniums and maleic anhydride. Independent from the structure of the surfactant, hydrogens of the maleic anhydride placed above the hexagonal cavity (Figure 6.18).

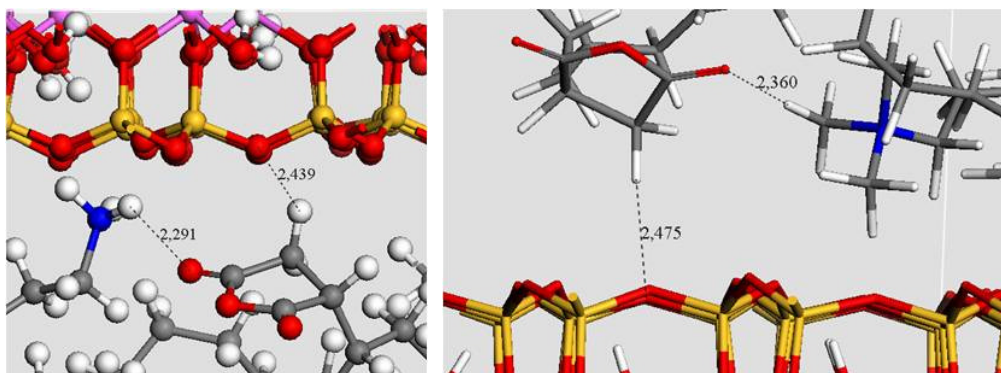


**Figure 6.18:** Snapshot picture showing the interactions of MA, ammonium head group and MMT surface.

The interaction of pyridinium and imidazolium ions which placed parallel to the clay surface at equilibrium had ion-dipole interaction with oxygen atoms of anhydride groups with the 2.3-2.5 Å distance. The possibility of this type of interaction was increased for imidazolium and pyridinium with respect to ammonium because of the number of hydrogens in their rings that all have similar charge and similar distance from the clay surface as seen from the Figure 6.19.



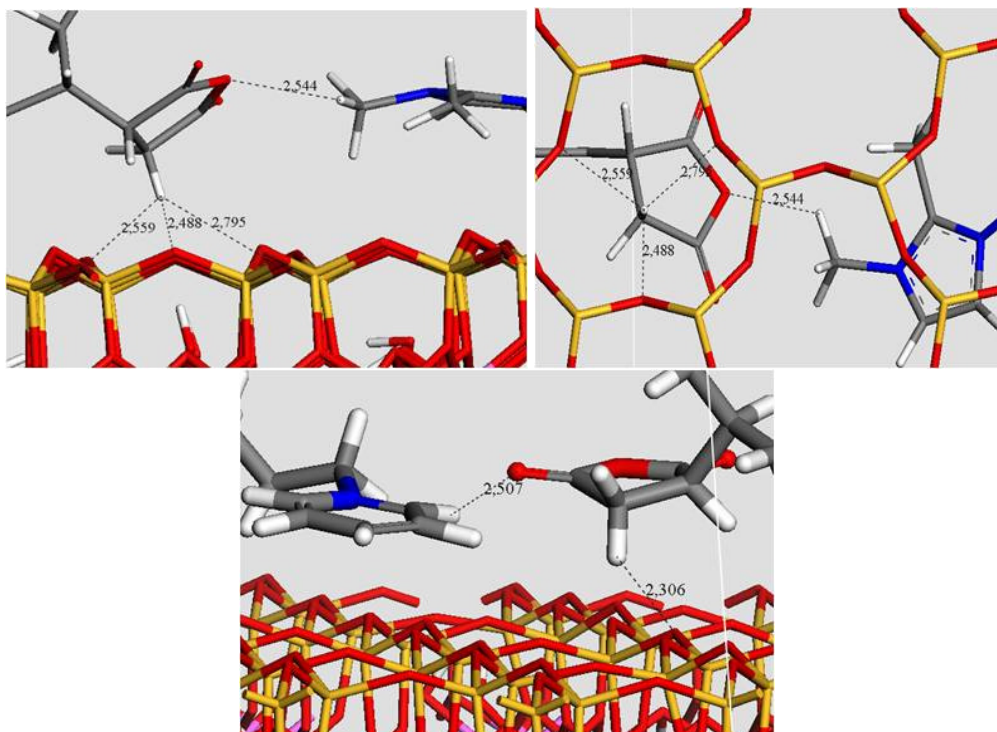


**Figure 6.19:** Snapshot picture showing the interactions of MA, ring shaped surfactants and MMT surface.

As explained above, IA and AA have the advantage of constituting strong hydrogen bonds with clay and surfactants and MA has the advantage of having three hydrogens that can interact at the same time due to the parallel conformation with the hexagonal cavities formed by oxygens of clay surface as well as with the surfactants. Another important advantage of the parallel conformation of MA is the double sided symmetric sp<sup>2</sup> hybridized oxygen and one sp hybridized oxygen that can possibly interact with more than one surfactant at the same time as given in one of the snapshot in Figure 6.20.

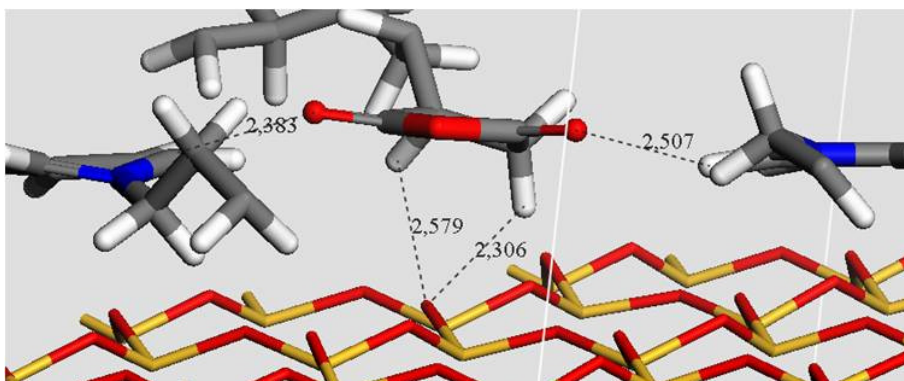


**Figure 6.20:** Snapshot picture showing the interactions of MA, imidazolium groups and MMT surface.

For the large and charge delocalized surfactant structures such as HDTBP have lower interaction and higher CH...O distance with maleic anhydride group as given in the Figure 6.21. These structures can also cause the increase in the clay surface distance with compatibilizers due to the steric hindrance of the 3 butyl chains lying parallel to the surface.

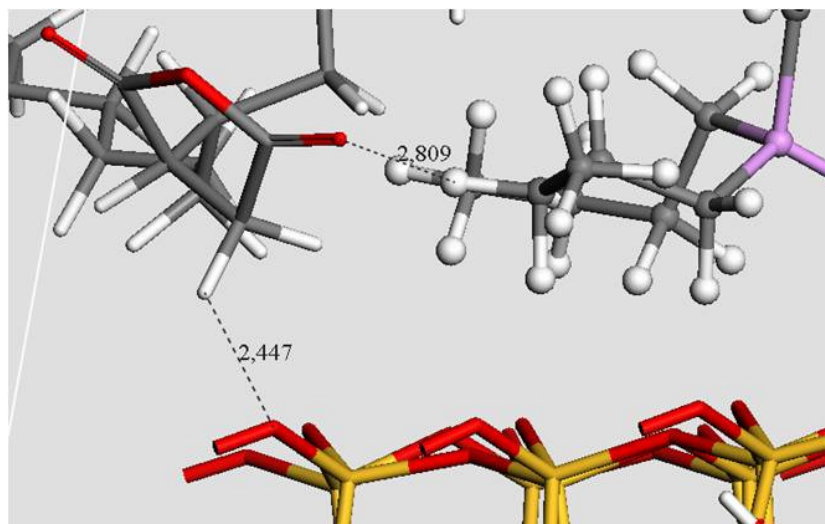


**Figure 6.21:** Snapshot picture showing the interactions of MA, HDTBP and MMT surface.

Another shielding of functional group from the clay surface is observed for the high amounts of compatilizer case. As seen from the Figure 6.22, when two of three PE chains are grafted by two different IA groups at the same time, only one of the IA group reaches to the surface at equilibrium. Other IA groups stay between layers in the PE chain phase which is unfavorable for nanocomposite formation. It can be concluded that the grafting of IA groups at higher ratios or with high intensities at the same time may cause declining of pinned IA groups to the clay surface.

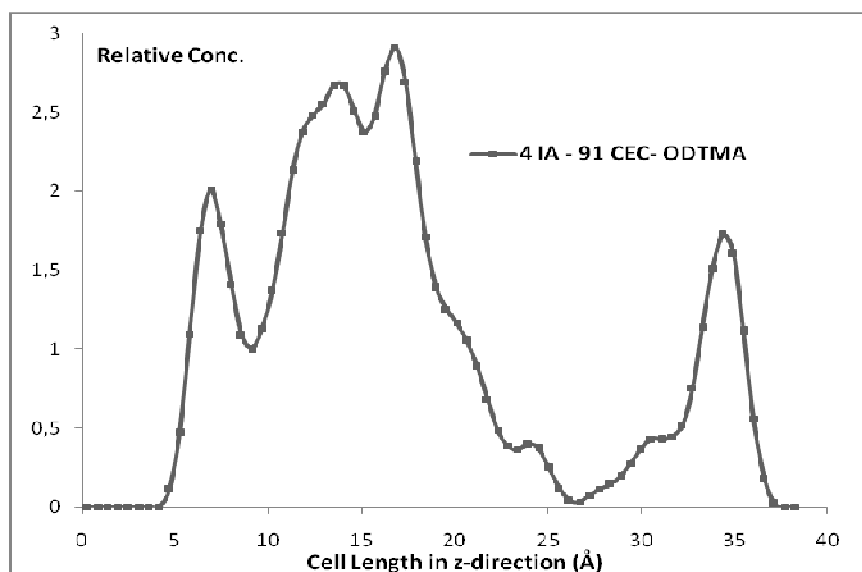


**Figure 6.22:** The concentration profile of –OH in high amount of IA groups.

The last case for the unfavorable interactions of IA in the gallery is due to the high density of surfactant alkyl tails. As seen from the Figure 6.23, when trioctadecylmethyammonium chains used at high cation exchange capacities, the alkyl chains causes a hydrophobic wall where the interaction between clay surface and compatibilizer prevented. All IA groups are forced to place in the middle part of gallery and have repulsive interactions.

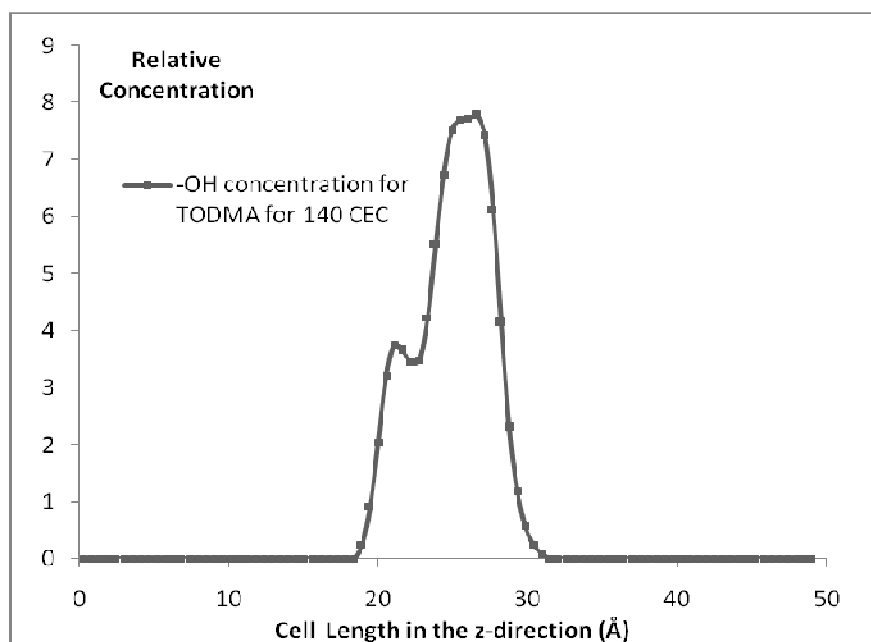


**Figure 6.23:** The concentration profile of –OH in TODMA based organoclay with high CEC.

Different from previous cases, the favorable interaction between high density of surfactant head groups and IA groups were also determined to be shielded. The IA groups that could not reach to the clay surface due to the steric hindrance of alkyl tails of TODMA, stay near the methyl end groups of alkyl tails where the highest charges of intergallery exists (Figure 6.24).

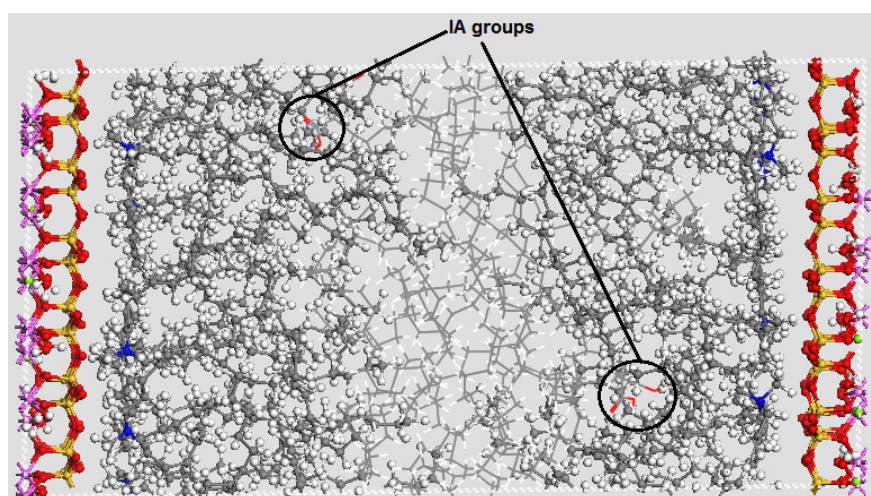


**Figure 6.24:** Snapshot picture showing the interactions of TODMA and IA groups in MMT3.

Another important factor in the formation of polymer-organoclay nanocomposites is the polyethylene chain organisation between the clay layers. As it can be seen in the Figure 6.25 where carbon atom concentrations of PE chains are given, there is not any crystal or ordered structure of PE chains in the confined system. However, there is a very important results about the organisation of chains near the clay surface for different surfactants having different number of alkyl tails. The distance of the first carbon atoms in PE chains from the clay surface is at 1.8 Å, 2.2 Å and 5 Å for ODTMA, DODDMA and TODMA. This means for the high number of alkyl chains in the surfactants, PE can be transported more hardly to the clay surface. This is what expected from a surfactant to prevent the unfavorable interaction resulted from the hydrophilic clay surface and apolar PE chains.

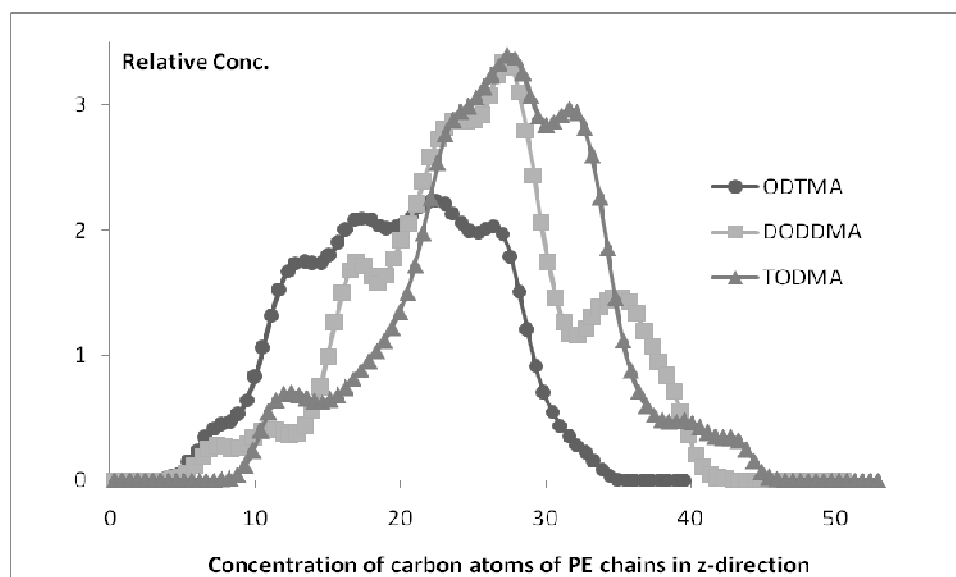


**Figure 6.25:** The concentration profile of  $-\text{CH}_2$  in ODTMA, DODDMA and TODMA based organoclays.

Similar effects are also valid for the increased cation exchange capacities with same surfactant. The PE chains are exist at 1.8 Å distant from the cation surface when only 6 ODTMA ammonium atoms covers the 5x3 supercell of clay surface with 56 meq/100g CEC. If the number of surfactants were increased to 16, dependent upon the usage of clay layer with 143 meq/100g, the PE chains were shielded more by the increased number of alkyl tails which is a desired situation in the between the clay layers (Figure 6.26).

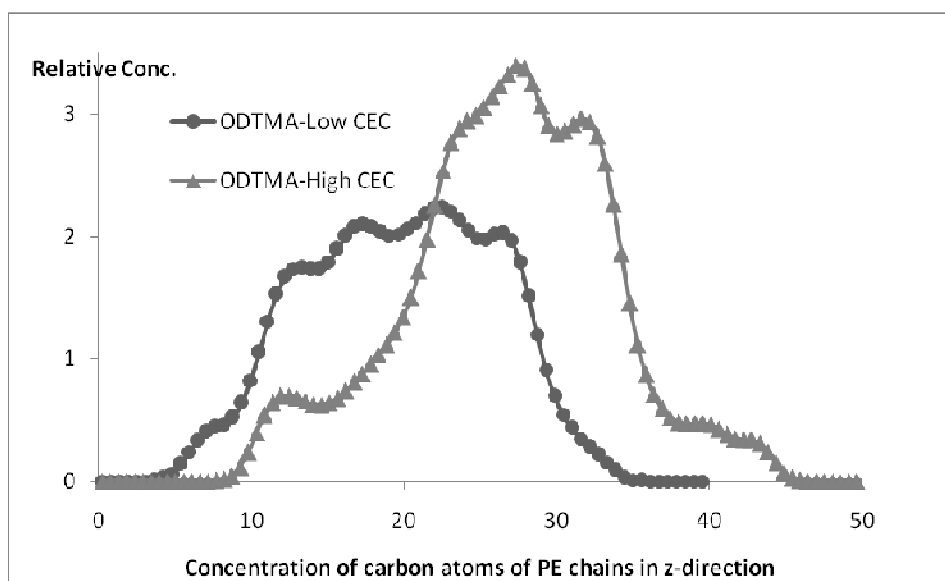


**Figure 6.26:** The concentration profile of  $-\text{CH}_2$  in ODTMA based organoclay with low and high CEC.

### 6.3.2 Interaction energies between the constituents

The important binding energies between constituents of polyethylene-organoclay, are analyzed with respect to CEC of the clay layers, structure of the surfactant and the compatibilizer used. All the energies given in this part are in kcal/mol.

The binding energies for the 91 CEC clay (MMT2) layer which is the most commercially used CEC in the experiments and industrially, are given in the Figure 6.27. The highest energy was found to be between surfactants and clay surface as expected. These energies are high for primary alkyl ammoniums (DDA and ODA) and low for the larger head groups and increased number of alkyl tails (HDTBP, DODDMA and TODMA). As shown above, primary alkyl ammoniums have the lowest distance and strong hydrogen bonding with the oxygens of the clay surface. The interactions between the surfactants and PE chains are lower in amount with respect to clay-surfactant, but still important in amount. Contrary to the clay-surfactant interactions, the energies between surfactant and PE chains are vdW interactions between alkyl tails and PE backbone. That is the reason why they have lowest values for primary alkyl ammoniums and increased with respect to number of chains in the tails. They are also higher for the increased volume of head groups such as for the HDTBP, DODDMA and TODMA. The lowest energy is between the polar clay surface and apolar PE chains as expected (Figure 6.27).

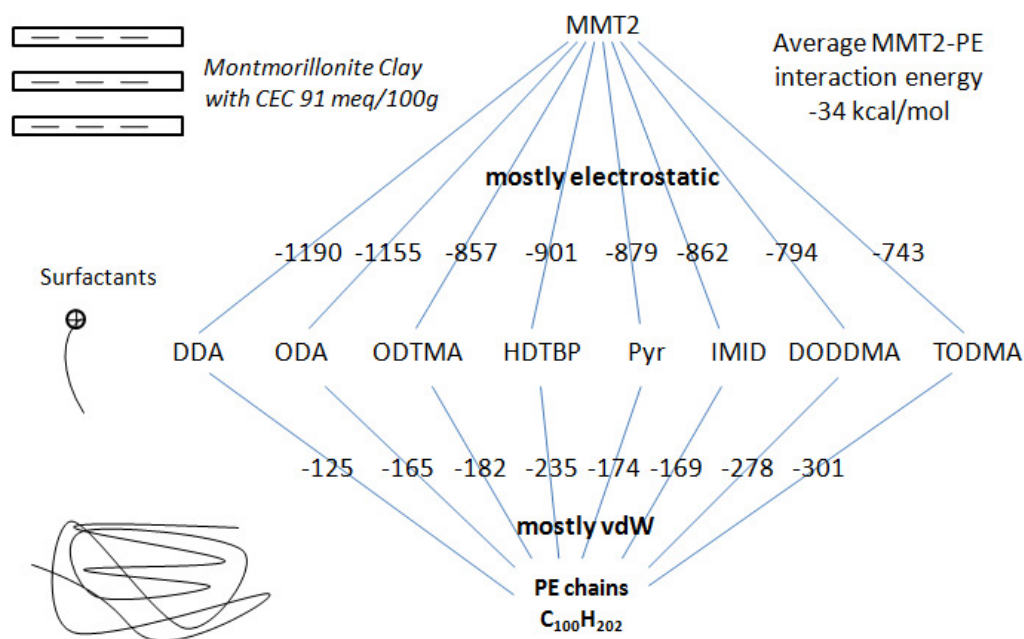


**Figure 6.27:** The binary interaction energies in nanocomposites formed by MMT2, pristine PE and different surfactants.

The energies between clay layers and intergallery constituents for low cation exchange capacity are given below. The general trends of interaction energies are all same with the previous energies in Figure 6.28. All the energies are decreased due to the decreased number of surfactant chains between clays. These results are consistent with the snapshots from simulations given in the previous section.

Since the surfactants are both interacted strongly with clay and polyethylene, the number and structure of surfactants are strongly effective on the energy values in addition to be effective on the shielding of the interactions between clay layers and PE chains for high CEC of clays. Higher number, length and size of the head group causes the more negative interaction energies with polyethylene chains, as the binding between the clay and surfactant lowered respectively. However, it must be noted that the organoclay formed by low CEC clay and TODMA surfactant still have -557 kcal/mol interaction energy and is very stable like all the other organoclay structures. Less negative interaction energy between MMT and PE backbones can be seen controversial at the first sight. However, the repulsive (positive) electrostatic interactions between apolar PE chains and polar clay surface are promoted by low CEC and low number of surfactants that causes the less negative interaction energy between MMT and PE chains (Figure 6.28).

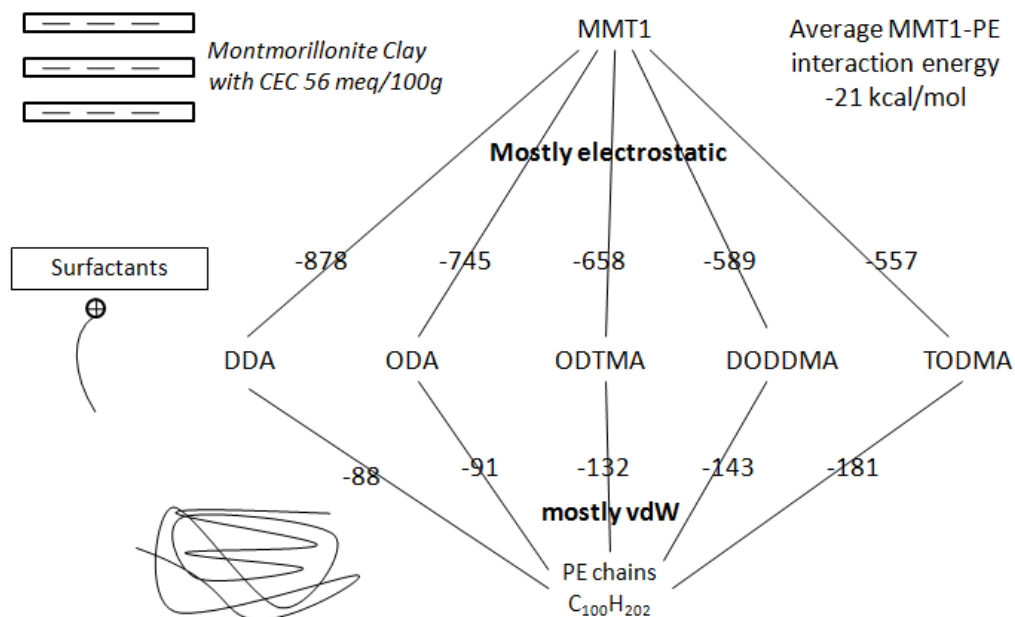


**Figure 6.28:** The binary interaction energies in nanocomposites formed by MMT1, pristine PE and different surfactants.

The pairwise interaction energies between constituents are given for the 143 meq/100g clay (MMT3) in Figure 6.29. All the interactions between MMT-surfactants, PE-surfactants and MMT-PE are increased due to the more surfactants chains present between the layers. The highest interaction between surfactants and clays are for primary alkyl ammoniums where 16 ammonium head groups have ionic and hydrogen bonding with clay oxygens. The highest interaction between surfactants and PE chains are observed for TODMA as expected where 48 octadecyl alkyl chains are lie out towards the PE chains. More negative interaction energy between MMT and PE chains are calculated for high CEC, due to the decreased repulsive (positive) electrostatic interactions between apolar PE chains and polar clay surface by high number of surfactants.



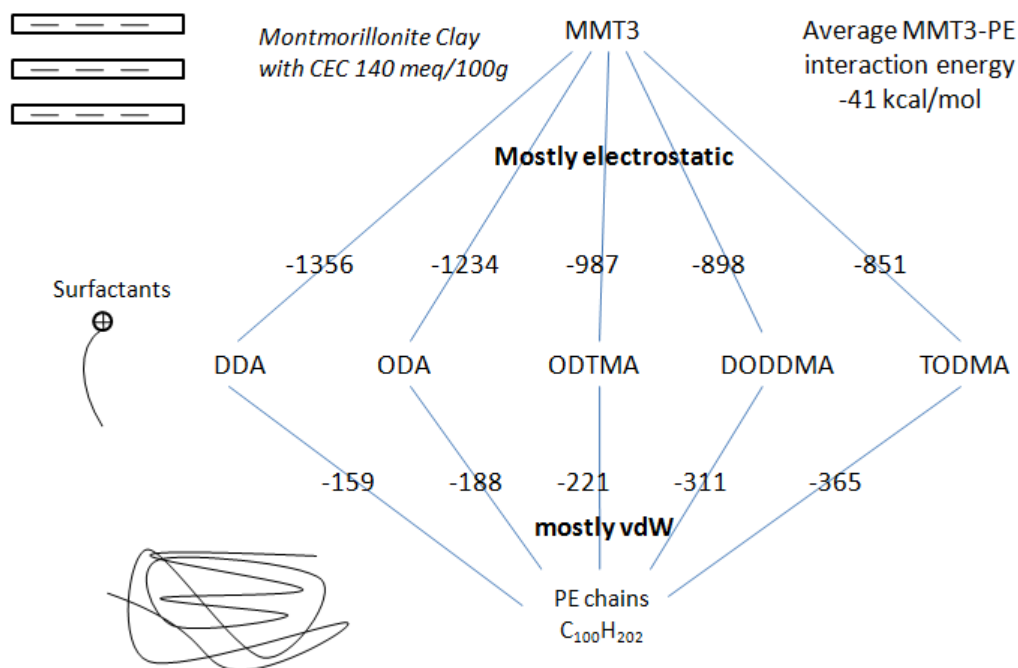


**Figure 6.29:** The binary interaction energies in nanocomposites formed by MMT3, pristine PE and different surfactants.

The interactions in the nanocomposite formed by PE-g-IA, middle CEC clay (MMT2) and different surfactants are shown in Figure 6.30. Two important enhancements observed in energies for compatibilizers with respect to pure PE chains. One is in the interaction between the surfactants and compatibilizers. This enhancement is resulted from the head groups of surfactants interacted with the functional groups of compatibilizer. This effect is more obvious and reach % 40-50 higher than pure PE interactions for primary alkyl ammoniums. Since the alkyl chains are less effective in shielding IA groups in primary alkyl ammoniums, IA groups can reach head groups of ammonium head groups. Secondly, the primary ammonium groups can make stronger hydrogen bonds with IA groups after reaching the surface.

The enhancement in the interaction energies by adding compatibilizer are lowered by the larger head groups and higher number of alkyl tails such as HDTBP, DODDMA and TODMA. The enhancement is at 3-10% levels for these systems. The first reason for that is the less polarity of the head groups and second reason is the shielding by hydrophobic alkyl tails that lowers the effects of compatibilizers.

The most important contribution of compatibilizers to the formation of PE-organoclay nanocomposites are based on the improved bonding due to the hydrogen bonding between clay surface oxygens and hydroxyl groups of IA groups. This improvement is very effective at more than 5 fold increase (-34 to -178) observed with respect to pure PE chains.

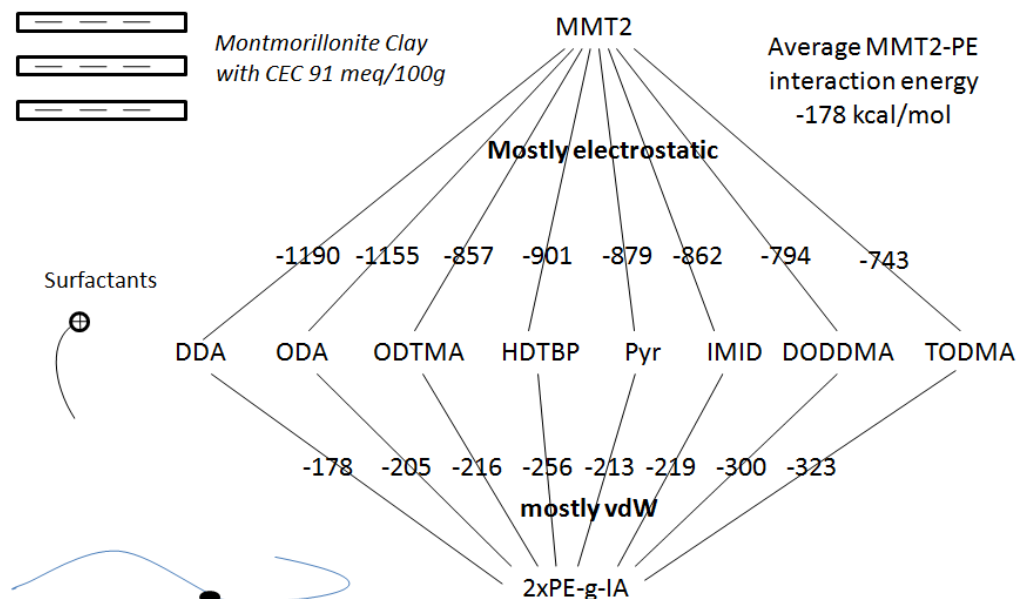


**Figure 6.30:** The binary interaction energies in nanocomposites formed by MMT3, PE-g-IA and different surfactants.

Another factor interested by experimentalists is the amount of compatibilizer between the clay layers [261]. Results for one of the example for this factor given in the Figure 6.31 for most used MMT2 and ODTMA surfactants. It is found that both the clay-polyethylene interaction and polyethylene-surfactant interaction improved by the amount of IA in the simulation cell. The compatibilizer between the cell must be increased for the stability and physical integrity of nanocomposite phases.

We have to remind that, it is not true universally for all surfactants and compatibilizers. As given in the previous Figures, for increased number of alkyl tails and larger volume of head groups such as TODMA, increased number of IA groups can not reside on the clay surface that causes repulsive interaction between both alkyl tails and clay layers. As a result, decrease in the interaction energies are observed for both with clay layers and surfactants with the increased amount of compatibilizers between clay layers.

For TODMA surfactant, the interaction between compatibilizer chains and surfactants is still more negative than ODTMA. The reason for this is the compatibilizer structure where only one IA group is grafted on the apolar PE chain in a 100 carbon atom backbone. Since TODMA also have apolar alkyl chains, the interaction of all compatibilizers with TODMA will be more negative than others. The key point here is the amount of compatibilizer used. The maximum interaction between TODMA and compatibilizer is reached for only two IA while the maximum interaction between compatibilizer and MMT is reached for one IA group is between the clay layer (for TODMA surfactant). The preceding one is more important than the second one in amount, since polymer phase is faced with surfactant rather than MMT, so two chain of compatibilizers are enough for the lowest energy structure in our cell composition.

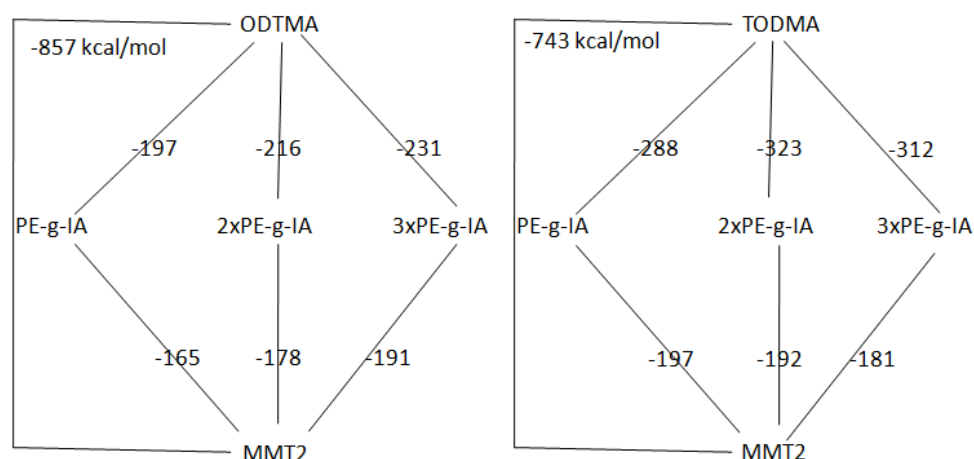


**Figure 6.31:** The binary interaction energies in nanocomposites formed by MMT2 and PE-g-IA with ODTMA and TODMA surfactants.

All these energetical discussions are also supported by the previous section where structures and concentration profiles between clay layer were analyzed. We can conclude this discussion by “when surfactants with single alkyl tail (ODA, ODTMA) are used, the higher amounts of compatibilizer can be used. However the compatibilizer amount can be lower for the larger volume of surfactants and CEC of the clay that resulted in less hydrophilic organoclay.”

The last factor important for the nanocomposite stability is the type of the functional group in the compatibilizer. Although all the energies are close in values, the highest interaction between ODTMA surfactant and compatibilizer is calculated with the

MA functional group given in the Figure 6.32. The IA group is better than AA due to the bicarboxylic acid groups. The interaction between different compatibilizers with clay surface is different in order. Since IA and AA can form strong hydrogen bonds with clay surface, their interactions are higher than MA based compatibilizers. We can conclude that MA have higher interaction with ammonium based surfactants, while IA and AA supply higher interaction with the clay surface. All these values are very close which means the addition of compatibilizer is crucial for the formation of nanocomposite, while the kind of functional group have less importance.

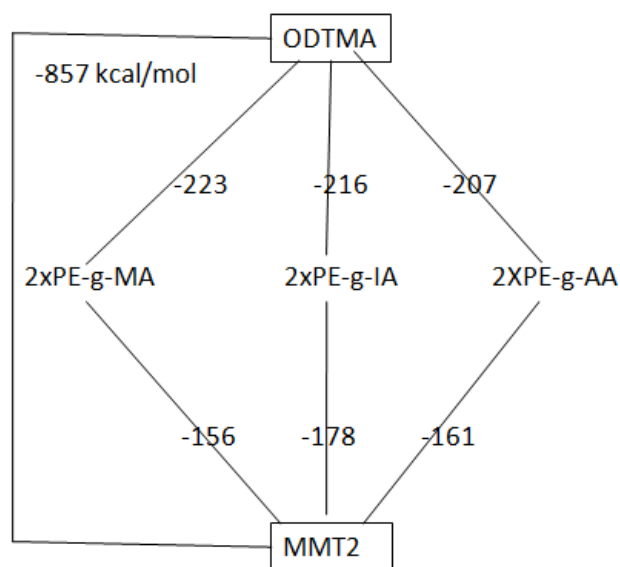


**Figure 6.32:** The binary interaction energies in nanocomposites formed by MMT2 and ODTMA with different compatibilizers.

By analyzing the total energies, it is found that the grafted polyethylenes (PE) interact better than pristine PE homopolymers with the organoclay at all cases, then grafting favors the interaction between polymer and organoclay. This causes exfoliation during melt compounding and enhances the physical and mechanical properties of the nanocomposite material. General interactions responsible for the PE-organoclays between constituents are given in Figure 6.33. Molecular dynamics simulations showed that vdw interactions determine the main interaction between polyethylene and alkyl tails in surfactants of organoclays. The strongest interaction between all constituents is the surfactant-MMT electrostatic interactions that causes the formation of stable organoclays. Experiments showed that interfacial action between MMT and PE compatibilizer is very important for the resulting mechanical properties of the nanocomposite [262-264].

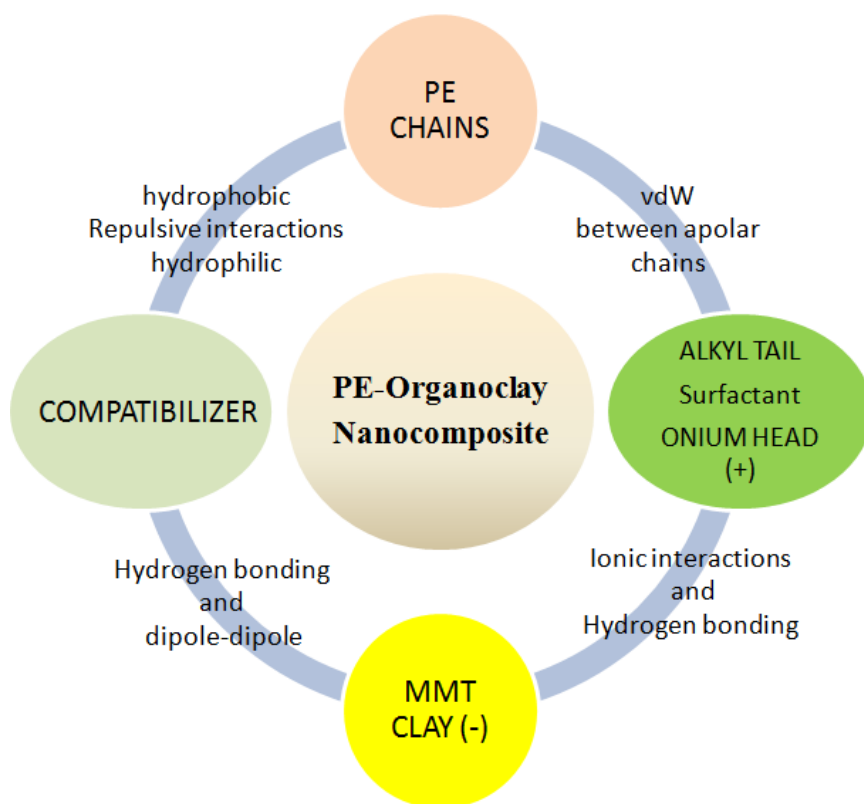


**Figure 6.33:** Type of pairwise interactions in PE-organoclay nanocomposites.

The interactions between MMT clay and surfactant head groups are much stronger than the interactions between polyethylene and surfactant tails. That is the reason why exfoliation can be accomplished in melt blending if only the interaction between the clay and polymer phase exists.

As a result of shielding some surfactants strongly bonded to clay surface and with larger volume can lowered the interactions between the polyethylene and the MMT layers. Even, in some experiments it was found that the system composed by pure MMT and a polar polymer such as polyamides or polyethylene oxides can have the highest binding energy [257,265]. The interaction energy between the polyethylene and the montmorillonite layer was calculated to have declining trend with increasing molecular volumes of surfactants. Similarly, the attractive interaction between the compatibilizers and the clay layers increase with decreasing volume of head groups and shorter hydrocarbonic chains in tails. These small surfactants are however effective in having unfavorable interaction energies with respect to longer ones for the surfactant with the polyethylene backbones. Since the ratio of polyethylene chains in nanocomposite is usually over %90 w/w, the interaction between alkyl tails

and PE chains is an important factor. The aspect ratio the clay is very high and compatibilizers will interact with the clay surface during the melt blending. This interaction between compatibilizer and the clay surface is important for the exfoliation of the platelets as also shown by experiments [266]. The alkyl tails of the surfactants must be long enough, but the surface coverage of these molecules must be smaller than 100% to let interaction of compatibilizers functional groups with the clay surface.

In summary, molecular dynamics simulation methods are used to determine the interaction energy between organoclay and polymer. The most effective interaction between the organoclay and different compatibilizers are sought. To increase polyethylene-clay interaction, the clay interlayer surfaces of the silicate must be modified with surfactants to change clay layer to have less hydrophilic character to have attractive interaction with hydrophobic polyethylene. The strongest interfacial interaction was found to be between the clay surface and ammonium heads of the surfactant molecules due to the H-bonding interactions of hydrogen's ( in  $\text{-NH}_3^+$  ) with the lone pairs of the framework oxygens. Our MD studies on the structure of the montmorillonite (MMT) based organoclay showed that the ammonium ( $\text{-NH}_3^+$ ) headgroups are coordinated to the hexagonal cavities. The incomparably high interaction energy between MMT and surfactant makes us to consider the organoclay as a whole. The main factor then determining the physical properties of the material is the grafted polymer and organoclay interaction. Then, the improvement in the experimental mechanical properties are found to be related with the increased attractive interaction energies between the functional groups of compatibilizer and highly stable organically modified clay. Grafting of the polar groups increases the attractive forces between PE and organoclay and this may be the driving force for the exfoliation during melt compounding which was confirmed by the high correlation between the calculated interaction energies and experimentally measured mechanical properties. All molecular modeling methods was carried out on the basis of input data obtained from lower-scale calculations. Each step of molecular simulations procedure has been confirmed by the experimental studies. This result is of great significance since it enables to estimate the optimum ratios of the constituents making up the nanocomposite and helps experimentalists to synthesize materials with enhanced properties.

## 7. CONCLUSIONS AND RECOMMENDATIONS

In this thesis, the major factors such as structure, formation and strength of interfacial interactions leading to enhanced physical and mechanical properties of polymer-clay nanocomposites were investigated by multi-scale studies. The structures of polyethylene chains, compatibilizers, clay layer, surfactants and interfaces were modeled and the interfacial interactions between polymer (PE) chains and compatibilizers, clay (MMT) surface and surfactants for polyethylene-organoclay nanocomposite systems were studied explicitly by employing quantum mechanical (QM), density functional theory (DFT) and statistical mechanical (MD and MC) methods. The initial structures were modeled according to the XRD data if available. The simulations were performed at experimental temperatures and cation exchange capacities of clay layers. The effects of grafting, structure and polarity of the functional groups, grafting ratio of compatibilizers, chain length and the type of the head groups of surfactants, cation exchange capacity of montmorillonite clay on the aforementioned properties were considered separately to elucidate their contribution to the energetics of the overall system.

We showed that the exfoliation of clay layers occurred due to the strong interaction between the polyethylene and clay in the PE matrix and as reported in the literature, exfoliation is required to improve the morphology and mechanical properties of such nanocomposites. The interactions have greatly strengthened by introducing compatibilizer which were prepared by the incorporation of a polar functional group onto the PE backbone. The compatibilizers achieved their function mostly by non-bonded interactions such as dipole-dipole and hydrogen bond interactions. The Fukui reactivity indices were calculated to demonstrate that the most reactive sites involved in physical or chemical interactions were the polar groups. The best compatibilizing performance of PECs were observed at low grafting ratios. The increase in the grafting ratios had negative effects on the structure. In the structural analyses of PE/PEC blends, we have seen that the polar functional groups tended to escape from

the nonpolar PE chains and reside on the surface or at the interfacial region. When the grafting ratios were increased, the functional groups were present also in the bulk phase, inside a cavity created due to their repulsive interaction with the PE environment. These cavities were called defects and they caused loss in the mechanical properties as observed experimentally. According to the interactions parameters calculated, the MA and IA grafted PEs served as the best PE compatibilizers and the latter could be used as an alternative to MA due to its biodegradability.

DFT calculations on periodic MMT clay structure showed that the hydroxyl hydrogen atoms in the octahedral layer had mostly trans configurations and acted as nucleophilic centers whereas oxygen atoms in the tetrahedral layer were electrophilic centers. In this respect, oxygen atoms on layer surfaces play an important role in adsorption and intercalation of surfactants and compatibilizers by their H-bond making ability. The high hydrophilic activity of MMT was proven with the high atomic charges of oxygen atoms on the clay surface.

Molecular mechanics and classical molecular dynamics simulations were carried out by using the force fields especially developed for organoclays. The MD simulations showed that vdW type interactions were the major interactions between PE chains and the alkyl tails of surfactants in the hydrophobic gallery zone. The strongest interaction among the all interfacial interactions was the electrostatic interactions between the surfactant's polar head group and MMT and it contributed highly to the formation of stable organoclays as also shown experimentally. We showed that the modification of MMT surface using surfactants played a very important role in the formation of PE/MMT nanocomposites by allowing energetically favorable penetration of the PE into the intergallery region. Another important function of surfactants is that they assist the exfoliation. We showed that this ability of surfactants were dependent on the chemical structure of the onium ions and cation exchange capacity and surface polarity of the clay. It is known that the structure and function of a molecule is highly interrelated. A priori organoclay and nanocomposite simulations, the optimized organoclay constituent geometries were compared to the XRD results and validated. Effect of alkyl ammonium chain lengths on the interlayer interactions and basal spacing were studied by modeling clays with different cation exchange capacities and different surfactants. The most stable positions of polar



alkyl ammonium heads on the clay surface were found to be at the center of the hexagonal cavities and were determined by the interfacial interaction between clay and surfactant. This interaction was calculated to be the strongest interaction among the all other interfacial interactions due to the H-bond formed between the hydrogen atoms of the head groups and the lone pairs of framework oxygen atoms in the tetrahedral layer. It is reasonable to expect that the strength of this interaction is highly correlated to the size matching between the head groups and the hexagonal cavities and it is increased if the polar head group is accommodated better. The incomparably high interaction energy between MMT and surfactant made us consider the resulting organoclay as a whole in further studies of the nanocomposite.

The interaction between clay surface and the hydrophobic tail of the surfactant was very repulsive and they did not mix at all. This caused the increase in the basal spacing and the tails were pointed out towards the interlayer. Basal spacing and layering behavior was seen to be controlled by the size of the head group, concentration of surfactant molecules, the number of the tail groups attached to the head and the length of the tail group. Upon increase in the alkyl chain length, the gradual transition from monolayer to bilayer, trilayer and paraffin-like structures of the tails was observed within the clay gallery.

When the calculated binary interaction energies between the compatibilizers, PE chains, MMT samples and surfactants were analyzed, it was seen that they all had negative values except the compatibilizer-PE energy. Negative mixing energies proved that nanocomposite formation and intercalation processes were favored. This result is very consistent with the experimentally reported high stability of organoclays even at their very low concentrations.

We showed that the grafted PEs interacted better than the homopolymers both with clay and surfactant's head groups. Grafting made the interaction between polymer and organoclay possible which would otherwise not possible and enabled the usage of commodity hydrophobic polymers in synthesis of nanocomposite materials. Presence of the functional groups on the PE surface enabled the access of PE chains to the clay layers. The compatibilizers functioned by orienting polar groups towards the clay surface. The experimentally observed enhanced mechanical properties were due to the better exfoliation caused by the increased interactions between the compatibilizer and organoclay.

The effects of the concentration of constituents that the nanocomposite is made of were studied by the periodic MD simulations. The modeling of nanocomposite was achieved by carrying the information obtained by the lower scale calculations. The most effective interaction between the organoclay and different compatibilizers were sought by calculating the total potential energy of the system. We have seen that when surfactants with single alkyl tail (ODA, ODTMA) are used, the high amounts of compatibilizer can be used. However, if larger surfactants and clay with higher CEC are used, the amount of compatibilizer should be lessened not to introduce interactions which have negative effects on the stability of nanocomposite.

In summary, we showed that:

- the choice of the surfactant and the compatibilizer was a very delicate issue due to their size- and amount-dependent complex behaviors,
- the overall stability of the nanocomposite depends on both vdW and electrostatic type interactions between the constituents of the PE/MMT nanocomposite and could be quantified by the calculation of accurate potential energies of interactions,
- the functional groups of the compatibilizer had a very important role in penetration of nonpolar polymer chains to the polar surfaces,
- the interaction energy between the PE and the montmorillonite layer was inversely proportional to the volume of the surfactant due to the decreased electrostatic interactions between the compatibilizer and the hydrophilic clay surface by the shielding effect.
- the shielding effect of the surfactants become more pronounced at high loadings or when the head groups were large or when the clay with high cation exchange capacity were used. All these factors increasing shielding, on the other hand, made the vdW interactions between alkyl tails and PE chains more attractive and resulted in larger basal spacing. The shielding effect except at very extreme cases were found to be negligible and had no negative effect on the stability.

## REFERENCES

- [1] URL < <http://goldbook.iupac.org/CT07545.html>>, accessed at 29.08.2010.
- [2] **Callister, W. D. Jr.**, 2000: *Materials Science and Engineering-An Introduction*, 5th edition, John Wiley and Sons, New York.
- [3] URL < <http://goldbook.iupac.org/NT07243.html> >, accessed at 29.08.2010.
- [4] **Rao, C. N. R., Müller, A., and Cheetham, A. K.**, 2005. The Chemistry of Nanomaterials: Volume 1, Synthesis, Properties and Applications” Edited by; John-Wiley and Sons Inc., New York.
- [5] **Koch, C. C.**, 2007. Nanostructured materials : processing, properties, and applications, Knovel, William Andrew Pub, Norwich, NY.
- [6] **Kassing, R.**, 2006. Functional properties of nanostructured materials North Atlantic Treaty Organization Dordrecht : Springer, 2006.
- [7] **Cagin, T., Che, J., Qi, Y., Zhou, Y., Demiralp, E., Gao, G., and et al.**, 1999. Computational materials chemistry at the nanoscale, *J. Nanopart. Res.*, **1**, 51–69.
- [8] **Rothon, R. L.**, 1995. Particulate-Filled Polymer Composites, Longman Scientific and Technical, New York.
- [9] **Vilgis, T., Heinrich, G., and Klüppel, M.**, 2009. Reinforcement of Polymer Nano-Composites Theory, Experiments and Applications, Cambridge university Press, New York.
- [10] **Xanthos, M.**, 2010. Functional Fillers for Plastics, Wiley, Weinheim.
- [11] **Wypych, G.**, 2000. Handbook Of Fillers, ChemTec Publishing, , New York.
- [12] **Work, W. J., Horie, K., Hess, M., and Stepto R. F. T.**, 2004. Definition of terms related to polymer blends, composites, and multiphase polymeric materials, *Pure and Applied Chemistry*, **62**, 1985–2007.
- [13] **Leblanc, J. L.**, 2009. Science and Industrial Applications Filled Polymers, CRC Press Taylor & Francis Group, New York.
- [14] **Okada, A., and Usuki, A.**, 2006. Twenty years of polymer–clay nanocomposites, *Macromol. Mater. Eng.*, **291**, 1449–76.
- [15] **Medalia, A. J.**, 1987. “Effect of Carbon Black on Ultimate Properties of Rubber Vulcanizates”, *Rubb. Chem. Technol.*, **60**, 45-61.
- [16] **Joseph, H. K.**, 2006. Polymer nanocomposites processing, characterization and applications, The McGraw-Hill, New York.

- [17] **Utracki, L. A.**, 2004. Clay-containing Polymeric Nanocomposites. Vol. 1., Shrewsbury: Rapra Technology Limited, London, U.K.
- [18] **Alexandre, M., and Dubois, P.**, 2000. Polymer-Layered Silicate Nanocomposites: preparation, properties and uses of a new class of materials, *Mat. Sci. Eng.*, **28**, 1-63.
- [19] **Pinnavaia, T. J., and Beall, G. W.**, 2000. Polymer–Clay Nanocomposites, Wiley Chichester, London, U.K.
- [20] **Oriakhi, C., and Lerner, M.**, 1999. Surface and interfacial properties of polymer-intercalated layered double hydroxide nanocomposites, *Appl. Clay Sci.*, **15**, 265-279.
- [21] **Chen, B., and Evans, J. R. G.**, 2005. On the driving force for polymer intercalation in smectite clays, *Philosophical Magazine*, **85**, 1519–1538.
- [22] **Crosby, A. J., and Lee, J. Y.**, 2007. Polymer Nanocomposites: the ‘‘nano’’ effect on mechanical properties, *Polym. Rev.*, **47**, 217–229.
- [23] **Friedrich, K., Fakirov, S., and Zhang, Z.**, 2005. Polymer Composites: from nano-to-macro-scale, Springer Science-Business Media, Inc. New York.
- [24] **Wang, Z. X., Guo, S., Fu, W., and Wu, D. Z.**, 2004. Polymers containing fullerene or carbon nanotube structures, *Prog. Polym. Sci.*, **29** (11), 1079–1141.
- [25] **Meunier, A.**, 2005. Clays, Springer-Verlag, Heidelberg.
- [26] **Mering, J., and Brindley, G. W.**, 1967. “X-ray Diffraction Band Profiles of Montmorillonite- Influence of Hydration and of the Exchangeable Cations”, *Clays and Clay Minerals*, **15**, 51-60.
- [27] **Moore, D. M., and Reynolds, R. C.**, 1989. X-ray diffraction and the identification and analysis of clay minerals. Oxford University Press, New York.
- [28] **Newman, A. C. D.**, 1987. Chemistry of clays and clay minerals. Mineralogical Society Monograph 6, Mineralogical Society, London.
- [29] **Brindley, G. W., and Brown, G.**, 1980. Crystal Structure of Clay Minerals and their X-ray Identification, Mineral Society Monograph 5, Mineralogical Society. 485 pp., London.
- [30] **Ray S. S., and Okamoto M.**, 2003. Polymer/layered silicate nanocomposites: a review from preparation to processing, *Prog. Polym. Sci.*, **28**, 1539–1641.
- [31] **Klein, C.**, 2002. Mineral Science, John Wiley and Sons, New York.
- [32] **Zvyagin, B. B., Mishchenko, K. S., and Soboleva, S. V.**, 1969. Structures of pyrophyllite and talc in relation to the polytypes of mica-type minerals, *Sov. Phys. Crystallogr.*, **13**, 511–515.

- [33] **Ali Olad, A.**, 2011. Polymer/Clay Nanocomposites in Advances in Diverse Industrial Applications of Nanocomposites, **Boreddy Reddy (Ed.)**, URL<<http://www.intechopen.com/articles/show/title/polymer-clay-nanocomposites>>
- [34] **Greathouse, J. A., Refson, K., and Sposito, G.**, 2000. Molecular Dynamics Simulation of Water Mobility in Magnesium-Smectite Hydrates, *J. Am. Chem. Soc.*, **122**, 11459-11464.
- [35] **Klapyta, Z., Fujita, T., and Iyi, N.**, 2001. Adsorption of dodecyl- and octadecyltrimethyl ammonium ions on a smectite and synthetic micas, *Applied Clay Science*, **19**, 5-10.
- [36] **Pozsgay, A., Fráter, T., Százdi, L., Müller, P., Sajó, I., and Pukánszky, B.**, 2004. Gallery structure and exfoliation of organophilized montmorillonite: effect on composite properties, *European Polymer Journal*, **40**, 27-36.
- [37] **Kaynak, C., and Tasan, C. C.**, 2006. Effects of production parameters on the structure of resol type phenolic resin/layered silicate nanocomposites, *European Polymer Journal*, **42**, 1908-1921.
- [38] **Kozák, O., Praus, P., Machovič, V., and Klika, Z.**, 2010. Adsorption Of Zinc And Copper Ions On Naturaland Ethylenediamine Modified Montmorillonite Ceramics, *Silikate*, **54 (1)**, 78-84.
- [39] **Fornes, T. D., and Paul, D. R.**, 2003. Modeling properties of nylon 6/clay nanocomposites using composite theories, *Polymer*, **44**, 4993-5013.
- [40] **Thomas, F., Michot, L. J., Vantelon, D., Montarges, E., Prelot, B., Cruchaudet M., and Delon, J. F.**, 1999. *Colloids Surfaces*, **159**, 351-358.
- [41] **Sainz-Diaz, C. I., Hernandez-Laguna, A., and Dove, M. T.**, 2001. Modelling of dioctahedral 2:1 phyllosilicates by means of transferable empirical potentials, *Phys. Chem. Miner.*, **28**, 130–141.
- [42] **Data Sheet**, Montmorillonite clay, Southern Clay Products Inc.
- [43] **Ray, S. S., Okamoto, K., and Okamoto, M.**, 2003. Structure-Property Relationship in Biodegradable Poly(butylenesuccinate)/Layered Silicate Nanocomposites, *Macromolecules*, **36**, 2355-2367.
- [44] **Paul, D. R., and Robeson, L. M.**, 2008. Polymer Nanotechnology: Nanocomposites, *Polymer*, **49**, 3187–3204.
- [45] **Low, P. F.**, 1980. The swelling of clay, II montmorillonites, *Journal of the Soil Science Society of America*, **4 (4)**, 667–676.
- [46] **Karaborni, S., Smit, B., Heidug, W., Urai, J., and Oort, E.**, 1996. The Swelling of Clay: Molecular Simulations of Hydration of Montmorillonite, *Science*, **271**, 1102-1104.
- [47] **Zhu, L., and Wool, R.P.**, 2006. Nanoclay reinforced bio-based elastomers: Synthesis and characterization, *Polymer*, **47**, 8106-8115.
- [48] **Winkler, B., Milman, V., Hennion, B., Payne, M. C., Lee, M. H., and Lin, J. S.**, 1995. Ab initio total energy study of brucite, diaspore and hypothetical hydrous wadsleyite, *Phys. Chem. Minerals*, **22**, 461-467.

- [49] **Teppen, B. J., et al.**, 1997. Molecular dynamics modeling of clay minerals .1. Gibbsite, kaolinite, pyrophyllite, and beidellite, *Journal of Physical Chemistry B*, **101**, 1579-1587.
- [50] **Minisini, B., and Tsobnang, F.**, 2005. Ab initio comparative study of montmorillonite structural models, *Applied Surface Science*, **242**, 21–28.
- [51] **Sainz-Diaz, C. I., Timon, V., Botella, V., Artacho, E., and Hernandez-Laguna, A.**, 2002. Quantum mechanical calculations of dioctahedral 2:1 phyllosilicates: effect of octahedral cation distributions in pyrophyllite, illite and smectite, *Am. Miner.*, **87**, 958–965.
- [52] **Boek, F. E. S., Coveney, P. V., and Skipper, N. T.**, 1995. Monte Carlo Molecular Modeling Studies of Hydrated Li-, Na-, and K-Smectites: Understanding the Role of Potassium as a Clay Swelling Inhibitor, *J. Am. Chem. Soc.*, **117** (50), 12608–12617.
- [53] **Skipper, N. T., Sposito, G., and Chang, F. R.**, 1995. Monte Carlo Simulations of interlayer molecular structure in swelling clay minerals. 1. Methodology, *Clays Clay Minerals*, **43**, 285-293.
- [54] **Park, S. H., and Sposito, G.**, 2000. Monte Carlo simulation of total radial distribution functions for interlayer water in Li-, Na-, and K-montmorillonite hydrates. *J. Phys. Chem. B*, **104**, 4642-4648.
- [55] **Greathouse, J. A., Refson, K., and Sposito, G.**, 2000. Molecular Dynamics Simulation of Water Mobility in Magnesium-Smectite Hydrates, *J. Am. Chem. Soc.*, **122**, 11459-11464.
- [56] **Lee, S. Y., and Kim, S. J.**, 2002. Expansion characteristics of organoclay as a precursor to nanocomposites, *Colloids Surf. A Physicochem. Eng. Aspects*, **211**, 19–26.
- [57] **Wei, R.X., Wei-Ping, P., Doug, H., Bryan, K., Loon-Seng, T., and Vaia, R.**, 2002. Thermal stability of quaternary phosphonium modified montmorillonites, *Chemistry of Materials*, **14**, 4837–4845.
- [58] **Wang, D., and Wilkie, C. A.**, 2003. A stibonium-modified clay and its polystyrene nanocomposite, *Polymer Degradation and Stability*, **82**, 309–315.
- [59] **Awad, W. H., Gilman, J. W., Nyden, M., Harris, J., R.H., Sutto, T. E., Callahan, J., Truvole, P. C., DeLong, H. C., and Fox, D. M.**, 2004. Thermal degradation studies of alkyl-imidazolium salts and their application in nanocomposites, *Thermochim. Acta*, **409**, 3–11.
- [60] **Beall, G. W., and Goss, M.**, 2004. Self-assembly of organic molecules on montmorillonite, *Appl. Clay Sci*, **27**, 179–186.
- [61] **Burmistr, M. V., Sukhy, K. M., Shilov, V. V., Pissis, P., Spanoudaki, A., Sukha, I. V., Tomilo, V. I., and Gonza, Y. P.**, 2005. Synthesis, structure, thermal and mechanical properties of nanocomposites based on a linear polymers and layered silicates modified by polymeric quaternary ammonium salts (ionenes), *Polymer* **46**, 12226–12232.

- [62] **Klapyta, Z., Fujita, T., and Iyi, N.,** 2001. Adsorption of dodecyl- and octadecyltrimethyl ammonium ions on a smectite and synthetic micas, *Applied Clay Science*, **19**, 5-10.
- [63] **Bilgiç, C.,** 2005. Investigation of the factors affecting organic cation adsorption on some silicates minerals, *J. Colloid Interface Sci.*, **281**, 33–38.
- [64] **Ruiz-Hitzky, E., and Meerbeek, V., A.,** 2006. Clay mineral-and organoclay- polymer nanocomposites. In: Bergaya, F., Theng, B.K.G., Lagaly, G. (Eds.), *Handbook of Clay Science*. Elsevier, Amsterdam, pp. 583–621.
- [65] **Li, J., Ton-That, M. T., and Tsai, S. J.,** 2006. PP-Based nanocomposites with various intercalant types and intercalant coverages, *Polym. Eng. Sci.*, **46**, 1060–1068.
- [66] **Hackett, E., Manias, E., and Giannelis, E. P.,** 1998. Molecular dynamics simulations of organically modified layered silicates, *J. Chem. Phys.*, **108**, 7410-7415.
- [67] **Gemeay, A. H., El-Sherbiny, A. S., and Zaki, A. B.,** 2002. Adsorption and kinetic studies of the intercalation of some organic compounds onto Na<sup>+</sup>-montmorillonite, *J. Colloid Interface Sci.*, **245**, 116–125.
- [68] **Wu, S. H., Wang, F. Y., Ma, C. C. M., Chang, W. C., Kuo, C. T., and Kuan, H. C.,** 2001. Mechanical, thermal and morphological properties of glass fiber and carbon fiber reinforced polyamide 6 and polyamide 6/clay nanocomposites. *Mater. Lett.*, **49**, 327–333.
- [69] **Park, S. J., Seo, D. I., and Lee, J. R.,** 2002. Surface modification on montmorillonite on surface acid–base characteristics of clay and thermal stability of epoxy/clay nanocomposites, *J. Colloid Interface Sci.*, **251**, 160–165.
- [70] **Patel, H. A., Somani, R. S., Bajah, H. C., and Jasra, R. V.,** 2007. Preparation and characterization of phosphonium montmorillonite with enhanced thermal stability, *Appl. Clay Sci.*, **35**, 194–200.
- [71] **Gilman, J. W., Awad, W. H., Davis, R. D, Shields, J., Harris, J. R. H., and Davis, C.,** 2002. Polymer/layered silicate nanocomposites from thermally stable trialkylimidazolium-treated montmorillonite, *Chem. Mater.*, **14**, 3776–3785.
- [72] **Xi, Y., Ding, Z., and Hongping, H.,** 2005. Infrared spectroscopy of organoclays synthesized with the surfactant octadecyltrimethylammonium bromide, *Spectrochim. Acta, Part A*, **61**, 515–525.
- [73] **Xie, W., Gao, Z., Liu, K., Pan, W. P., Vaia, R., and Hunter, D.,** 2001. Thermal characterization of organically modified montmorillonite, *Thermochim. Acta*, **367**, 339–350.
- [74] **Pauli, D. R., Zeng, Q. H., Yu, A. B., and Lu, G. Q.,** 2005. The interlayer swelling and molecular packing in organoclays, *J. Colloid Interface Sci.*, **292**, 462–4688.

- [75] **Zeng, Q. H., Yu, A. B., and Lu, G. Q.**, 2003. Standish RK. Molecular dynamics simulation of organic-inorganic nanocomposites: layering behavior and interlayer structure of organoclays, *Chem. Mater.*, **15**, 4732–4738.
- [76] **Pozsgay, A., Fráter, T., Százdí, L., Müller, P., Sajó, I., and Pukánszk, B.**, Gallery structure and exfoliation of organophilized montmorillonite: Effect on composite properties, *European Polymer Journal*, **40**, 27-36.
- [77] **Vaia, R. A., Teukolsky, R. K., and Giannelis, E. P.**, 1994. Interlayer structure and molecular environment of alkylammonium layered silicates, *Chem. Mater.*, **6**, 1017-1022.
- [78] **Heinz, H., Vaia, R. A., Krishnamoorti, R., and Farmer, B. L.**, 2007. Self-assembly of alkylammonium chains on montmorillonite: effect of chain length, head group structure, and cation exchange capacity, *Chem Mater*, **19**, 59–68.
- [79] **Zhu, J., He, H., Zhu, L., Wen, X., Deng, F.**, 2005. Characterization of organic phases in the interlayer of montmorillonite using FTIR and <sup>13</sup>C NMR, *J. Colloid Interface Sci.*, **286**, 239–244.
- [80] **Reichert, P., Kressler, J., Thomann, R., Muelhaupt, R., and Stoeppelmann, G.**, 1998. Nanocomposites based on a synthetic layer silicate and polyamide-12, *Acta Polym.*, **49**, 116-123.
- [81] **Kim, Y., and White, J. L.**, 2006. Modeling of polymer/clay nanocomposite formation, *J. Appl. Polym. Sci.*, **101**, 1657–1663.
- [82] **Zhang, Y. Q., Lee, J. H., Jang, H. J., and Nah, C. W.**, 2004. Preparing PP/clay nanocomposites using a swelling agent, *Composites: Part B*, **35**, 133–138.
- [83] **He, H. P., Galy, J., and Gerard, J. F.**, 2005. Molecular simulation of the interlayer structure and the mobility of alkyl chains in HDTMA+/montmorillonite hybrids, *J. Phys. Chem. B*, **109**, 13301–13306.
- [84] **Pavlidou, S., and Papaspyrides, C. D.**, 2008. A review on polymer-layered silicate nanocomposites, *Progress in Polymer Science*, **33**, 1119–1198.
- [85] **Langat, J.**, 2006. Synthesis of imidazolium salts and their application in epoxy montmorillonite nanocomposites, *Polymer*, **47**, 6698-6709.
- [86] **de Paiva, L. B., Morales, A. R., Díaz, F. V. R.**, 2008. Organoclays: Properties, preparation and applications, *Applied Clay Science*, **42**, 8–24
- [87] **Zhu, J. X., He, H. P., Guo, J. G., Yang, D., and Xie, X. D.**, 2003. Arrangement models of alkylammonium cations in the interlayer of HDTMA+ pillared montmorillonite, *Chin. Sci. Bull.*, **48**, 368–372.
- [88] **Bergaya, F., and Lagaly, G.**, 2001. Surface modifications of clay minerals, *Appl. Clay Sci.*, **19**, 1–3.



- [89] **Austin, J. R., and Kontopoulou, M.,** 2006. Effect of organoclay content on the rheology, morphology, and physical properties of polyolefin elastomers and their blends with polypropylene, *Polymer Engineering and Science*, **46**, 1491-1501.
- [90] **Katti, D. R., Ghosh, P., Schmidt, S., and Katti, K. S.,** 2005. Mechanical Properties of the Sodium Montmorillonite Interlayer Intercalated with Amino Acids, *Biomacromolecules*, **6**, 3276-3282.
- [91] **Pospíšil, M., Kalendová, A., Čapková, P., Šimoník J., and Valášková, M.,** 2004. Structure analysis of intercalated layer silicates. combination of molecular simulations and experiment, *Journal of Colloid and Interface Science*, **277**, 154-161.
- [92] **Pospisil, M., Capkova, P., Merinska, D., Malac, Z., and Simonik, J.,** 2001. Structure Analysis of Montmorillonite Intercalated with Cetylpyridinium and Cetyltrimethylammonium: Molecular Simulations and XRD Analysis, *Journal of Colloid and Interface Science*, **236**, 127-131.
- [93] **Zeng, Q. H., Yu, A. B., Lu, G. Q., and Standish, R. K.,** 2004. Molecular dynamics simulation of the structural and dynamic properties of dioctadecyl dimethyl ammoniums in organoclays, *J. Phys. Chem. B.*, **108**, 10025-10033.
- [94] **Heinz, H., Castelijns, H. J., and Suter, U. W.,** 2003. Structure and phase transitions of alkyl chains on mica, *Journal of the American Chemical Society*, **125**, 9500-9510.
- [95] **Biswas, M., and Ray, S. S.,** 2001. Recent progress in synthesis and evaluation of polymer-montmorillonite nanocomposites, *Adv. Polym. Sci.*, **155**, 167-221.
- [96] **Crosby, A. J., and Lee, J. Y.,** 2007. Polymer nanocomposites: the “nano” effect on mechanical properties, *Polym. Rev.*, **47**, 217-29.
- [97] **Okada, A., Kawasumi, M., Usuki, A., Kojima, Y., Kurauchi, T., and Kamigaito, O.,** 1990. Synthesis and properties of nylon-6/clay hybrids. In: Schaefer DW, Mark JE, editors. Polymer based molecular composites, MRS Symposium Proceedings, *Pittsburgh*, **171**, 45-50.
- [98] **Wang, S. J., Long, C., Wang, X., Li, Q., and Qi, Z.,** 1998. Synthesis and properties of silicone rubber organomontmorillonite hybrid nanocomposites, *J. Appl. Polym. Sci.*, **69**, 1557-61.
- [99] **Goettler, L. A., and Recktenwald, D. W.,** 1998. Nylon nanocomposites: performance attributes and potential applications. *Additives'98*, February 17, Orlando.
- [100] **Usuki, A., Kojima, Y., Kawasumi, M., Okada, A., Fukushima, Y., Kurauchi, T., and et al.,** 1993. Synthesis of nylon 6-clay hybrid, *J. Mater. Res.*, **8**, 1179-84.
- [101] **Vaia, R., Vasudevan, S., Krawiec, W., Scanlon, L., and Giannelis, E.,** 1995. New Polymer Electrolyte Nanocomposites: Melt Intercalation of Poly(ethylene oxide) in Mica- Type Silicates, *Advanced Materials*, **7**, 154-156.

- [102] **Bergman, J. S., Chen, H., Giannelis, E. P., Thomas, M. G., and Coates, G. W.,** 1999. Synthesis and characterization of polyolefin-silicate nanocomposites: a catalyst intercalation and in situ polymerization approach, *J. Chem. Soc. Chem. Commun.*, **21**, 2179–2180.
- [103] **Sun, T., and Garces, J. M.,** 2002. High-performance polypropylene-clay nanocomposites by in-situ polymerization with metallocene/clay catalysts, *Adv. Mater.*, **14**, 128–130.
- [104] **Liang, G., Xu, J., Bao, S., and Xu, W.,** 2004. Polyethylene/maleic anhydride grafted polyethylene/organic montmorillonite nanocomposites. Preparation, microstructure, and mechanical properties, *J. Appl. Polym. Sci.*, **91**, 3974–3980.
- [105] **Mitchell, C. A., and Krishnamoorti, R.,** 2002. Rheological properties of diblock copolymer/layered-silicate nanocomposites, *J. Polym. Sci., Part B: Polym. Phys.*, **40**, 1434–1443.
- [106] **Kiliaris, P., Papaspyrides, C.D.,** 2010. Polymer/layered silicate (clay) nanocomposites: An overview of flame retardancy, *Progress in Polymer Science*, **35**, 902–958.
- [107] **Wang, Z., and Pinnavaia, T. J.,** 1998. Hybrid organic-inorganic nanocomposites: exfoliation of magadiite nanolayers in an elastomeric epoxy polymer, *Chem. Mater.*, **10**, 1820-1826.
- [108] **Mittal, V.,** 2009. Polyamide Nanocomposites As Gas Permeation Barrier: in Barrier Properties of Polymer Clay Nanocomposites, Nova Science Publishers Inc, New York.
- [109] **Jin, Y. H., Park, H. J., Im, S. S., Kwak, S. Y., and Kwak, S.,** 2002. Polyethylene/ clay nanocomposite by in-situ exfoliation of montmorillonite during Ziegler–Natta polymerization of ethylene, *Macromol. Rapid. Commun.*, **23**, 135–140.
- [110] **LeBaron, P. C., Wang, Z., and Pinnavai, T. J.,** 1999. Polymer layered silicate nanocomposites: An overview. *Applied Clay Science*, **15**, 11–29.
- [111] **Nwabunma, D., and Kyu, T.,** 2008. Polyolefin Composites, John Wiley and Sons Inc., New Jersey.
- [112] **Krishnamoorti, R, and Vaia, R. A.,** 2001. Polymer nanocomposites: synthesis, characterization, and modeling, American Chemical Society, Washington DC.
- [113] **Ogata, N., Jimenez, G., Kawai, H., and Ogihara, T.,** 1997. Structure and thermal/mechanical properties of poly(L-lactide)–clay blend, *J. Polym. Sci. Part B: Polym. Phys.*, **35**, 389–396.
- [114] **Jin, Y. H., Park, H. J., Im, S. S., Kwak, S. Y., and Kwak, S.,** 2002. Polyethylene/ clay nanocomposite by in-situ exfoliation of montmorillonite during Ziegler–Natta polymerization of ethylene, *Macromol. Rapid. Commun.*, **23**, 135–40.
- [115] **Vaia, R. A., and Giannelis, E. P.,** 1997. Polymer melt intercalation in organically-modified layered silicates: model predictions and experiment, *Macromolecules*, **30**, 8000-8009.

- [116] **Ke, Y. C.**, 2005. Polymer-Layered Silicate and Silica Nanocomposites, Elsevier, Amsterdam.
- [117] **Ke, Y. C., and Long, C., Qi, Z.**, 1999. Crystallization, properties, and crystal and nanoscale morphology of PET-clay nanocomposites, *J. Appl. Polym. Sci.*, **71**, 1139–1146.
- [118] **Gopakumar, T.G., Lee, J.A., Kontopoulou, M., and Parent, J.S.**, 2002. Influence of clay exfoliation on the physical properties of montmorillonite/polyethylene composites. *Polymer*, **43**, 5483–5491.
- [119] **Treece, M. A., Zhang, W., Moffitt, R. D., and Oberhauser, J. P.**, 2007. Twin-Screw Extrusion of Polypropylene-Clay Nanocomposites: Influence of Masterbatch Processing, Screw Rotation Mode and Sequence, *Polymer Engineering and Science*, 898-911.
- [120] **Paul, D. R., and Robeson, L. M.**, 2008. Polymer nanotechnology: Nanocomposites, *Polymer*, **49**, 3187–3204.
- [121] **Zheng, X., and Wilkie, C. A.**, 2003. Flame retardancy of polystyrene nanocomposites based on an oligomeric organically modified clay containing phosphate. *Polymer Degradation and Stability*, **79**, 551–557.
- [122] **Chang, J. H., Uk-An, Y., and Sur, G. S.**, 2003. Poly(lactic acid) nanocomposites with various organoclays. I. Thermomechanical properties, morphology, and gas permeability, *J Polym Sci Part B: Polym. Phys.*, **41**, 94-103.
- [123] **Sinha, R. S., Yamada, K., Okamoto, M., Ogami, A., and Ueda, K.**, 2003. New polylactide/ layered silicate nanocomposites: structure, properties and biodegradability, *Comp Interfaces*, **10**, 435-50.
- [124] **Zanetti, M., Kashiwagi, T., Falqui, L., and Camino, G.**, 2002. Cone calorimeter combustion and gasification studies of polymer layered silicate nanocomposites, *Chemistry of Materials*, **14**, 881-887.
- [125] **Maiti, P., Nam, P. H., Okamoto, M., Kotaka, T., Hasegawa, N., and Usuki, A.**, 2002. The effect of crystallization on the structure and morphology of polypropylene/clay nanocomposites, *Polym. Eng. Sci.*, **42** (9), 1864-1871.
- [126] **Grunlan, J. C., Grigorian, A., Hamilton, C. B., and Mehrabi, A. R.**, 2004. Effect of clay concentration on the oxygen permeability and optical properties of a modified poly(vinyl alcohol), *J. Appl. Polym. Sci.*, **93**, 1102-9.
- [127] **Nielsen, L.**, 1967. Models for the permeability of filled polymer systems. *Journal of Macromolecular Science Part A: Pure and Applied Chemistry*, **1**, 929–942.
- [128] **Beall, G. W.**, 2001. A new model for interpreting nanocomposite behavior, *Annual Technical Conference, Society of Plastics Engineers*, **59**, 2195-2202.
- [129] **Ellis, T. S. and D'Angelo, J. S.**, 2003. Thermal and Mechanical Properties of a Polypropylene Nanocomposite, *J. Appl. Polym. Sci.*, **90**, 1639-1647.

- [130] **Morgan, A. B., Harris Jr., R. H., Kashiwagi, T., Chyall, L. J., and Gilman, J. W.,** 2002. Flammability of Polystyrene Layered Silicate (Clay) Nanocomposites: Carbonaceous Char Formation, *Fire Mater.*, **26**, 247–253.
- [131] **Morgan, A. B.,** 2006. Flame retarded polymer layered silicate nanocomposites: a review of commercial and open literature systems, *Polym. Adv. Technol.*, **17**, 206–217.
- [132] **Yung, K. C., Wang, J., and Yue, T. M.,** 2006. Modeling Young's modulus of polymer-layered silicate nanocomposites using a modified Halpin–Tsai micromechanical model, *J Reinf. Plast. Compos.*, **25**, 847–861.
- [133] **Gu, A., and Chang, F. C.,** 2001. A novel preparation of polyimide/clay hybrid films with low coefficient of thermal expansion, *J. Appl. Polym. Sci.*, **79**, 289–294.
- [134] **Grunlan, J. C., Grigorian, A., Hamilton, C. B., and Mehrabi, A. R.,** 2004. Effect of clay concentration on the oxygen permeability and optical properties of a modified poly(vinyl alcohol), *J. Appl. Polym. Sci.*, **93**, 1102–1109.
- [135] **Paul, M. A., Alexandre, M., Degee, P., Henrist, C., Rulmont, A., and Dubois, P.,** 2003. New nanocomposite materials based on plasticized poly(L-lactide) and organo-modified montmorillonites: thermal and morphological study, *Polymer*, **44**, 443–450.
- [136] **Zeng, Q. H., Yu, A. B., Lu, G. Q., and Paul, D. R.,** 2005. Clay-based polymer nanocomposites: research and commercial development, *J. Nanosci. Nanotechnol.*, **5**, 1574–1592.
- [137] **Maiti, P., and Okamoto, M.,** 2003. Crystallization controlled by silicate surfaces in nylon 6–clay nanocomposites, *Macromol. Mater. Eng.*, **288**, 440–445.
- [138] **Porter, D., Metcalfe, E., and Thomas, M. J. K.,** 2000. Nanocomposite fire retardants-a review, *Fire Mater.*, **24**, 45–52.
- [139] **Jinnai, H., Spontak, R. J., and Nishi, T.,** 2010. Transmission Electron Microtomography and Polymer Nanostructures, *Macromolecules*, **43**, 1675–1688.
- [140] **Vaia, R. A., Jandt, K. D., and Giannelis, E. P.,** 1995. Kinetics of polymer melt intercalation, *Macromolecules*, **28**, 8080–8085.
- [141] **Manias, E., Chen, H., Krishnamoorti, R., Genzer, J., Kramer, E. J., and Giannelis, E. P.,** 2000. Intercalation Kinetics of Long Polymers in 2 nm Confinements, *Macromolecules*, **33**, 7955–7966.
- [142] **Mark, J. E.,** 2007. Physical Properties of Polymer/Clay Nanocomposites in Physical Properties of Polymers Handbook, Springer, New York, 563–580.
- [143] **Alexander B. Morgan and Charles A.** 2007. Wilkie “Flame Retardant Polymer Nanocomposites,” John Wiley and Sons, Hoboken, NJ.

- [144] **Fornes, T. D., Yoon, P. J., Hunter, D. L., Keskkula, H., and Paul, D. R.,** 2002. Effect of organoclay structure on nylon 6 nanocomposite morphology and properties. *Polymer*, **43**, 5915–5933.
- [145] **Fan, J., Liu, S., Chen, G., and Qi, Z.,** 2002. SEM Study of a Polystyrene/Clay Nanocomposite, *Journal of Applied Polymer Science*, **83**, 66–69.
- [146] **Lincoln, D. M., Vaia, R. A., Wang, Z. G., and Hsiao, B. S.,** 2001. Secondary structure and elevated temperature crystallite morphology of nylon6/layered silicate nanocomposites, *Polymer*, **42**, 1621–31.
- [147] **Biswas, M., and Sinha, R. S.,** 2001. Recent progress in synthesis and evaluation of polymer montmorillonite nanocomposites, *Adv. Polym. Sci.*, **155**, 167–221.
- [148] **Carastan, D. J., and Demarquette, N. R.,** 2007. Polystyrene/clay nanocomposites, *International Materials Reviews*, **52**, 345–380.
- [149] **Goettler, L. A., Lee, K. Y., and Thakkar, H.,** 2007. Layered Silicate Reinforced Polymer Nanocomposites: Development and Applications, *Polymer Reviews*, **47**, 291–317.
- [150] **Okamoto, M.,** 2003. Polymer/Layered Silicate Nanocomposites, Rapra Technology Limited, Shawbury, Shrewsbury.
- [151] **Smith, G. D., Bedrov, D., Li, L., and Bytner, O.,** 2002. A molecular dynamics simulation study of the viscoelastic properties of polymer nanocomposites, *J. Chem. Phys. A*, **117**, 9478–9480.
- [152] **Fermeglia, M., Ferrone, M., and Priol, S.,** 2003. Computer simulation of nylon-6/organoclay nanocomposites: prediction of the binding energy, *Fluid Phase Equilib*, **212**, 315–329.
- [153] **Kato, M., Okamoto, H., Hasegawa, N., Tsukigase, A., and Usuki, A.,** 2003. Preparation and properties of polyethylene-clay hybrids, *Polym. Eng. Sci.*, **43**, 1312–1316.
- [154] **Andrew Peacock,** 2000. Handbook of Polyethylene: Structures: Properties, and Applications, Mark Dekker, New York.
- [155] **Gracias, D. H., Zhang, D., Shen, Y. R., and Somorjai, G. A.,** 1998. Surface chemistry mechanical property relationship of low density polyethylene: an IR-visible sum frequency generation spectroscopy and atomic force microscopy study, *Tribology Letters*, **4**, 231–235.
- [156] **Eyerer, P., and Ke, Y. C.,** 1984. Property changes of UHMW polyethylene hip cup endoprostheses during implantation, *Journal of Biomedical Materials Research*, **18**, 1137–1151.
- [157] **Morawiec, J., Pawlak, A., Slouf, M., Galeski, A., Piorkowska, E., and Krasnikowa, N.,** 2005. Preparation and properties of compatibilized LDPE/organo-modified montmorillonite nanocomposites, *Eur. Polym. J.*, **41**, 1115–22.
- [158] **Malpass, D. B.,** 2010. Introduction to Industrial Polyethylene Properties, Catalysts, Processes, John Wiley and Sons Ltd Scrivener Publishing, Hoboken, New Jersey.

- [159] **Li, C., Zhao, J., Zhao, D., and Fan, Q.,** 2004. Linear low-density polyethylene/poly(ethylene-ran-butene) elastomer blends: Miscibility and crystallization behavior, *Journal of Polymer Research*, **11**, 4, 323-331.
- [160] **Pracella, M., and Chionna, D.,** 2003. Reactive compatibilization of blends of PET and PP modified by GMA grafting, *Macromol. Symp*, **198**, 161–171.
- [161] **Bruna, J., Yazdani-Pedram, M., Quijada, R., Valentin, J. L., and Lopez-Manchado, M. A.,** 2005. Melt grafting of itaconic acid and its derivatives onto an ethylene-propylene copolymer, *Reactive & Functional Polymers*, **64**, 169–178.
- [162] **Arostegui, A., and Nazabal, J.,** 2003. Stiffer and super-tough poly(butylene terephthalate) based blends by modification with phenoxy and maleated poly(ethylene-octene) copolymers, *Polymer*, **44**, 239–249.
- [163] **Qiu, W., Mai, K., Fang, K., Li, Z., and Zeng, H.,** 1999. Morphology and Thermal Behavior of PA1010/LLDPE Blends using PE-g-AA as a Compatibilizer, *Journal of Applied Polymer Science*, **71**, 847–853.
- [164] **Yanqing, M., Li, Z., Zhuang, D., Jiruo, Z., Ying, F., and Jinghua, Y.,** 2010. 'The Preparation of Malefic Anhydride Modified Polyethylene via in-situ Chlorinating Graft Copolymerization', *Polymer-Plastics Technology and Engineering*, **49**, 1, 24-31
- [165] **Gaylord, N. G., and Mehta, R.,** 2006. Radical-catalyzed homopolymerization of maleic anhydride in presence of polar organic compounds, *Progress in Organic Coatings*, **55**, 20-26.
- [166] **Bruna, J., Yazdani-Pedram, M., Quijada, R., Valentin, J. L., and Lopez-Manchado, M. A.,** 2005. Melt grafting of itaconic acid and its derivatives onto an ethylene-propylene copolymer, *Reactive and Functional Polymers*, **64**, 169–178.
- [167] **Pesetskii, S. S., Krivoguz, Y. M., and Jurkowski, B.,** 2004. Structure and Properties of Polyamide 6 Blends with Low-Density Polyethylene Grafted by Itaconic Acid and with Neutralized Carboxyl Groups, *Journal of Applied Polymer Science*, **92**, 1702–1708.
- [168] **Roeder, J., Oliveira, R. V. B., Goncalves, M. C., Soldi, V., and Pires, A. T. N.,** 2002. polypropylene-polyamide-6 blends: Influence of compatibilizing agent on interface domains. *Polym. Test*, **21**, 815–821.
- [169] **Tang, Y., Hu, Y., Song, L., Zong, R. W., Gui, Z., Fan, W. C.,** 2006. Preparation and combustion properties of flame retarded polypropylene-polyamide-6 alloys. *Polym. Degradation. Stab.*, **91**, 234–241.
- [170] **Huang, J. J., Keskkula, H., and Paul, D. R.,** 2006. Comparison of the toughening behavior of nylon 6 versus an amorphous polyamide using various maleated elastomers, *Polymer*, **47**, 639–651.

- [171] **Al-Malaika, S., and Kong, W.,** 2005. Reactive processing of polymers: effect of in situ compatibilisation on characteristics of blends of polyethylene terephthalate and ethylene-propylene rubber, *Polymer*, **46**, 209–228.
- [172] **Lopez-Quintana, S., Rosales, C., Gobernado-Mitre, I., Merino, J. C., and Pastor, J. M.,** 2008. Mechanical characterization of toughened polyamide-6 blends with metallocene copolymers, *J. Appl. Polym. Sci.*, **107**, 3099–3110.
- [173] **Pedroso, A. G., and Rosa, D. S.,** 2005. Effects Of The Compatibilizer PE-g-GMA On The Mechanical, Thermal And Morphological Properties Of Virgin And Reprocessed LDPE/Corn Starch Blends, *Polym Adv Technol*, **16**, 310–317.
- [174] **Jang, B. C., Huh, S. Y., Jang, J. G., and Bae, Y. C.,** 2001. Mechanical Properties And Morphology Of The Modified HDPE/Starch Reactive Blend, *Journal of Applied Polymer Science*, **82**, 3313–3320.
- [175] **Ermolovich, O. A., and Makarevich, A. V.,** 2006. Effect Of Compatibilizer Additives On The Technological And Performance Characteristics Of Biodegradable Materials Based On Starch-Filled Polyethylene, *Russian Journal of Applied Chemistry*, **79**, 1526-1531.
- [176] **Roy, D., Simon, G. P., and Forsyth, M.,** 2001. Blends of maleic-anhydride-grafted polyethylene with polyethylene for improved cathodic disbondment performance, *Polymer International*, **20**, 115-1123.
- [177] **Griffin, G. J. L.,** 1994. Chemistry and Technology of Biodegradable Polymers, Blackie Academic and Professional (Chapman and Hall), Suffolk, U.K.
- [178] **Hasegawa, N., Kawasumi, M., Kato, M., Usuki, A., and Okada, A.,** 1998. Preparation and mechanical properties of polypropylene-clay hybrids using a maleic anhydride-modified polypropylene oligomer, *J. Appl. Polym. Sci.*, **67**, 87-92.
- [179] **Reichert, P., Nitz, H., Klinke, S., Brandsch, R., Thomann, R., and Mülhaupt, R.,** 2000. Poly(propylene)/organoclay nanocomposite formation: influence of compatibilizer functionality and organoclay modification. *Macromol. Mater. Eng.*, **275**, 8–17.
- [180] **Katti, K. S., Sikdar, D., Katti, D. R., Ghosh, P., and Verma, D.,** 2006. Molecular interactions in intercalated organically modified clay and clay–polycaprolactam nanocomposites: experiments and modeling, *Polymer*, **47**, 403–14.
- [181] **Xie, S. B., Zhang, S. M., and Wang, F. S.,** 2004. Synthesis and characterization of poly(propylene)/montmorillonite nanocomposites by simultaneous grafting-intercalation, *Journal of Applied Polymer Science*, **94**(3), 1018-1023.
- [182] **Jeon, H. G., Jung, H. T., Lee, S. W., and Hudson, S. D.,** 1998. Morphology of polymer/silicate nanocomposites, *Polym. Bull.*, **41**, 107–113.

- [183] **Zhang, J., and Wilkie, C. A.,** 2003. Preparation and flammability properties of polyethylene-clay nanocomposites, *Polym Degrad Stability*, **80**, 163–169.
- [184] **Wang, K. H., Choi, M. H., Koo, C. M., Choi, Y. S., and Chung, I. J.,** 2001. Synthesis and characterization of maleated polyethylene/clay nanocomposites, *Polymer*, **42**, 9819–9826.
- [185] **Hotta, S., and Paul, D. R.,** 2004. Nanocomposites formed from linear low density polyethylene and organoclays, *Polymer*, **45**, 7639–54.
- [186] **Galeski, A.,** 2010. University of Lodz, Personal Communication.
- [187] **Kato, M., Okamoto, H., Hasegawa, N., Tsukigase, A., and Usuki, A.,** 2003. Preparation and properties of polyethylene-clay hybrids, *Polymer Engineering and Science*, **43**, 1312–1316.
- [188] **Mohaddespour, A., Ahmadi, S. J., Abolghasemi, H., and Jafarinejad, S.,** 2007. Investigation of mechanical, thermal and chemical properties of HDPE/PEG/OMT nanocomposites, *J. Appl. Sci*, **7**, 2591–2597
- [189] **Zanetti, M., and Costa, L.,** 2004. Preparation and combustion behaviour of polymer/layered silicate nanocomposites based upon PE and EVA, *Polymer*, **45**, 4367–4373.
- [190] **Zhai, H. B., Xu, W. B., Guo, H. Y., Zhou, Z. F., Shen, S. J., and Song Q. S.,** 2004. Preparation and characterization of PE and PE-g-MAH/montmorillonite nanocomposites. *European Polymer Journal*, **40**, 2539–2545.
- [191] **Jacquelot, E., Espuche, E., Gerard, J. F., Duchet, J., and Mazabraud, P.,** 2006. Morphology and gas barrier properties of polyethylene-based nanocomposites, *J Polym Sci Part B: Polym Phys*, **44**, 431–440.
- [192] **Dumont, M. J., Reyna-Valencia, A., Emond, J. P., and Bousmina, M.,** Barrier properties of polypropylene/organoclay nanocomposites, *Journal of Applied Polymer Science*, **103**, 618–625.
- [193] **Fermeglia, M., and Pricl, S.,** 2007. Multiscale modeling for polymer systems of industrial interest, *Progress in Organic Coatings*, **58**, 187–199.
- [194] **Zeng, Q. H., Yu, A. B., and Lu, G. Q.,** 2008. Multiscale modeling and simulation of polymer nanocomposites, *Prog. Polym. Sci*, **33**, 191–269
- [195] **Sikdar, D., Katti, D. R., and Katti, K. S.,** 2006. A molecular model for epsilon-caprolactam based intercalated polymer clay nanocomposite: integrating modeling and experiments, *Langmuir*, **22**, 7738–7747.
- [196] **Ozmusul, M. S., Picu, C. R., Sternstein, S. S., and Kumar, S. K.,** 2005. Lattice Monte Carlo simulations of chain conformations in polymer nanocomposites, *Macromolecules*, **38**, 4495–500.
- [197] **Sides, S. W., Kim, B. J., Kramer, E. J., and Fredrickson, G. H.,** 2006. Hybrid particle-field simulations of polymer nanocomposite, *Phys. Rev. Lett.*, **96**, 250601–250605.



- [198] **Scocchi, G., Posocco, P., Fermeglia, M., and Pricl, S.,** 2007. Polymer-clay nanocomposites: a multiscale molecular modeling approach, *J. Phys. Chem. B*, **111**, 2143–2151.
- [199] **Vaia, R. A., and Giannelis, E. P.,** 1997. Lattice model of polymer melt intercalation in organically-modified layered silicates, *Macromolecules*, **30**, 7990–7999.
- [200] **Kuznetsov, D. V., and Balazs, A. C.,** 2000. Phase behavior of end functionalized polymers confined between two surfaces, *J. Chem. Phys.*, **113**, 2479–83.
- [201] **Balazs, A. C., Singh, C., Zhulina, E., and Lyatskaya, Y.,** 1999. Modeling the phase behavior of polymer/clay nanocomposites, *Acc Chem Res*, **32**, 651–7.
- [202] **Gardebien, F., Gaudel-Siri, A., Bredas, J. L., and Lazzaroni, R.,** 2004. Molecular Dynamics Simulations of Intercalated Poly(E-Caprolactone)-Montmorillonite Clay Nanocomposites, *J. Phys. Chem. B*, **108**, 10678-10686.
- [203] **Yung, K. C., Wang, J., and Yue, T. M.,** 2006. Modeling Young modulus of polymer-layered silicate nanocomposites using a modified Halpin–Tsai micromechanical model, *J. Reinf. Plast. Compos.*, **25**, 847–61.
- [204] **Sheng, N., Boyce, M. C., Parks, D. M., Rutledge, G. C., Abes, J. I., and Cohen, R. E.,** 2004. Multiscale micromechanical modeling of polymer/clay nanocomposites and the effective clay particle, *Polymer*, **45**, 487–506.
- [205] **Vacatello, M.,** 2003. Predicting the molecular arrangements in polymer-based nanocomposites, *Macromol. Theory Simul.*, **12**, 86–91.
- [206] **Manias, E., Chen, H., Krishnamoorti, R., Genzer, J., Kramer, E. J., and Giannelis, E. P.,** 2000. Intercalation Kinetics of Long Polymers in 2 nm Confinements, *Macromolecules*, **33**, 7955-7966.
- [207] **Lee, J. Y., Baljon, A. R. C., Sogah, D. Y., and Loring, R. F.,** 2000. Molecular dynamics study of the intercalation of diblock copolymers into layered silicates, *J. Chem. Phys.*, **112**, 9112–9119.
- [208] **Minisini, B., and Tsobnang, F.,** 2005. Molecular mechanics studies of specific interactions in organomodified clay nanocomposite, *Composites: Part A*, **36**, 531–537.
- [209] **Maly, M., Posocco, P., Pricl, S., and Fermeglia, M.,** 2008. Self-Assembly of Nanoparticle Mixtures in Diblock Copolymers: Multiscale Molecular Modeling, *Ind. Eng. Chem. Res*, **47**, 5023–5038.
- [210] **Luo, J. J., Daniel, I. M.,** 2003. Characterization and modeling of mechanical behavior of polymer/clay nanocomposites, *Compos. Sci. Technol.*, **63**, 1607–1616.
- [211] **Anderson, K. L., Sinsawat, A., Vaia, R. A., and Farmer, B. L.,** 2005. Control of silicate nanocomposite morphology in binary fluids: Coarse-grained molecular dynamics simulations, *J Polym Sci Part B: Polym Phys*, **43**, 1014–1024.

- [212] **Gaudel-Siri, A., Brocorens, P., Siri, D., Gardebien, F., Bredas, J. L., and Lazzaroni, R.,** 2003. Molecular Dynamics Study of E-Caprolactone Intercalated in Wyoming Sodium Montmorillonite, *Langmuir*, **19**, 8287-8291.
- [213] **Sikdar, D., Katti, D. R., Kalpana S. Katti, K. S., and Bhowmik, R.,** 2006. Insight into molecular interactions between constituents in polymer clay nanocomposites, *Polymer*, **47**, 5196–5205.
- [214] **Sikdar, D., Katti, D. R., and Katti, K. S.,** 2008. The Role of Interfacial Interactions on the Crystallinity and Nanomechanical Properties of Clay–Polymer Nanocomposites: A Molecular Dynamics Study, *J. Appl. Polym. Sci.*, **107**, 3137–3148.
- [215] **Manias, E., and Kупpa, V.,** 2001. Relaxation of polymers in 2-nm slitpores: confinement induced segmental dynamics and suppression of the glass transition. *Colloids Surf. A*, **187–188**, 509–21.
- [216] **Vaia, R. A., and Giannelis, E. P.,** 1997. Polymer melt intercalation in organically-modified layered silicates: model predictions and experiment, *Macromolecules*, **30**, 8000-8009.
- [217] **Balazs, A. C., Ginzburg, V. V., Qiu, F., Peng, G. W., and Jasnow, D.,** 2000. Multi-scale model for binary mixtures containing nano- scopic particles, *J. Phys. Chem. B*, **104**, 3411–22.
- [218] **Balazs, A. C., Singh, C., and Zhulina, E.,** 1998. The interactions between polymers and clay surfaces through self-consistent field theory, *Macromolecules*, **31**, 8370-8381.
- [219] **Balazs, A. C., Singh, C., Zhulina, E., and Lyatskaya, Y.,** 1999. Modeling the phase behavior of polymer/clay nanocomposites, *Acc. Chem. Res.*, **32**, 651–657.
- [220] **Manias, E., Kупpa, V., Yang, D. K., and Zax, D. B.,** 2001. Relaxation of polymers in 2 nm slit-pores: confinement induced segmental dynamics and suppression of the glass transition, *Colloids Surf.*, **187**, 509–21.
- [221] **Chung, T. C.,** 2002. Synthesis of Functional Polyolefin Copolymers with Graft and Block Structures, *Prog. Polym. Sci.*, **27**, 40-85.
- [222] **Pracella, M., Pazzagli, F., Galeski, A.,** 2002. Reactive Compatibilization And Properties Of Recycled Poly(ethylene terephthalate)/Polyethylene Blends, *Polymer Bulletin*, **48**, 67-74.
- [223] **Singh, G., Bhunia, H., Rajor, A., and Choudhary, V.,** 2011. Thermal Properties And Degradation Characteristics of Polylactide, Linear Low Density Polyethylene, and their Blends, *Polym. Bull.*, **66**, 939–953.
- [224] **Gaylord, N. G.,** 1992. In: Reactive Extrusion: Principles and Practice. Hanser, New York, 55–71.
- [225] **Flory, P. J.,** 1953. *Principles of Polymer Chemistry*. Cornell University Press, Ithaca.
- [226] **Accelrys Material Studio Release 5.0,** 2009. Accelrys software Inc., San Diego.

- [227] **Sun, H.**, 1995. Ab initio calculations and force field development for computer simulation of polysilanes, *Macromolecules*, **28**, 701-712.
- [228] **Frisch, M. J.**, 2009. Gaussian09, Revision A.1, Gaussian, Inc., Wallingford, CT.
- [229] **Fan, C. F., Olafson, B. D., Blanco, M., and Hsu, S. L.**, 1992. Application of molecular simulation to derive phase diagrams of binary mixtures, *Macromolecules*, **25**, 3667-76.
- [230] **Hildebrand, J. H.**, 1979. Is there a "hydrophobic effect"? *Proc. Natl. Acad. Sci. USA*, **76**, 6040-41.
- [231] **Filippi, S., Chiono, V., Polacco, G., Paci, M., Minkova, L. I., and Magagnini, P.**, 2002. Reactive Compatibilizer Precursors For LDPE/PA6 Blends, 1. Ethylene/Acrylic Acid Copolymers, *Macromol. Chem. Phys.*, **203**, 1512-1525.
- [232] **Chuai, C., Iqbal, M., and Tian, S.**, 2010. A study on melt grafting of maleic anhydride onto low-density polyethylene and its blend with polyamide 6, *Journal of Polymer Science Part B: Polymer Physics*, **48**, 267-275.
- [233] **Singh, G., Bhunia, H., Rajor, A., and Choudhary, V.**, 2011. Thermal Properties And Degradation Characteristics of Polylactide, Linear Low Density Polyethylene, and Their Blends, *Polym Bull*, **66**, 939-953.
- [234] **Sailaja, R. R. N.**, 2005. Mechanical properties of esterified tapioca starch-LDPE blends using LDPE-co-glycidyl methacrylate as compatibilizer, *Polym. Int.*, **54**, 286-296.
- [235] **Stackhouse, S., and Coveney, P. V.**, 2002. Study of thermally treated lithium montmorillonite by Ab Initio methods, *J Phys Chem B*, **106**, 12470-77.
- [236] **Tsipursky, S., and Drits, V. A.**, 1984. The distribution of octahedral cations in the 2:1 layers of dioctahedral smectites studied by oblique-texture electron diffraction, *Clay Miner*, **19**, 177-193.
- [237] **Pearson, R. G.**, 1963. Hard and Soft Acids and Bases, *J. Am. Chem. Soc.*, **85**, 3533-3553.
- [238] **Parr, R. G., and Yang, W.**, 1984. Density functional approach to the frontier-electron theory of chemical reactivity, *J. Am. Chem. Soc.*, **106**, 4049-4050.
- [239] **MacKenzie, K. J. D., Brown, I. W. M., Meinhold, R. H., and Bowden, M. E.**, 1985. Thermal reactions of pyrophyllite studied by high-resolution solid-state Al and Sn nuclear magnetic resonance spectroscopy, *J. Am. Ceram. Soc.*, **68**, 266-272,
- [240] **Evans, B. W., and Guggenheim, S.**, 1988. Talc, pyrophyllite, and related minerals. In: Bailey SW (ed) Hydrous phyllosilicates, vol 19. Reviews in Mineralogy, Mineralogical Society of America, Washington, D.C. pp 225-294

- [241] **Wardle, R., and Brindley, G. W.,** 1972. The crystal structure of pyrophyllite, ITc and of its dehydroxylate, *Am. Mineral*, **57**, 732-750.
- [242] **Sainz-Diaz, C. I., Hernandez-Laguna, A., and Dove, M. T.,** 2001. Theoretical modelling of cis-vacant and trans-vacant configurations in the octahedral sheet of illites and smectites, *Phys. Chem. Miner*, **28**, 322-331.
- [243] **Kwilek, T., Hodorowicz, M., Standnick, K., and Czapkiewicz, J.,** 2003. Adsorption isotherms of homologous alkyltrimethyl-benzylammonium bromides on sodium montmorillonite, *J. Colloid Interface Sci.*, **264**, 14-19.
- [244] **Chigwada, G., Wang, D. D., and Wilkie, C. A.,** 2006. Polystyrene nanocomposites based on quinolinium and pyridinium surfactants, *Polym. Degrad. Stab.*, **91**, 848-855.
- [245] **Vaia, R., Teukolsky, R., and Giannelis, E.,** 1994. Interlayer Structure and Molecular Environment of Alkylammonium Layered Silicates, *Chem. Mater.*, **6**, 1017.
- [246] **Zhu, J., He, H., Zhu, L., Wen, X., Deng, F.,** 2005. Characterization of organic phases in the interlayer of montmorillonite using FTIR and <sup>13</sup>C NMR. *J. Colloid Interface Sci.*, **286**, 239-244.
- [247] **Hendrik Heinz, Hilmar Koerner, Kelly L. Anderson, Richard A. Vaia, and B. L. Farmer,** 2005. Force Field for Mica-Type Silicates and Dynamics of Octadecylammonium Chains Grafted to Montmorillonite, *Chem. Mater.*, **17**, 5658-5669.
- [248] **Heinz, H., Vaia, R. A., Krishnamoorti, R., and Farmer, B. L.,** 2007. Self-assembly of alkylammonium chains on montmorillonite: effect of chain length, head group structure, and cation exchange capacity, *Chem. Mater.*, **19**, 59-68.
- [249] **Li, Y.Q., and Ishida, H.,** 2003. Concentration-dependent conformation of alkyl tail in the nanoconfined space: hexadecylamine in the silicate galleries, *Langmuir*, **19**, 2479-2484.
- [250] **Lagaly, G.,** 1999. From clay mineral-polymer interactions to clay mineral-polymer nanocomposites, *Appl. Clay Sci.*, **15**, 1-9.
- [251] **Madejova, J.,** 2003. FTIR techniques in clay mineral studies, *Vib. Spectrosc.*, **31**, 1-10.
- [252] **He, H. P., Frost, R. L., Zhu, J. X.,** 2004. Infrared study of HDTMA+ intercalated montmorillonite, *Spectrochim. Acta, Part A: Mol. Biomol. Spectrosc.*, **60**, 2853-2859.
- [253] **Ren, C., Jiang, Z., Du, X., Men, Y., and Tang, T.,** 2009. Microstructure and Deformation Behavior of Polyethylene/Montmorillonite Nanocomposites with Strong Interfacial Interaction, *J. Phys. Chem. B*, **113**, 14118-14127.
- [254] **Parija, S., Nayak, S. K., Verma, S. K., and Tripathy, S. S.,** 2004. Studies on Physico-Mechanical Properties and Thermal Characteristics of Polypropylene/Layered Silicate Nanocomposites, *Polym. Compos.*, **25**, 646-652.

- [255] **Karian, H. G.**, 2002. Handbook of Polypropylene and Polypropylene Composites, Marck Dekker Inc., New York.
- [256] **Zeng, Q. H., Yu, A. B., and Lu, G. Q.**, 2005. Interfacial interactions and structure of polyurethane intercalated nanocomposite, *Nanotechnology*, **16**, 2757-2763.
- [257] **Kuppa, V., Menakanit, S., Krishnamoorti, R., and Manias, E.**, 2003. Simulation insights on the structure of nanoscopically confined poly(ethylene oxide), *J. Polym. Sci. Part B: Polym. Phys.*, **41**, 3285–98.
- [258] **Toth, R., Coslanich, A., Ferrone, M., Fermeglia, M., Priol, S., Miertus, S., and Chiellini, E.**, 2004. Computer simulation of polypropylene/organoclay nanocomposites: characterization of atomic scale structure and prediction of binding energy, *Polymer*, **45**, 8075–8083.
- [259] **Mai, Y.W., and Yu, Z.Z.**, 2006. Polymer Nanocomposites, Woodhead Publishing Limited, Abington Hall, Abington.
- [260] **Manias, E., Touny, A., Wu, L., Strawhecker, K., Lu, B., and Chung, T.C.**, 2001. Polypropylene/Montmorillonite Nanocomposites. Review of the Synthetic Routes and Materials Properties, *Chem. Mater.*, **13**, 3516-3523.
- [261] **Passaglia, E., Sulcis, R., Ciardelli, F., Malvaldi, M., and Narducci, P.**, 2005. Effect of functional groups of modified polyolefins on the structure and properties of their composites with lamellar silicates, *Polym. Int.*, **54**, 1549–1556.
- [262] **Passaglia, E., Bertoldo, M., Coiai, S., Augier, S., Savi, S., and Ciardelli, F.**, 2008. Nanostructured polyolefins/clay composites: role of the molecular interaction at the interface, *Polym. Adv. Technol.*, **19**, 560–568.
- [263] **Deshmane, Q., Yuan, R.S., Perkins, and R.D.K. Misra**, 2007. On striking variation in impact toughness of polyethylene–clay and polypropylene–clay nanocomposite systems: The effect of clay–polymer interaction, *Materials Science and Engineering A*, **458**, 150–157.
- [264] **Eriman, B.**, 2008. The effects of the polyethylene grafted copolymers to the structures and mechanical properties of polyethylene/organoclay nanocomposites, *Ms.Sci. Thesis*, ITU Institute of Science and Technology.
- [265] **Kuppa, V.K.**, 2003. Poly(Ethylene Oxide)/Layered-Inorganic Nanocomposites: A Molecular Modeling Perspective, *Ph.D Thesis*, The Pennsylvania State University The Graduate School Department of Materials Science and Engineering.
- [266] **Spencer, M.W., Cui, L., Yoo, Y., Paul, D.R.**, 2003. Morphology and properties of nanocomposites based on HDPE/HDPE-g-MA blends, *Polymer*, **51**, 1056–1070.



## CURRICULUM VITAE



**Candidate's full name** : Erol YILDIRIM  
**Place and date of birth** : Diyarbakır - 1980  
**Permanent Address** : İTÜ, Faculty of Science, Department of Chemistry,  
Room: B3-312  
**Universities and  
Colleges attended** : Bilkent University and İTÜ

### Publications:

1. E. Yurtsever, **E. Yıldırım**, M. Yurtsever, E. Bodo, F.A. Gianturco, '*Solvation of  $K^+$  in Helium droplets*', Eur. Phys. J. D, 43, 105-108 (2007)
2. F. Marinetti, E. Coccia, E. Bodo, F. A. Gianturco, E. Yurtsever, M. Yurtsever, **E. Yıldırım**, '*Bosonic Helium Clusters Doped By Alkali Cations: Interaction Forces and Analysis of Their Most Stable Structures*', Theoretical Chemistry Accounts, 118, 53-65 (2007)
3. E. Coccia, E. Bodo, F. Marinetti, F.A. Gianturco, **E. Yıldırım**, M. Yurtsever, E. Yurtsever, '*Bosonic Helium Droplets with Cationic Impurities: Onset of electrostriction and Snowball effects from Quantum Calculations*', Journal of Chemical Physics, 126(12), 124319-1-8 (2007)
4. E. Coccia, E. Bodo, F.A. Gianturco, E. Yurtsever, M. Yurtsever, **E. Yıldırım** '*Quantum Structuring of  $^4\text{He}$  Atoms Around Ionic Dopants: Energetics of  $\text{Li}^+$ ,  $\text{Na}^+$  and  $\text{K}^+$  From Stochastic Calculations*', WSPC Proceedings (2007)
5. **E. Yıldırım**, D. Aksoy, N. Tuzun, M. Yurtsever, '*A QSPR Study on the Physical Properties of Substituted Polypyrroles and Poly(paraphenylenes)*' Designed Monomers & Polymers, Volume 14, 79-91, (2011)
6. **E. Yıldırım**, M. Yurtsever, B. Kenarlı, A.L. Demirel, '*Dissipative Particle Dynamics Study On The Microphase Separation Of Phenylene Oligomers with Polymeric Side Chains*', Macromolecular Theory and Simulations, 20: 340-349 (2011)
7. **E. Yıldırım**, M. Yurtsever, E. Yurtsever, I. Yilgor, E. Yilgor, '*Multiscale Modeling of the Morphology and Properties of Segmented Silicone-Urea Copolymers*', Journal of Inorganic and Organometallic Polymers, **published online** DOI: 10.1007/s10904-011-9588-1 (2011)
8. **E. Yıldırım**, M. Yurtsever, '*A Theoretical Study on Comparison of Efficiency of Polyethylene Compatibilizers*', Journal of Polymer Research, **Accepted**, (2011)
9. **E. Yıldırım**, M. Yurtsever, '*Morphological Properties of Pyrrole and Phenylene Rod-Coil Diblock Copolymers by Dissipative Particle Dynamics*', Macromolecular Research, **Submitted**, (2011)
10. **E. Yıldırım**, M. Yurtsever, '*Investigation of intercalation and layering behaviors of cationic surfactants in organoclays: MD Study*', **In preparation.**
11. **E. Yıldırım**, M. Yurtsever, '*Modeling and MD simulation studies of Polyethylene/Montmorillonite Nanocomposites*', **In preparation.**

